Argonne NATIONAL LABORATORY

ANL-10/35
ISSN 1931-5007
May 2011

APS Science 2010

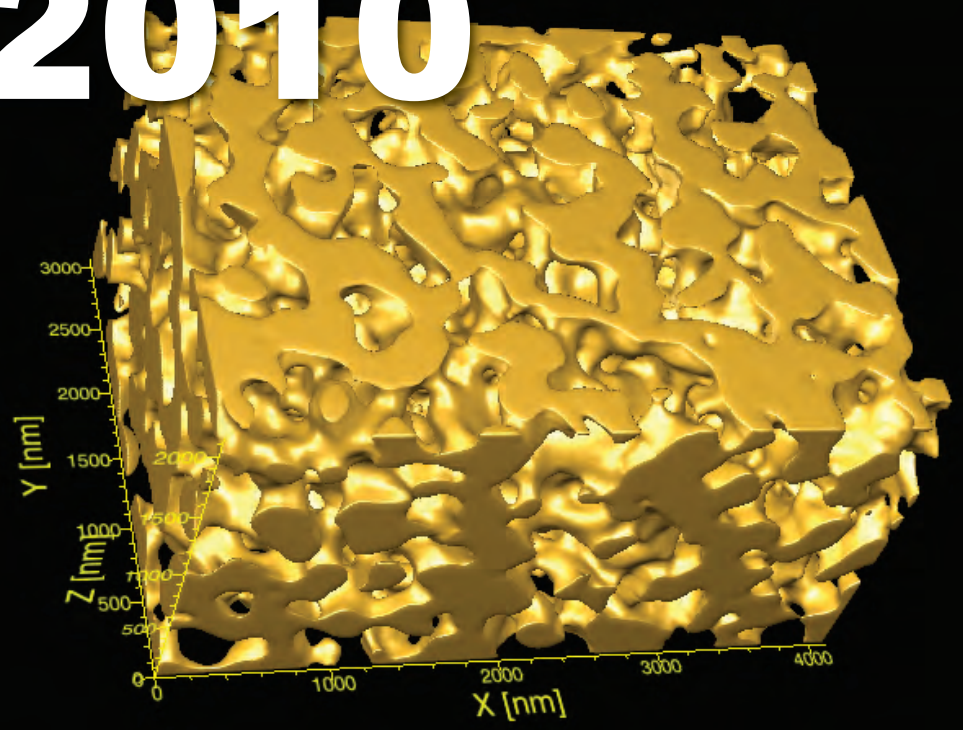

Research and engineering highlights from the Advanced Photon Source at Argonne National Laboratory

ANL-10/35
ISSN 1931-5007
May 2011

The Advanced Photon Source at Argonne National Laboratory is supported by the U.S. Department of Energy, Office of Science, Office of Basic Energy Sciences, under Contract No. DE-ACO2-06CH11357.

About Argonne National Laboratory
Argonne is a U.S. Department of Energy laboratory managed by UChicago Argonne, LLC under contract DE-ACO2-06CH11357. The Laboratory's main facility is outside Chicago, at 9700 South Cass Avenue, Argonne, Illinois 60439. For information about Argonne and its pioneering science and technology programs, see www.anl.gov.

Availability of This Report
This report is available, at no cost, at http://www.osti.gov/bridge. It is also available on paper to the U.S. Department of Energy and its contractors, for a processing fee, from: U.S. Department of Energy
Office of Scientific and Technical Information
P.O. Box 62
Oak Ridge, TN 37831-0062
phone (865) 576-8401
fax (865) 576-5728

reports@adonis.osti.gov

On the cover: A three-dimensional reconstruction of a nanoporous gold sample, annealed at 400oC for 30 min., imaged at XSD beamline 32-ID utilizing transmission x-ray micros-copy. See the article "El Dorado in the Lab: 3-D Imaging of Nanoporous Gold" on page 106.

ANL-10/35
ISSN 1931-5007
May 2011

APS SCIENCE 2010

Research and Engineering Highlights from the Advanced Photon Source at Argonne National Laboratory

Argonne is a U.S. Department of Energy laboratory managed by UChicago Argonne, LLC
The Advanced Photon Source is an Office of Science User Facility operated for the U.S. Department of Energy Office of Science by Argonne National Laboratory.

The Advanced Photon Source facility at Argonne National Laboratory

The APS occupies an 80-acre site on the Argonne campus, about 25 miles from downtown Chicago, Illinois. For directions to Argonne, see www.anl.gov/Visiting/anlil.html.

Access to beam time at the APS

Beam time at the APS can be obtained either as a general user (a researcher not associated with a particular beamline) or as a partner user (e.g., a member of a collaborative access team [CAT], a partner user proposer, or a member of a collaborative development team). If you are a CAT member, contact your CAT for instructions on applying for CAT beam time. At minimum, 25% of the time at all operating beamlines is available to general users, but many offer considerably more general user time—up to 80% on X-ray Operations and Research beamlines, for example.

How general users can apply for beam time at the APS:
1) First-time users should read the information for new users found on our Web site at http://www.aps.anl.gov/Users/Prospective/ before applying for beam time. Also, certain administrative requirements must be completed. In particular, a user agreement between the APS and each research-sponsoring institution must be in place.

2) To choose the appropriate technique(s) and beamline(s), see the beamlines directory in the “Data” section of this volume or at https://beam.aps.anl.gov/pls/apsweb/beamline_display_pkg.beamline_dir.

3) Submit a proposal via the Web-based system. Proposals are evaluated before each user run. For more information see the proposal system overview at: www.aps.anl.gov/Users/Scientific_Access/General_User/General_User_Proposal/Instructions/Proposer/.

Contact us

For more information about the Advanced Photon Source or to order additional copies of this, or previous, issues of *APS Science*, send an e-mail to apsinfo@aps.anl.gov, or write to APS info, Bldg. 401, Rm. A4115, Argonne National Laboratory, 9700 S. Cass Ave., Argonne, IL 60439. Visit the APS on the Web at www.aps.anl.gov.

Table of Contents

For links to online content including animations, videos, etc., look for URLS or (for readers of the print version of this book) QR codes.
QR codes quickly link smartphone users to the content.
A code reader can be downloaded from http://www.quickmark.com.tw/En/basic/download.asp
Adobe Flash may be required for some films.

lightsources.org For news from, and information about, light sources worldwide, visit www.lightsources.org

Welcome

Brian Stephenson

April 2011

The year since the last issue of *APS Science* has been a period of transition for the Advanced Photon Source (APS). Murray Gibson, who served as Argonne Associate Laboratory Director for Photon Sciences and Director of the APS, and who began publication of these yearly highlight compendiums, left the Laboratory to take a new position as founding dean of the College of Science at Northeastern University in Boston. Murray left the APS a better place: stronger, more focused, more diverse, and more open to a broader research community, while maintaining the scientific, engineering, and personnel excellence for which the APS is deservedly renowned.

Murray also left us with a solid foundation for the APS Upgrade project. We are working with our sponsor, the U.S. Department of Energy Office of Science, to bring about an evolution of the APS that will place this facility at the forefront of high-energy synchrotron x-ray science so that our users can continue to serve the nation and justify the investment made by Congress and the Administration. You can read more about the Upgrade in the article on page 6. But here we emphasize that the Upgrade would not have successfully progressed to its current state without Murray's vision and leadership.

When Argonne's Director, Eric Isaacs, asked me to serve as Interim Associate Laboratory Director for Photon Sciences, it was easy to say yes. All of us who are users and staff of the APS want to do whatever we can to see that this facility continues to prosper and that the photon sciences program at Argonne meets the expectations of our sponsor, Argonne management, and the University of Chicago Argonne, LLC.

One of our strongest resources is the APS Scientific Advisory Committee (SAC). This group and its membership of distinguished scientists have for years provided the APS with sound advice and wise counsel about our research program. In recent years the SAC has taken on new, essential responsibilities as an important source of wisdom and guidance for the evolution of the Upgrade.

Equally important to the current success of the APS and the future success of the Upgrade are the APS Users Organization Steering Committee, which represents our user community to APS management and advocates on behalf of science, and the APS Partner User Council, which represents user groups that partner with the APS to build and operate facilities here. In October of 2010, these groups held a joint meeting that had the Upgrade as a primary focus. A series of presentations by APS staff covered the technical aspects of Upgrade accelerator and x-ray beamline planning, and set the stage for wide-ranging discussions by attendees.

As has been the case for all of these highlights volumes since they began in 2003, we trust you will see the breadth and depth and importance of the science reported here. Collectively, these experimental results are a testimony to the scientific curiosity and imagination of our users, the dedication and hard work of the APS staff, and the faith our nation places in science for the common good.

G. Brian Stephenson
(aps-director@aps.anl.gov)

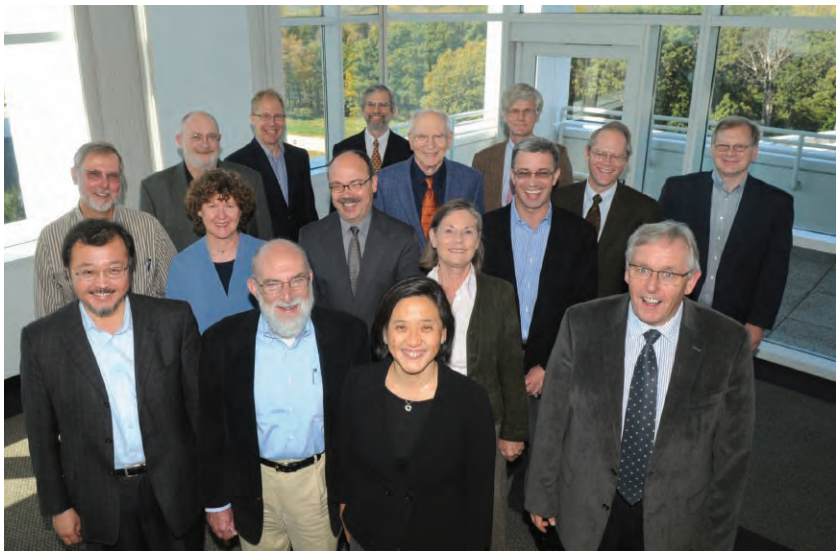

The Advanced Photon Source Scientific Advisory Committee, October 7, 2010. *Front row (l to r)*: Soichi Wakatsuki (Photon Factory), Janos Kirz (Advanced Light Source), Ka Yee C. Lee (The University of Chicago), William Stirling (SAC Chair, European Synchrotron Radiation Facility and CEA-G) *Second row (l. to r.):* Dan Neumann (National Institute of Standards and Technology Center for Neutron Research), Louise N. Johnson (Diamond Light Source), John Corlett (Lawrence Berkeley National Laboratory) *Third row (l. to r.):* Britt Hedman (Stanford Synchrotron Radiation Laboratory), Glenn Waychunas (Lawrence Berkeley National Laboratory), Howard Einspahr (Retired, Bristol-Myers Squibb), Miles V. Klein (Emeritus, University of Illinois), G. Brian Stephenson (Argonne National Laboratory) *Back row:* Roger A. Leach (E.I DuPont de Nemours & Company), Philip H. Bucksbaum (Stanford University), J. Friso van der Veen (Paul Scherrer Institüt) *Not pictured:* David Tiede (Argonne National Laboratory; Chair, APS Users Organization, *ex-officio*), and Thomas Irving (Illinois Institute of Technology; Chair, APS Partner User Council, *ex-officio*)

The Advanced Photon Source Users Organization Steering Committee, January 21, 2011. *Front row (l. to r.):* Peter Eng (The University of Chicago), Brian Stephenson (Argonne National Laboratory) *Back row (l. to r.):* Robert Suter (Carnegie Mellon University), Eric Dufresne (Argonne National Laboratory), Matthew Miller (Cornell University), Alec Sandy (Argonne National Laboratory), Jeremy Kropf (Argonne National Laboratory) *Not pictured:* Dennis Brown (Northern Illinois University), Carl Correll (Rosalind Franklin University of Medicine and Science), Pamela Focia (Northwestern University), Paul Fuoss (*ex officio*; Argonne National Laboratory), Wendy Mao (Stanford University), Alfonso Mondragón (Northwestern University), and David Tiede (Argonne National Laboratory; APSUO Chair)

The Advanced Photon Source Partner User Council Executive Board, January 21, 2011. *Front row (l. to r.):* Lisa Keefe (IMCA-CAT), Keith Brister (LS-CAT; PUC Vice-Chair), Brian Stephenson (Advanced Photon Source), Denis Keane (DND-CAT). *Back row (l. to r.):* Andrzej Joachimiak (SBC-CAT), Bruce Bunker (MR-CAT), James Viccaro (ChemMatCARS-CAT), Wayne Anderson (LS-CAT), Robert Gordon (XSD), Robert Winarski (CNM/XSD), Guoyin Shen (HP-CAT), Robert Fischetti (GM/CA-CAT) *Not pictured:* Malcolm Capel (NE-CAT), John Chrzas (SER-CAT), Thomas Irving (Bio-CAT; PUC Chair), and Stephen Wasserman (LRL-CAT)

THE ADVANCED PHOTON SOURCE UPGRADE PROJECT

April 2011

The last year has been one of great progress for the Advanced Photon Source Upgrade (APS-U) project at Argonne National Laboratory, which Argonne Director Eric Isaacs has identified the Laboratory's number one priority.

The goal of the APS-U project is to enhance the capacity and capabilities of the APS by harnessing innovative physics and technologies developed and implemented by Argonne scientists and engineers, resulting in an improved, world-class source of high-energy, high-brightness, tunable x-rays for scientific research. With nanometers of spatial resolution for imaging and picoseconds of timing resolution for dynamics research, the upgraded Advanced Photon Source will enhance the Department of Energy (DOE) Office of Science research missions in energy, the environment, and national security for the coming decades.

On April 27, 2010, Bill Brinkman, Director of the U.S. Department of Energy Office of Science, signed the formal authorization for Approval of Critical Decision-0, Approve Mission Need (CD-0) for the APS-U, marking the formal beginning of the project, and authorizing preparation of a detailed conceptual design report (CDR). The CD-0 approval was announced on May 3 at the opening session of the annual APS Users Meeting by Pedro Montano, then Director of the DOE Scientific User Facilities Division, on behalf of Harriet Kung, Director of the Office of Basic Energy Sciences.

The process leading up to granting of CD-0 by the DOE was guided by the APS user community as represented by the APS-U Steering Committee (Michael Borland, Robert Fischetti, Paul Fuoss, Rod Gerig, John Maclean, Denny Mills, George Srajer, [all Argonne], Dan Neumann [National Institute of Standards and Technology], and Thomas Irving [Illinois Institute of Technology] and 60 members of 10 "science teams," all of whom were appointed by then-Associate Laboratory Director for Photon Sciences Murray Gibson.

A project management team is now in place, led by Derrick Mancini, Argonne Deputy Associate Laboratory Director for Facility Development in Photon Sciences and APS-U project Director. Mancini's nascent Project Management Team includes Argonne personnel Project Manager Geoff Pile; Associate Project Managers Yeldez Amer (Project Support), Mohan Ramanathan (Engineering Support), Dean Haeffner (Beamline Upgrades), and Marion White (Accelerator Upgrades);Tom Barkalow (ES&H); and Tom Barsz (QA), with Edward Temple serving as Project Advisor. Ronald Lutha of the DOE Chicago Office is the APS-U Federal Project Director on behalf of DOE.

Derrick Mancini

The first task for the APS-U project team is completion of the CDR, which addresses ways to make improvements throughout the APS technical facility. In addition to the proposed baseline capabilities funded by the APS-U, the CDR documents alternatives as contingent additional scope, which will continue to be developed, tracked, and reviewed. At this writing, that document is nearing finished form.

The proposed scope of the project is now well defined, thanks to the beamline proposals put forth and then fleshed out by the APS user community and the APS beamline staff, and vetted by the APS Scientific Advisory Committee (SAC, page 5) and APS management. The APS-U project organization is now fully interfaced with the APS organization, bringing local expertise fully to bear on the technological innovations that the Upgrade represents.

A website dedicated to the APS-U project includes the ability for APS users to view the current draft of the CDR and provide input to and discussions about the Upgrade via APS-U discussion forums and postings to the APS-U Steering Committee.

The project team is preparing for a DOE review in May 2011 that precedes the granting of Critical Decision 1 - Approve Alternative Selection and Cost Range.

All APS-U project activites are carried out under codified "Guidelines for Accelerator Improvements and Beamline Upgrade Selection":

- Appropriate scale for APS user facility
- Supports the identified scientific themes
- Theme leaders heavily involved in defining equipment priorities
- Supports the needs of the user community
- Continuing input from users has been and will be obtained
- Compatibility with existing and planned operations
- Coordination with existing facility layout, roadmap for beamline development, and strategic plans for off-project beamlines
- Subject to review by the APS-U Project Scientific Advisory Committee and APS SAC
- Recent SAC review determined beamline prioritization

Outreach to the user community is of paramount importance. APS User Meetings, the APS Monthly Operations Meeting, APS-U Project Monthly Meetings, and the aforementioned APS-U website are a few of the avenues for contact between the Project and stakeholders.

Contact: Derrick Mancini, mancini@anl.gov

THE APS-U PROJECT: BACKGROUND

The DOE's Basic Energy Sciences (BES) program has a mission to support "fundamental research to understand, predict, and ultimately control matter and energy at the electronic, atomic, and molecular levels in order to provide the foundations for new energy technologies and to support DOE missions in energy, environment, and national security."

There is a particular need for studies of real materials under real conditions in real time by the use of groundbreaking scientific tools that observe, understand, and ultimately control the functions of materials on the nanoscale to develop new technologies. In order to sustain this nation's position at the frontier of science and technology, there is a need for BES to acquire a new, or to upgrade an existing third-generation, synchrotron light source facility that provides an unprecedented combination of high-energy, high-average-brilliance, and short-pulse x-rays together with state-of-the-art x-ray beamline instrumentation. Such a facility is specifically identified as a priority in the Office of Science strategic plan. In this context, the most practical alternative to achieve this mission is to upgrade the APS at Argonne.

Among the various BES user facilities, such as neutron sources, nanoscience centers, and electron microscopy centers, the synchrotron light sources have proven especially valuable. These light sources can be categorized as either storage ring type or free-electron laser (FEL) type, and as producing x-rays optimized in the low-energy (<3 keV) , medium-energy(<20 keV) or high-energy (>25 keV) ranges. Storage ring and FEL sources have complementary capabilities, as do light sources optimized for each of the three x-ray energy ranges. Storage ring sources typically have many beamlines and so can accommodate a large user community. To address its critical mission needs, the DOE expects to provide leading capabilities for each energy range and both source types.

The four DOE-operated, storage-ring-based light sources —APS, Advanced Light Source (ALS), National Synchrotron Light Source, and Stanford Synchrotron Radiation Lightsource (SSRL) — have provided research opportunities for an ever-expanding scientific user community of almost 10,000 scientists, leveraging individual research grants from DOE, the U.S. National Science Foundation, the National Institutes of Health, the U.S. Environmental Protection Agency, the U.S. Department of Agriculture, and many other U.S. federal agencies.

The APS is the only DOE light source in the U.S. Midwest; is the only modern high-energy storage ring source in the U.S.; and, after the APS-U project is complete, will be the best source for x-rays above 20-keV worldwide. The upgraded APS will complement the other existing and planned DOE light sources; the National Synchrotron Light Source II will be a high-performance storage ring radiation source located in the U.S. Northeast, and will be the brightest source of medium-energy x-rays worldwide; the ALS is the only modern low-energy storage ring source in the U.S; the SSRL , which has recently been modernized and offers medium- to high-energy x-rays; and the new FEL Linac Coherent Light Source, the only operating source of its kind in the world, offering ultra-intense, ultra-short pulses of medium-energy x-rays.

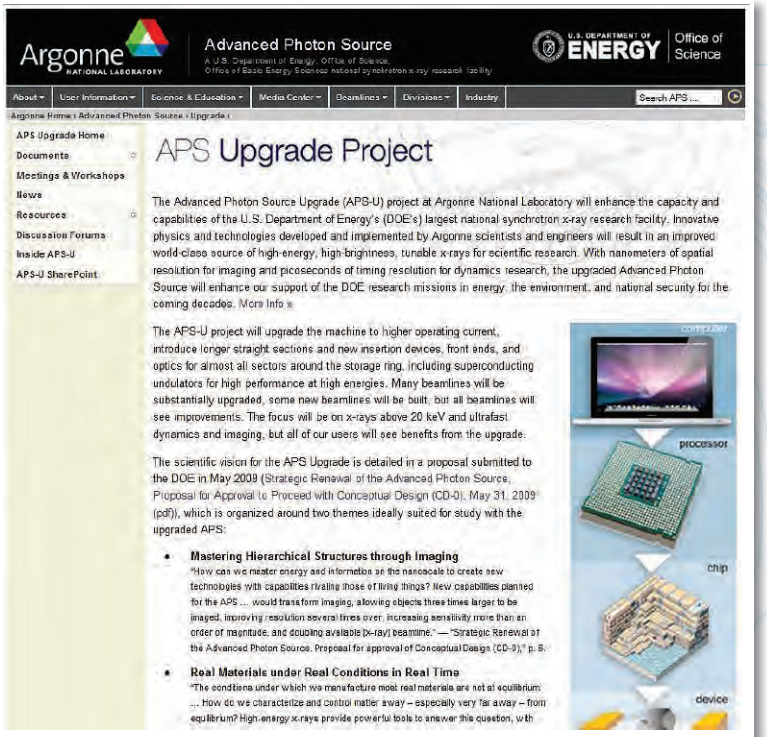

Fig. 1. The APS-U project home page at http://www.aps.anl.gov/Upgrade/.

Upgrading the APS will provide the U.S. with a suite of state-of-the-art complementary research tools needed to carry out the revolutionary research described in the Basic Energy Sciences Advisory Committee report, "New Science for a Secure and Sustainable Energy Future." In particular, the route to new functional materials involves better control during the synthesis and processing of materials. High-energy x-rays uniquely allow structural and chemical studies at the nanometer and picosecond scale under the realistic conditions of materials manufacturing. The vision of going beyond a "discovery" approach to a "controlled" approach for making functional materials will rely on a new high-energy x-ray capability with enough brilliance to provide nanoscale spatial resolution in such environments, which is not possible with any U.S. source today.

A videos about the APS-U project can be viewed at: http://tinyurl.com/3kb5hvj.

APS sectors:

Sector 1: X-ray Science Division (XSD) 1

Sector 2: XSD 2

Sector 3: XSD 3

Sector 4: XSD 4

Sector 5: DuPont-Northwestern-Dow Collaborative Access Team (DND-CAT)

Sector 6: XSD 6

Sector 7: XSD 7

Sector 8: XSD 8

Sector 9: XSD 9

Sector 10: Materials Research CAT (MR-CAT)

Sector 11: XSD 11

Sector 12: XSD 12

Sectors 13 through 15: Center for Advanced Radiation Sources (CARS)
Sector 13: GeoSoilEnviroCARS-CAT
Sector 14: BioCARS-CAT
Sector15: ChemMatCARS-CAT

Sector 16: High Pressure CAT (HP-CAT)

Sector 17: Industrial Macromolecular Crystallography Association CAT (IMCA-CAT)

Sector 18: Biophysics CAT (Bio-CAT)

Sector 19: Structural Biology Center CAT (SBC-CAT)

Sector 20: XSD 20

Sector 21: Life Sciences CAT (LS-CAT)

Sector 22: Southeast Regional CAT (SER-CAT)

Sector 23: General Medicine and Cancer Institutes CAT (GM/CA-CAT)

Sector 24: Northeastern CAT (NE-CAT)

Sector 26: Center for Nanoscale Materials/XSD (CNM/XSD)

Sector 29: Intermediate-Energy X-ray Collaborative Development Team (IEX/CDT)

Sector 30: XSD 30

Sector 31: Lilly Research Laboratories CAT (LRL-CAT)

Sector 32: XSD 32

Sector 33: XSD 33

Sector 34: XSD 34

Key to the beamline descriptions:
Beamline designation • Sector operator • Disciplines • Techniques • Radiation source energy • User access modes • General-user status for particular beamlines are displayed with the science highlights in this book. This information can be viewed in whole at:
http://www.aps.anl.gov/Beamlines/Directory/

The Advanced Photon Source (APS), a national synchrotron radiation research facility at the U.S. Department of Energy's (DOE's) Argonne National Laboratory in Illinois, provides this nation's brightest x-ray beams for science. Research by APS users extends from the center of the Earth to outer space, from new information on combustion engines and microcircuits to new drugs and nanotechnologies whose scale is measured in billionths of a meter. The APS, which is funded by the Basic Energy Sciences program in the DOE Office of Science, enhances America's competitiveness in such areas as superconductors, semiconductors, pharmaceuticals, polymers, and catalysts, and promises to have far-reaching impact on our technology, economy, health, and fundamental knowledge of the materials that make up our world.

At the APS, a "sector" comprises the radiation sources (one bending magnets and one insertion device, although the number of insertion devices in the straight sections of the storage ring can vary), and the beamlines, enclosures, and instrumentation that are associated with a particular storage ring sector. The APS has 35 sectors, 34 of which are dedicated to user science and experimental apparatus. The 35th has limited space for instrumentation and is used primarily for accelerator-related studies.

- **X-ray Science Division** (XSD) sectors comprise those beamlines operated by the APS.

- **Collaborative access team** (CAT) sectors comprise beamlines operated by independent groups made up of scientists from universities, industry, and/or research laboratories.

- **Collaborative development teams** (CDTs) comprise an external partner group that drives the development of a beamline that will be ultimately operated by the APS.

To access the APS as general users (GUs), researchers submit proposals that can be active for up to two years. These proposals are reviewed and rated by one of nine proposal review panels comprising scientific peers, generally not affiliated with the APS. Beam time is then allocated by either of two APS beam-time allocation committees.

Those users who propose to carry out research programs beyond the scope of the GU program may apply to become partner users on any beamline operated by the APS. Prospective Partner User Proposals are peer reviewed by a subset of the APS Scientific Advisory Committee. Final decisions on the appointment of partner users are made by APS management.

Argonne NATIONAL LABORATORY

THE ADVANCED PHOTON SOURCE

Sector Allocations & Disciplines

Source Configuration

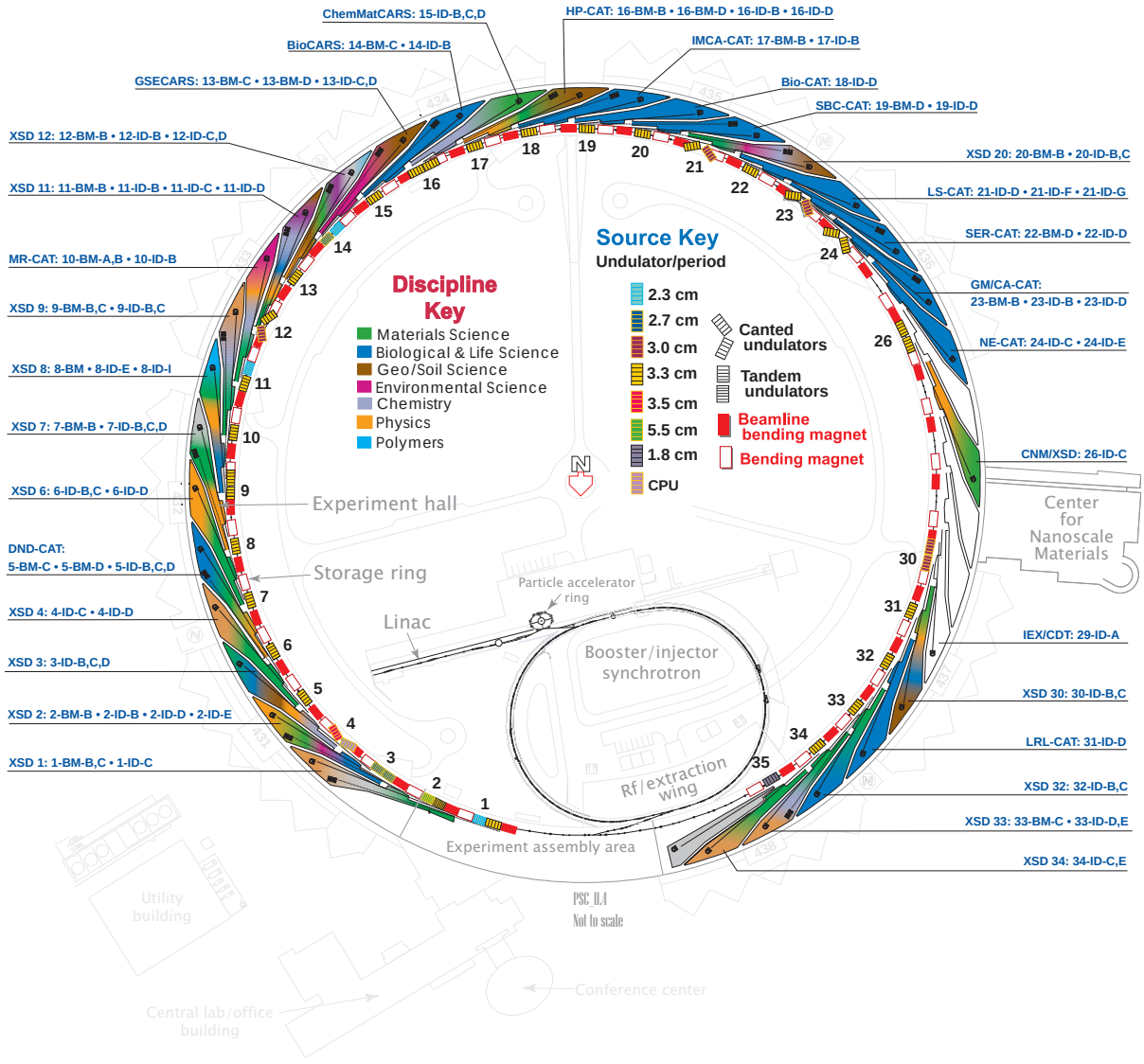

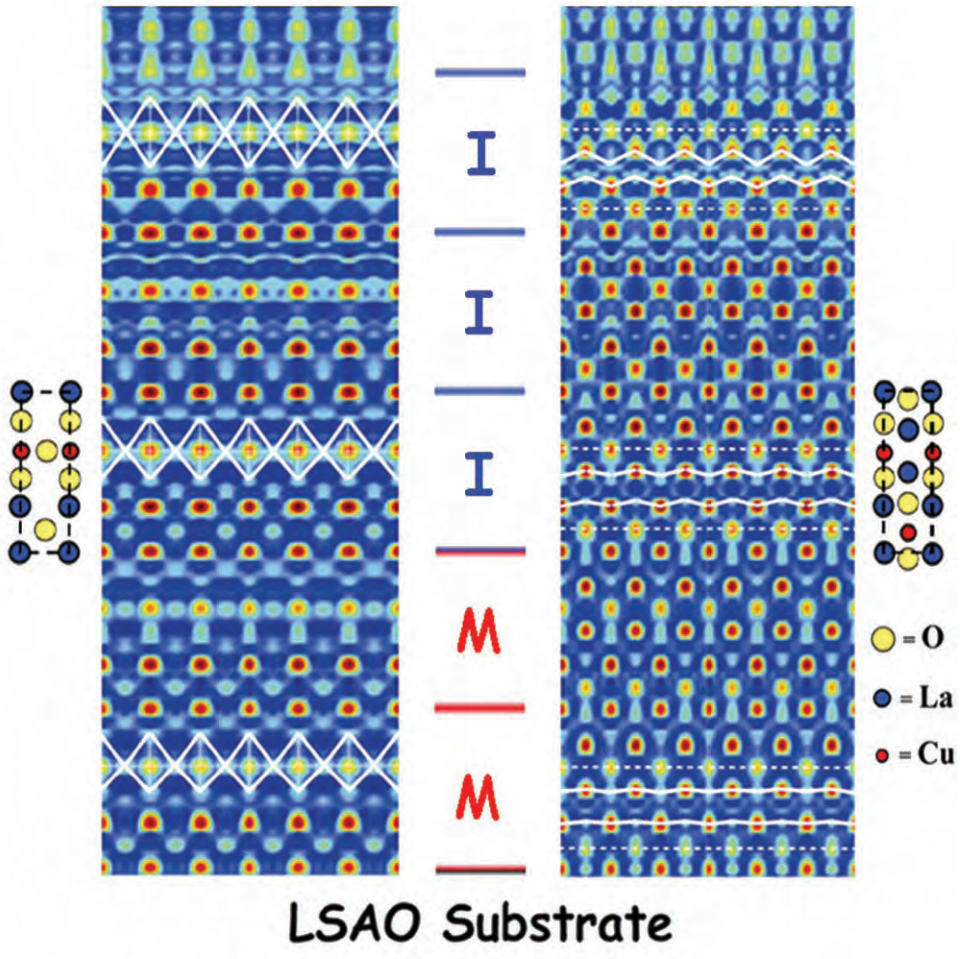

Fig. 1. The measured electron density in two atomic planes of the interfacial superconducting bilayer film showing the positions of the atoms in two metallic (M) and three insulating (I) unit cells. Left: In the (100) plane, the white lines highlight the projected shapes of the CuO_6 octahedra, in particular the elongation near the surface; Right: In the (110) plane, the white lines highlight the projected profiles of the La-apical O planes, in particular the enhanced corrugation near the surface.

How Superconductivity Emerges in Cuprate Bilayers

The recent discovery that superconductivity can exist at the interfaces of complex oxides even when neither of the oxides forming the bilayers is superconductive has generated considerable excitement and triggered a debate about the origin of this superconductivity. To explore this question, researchers from Brookhaven National Laboratory and Hebrew University used a unique atomic layer-by-layer molecular beam epitaxy (ALL-MBE) system to synthesize a number of La-cuprate ultrathin films and then investigated the atomic structures of the films at XSD beamline 33-ID of the APS by measuring diffraction intensities along substrate-defined Bragg rods. The study shows that cuprate crystal structure can be modified and superconductive properties may be dramatically altered. The researchers' work also emphasizes the need for detailed surface-structure determinations in conjunction with surface-sensitive probes of electronic states when studying the superconductive properties of cuprates.

The researchers analyzed their data with an improved x-ray phase-retrieval method they developed that converges with unprecedented speed and precision. In this way, they determined the complete atomic structures of the epitaxial $La_{2-x}Sr_xCuO_4$ ultrathin films with sub-angstrom resolution. Specifically, they found that, while the copper-apical-oxygen distance remains approximately constant in single-phase films, it shows a dramatic increase from the metallic-insulating interface of the bilayer towards the surface by as much as 0.45 Å. This is significant because the apical-oxygen displacement is known to have a profound effect on the superconducting transition temperature. The results show that the improved phase-retrieval diffraction method enables accurate measurement of structural modifications in near-surface layers, which may be critically important for an understanding of surface-sensitive experiments.

The ultrathin films formed using the ALL-MBE system included (i) single-phase films of optimally doped $La_{1.84}Sr_{0.16}CuO_4$ superconductor, (ii) metallic but nonsuperconducting $La_{1.55}Sr_{0.45}CuO_4$, and insulating La_2CuO_4, along with (iii) several different metal-insulator bilayers made from such films. Since atomic positions can vary from one unit cell layer to another in ultrathin films, the standard x-ray diffraction analysis algorithms must be replaced by Coherent Bragg Rod Analysis (COBRA). In general, COBRA uses the measured diffraction intensities and the fact that complex structure factors (CSFs) vary continuously along the substrate-defined Bragg rods in determining the diffraction phases and the CSFs. The CSFs are then Fourier transformed into real space to obtain the three-dimensional electron density of the film and the substrate ($LaSrAlO_4$ [LSAO]), which provides the atomic structures of both.

The COBRA method makes use of an approximation that allows COBRA to converge very quickly to nearly the right solution but not to the exact one. To overcome this limitation, the researchers further refined the CSFs using the so-called Difference-Map algorithm. Using the COBRA solution as the starting point for the Difference-Map algorithm along with a filter program that takes advantage of the fact that the CSFs vary continuously along the Bragg rods, the researchers made the Difference-Map algorithm converge after about 20 iterations, which accelerated convergence by about two orders of magnitude.

With ultrathin bilayers made of metallic nonsuperconducting $La_{1.55}Sr_{0.45}CuO_4$ (M) and insulating La_2CuO_4 (I) ultrathin films, the researchers observed interface superconductivity having a critical temperature of 34K to 36K along with the remarkable increase in the Cu-apical-O distance (Fig. 1). The researchers concluded that the crystal structure of cuprates can be modified in near-surface layers in such a way that superconductive properties may be dramatically altered, with subtle lattice contributions apparently playing an important role. This finding underscores the importance of making detailed surface-structure determinations in conjunction with surface-sensitive probes of electronic states such as scanning tunneling microscopy or angle-resolved photoemission spectroscopy when studying the superconductive properties of cuprates. — *Vic Comello*

See: Hua Zhou[1], Yizhak Yacoby[2], Vladimir Y. Butko[1], Gennady Logvenov[1], Ivan Božović[1], and Ron Pindak[1]*, "Anomalous expansion of the copper-apical-oxygen distance in superconducting cuprate bilayers," Proc. Natl. Acad. Sci. USA **107**(18), 8103 (May 4, 2010).
DOI: 10.1073/pnas.0914702107
Author affiliations: [1]Brookhaven National Laboratory, [2]Hebrew University
Correspondence: *pindak@bnl.gov

This work was supported by the U.S. Department of Energy (DOE) grant MA-509-MACA, Contract No. DE-AC02-98CH10886. Use of the Advanced Photon Source, an Office of Science User Facility operated for the U.S. Department of Energy (DOE) Office of Science by Argonne National Laboratory, was supported by the U.S. DOE under Contract No. DE-AC02-06CH11357.

33-ID • XSD • Chemistry, materials science, physics • Anomalous and resonant scattering (hard x-ray), diffuse x-ray scattering, general diffraction, surface diffraction, x-ray reflectivity, x-ray standing waves • 4-40 keV, 6-21 keV • On-site • Accepting general users

A Chilly Superconductor Warms Up Layer by Layer

An international team of researchers has used the microcrystallography facility operated by ChemMatCARS at Sector 15 of the APS to determine the crystallographic details of a novel, polymorphic form of a layered superconductor material. The material has a critical temperature five times higher than the original form. Finding novel materials that interleave antiferromagnetic, charge ordered, and superconducting layers holds great promise for developing new superconductors.

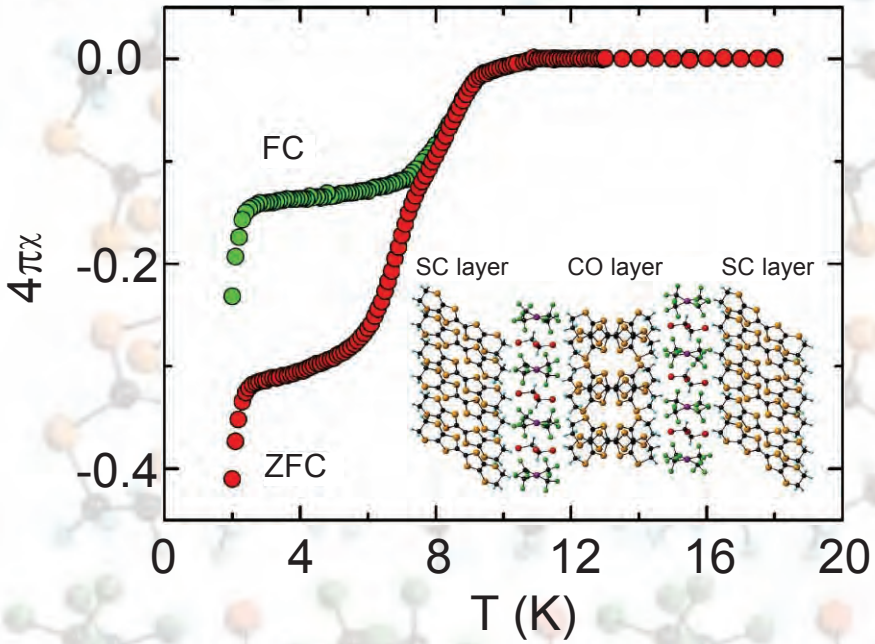

Fig. 1. Magnetic susceptibility for κ-α′-(BEDT-TTF)$_2$Ag(CF$_3$)$_4$(TCE) taken in zero-field-cooled and field-cooled measurements. Inset: Dual-layer packing motif of κ-α′-(BEDT-TTF)$_2$Ag(CF$_3$)$_4$(TCE).

Superconducting materials have zero electrical resistance below a characteristic temperature. This arises because of the quantum mechanical behavior of conducting particles within their structures. Although the effect was discovered in 1911 by Heike Kamerlingh Onnes, it is only in the last few decades that advances have led to significant applications. For example, superconductors are used in magnetic resonance imaging and nuclear magnetic resonance spectroscopy because superconducting magnets are extremely quiet and energy efficient.

Superconductors are also used in particle accelerators and highly sensitive research instrumentation, including the devices used to measure the magnetic and electrical properties of experimental superconducting materials themselves. One major potential benefit of superconductivity lies in the energy-saving possibilities of building an electrical power plant. The zero electrical resistance of superconductors would preclude the inherent energy losses due to the heating effects of conventional components.

Over a decade ago, John A. Schlueter's group at Argonne National Laboratory discovered a highly versatile family of molecule-based superconductors with the general formula $(BEDT\text{-}TTF)_2M(CF_3)_4(solvent)$; BEDT-TTF is bis(ethylenedithio)tetrathiafulvalene, the solvent is a halogen-containing hydrocarbon, 1,1,2-trihaloethane, and M is a coinage metal (copper, silver, or gold). The sulfur atoms in the BEDT-TTF molecules can form bonds with each other between otherwise separate molecules, resulting in a conducting network. In addition, hydrogen bonds, which can form between oxygen or halogen atoms on one molecule and hydrogen atoms on another, compete with the formation of these sulfur-sulfur bonds. This intermolecular competition for bonding means that the material can crystallize in various different forms, or polymorphs, as the different types of bonds form giving rise to different types of connectivity within the structure.

The Argonne group found two crystalline phases of these silver-containing superconductors. The first compound, in which all BEDT-TTF layers are metallic, is a superconductor below 2.1K. The crystal structure of a new morphology, which grows as filamentous molecular crystals, could not be determined by traditional methods and required use of the APS. This phase was found to be superconducting at 11.1° above absolute zero. This is within half a degree Kelvin, of the "warmest" of the cation radical salt class of materials.

Now, Schlueter and his colleagues at Argonne, the Goethe-University Frankfurt, Kyung Hee University, and North Carolina State University, utilizing the ChemMatCARS 15-ID beamline, have discovered that the polymorph with the improved superconducting properties has a dual-layer structure. In this compound, superconducting layers alternate with insulating charge-ordered layers. This layered structure is, they explain, reminiscent of the more conventional, copper-containing (cuprate) superconductors. Those materials have a multi-layered structure and are active at much higher temperatures, perhaps even hinting at superconducting temperatures higher than the boiling point of liquid nitrogen at 77K.

The latest study reveals a novel polymorphic form of their archetypal silver compound that is unique among the class as a whole by virtue of its dual-layered crystal structure (Fig. 1). The team points out that such layered materials have become especially intriguing to researchers because it seems that for many superconductors, the antiferromagnetic and superconducting regions of a materials phase diagram often lie close together. Finding novel materials that interleave antiferromagnetic, charge ordered, and superconducting layers holds great promise for developing new superconductors.

There are only scant clues as to why this novel polymorph with its fibrous structure has such a high critical temperature at 11.1K. It might be due to the greater order of anions and solvent molecules in the charge-compensating layers of the material or perhaps a type of electronic coupling between the "superconducting" and "antiferromagnetic" layers. The next step for these researchers will be to investigate these possibilities more closely through a combined theoretical, synthetic, and experimental approach.

— David Bradley

See: John A. Schlueter[1]*, Leonore Wiehl[2], Hyunsoo Park[1], Mariano de Souza[2], Michael Lang[2], Hyun-Joo Koo[3], and Myung-Hwan Whangbo[4], "Enhanced Critical Temperature in a Dual-Layered Molecular Superconductor," J. Am. Chem. Soc. **132**, 16308 (2010).
DOI:10.1021/ja105854m
Author affiliations: [1]Argonne National Laboratory, [2]Goethe-University Frankfurt, [3]Kyung Hee University, [4]North Carolina State University
Correspondence:
*JASchlueter@anl.gov

Sector 15 is principally supported by the National Science Foundation and the U.S. Department of Energy (DOE) under grant number NSF/CHE-0822838. Work at North Carolina State University (NCSU) was supported by the Office of Basic Energy Sciences, Division of Materials Sciences, U.S. DOE, under Grant DE-FG02-86ER45259, and by the resources of the National Energy Research Scientific Computing Center and the High Performance Computing center of NCSU. Use of the Advanced Photon Source, an Office of Science User Facility operated for the U.S. DOE Office of Science by Argonne National Laboratory, was supported by the U.S. DOE under Contract No. DE-AC02-06CH11357.

15-ID • ChemMatCARS • Chemistry, materials science • Anomalous and resonant scattering (hard x-ray), liquid scattering, microdiffraction, single-crystal diffraction, small-angle x-ray scattering, surface diffraction, wide-angle x-ray scattering • 6-32 keV • On-site • Accepting general users

ELECTRONIC ANISOTROPY IN AN IRON ARSENIDE SUPERCONDUCTOR

Iron-based superconductors are a relatively recent development. Discovered in 2008, these iron compounds present both challenges and opportunities to theorists and experimentalists alike in attempting to understand the mechanisms behind high-temperature superconductivity. One particular question is the role played by a pervasive structural transition found for certain ranges of composition in this class of compounds. The materials are layered, and the structural transition corresponds to a change from a square to rectangular symmetry of the planar iron network. Understanding the origin and significance of this "broken" rotational symmetry (the high-temperature square lattice has a 4-fold symmetry, whereas the low-temperature rectangular lattice has a 2-fold symmetry) requires characterization of the associated electronic anisotropy. In this research, carried out in part at XSD beamline 4-ID-D at the APS, the structural transition related to in-plane resistivity anisotropy of a representative iron arsenide superconductor, cobalt-doped $BaFe_2As_2$, was investigated.

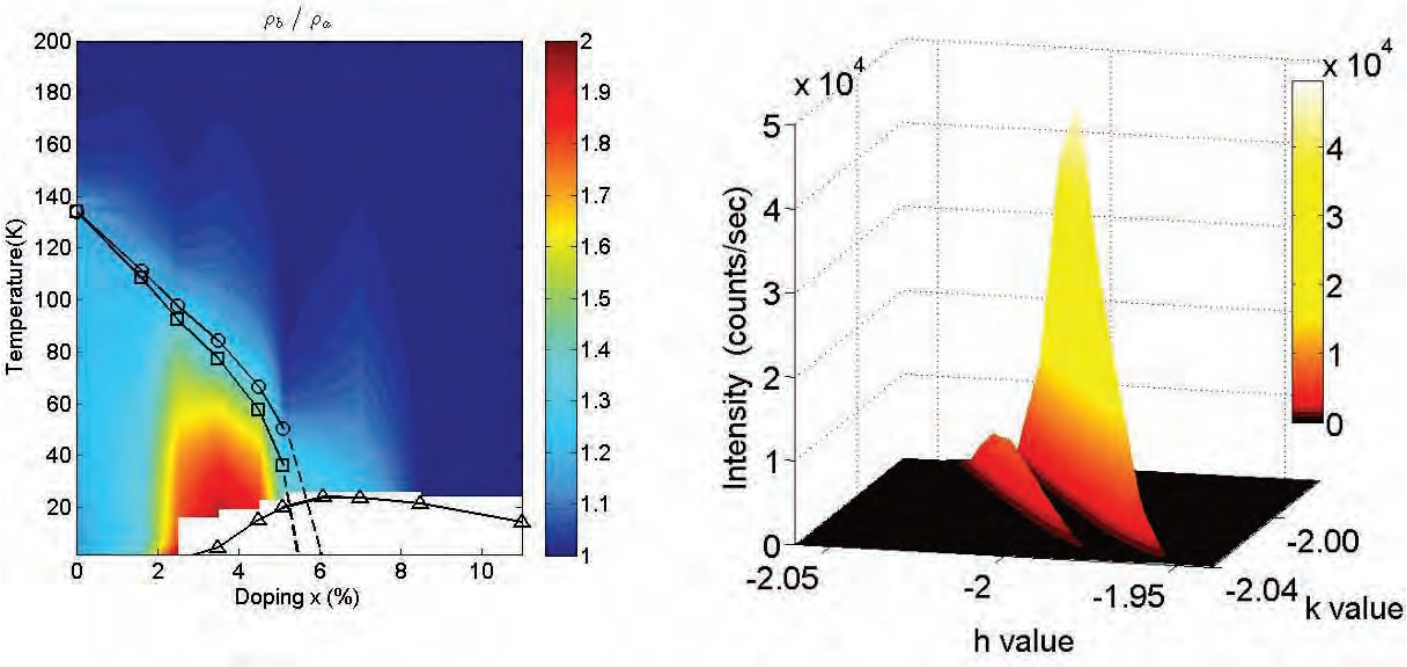

Fig. 1. (a) The left panel shows the degree of resistivity anisotropy (the ratio of resistivity along the a- and b-directions) plotted as a color scale on the temperature vs. doping phase diagram. The large anisotropy (up to a factor of 2) emerges at the proximity of superconductivity. (b) The right panel shows the (-2 -2 20) Bragg peak intensity map on the h-k mesh. The highly asymmetric twin peaks indicate that the crystal is mostly "detwinned." The more asymmetric the peaks, the more detwinned the crystal. With this confirmation the researchers were able to reveal the striking in-plane anisotropy hidden in the iron arsenide sample.

An interesting feature of the iron arsenides is that of crystalline "twinning." The square-to-rectangular structural transition can occur by stretching the square lattice in one of two possible directions (up-down or left-right), both of which occur naturally in any given crystal and are referred to as "twins." Although the properties of the material might be very different if seen along the long or short rectangular axes, the presence of two twin orientations in a macroscopic sample obscures this "anisotropy," leading to the observation of just an average of the two values.

To overcome this problem, the researchers, from Stanford University, SLAC National Accelerator Laboratory, Argonne, and the National Institute of Informatics developed a device that "detwins" the crystals through application of uniaxial pressure. Squeezing the material in one direction favors the twin orientation for which the short rectangular axis is in the direction of the applied pressure, and ultimately leads to a "single-twin" orientation. The team accomplished the detwinning by sandwiching the iron arsenide sample between a substrate and an adjustable cantilever; turning a screw in the center of a cantilever increased the pressure applied to the sample until it was detwinned.

High-resolution x-ray diffraction carried out at the beamline 4-ID-D confirmed the success of the detwinning performed by the cantilever device (Fig. 1, right panel). The measurements were performed using 20-keV photons in a highly asymmetric reflection geometry to ensure a bulk sampling of the crystal. These measurements revealed that the relative twin population (i.e., the relative amount of the material with the long rectangular axis oriented in one particular direction) was close to 100%. Measurements could then be performed on crystals comprising a single twin orientation, and hence the electronic anisotropy (the difference in the electronic properties) along the long and short rectangular directions could be determined.

Systematic measurements of the electrical resistivity of detwinned crystals of cobalt-doped $BaFe_2As_2$ as a function of temperature and composition revealed several unanticipated results.

First, the resistivity along the shorter rectangular axis (denoted ρ_b) was found to be larger than the resistivity along the longer axis (ρ_a). Resistivity measures how hard it is for a material to conduct electricity — a larger resistivity corresponds to a poorer conductor. For a simple material, the resistivity is ordinarily expected to be smaller when atoms are moved closer together. Evidently the iron arsenide compounds are not simple materials. Furthermore, the observed differences in ρ_b and ρ_a were large, up to a factor of 2, in comparison to the actual difference in the long and short axes of the rectangular structure, which were significantly smaller.

Secondly, the resistivity anisotropy, measured by ρ_b/ρ_a, was found to vary non-monotonically with progressive changes in the chemical composition. In contrast, cobalt substitution gradually suppressed the structural transition, and the corresponding difference in the in-plane lattice parameters (the difference between the long and short axes of the rectangle) also smoothly diminished. Given this smooth evolution of the crystal structure, it was especially surprising to find that the associated in-plane electronic anisotropy varies in such a complicated way (Fig. 1, left panel). Of particular note, the onset of the large in-plane anisotropy (the red region in the figure's left panel) occured for a composition close to the onset of superconductivity.

It remains to be seen to what extent these results are generic to all Fe-arsenide superconductors. However, at least for the example studied in this case, it appears that the onset of superconductivity might be associated with changes in the electronic properties which are related to the degree of in-plane electronic anisotropy. — *Philip Koth*

See: Jiun-Haw Chu[1,2], James G. Analytis[1,2], Kristiaan De Greve[1], Peter L. McMahon[1], Zahirul Islam[3], Yoshihisa Yamamoto[3,4], and Ian R. Fisher[1,2]*, "In-Plane Resistivity Anisotropy in an Underdoped Iron Arsenide Superconductor", Science **329**, 824 (13 August 2010).
DOI:10.1126/science.1190482
Author affiliations: [1]Stanford University, [2]SLAC National Accelerator Laboratory, [3]Argonne National Laboratory, [4]National Institute of Informatics
Correspondence:
*irfisher@stanford.edu

This work was supported by the U.S. Department of Energy (DOE), Office of Sciences, under contract DE-AC02-76SF00515. Use of the Advanced Photon Source, an Office of Science User Facility operated for the U.S. DOE Office of Science by Argonne National Laboratory, was supported by the U.S. DOE under Contract No. DE-AC02-06CH11357.

4-ID-D • XSD • Materials science, physics • Anomalous and resonant scattering (hard x-ray), magnetic circular dichroism (x-ray magnetic circular dichroism, hard x-ray), magnetic x-ray scattering • 2.5-50 keV • On-site • Accepting general users

Chasing a Restless Electron in CeAl Metallic Glass

Metals and glasses are handy materials, but combining the qualities of both in metallic glass can provide some unique advantages, resulting in materials with greater durability than ordinary metals while avoiding the brittleness of typical glasses. The amorphous structure of metallic glass also allows intriguing electronic behaviors that could prove useful for various applications. By putting the pressure on a cerium-aluminum metallic glass, researchers using three x-ray beamlines at the APS have confirmed a polyamorphic phase transition involving unusual behavior of the cerium 4*f* electrons. The results are a milestone in understanding the structure of these metallic glasses and their behavior under different conditions, which can be important in using the materials to best advantage and tailoring them for specific applications.

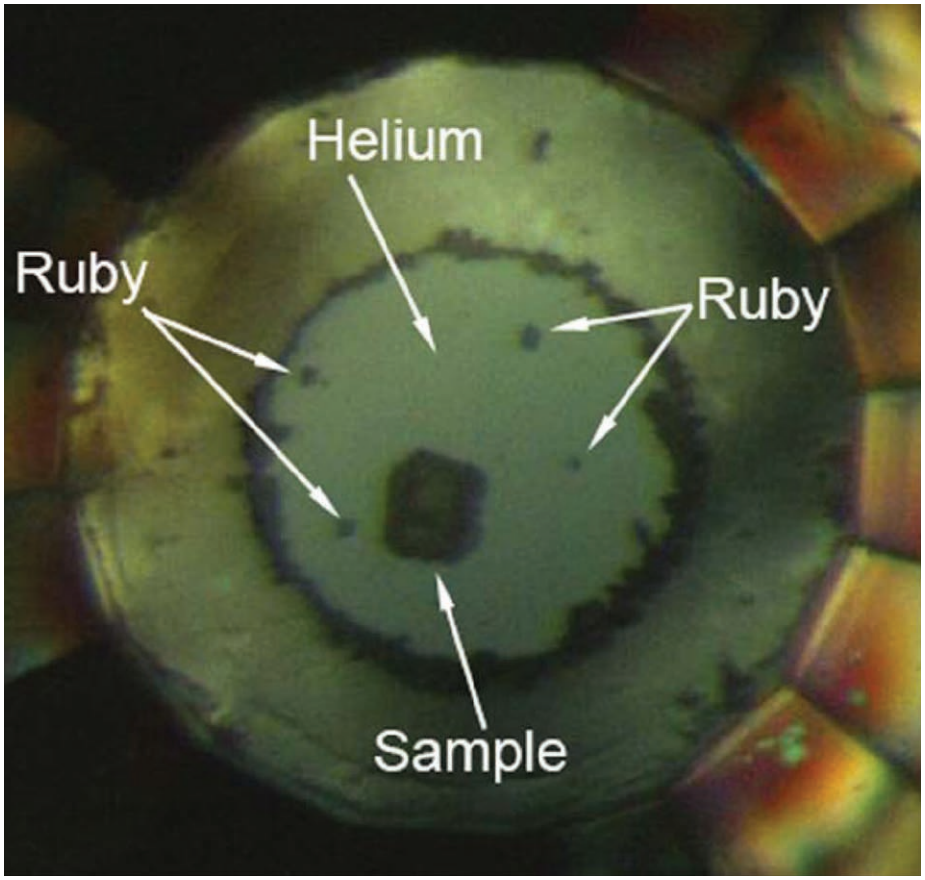

Fig. 1. Photomicrograph of sample loaded with helium in diamond anvil cell at 0.8 GPa. All figures from Q.-s. Zeng et al., Phys. Rev. Lett. **104,** 105702 [2010]. http://prl.aps.org/abstract/PRL/v104/i10/e105702

The experimenters from Zhejiang University, the Carnegie Institution, Stanford University, and the SLAC National Accelerator Laboratory employed the x-ray diffraction (XRD) and x-ray absorption spectroscopy (XAS) techniques to examine polyamorphic transformations in the $Ce_{75}Al_{25}$ metallic glass samples. Because recent previous work had suggested involvement of the 4*f* cerium electrons in pressure-induced metallic glass polyamorphism, the team used samples with the highest possible Ce content to avoid contamination of the results with other materials.

Previous experiments with other amorphous solids had shown that polyamorphism and the resulting greater density under high pressures were due to increased atomic coordination and bond shortening that allowed closer packing of atoms. But such phenomena were considered impossible in metallic glasses, in which atoms are generally already at their maximum possible coordination. After several 2007 studies demonstrated that metallic glasses containing cerium could indeed undergo polyamorphic changes (suggested by sharp kinks in the measured pressure shifts of XRD peaks), a different mechanism was suggested involving delocalization of the 4*f* Ce electrons, which is known to occur in pure Ce and its compounds. However, the 2007 experiments could not provide direct evidence of this electron delocalization.

The researchers in this study set out to find such evidence and the mechanism behind the unexpected polyamorphism observed in cerium-rich metallic glass. As pressure was increased on the $Ce_{75}Al_{25}$ metallic glass samples at the HP-CAT 16ID-B and 16-BM-D beamlines of the APS (Fig.1), XRD studies showed a broad transition range from their low-density amorphous state to higher densities (Fig.2). This transition range can be divided into three fairly distinct regimes: a low-density amorphous state below

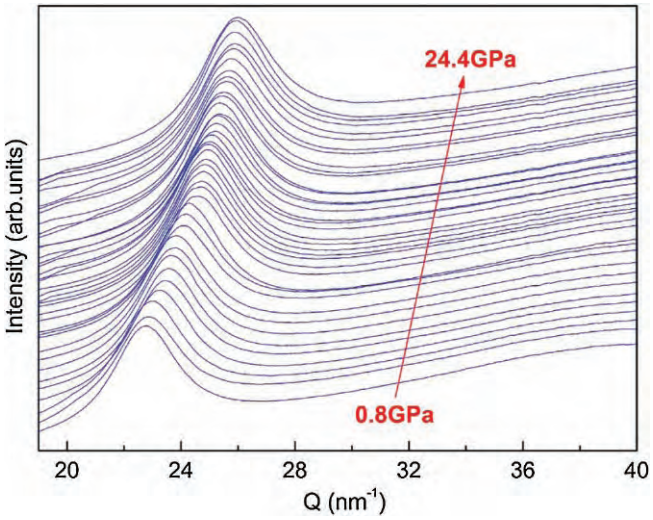

Fig. 2. *In situ* high-pressure XRD patterns of $Ce_{75}Al_{25}$ metallic glass from 0.8 to 24.4 GPa. The position of FSDP shifts to the higher Q values with increasing pressure as a result of densification.

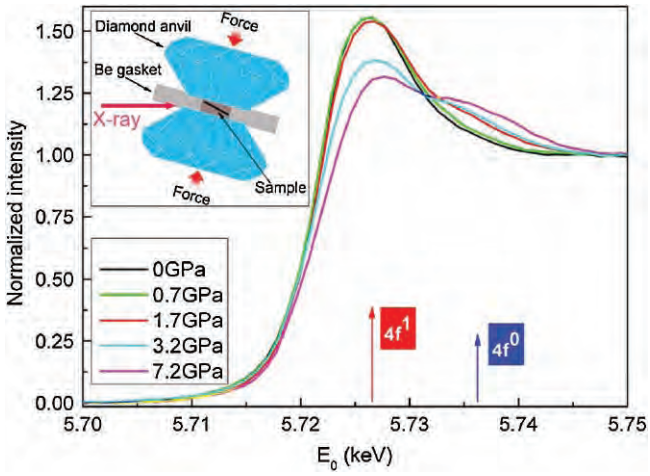

Fig. 3. *In situ* high-pressure Ce L_3-edge XAS spectra of $Ce_{75}Al_{25}$ metallic glass. The arrows point to the $4f^0$ and $4f^1$ components. The appearance of the $4f^0$ feature indicates the delocalization of $4f$ electrons, and coincides with the volume collapse in XRD results. The inset shows a schematic of the *in situ* high-pressure XAS experimental geometry.

1.5 GPa; an intermediate state between 1.5 and 5 GPa; and a high-density amorphous state above 5 up to 24.4 GPa. In the intermediate regime, the samples showed a reduction in volume of almost 9%, indicating the transition to a polyamorphic state.

Using XAS at the XSD 20-BM beamline at the APS, the experimenters then set out to confirm the proposed itinerant behavior of the $4f$ Ce electrons in the CeAl metallic glass samples. This posed an experimental challenge, because the diamond anvil cell (DAC) in which the samples are mounted tends to sharply attenuate the x-ray beam at the Ce L_3 edge spectrum, the energy range in which this delocalization would be best observed. The team overcame this problem by tilting the DAC in the optical path by 18° to reduce the amount of diamond material penetrated by the x-ray beam.

The XAS spectra obtained at the Ce L_3 edge (Fig.3) showed that under increased pressure, the $4f$ electrons indeed became itinerant. The delocalization began in the low pressure regime at 1.5 GPa and intensified in the intermediate pressure regime, until the $4f$ electrons are observed to be fully itinerant above 5 GPa. This confirms a new type of electronic polyamorphism that is strongly correlated with cerium content, quite distinct from the polyamorphism seen in other types of amorphous solids, and provides the first direct experimental evidence of the $4f$ electron behavior proposed to explain the phenomenon.

Because other metallic glasses with high amounts of cerium or other rare-earths could display similar electronic properties, the researchers expect that this work will prove a valuable milestone in understanding how these metallic glasses are structured and how they behave under different conditions. That understanding will be vital in the quest to not only use these materials to best advantage, but also tailor them for specific applications.

— Mark Wolverton

See: Qiao-shi Zeng[1,2], Yang Ding[2], Wendy L. Mao[1,3,4], Wenge Yang[2], Stas.V. Sinogeikin[2], Jinfu Shu[2], Ho-kwang Mao[1,2], and J. Z. Jiang[1]*, "Origin of Pressure-Induced Polyamorphism in $Ce_{75}Al_{25}$ Metallic Glass," Phys. Rev. Lett. **104**, 105702 (12 March 2010). DOI:10.1103/PhysRevLett.104.105702

Author affiliations: [1]Zhejiang University, [2]Carnegie Institution of Washington, [3]Stanford University, [4]SLAC National Accelerator Laboratory

Correspondence: *jiangjz@zju.edu.cn

Research supported as part of EFree, an Energy Frontier Research Center funded by the U.S. Department of Energy (DOE), Office of Science, Office of Basic Energy Sciences (BES) under Grant No. DE-SC0001057. Use of HP-CAT was supported by DOE-BES, DOE-NNSA (CDAC), and the National Science Foundation. XSD 20 and research at these facilities, are supported by DOE-BES, a major facilities access grant from Natural Sciences and Engineering Research Council of Canada, University of Washington, Simon Fraser University, and the APS. This work was supported by the Balzan Foundation, National Natural Science Foundation of China (Grants No. 50601021, No. 50701038, No. 60776014, No. 60876002, No. 50920105101, and No. 10979002), the Zhejiang University-Helmholtz Cooperation Fund, the Ministry of Education of China (the Changjiang Foundation, the Doctoral Education Foundation, China State Oversea Foundation), the Department of Science and Technology of Zhejiang Province, and Baoyugang Foundation of Zhejiang University. Use of the Advanced Photon Source, an Office of Science User Facility operated for the U.S. DOE Office of Science by Argonne National Laboratory, was supported by the U.S. DOE under Contract No. DE-AC02-06CH11357.

16-BM-D • HP-CAT • Chemistry, geoscience, materials science, physics • Energy dispersive x-ray diffraction, high-pressure diamond anvil cell, white Laue single crystal-diffraction • 10-120 keV • On-site • Accepting general users

16-ID-B • HP-CAT • Chemistry, geoscience, materials science, physics • High-pressure diamond anvil cell, microdiffraction, single-crystal diffraction• 24-35 keV • On-site • Accepting general users

20-BM • XSD • Chemistry, environmental science, geoscience, materials science • Micro x-ray absorption fine structure, microfluorescence (hard x-ray), x-ray absorption fine structure • 2.7-25 keV, 2.7-30 keV, 2.7-35 keV • On-site • Accepting general users

Different Layers in Complex Oxide Superlattices Show Surprisingly Similar Behavior

Superlattices are crystals built from a repeating pattern of different but structurally compatible molecular layers. Because superlattices combine the physical properties of their component materials in sometimes unusual ways, they open up the possibility of designing novel structures with desirable characteristics. Using the XSD beamline 7-ID at the APS, researchers conducted time-resolved x-ray diffraction studies on a superlattice in a varying electric field in order to understand how its electrical properties derive from the very different properties of its constituents, two complex metal oxides. Their findings offer lessons for the design and construction of novel superlattices.

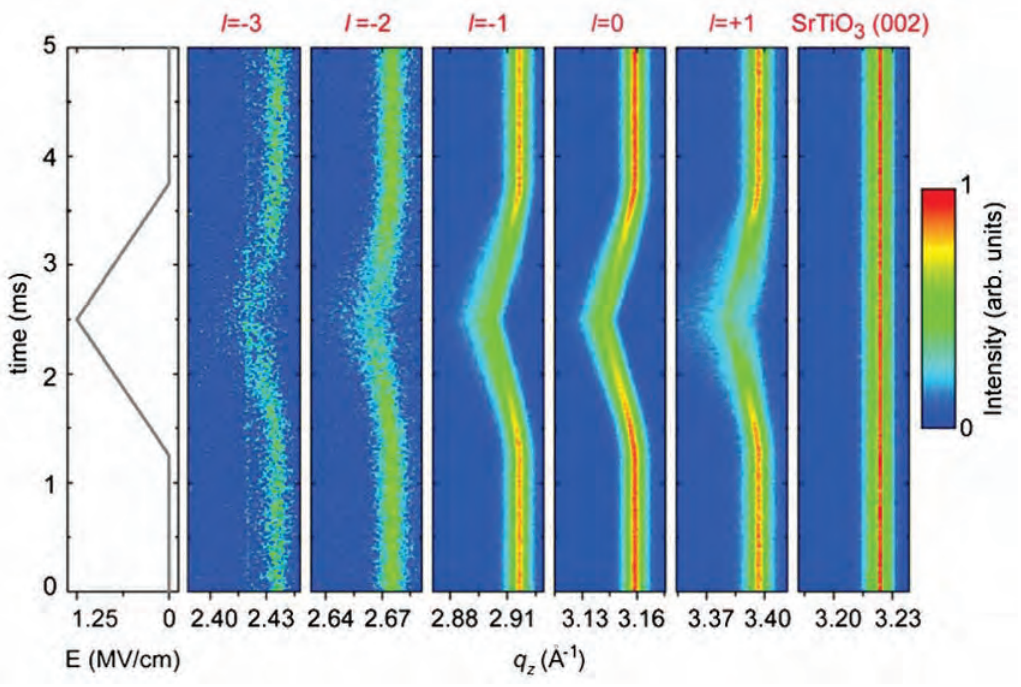

Fig. 1. Time-dependent x-ray diffraction patterns for the l = –3, –2, –1, –0, and –1 reflections of the superlattice with m = 2, and the (002) reflection of the $SrTiO_3$ substrate.

The researchers, from the University of Wisconsin-Madison, Oak Ridge National Laboratory, and Argonne, have probed a complex oxide superlattice created by repeatedly depositing two layers of barium titanate ($BaTiO_3$) followed by four layers of calcium titanate ($CaTiO_3$) on a strontium ruthenate ($SrRuO_3$) electrode layer covering a strontium titanate ($SrTiO_3$) substrate. $BaTiO_3$ is ferroelectric, meaning that it develops a spontaneous electrical polarization even when no external electric field is present. It is also piezoelectric: Its polarization changes when the crystal structure is physically strained, and applying an external field distorts the lattice. $CaTiO_3$ is dielectric, so it develops a polarization when placed in an electric field.

Sandwiched between the ferroelectric layers, the dielectric layers in this superlattice become effectively both ferroelectric and piezoelectric. They acquire a spontaneous polarization, and that polarization changes in response to external fields or physical stress. Exactly how the two different layers contribute to the behavior of the superlattice as a whole was unclear.

To measure the piezoelectric response of the superlattice, the researchers used time-resolved x-ray diffraction to probe its structure while applying a periodically varying electric field (Fig. 1). Measurements obtained during many cycles of the applied field were added to give statistically reliable results for the piezoelectrically induced strain at each magnitude of the applied field. Above approximately 0.4 MV/cm,

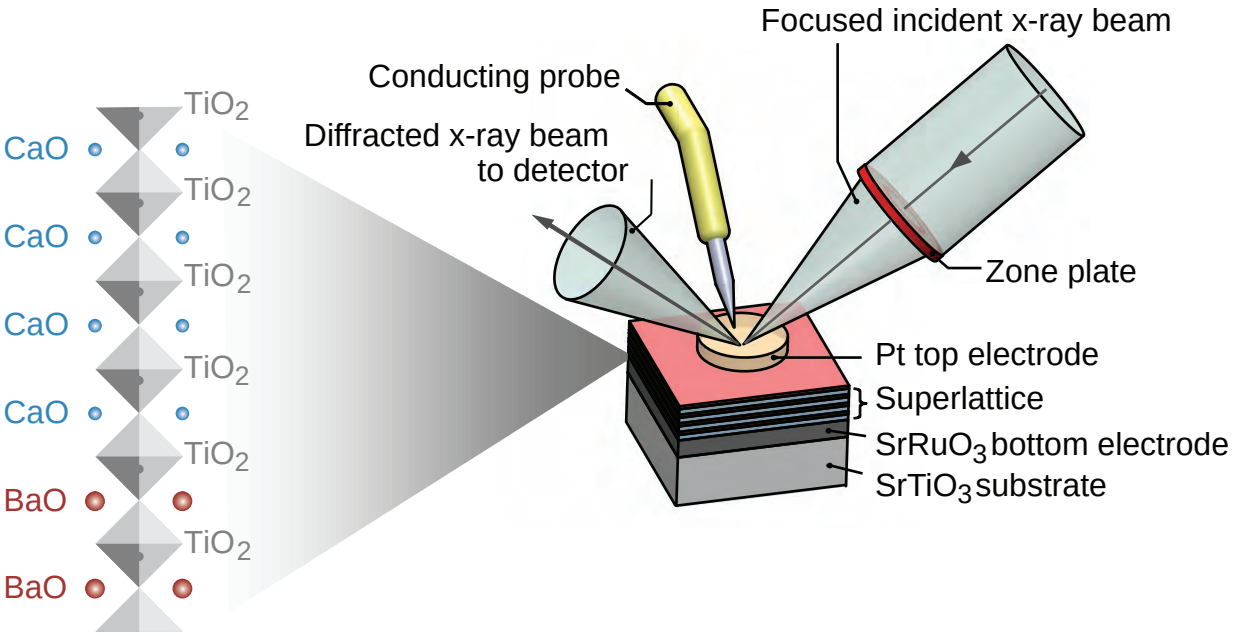

Fig. 2. X-ray diffraction measurements of a complex oxide superlattice reveal how an applied electric field distorts its structure. When the layers are only a few atomic spacings thick, the two different materials in the superlattice (left) behave similarly, even though in bulk they have very different electrical properties

the superlattice behaved like a typical piezoelectric material, with strain increasing linearly with field strength. For smaller fields, the results are slightly more complicated, due either to an initial re-alignment of larger-scale domains within the superlattice or a field-induced change in its atomic-scale symmetry before the linear piezoelectric response sets in.

A detailed analysis of the experimental results yielded two important insights. First, the measured piezoelectric response of the superlattice accurately tracked a theoretical prediction derived using density functional theory, and was also very close to what would be expected of pure $BaTiO_3$ attached to the same substrate, even though the superlattice has twice as many normally dielectric $CaTiO_3$ layers as $BaTiO_3$ layers. In creating the theoretical model the researchers assumed that, because of the way it was grown on the $SrTiO_3$ substrate, each molecular layer in the superlattice remains rigid in its own plane and that there is no complex multi-dimensional distortion of the lattice.

Second, the researchers used the intensities of different x-ray diffraction features to determine how the distortion of the superlattice as a whole was split into expansions of the two layers (Fig. 2). If the atomic layer spacings within the $CaTiO_3$ and the $BaTiO_3$ layers changed to different extents, the superlattice's diffraction pattern would vary in intensity as the electric field changed. In fact, the intensities remained the same, indicating that both the ferroelectric and the dielectric layers contribute equally to the piezoelectric response of the superlattice.

The polarization of the materials is the superlattice is nearly constant throughout the layers and as a result can be quite different from the materials' bulk properties. The researchers conclude that the components of the superlattice thus can take on functional properties that are dramatically different from those of the bulk materials. Materials scientists and engineers will be able to take such effects into account to design and build a variety of superlattices with comparable structures. — *David Lindley*

See: Ji Young Jo[1], Rebecca J. Sichel[1], Ho Nyung Lee[2], Serge M. Nakhmanson[3], Eric M. Dufresne[3], and Paul G. Evans[1]*, "Piezoelectricity in the Dielectric Component of Nanoscale Dielectric-Ferroelectric Superlattices," Phys. Rev. Lett. **104**, 207601 (2010). DOI:10.1103/PhysRevLett.104.207601

Author affiliations: [1]University of Wisconsin–Madison, [2]Oak Ridge National Laboratory, [3]Argonne National Laboratory

Correspondence:
*evans@engr.wisc.edu

This work was supported by the U.S. Department of Energy (DOE), Office of Basic Energy Sciences, through Contract No. DE-FG02-04ER46147. H.N.L. acknowledges support from the Division of Materials Sciences and Engineering, U.S. DOE, through Contract No. DEAC05-00OR22725. S.M.N. Use of the Advanced Photon Source, an Office of Science User Facility operated for the U.S. DOE Office of Science by Argonne National Laboratory, was supported by the U.S. DOE under Contract No. DE-AC02-06CH11357.

7-ID • XSD • Atomic physics, chemistry, materials science • Phase contrast imaging, time-resolved x-ray absorption fine structure, time-resolved x-ray scattering • 6-21 keV • On-site • Accepting general users

Stretching to Make Ferroelectric Ferromagnets

Thin films of europium titanate become both ferroelectric (electrically polarized) and ferromagnetic (exhibiting a permanent magnetic field) when stretched. Moreover, their properties are about 1000 times stronger than the next-best material that is simultaneously ferroelectric and ferromagnetic. If this stretching mechanism can be applied to other materials that transform into this state at higher temperatures, it could be useful for next-generation electronic devices. A research team utilizing two beamlines at the APS showed both experimentally and theoretically that biaxial tension causes a simultaneously ferroelectric and ferromagnetic state in the thin films, work that represents a paradigm shift in the search for new ferroelectric ferromagnets.

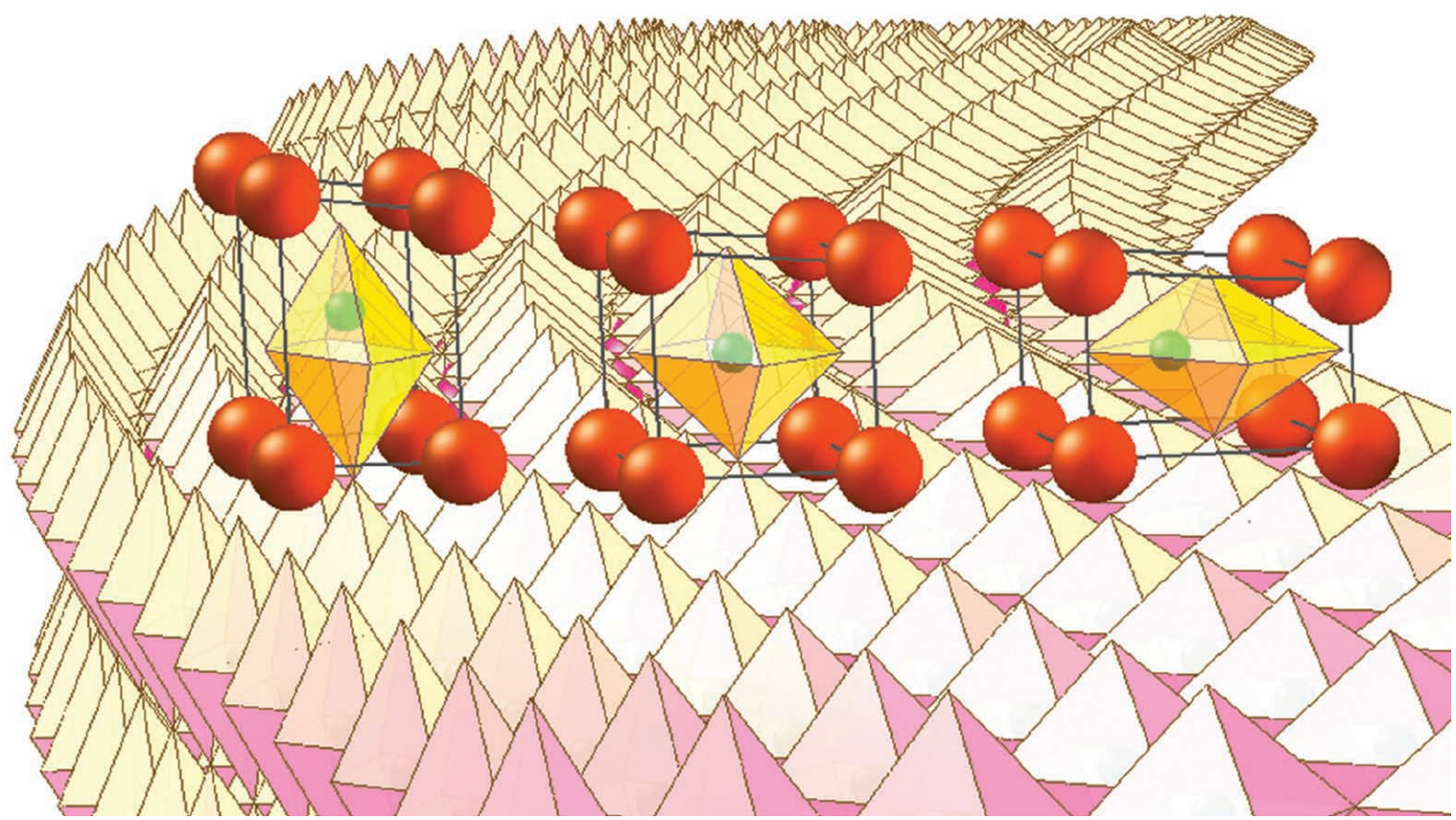

The road to potent ferromagnetic ferroelectrics involves stretching or squeezing a mundane starting material by depositing it on an underlying substrate with a smaller or larger spacing between its atoms. The deposited atoms replicate the spacing of those in the substrate.

Few materials are both ferroelectric and ferromagnetic, and in those that are, the effects are too weak to be useful. Materials with stronger effects could enable new technologies that combine the low power and high speed of field-effect electronics with the permanence of voltage-controlled ferromagnetism. These abilities could dramatically improve low-power, highly sensitive magnetic memory, magnetic sensors, or highly tunable microwave devices.

The researchers, from The Pennsylvania State University, Cornell University, Ohio State University, Argonne, Research Centre Jülich, Institute of Physics ASCR, JARA-Fundamentals of Future Information Technologies, Research Centre Jülich, the Leibniz Institute for Crystal Growth, Rutgers University, and the Kavli Institute at Cornell for Nanoscale Science focused on the oxide europium titanate ($EuTiO_3$). They stretched it by growing it as a thin film on another oxide having a slightly larger spacing between its atoms: dysprosium scandate ($DyScO_3$). The crystal structure of the europium titanate became strained because of the tendency of its atoms to align themselves with the underlying arrangement of atoms in the substrate.

One of the team had theorized that some magnetically ordered insulators, which are normally neither ferroelectric nor ferromagnetic, could be transformed into ferroelectric ferromagnets by applying strain along two axes. The multi-institution, multi-national group experimentally confirmed the work by creating a thin film that behaved as the strongest ferroelectric ferromagnet yet, and opened the door to investigating other materials that could work at higher temperatures thanks to this new mechanism.

The researchers needed to make sure that the thin film rigidly adhered to the substrate, affirm that the europium titanate was strained. They carried out x-ray diffraction utilizing a PSI-Huber diffractometer at XSD beamline 6-ID-B at the APS to measure all three lattice parameters of the film and substrate. Their results showed good in-plane lattice matching, indicating that the thin film was strained in the plane parallel to the surface. They also examined the samples using scanning transmission electron microscopy, electron energy-loss spectroscopy, Rutherford backscattering spectrometry, and x-ray absorption spectroscopy.

Element-resolved polarized x-ray absorption spectroscopy measurements of the $EuTiO_3/DyScO_3$ samples were performed at XSD beamline 4-ID-C at the APS. Data from this and the x-ray magnetic circular dichroism signal taken at a temperature of 6K in a 5-T magnetic field led to the conclusion that surface oxidation does not influence the magnetic order, and that the films were fully magnetic below the transition temperature at which the film changes from para-electric to ferroelectric.

The research team showed both experimentally and theoretically that biaxial tension causes a simultaneously ferroelectric and ferromagnetic state in the thin films. Their work is a paradigm shift in the search for new ferroelectric ferromagnets. Rather than searching directly for this rare state of matter, this work shows that one can, instead, search among materials that are neither ferroelectric nor ferroelectric, of which there are many, for those that transform into the simultaneously ferroelectric and ferromagnetic state when strained. Although strained europium titanate was only ferroelectric and ferromagnetic at very low temperatures, other higher-temperature ferroelectric and ferromagnetic materials could prove a boon for new electronics.

— Yvonne Carts-Powell

See: June Hyuk Lee[1,2], Lei Fang[3], Eftihia Vlahos[2], Xianglin Ke[2], Young Woo Jung[3], Lena Fitting Kourkoutis[1], Jong-Woo Kim[4], Philip J. Ryan[4], Tassilo Heeg[1], Martin Roeckerath[5], Veronica Goian[6], Margitta Bernhagen[7], Reinhard Uecker[7], P. Chris Hammel[3], Karin M. Rabe[8], Stanislav Kamba[6], Jürgen Schubert[5], John W. Freeland[4], David A. Muller[1,9], Craig J. Fennie[1], Peter Schiffer[2], Venkatraman Gopalan[2], Ezekiel Johnston-Halperin[3], and Darrell G. Schlom[1]*, "A strong ferroelectric ferromagnet created by means of spin–lattice coupling," Nature **466**, 954 (19 August 2010). DOI:10.1038/nature09331.

Author affiliations: [1]Cornell University, [2]The Pennsylvania State University, [3]The Ohio State University, [4]Argonne National Laboratory, [5]JARA-Fundamentals of Future Information Technologies, [6]Institute of Physics ASCR, [7]Leibniz Institute for Crystal Growth, [8]Rutgers University, [9]Kavli Institute at Cornell for Nanoscale Science

Correspondence: *schlom@cornell.edu

This work was supported by the National Science Foundation through grant DMR-0507146 and the Materials Research Science and Engineering Centers program (DMR-0520404, DMR-0820404 and DMR-0820414), and of the Czech Science Foundation (project no. 202/09/0682). Use of the Advanced Photon Source, an Office of Science User Facility operated for the U.S. Department of Energy (DOE) Office of Science by Argonne National Laboratory, was supported by the U.S. DOE under Contract No. DE-AC02-06CH11357.

4-ID-C • XSD • Materials science, physics • Anomalous and resonant scattering (soft x-ray), magnetic circular dichroism (x-ray magnetic circular dichroism, soft x-ray), magnetic x-ray scattering, x-ray magnetic linear dichroism, x-ray photoemission electron microscopy, x-ray photoemission spectroscopy • 500-3000 eV • On-site • Accepting general users

6-ID-B • XSD • Materials science, physics • Anomalous and resonant scattering (hard x-ray), general diffraction, grazing incidence diffraction, magnetic x-ray scattering, surface diffraction (UHV) • 3.2-38 keV • On-site • Accepting general users

HOW A LARGE MAGNETOELECTRIC COUPLING ARISES IN MULTIFERROIC HETEROSTRUCTURES

The drive to develop novel magnetoelectric devices has rekindled interest in multiferroics, which are materials having both ferroelectric and ferromagnetic properties. Because the magnetoelectric coupling in naturally occurring multiferroics is often weak, new artificially structured composites that combine dissimilar magnetic and ferroelectric materials are being developed. A team of researchers used an APS beamline to study the behavior of such a composite as the lead zirconate titanate was switched between the two ferroelectric states of polarization. Their work points to a new pathway to the electronic control of spin in complex oxide materials.

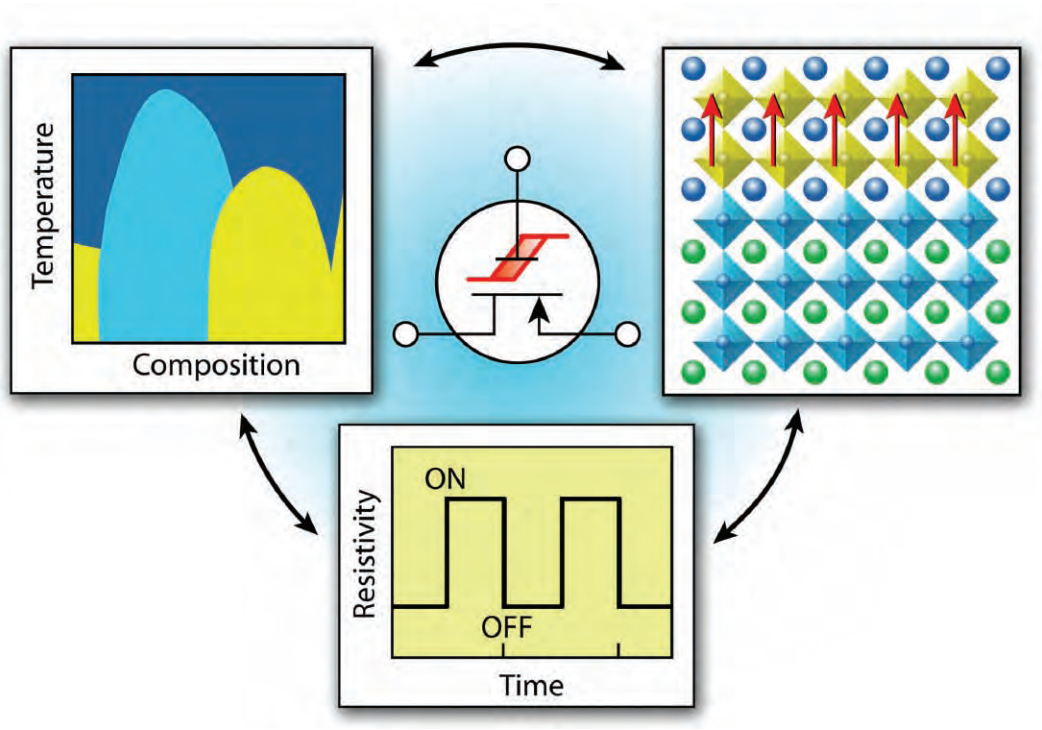

Fig. 1. Schematic representation of the coupling between charge, magnetism, and ferroelectricity, combined to modulate the magnetic order in a multiferroic heterostructure, suggesting how the electric field control of magnetism could find applications in spintronics devices for next-generation logic switches.

In charge-based multiferroic composites, such as strontium (Sr)-doped lanthanum manganite/ferroelectric heterostructures, the sensitivity of the electronic and spin states of the doped manganite to charge provides for the enhanced coupling. To uncover the microscopic origin of this magnetoelectric coupling, researchers from Yale University and Argonne used x-ray absorption near edge spectroscopy (XANES) to study the behavior of $Pb(Zr_{0.2}Ti_{0.8})O_3/La_{0.8}Sr_{0.2}MnO_3$ (PZT/LSMO) heterostructures as the PZT was switched between the two ferroelectric states of polarization. XANES measurements of the absorption edge of manganese (Mn) in the PZT/LSMO heterostructures, carried out at the XSD 33-ID beamline of the APS, revealed a temperature-independent shift in the absorption edge associated with a change in the electronic valence state of Mn induced by charge carrier modulation in the LSMO, demonstrating the electronic origin of the magnetoelectric effect. Spectroscopic, magnetic, and electric characterization of the system showed that the large magnetoelectric response was due to a modified interfacial spin configuration, opening a new pathway to the electronic control of spin in complex oxide materials (Fig. 1).

XANES is especially sensitive to changes in the atomic valence state, and therefore is especially suited to probing charge-induced changes in the atomic structure of LSMO; another advantage is the ability of XANES to probe buried layers. In this study, 250-nm PZT/LSMO epitaxial heterostructures were grown on strontium titanate ($SrTiO_3$) substrates, and the direction of the ferroelectric polarization of PZT was used to electrostatically modulate the hole-carrier density in the LSMO (hole charge depletion occurred when the PZT polarization pointed into the LSMO film, and hole accumulation occurred in the opposite case). The key experimental result of this work was the finding of an energy shift in the Mn absorption edge upon switching the PZT polarization from the depletion to the accumulation state. The observed energy shift between the depletion and accumulation states indicated a change in the average Mn valency induced by the electrostatic hole-carrier modulation. This change in the valency of Mn was responsible for the changes in the magnetic state of LSMO and is the origin of the large magnetoelectric effect observed in PZT/LSMO multiferroic heterostructures. Importantly, no change in the crystal lattice occurred during these measurements. Also, a similar change in the Mn valency was seen at both room temperature and 20K, showing that the charge carrier modulation of the Mn valence state was robust and occurred irrespective of temperature.

The researchers in this study estimated the change in Mn valency from the XANES spectra, finding that most surface charge at the ferroelectric interface was screened by charge carriers from the LSMO. The change in valency was thus seen to take place mostly at the PZT/LSMO interface, within a screening length of about 1 unit cell. The measured change in Mn valency gave a change in magnetic moment over about two unit cells, which was seen to originate from a modification in the spin exchange coupling at the interface whereby the spins coupled ferromagnetically within this interfacial layer and antiferromagnetically with the spins of the adjacent layers for the accumulation state. The results therefore provided an experimental signature of the magnetic interface reconstruction occurring at the PZT/LMSO interface, which is responsible for the dramatic change in the average magnetic moment and explains the very large magnetoelectric coupling found in PZT/LSMO multiferroic heterostructures. This work opens a new path to the electronic control of spin in complex oxide materials. — *Vic Comello*

See: C.A.F. Vaz[1]*, J. Hoffman[1], Y. Segal[1], J.W. Reiner[1], R.D. Grober[1], Z. Zhang[2], C.H. Ahn[1], and F.J. Walker[1], "Origin of the Magnetoelectric Coupling Effect in $Pb(Zr_{0.2}Ti_{0.8})O_3/La_{0.8}Sr_{0.2}MnO_3$ Multiferroic Heterostructures," Phys. Rev. Lett. **104**, 127202 (2010). DOI: 10.1103/PhysRevLett.104.127202

Author affiliations: [1]Yale University, [2]Argonne National Laboratory
Correspondence:
*carlos.vaz@cantab.net

This work was supported by the National Science Foundation through Materials Research Science and Engineering Center Grant DMR 0520495 (Center for Research on Interface Structures and Phenomena), Center on Functional Engineered Nano Architectonics, and the National Research Initiative. Use of the Advanced Photon Source, an Office of Science User Facility operated for the U.S. Department of Energy (DOE) Office of Science by Argonne National Laboratory, was supported by the U.S. DOE under Contract No. DE-AC02-06CH11357.

33-ID • XSD • Chemistry, materials science, physics • Anomalous and resonant scattering (hard x-ray), diffuse x-ray scattering, general diffraction, surface diffraction, x-ray reflectivity, x-ray standing waves • 4-40 keV, 6-21 keV • On-site • Accepting general users

The Weak Interaction of Graphene Electrons

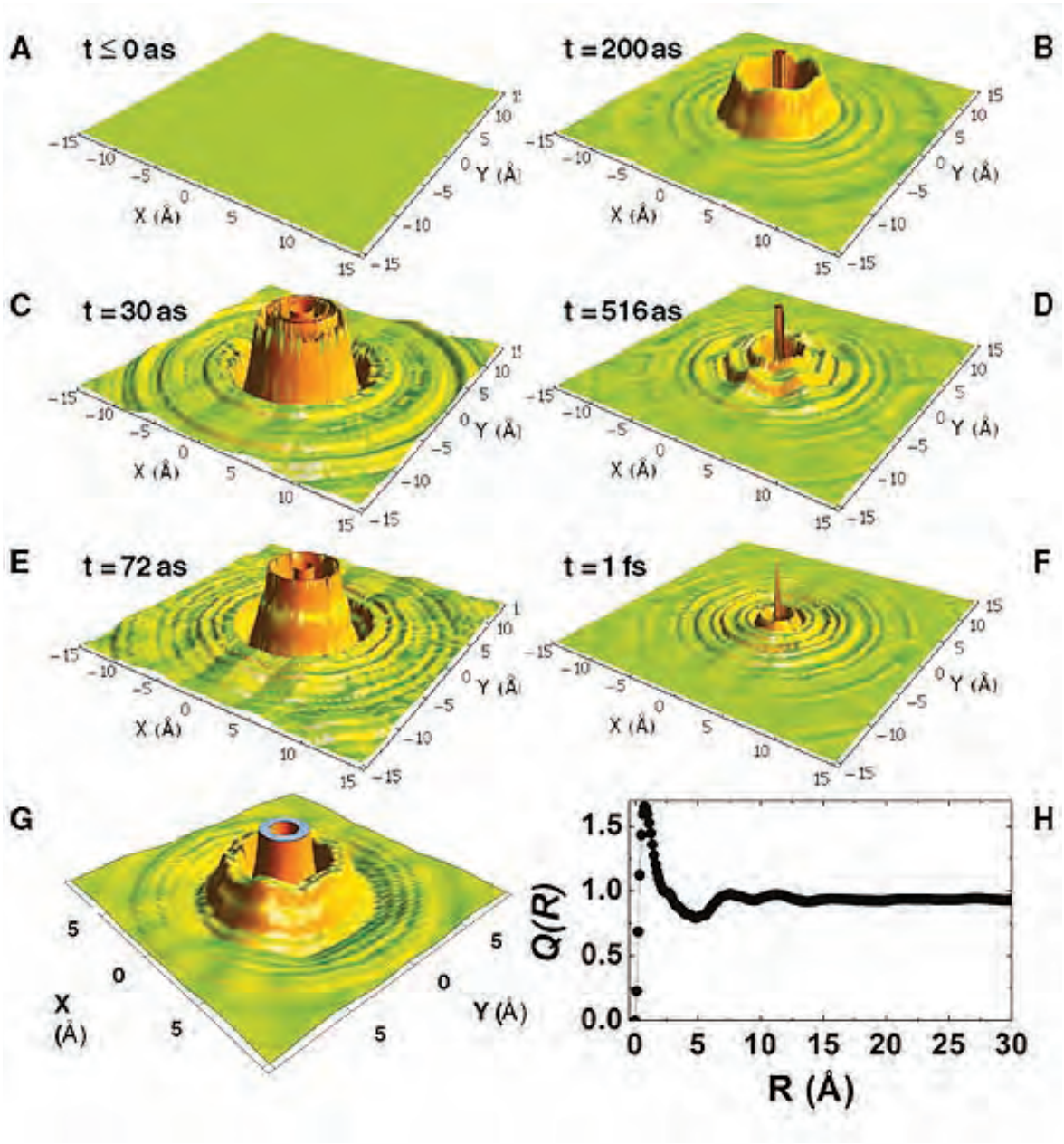

Fig. 1. Excitations in graphene electrons propagating in real time. The dynamical electron density, which is induced by a point source that appears at the origin and then quickly disappears, is shown at 200 as, or 2×10^{-15} sec, over a field of view of 30 Å × 30 Å (3×10^{-9} m). From James P. Reed et al., Science **330**, 805 (5 November 2010) © 2011 American Association for the Advancement of Science. All Rights Reserved. http://www.sciencemag.org/content/330/6005/805.abstract
A movie of the above can be viewed at
http://www.sciencemag.org/content/suppl/2010/11/02/330.6005.805.DC1/1190920s1.mov

Atomic-scale chicken wire might seem an apt description for high-tech fencing material, but it is actually a nickname for graphitic carbon, better known as graphene. This moniker is appropriate because of graphene's unique thickness (just one atom deep) and its special structure (rings of carbon atoms, similar to a honeycomb). In addition, electrons within graphene behave like relativistic (massless) Dirac fermions – with the ability to travel at very high speeds without much resistance. With this in mind, a team of researchers asked the question: Do the electrons in graphene behave independently, or are their motions correlated with one another? With an assist from the XSD 9-ID beamline at the APS, they discovered the interaction among the electrons of graphene to be surprisingly weaker than previously believed. Such a finding makes graphene even more potentially valuable for a wide range of practical applications, including high-tech application such as integrated circuits, gas sensors, solar cells, biodevices, and nanoelectronic circuits for even smaller, less expensive, faster, and more energy-efficient electronic devices.

To answer their question — whether electrons in graphene move independently of one another (i.e., are non-interacting and behave like relativistic fermions) or are tied to repulsive electrostatic forces (that is, are manipulated by Coulomb correlations and behave like classical electrons) — the researchers from the University of Illinois at Urbana-Champaign and Argone used inelastic x-ray scattering to scatter x-rays off sheets of graphene in order to image electron motion in graphene within graphite crystals. Graphite and graphene are similar enough to each other in physical characteristics so that by properly analyzing experimentally collected data the physicists were able to extract information about graphene from measurements on graphite.

The team measured the effective value of the fine-structure constant (α_g), which represents the magnitude of the force between electrically charged particles. (The unitless ratio equals potential energy divided by kinetic energy or, equivalently, electron charge squared divided by Planck's constant times Fermi velocity of the Dirac particle.) They then applied advanced reconstruction algorithms to image the dynamical screening of a point charge in a single graphene sheet. (Fig. 1.) Specifically, images of electron motion within graphene were taken with resolutions of 0.533 Å (5.3×10^{-11} m) and 10.3 as (10^{-17} sec).

The researchers discovered that the 1-nm charge cloud, which surrounds the graphene electrons, comes about from two divergences (called Van Hove singularities) within graphene's density of states. It effectively screens external charge through Coulomb interactions; that is, the spectral analysis revealed the interaction among graphene's electrons was surprisingly weaker than expected. This makes graphene act like a simple (free-electron) semi-metal.

Specifically, the effective fine-structure constant was measured within the study to have, in the limit of small energy, a value of 0.14 ± 0.092 (approximately 1/7), while the nominal value is 2.2. The much smaller value was found to occur because its electrons are highly polarizable.

This research explains the reason behind graphene's electrons behaving as if they do not interact with one another: The Coulomb interaction between the electrons is screened. It also demonstrates a new approach to studying ultrafast dynamics, creating a new window on the most fundamental properties of materials. In fact, during their experimentation these scientists produced the fastest movies ever made of electron motion.

For future high-tech applications in such areas as integrated circuits, gas sensors, solar cells, and biodevices, graphene offers important properties such as immense tensile strength (it is about 100 times stronger than steel) and flexibility, and strong electrical conductivity and heat resistance. This ultrafast dynamic study of provides additional knowledge on the fundamental properties of this increasingly important form of graphite, one of the most versatile and promising materials ever discovered. — *William Arthur Atkins*

See: James P. Reed[1], Bruno Uchoa[1], Young Il Joe[1], Yu Gan[1], Diego Casa[2], Eduardo Fradkin[1], and Peter Abbamonte[1]*, "The Effective Fine-Structure Constant of Freestanding Graphene Measured in Graphite," Science **330**, 805 (5 November 2010). DOI:10.1126/science.1190920
Author affiliations: [1]University of Illinois at Urbana-Champaign, [2]Argonne National Laboratory
Correspondence:
*abbamonte@mrl.uiuc.edu

This work was supported by the U.S. Department of Energy (DOE) under grants DE-FG02-07ER46459 and DE-FG02-07ER46453 through the Frederick Seitz Materials Research Laboratory. Use of the Advanced Photon Source, an Office of Science User Facility operated for the U.S. DOE Office of Science by Argonne National Laboratory, was supported by the U.S. DOE under Contract No. DE-AC02-06CH11357.

9-ID • XSD • Materials science, physics • Inelastic x-ray scattering, liquid scattering, resonant inelastic x-ray scattering • 4.5-24 keV, 8.9-30 keV • On-site • Accepting general users

Cementing the Structure of CSHs

Portland cement concrete is all around us, in the sidewalks we walk on, the buildings we live and work in, and the roads our vehicles ride on. One of the most versatile and useful building materials ever created, it is so commonplace that we hardly ever think of it (unless we happen to trip and scrape our knees on it). Yet surprisingly, although we worry about carbon emissions from cars, airplanes, and power plants, this everyday, seemingly innocent material is also a hidden and largely ignored global warming culprit. Now, new insights into the nanostructure of concrete are coming to light thanks to studies carried out at the APS. The work, by researchers from the University of California, Berkeley; and Argonne is an important milestone in the push for stronger, more environmentally friendly concrete.

The manufacture of cement is responsible for about 5% to 7% of all the CO_2 released by humans into the Earth's atmosphere every year. It is quite possible that the U.S. federal government will start putting charges on the use of concrete to account for its carbon footprint, a possibility for which the cement industry is already preparing. Such a "carbon tax" would inevitably lead to higher costs for concrete.

Those sobering facts have set the cement and concrete industry on an intensive quest to find ways to reduce CO_2 emissions while improving concrete's strength and versatility, qualities which are still not completely understood, even though Portland cement has been around for well over a century. A better understanding of the atomic-level structure of cement hydration products is the key to finding more environmentally-friendly ways to manufacture and use concrete.

The researchers studied the nanostructure of calcium silicate hydrate (CSH), the main ingredient that gives concrete its great strength, the glue that holds concrete together. Pinning down the crystalline structure of CSH in cement-paste matrix has proven elusive because of its broad diffraction properties and difficulty in separating it from the other complex phases of cement formation.

In previous times, people would refer to these calcium silicates as almost like an amorphous gel, indicating there was very little structure in the long

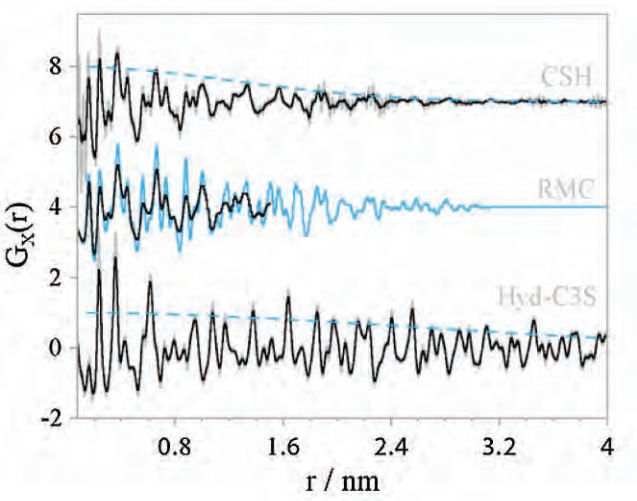

Fig. 1. The x-ray pair distribution functions of synthetic CSH(I) (top black line, obtained using a Lorch modification function, light grey is the raw transform) and hyd-C3S (lower black and grey lines). The lower dashed blue line shows the intensity damping present due to the finite Q resolution, whereas the upper dashed line approximates the damping present in the CSH(I) sample due to grain size. The middle curves are the distribution functions of 1.1 nm tobermorite before and after refinement to fit the measured data. Both figures: L.B. Skinner et al., Phys. Rev. Lett **104**, 195502 (2010). http://prl.aps.org/abstract/PRL/v104/i19/e195502

range. Only recently have more precise characterization techniques become available to probe into the details of CSH structure. Using synchrotron x-ray diffraction at the XSD 11-ID-C beamline of the APS, the researchers found that CSHs are more ordered than previously believed, and at a smaller scale.

The bulk behavior of CSHs has been explained theoretically by some colloidal models that posit the existence of nanograins of 5 nm or less, but experimental confirmation has been lacking because of the previously-mentioned diffraction and phase separation problems. Crystallographic work has also suggested a strong similarity to the rare toberomite minerals, but in a less structured form. To better investigate these possibilities and refine the models, the research team used pair distribution function techniques (Fig. 1) on samples of a synthetic CSH(1) and a hydrated tricalcium silicate paste (hyd-C3S). Each sample represents different phases of CSHs as they are found in real cement paste.

The experimenters found a lack of sharp Bragg peaks in the synthetic CSH(1) compared to the hyd-C3S, indicating that while the CSH is not truly amorphous, it also contains no large, ordered crystals. However, it shows striking similarity to a size-broadened 1.1-nm toberomite crystal structure. Damping of structural features is seen at scales larger than 3.5 nm (Fig. 2), confirming a nanocrystalline structure of the CSH with an approximately 3.5-nm particle diameter. This supports previously published work, including small-angle neutron scattering measurements that implied a similar nanostructure. Even using completely different techniques with x-rays, they arrived at complementary information.That is good validation, but the unique contribution of their work is that the nanocrystals are in fact very ordered and that the planes need only be slightly bent to inhibit growth.

The next step will be to investigate the possible role of polymers and other materials—possibly including fly-ash residue from coal—which could be used to make hybrid CSHs with improved cementitious properties and a reduced carbon footprint. These new insights into the nanostructure of concrete are an important milestone in optimizing the engineering of improved CSHs for creating stronger, more environmentally benign concrete.

— Mark Wolverton

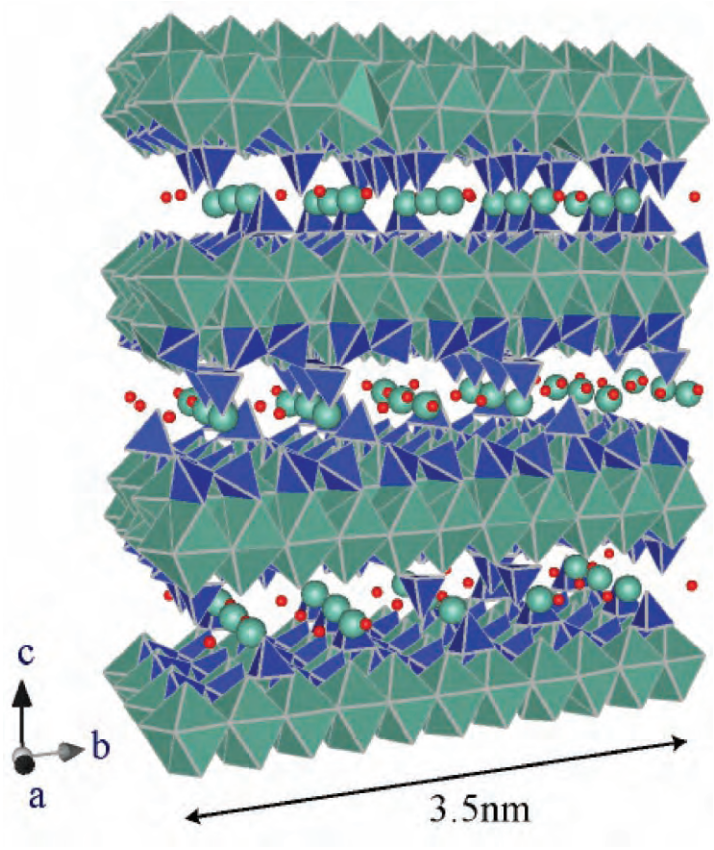

Fig. 2. The final structure of synthetic C-S-H that is refined to be consistent with the measured data. Green polyhedra = CaO, blue tetrahedra= SiO, red spheres = inter layer O (water), green spheres = interlayer Ca.

See: L.B. Skinner[1], S.R. Chae[1], C.J. Benmore[2], H.R. Wenk[1], and P.J.M. Monteiro[1]*, "Nanostructure of Calcium Silicate Hydrates in Cements," Phys. Rev. Lett. **104**, 195502 (2010). DOI:10.1103/PhysRevLett.104.195502

Author affiliations: [1]University of California, Berkeley; [2]Argonne National Laboratory

Correspondence:
*monteiro@ce.berkeley.edu

This work was supported in part by Grant No. KUS-I1-004021, made by King Abdullah University of Science and Technology (KAUST). Use of the Advanced Photon Source, an Office of Science User Facility operated for the U.S. Department of Energy (DOE) Office of Science by Argonne National Laboratory, was supported by the U.S. DOE under Contract No. DE-AC02-06CH11357.

See also: Physical Review Focus: "The Nanostructure of Buildings and Bridges," by Michelangelo D'Agostino, Phys. Rev. Lett. **104**, 195502 (14 May 2010).

Photo preceding page: Otay River Bridge in San Diego, Calif. This structure is one of nine winners in the Portland Cement Association's (PCA) Eleventh Biennial Bridge Awards Competition. Courtesy of South Bay Expressway and International Bridge Technologies, Inc., and the PCA (http://www.cement.org/index.asp).

11-ID-C • XSD • Materials science, geoscience, physics, chemistry • Diffuse x-ray scattering, high-energy x-ray diffraction, pair distribution function • 115 keV • On-site • Accepting general users

Why Materials Fail:
Characterizing Damage in Aluminum Matrix Composites

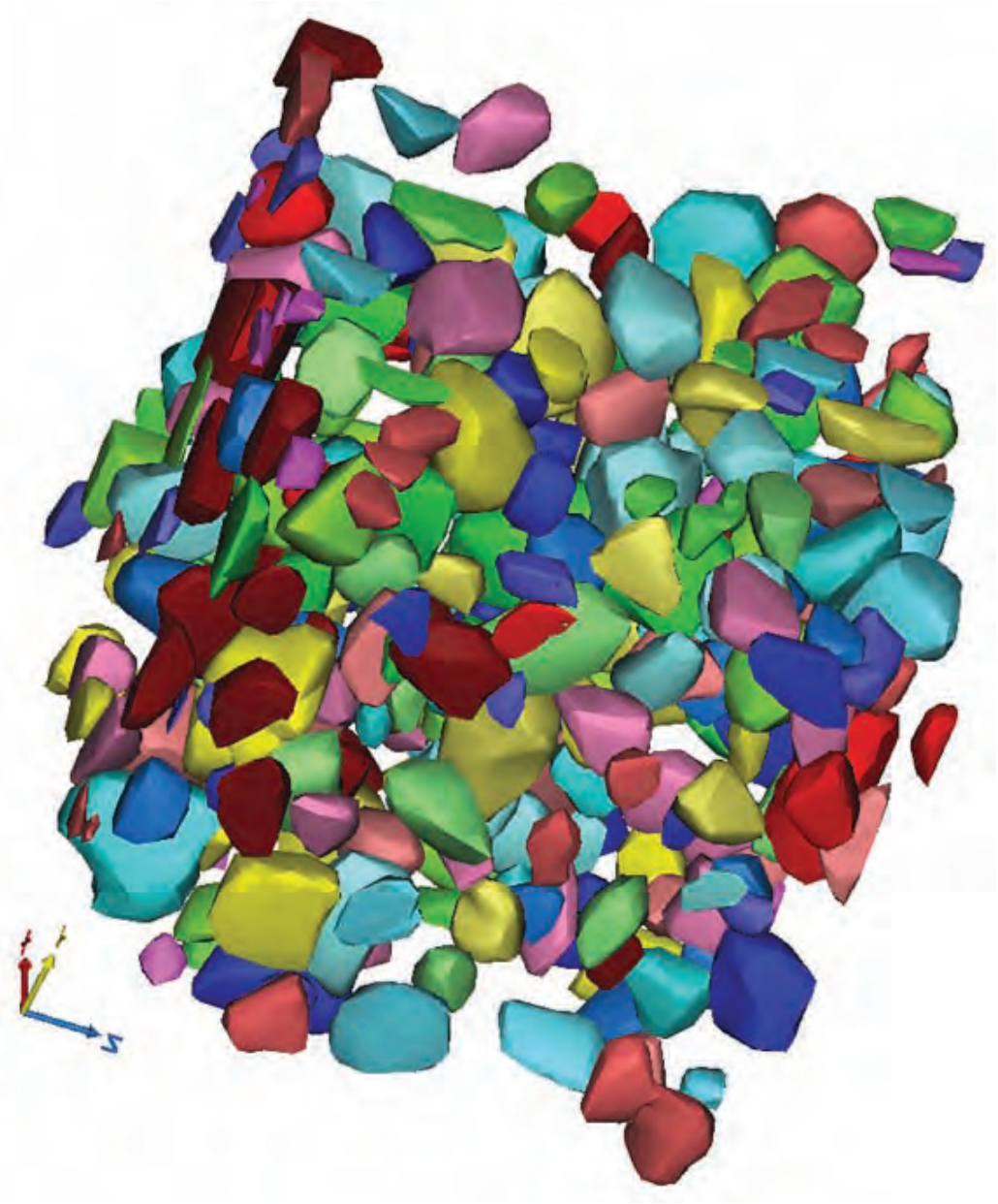

Fig. 1. 3-D reconstruction of SiC particles in an Al alloy matrix (matrix not shown) by x-ray synchrotron tomography. 360 SiC particles, edge of cube = 260 mm (200 voxels), SiC particle volume fraction = 20.1%. The various colors highlighting the particles are merely for aesthetics.

2-BM • XSD • Life sciences, physics • General diffraction, microdiffraction, phase contrast imaging, tomography .5-33 keV, 5-33 keV • On-site • Accepting general users

One way to improve the properties of various materials is to determine how and why they fail. In this study, researchers examined the microstructure of a metal matrix composite (MMC), both before and after tensile damage. MMCs are lightweight, high-stiffness materials that are of interest in automotive and aerospace applications, primarily from a fuel efficiency point of view. Techniques to investigate the microstructures within MMC materials are typically limited either to surface images that cannot yield information about the composite's three-dimensional (3-D) structure, or — in the case of 3-D imaging techniques — are time consuming and destructive to the sample. To avoid such drawbacks, the researchers in this study utilized x-ray tomography at XSD beamline 2-BM of the APS to capture high-resolution 3-D images of MMC samples. This technique is non-destructive and requires minimal time for sample preparation. The study produced several important findings and added information to our knowledge about damage evolution in MMCs.

The silicon carbide (SiC)/aluminum composite (2080/SiC) examined here is an Al-Cu-Mg alloy that is commercially important. The SiC particles possessed an average size of 25 μm. Small samples of 2080/SiC were probed before and after tensile damage.

Previous studies had shown that ceramic/metal composites fail due to fracturing of their tiny ceramic particles, and also due to void growth (voids are spaces that open up between the ceramic particles and the metal matrix). Regarding particle fracture, a clear description of how particle size and shape affects MMC failure has been lacking. These researchers wanted to delineate exactly how the sizes and aspect ratios of the silicon carbide particles within the 2080/SiC composite influenced the composite's failure. (A particle's aspect ratio equals its length divided by width.) The research team, from Arizona State University and Argonne, also wanted to better understand the mechanism of void creation.

The x-ray synchrotron tomography probed a sufficiently large volume of 2080/SiC (0.5 mm^3) so that a statistically-significant number of voids and SiC particles could be identified. The non-destructive tomography provided high-resolution imaging at the micrometer scale.

To delineate between various structures within the 2080/SiC composite, both absorption and scattering of x-rays were utilized as they passed through the sample. Low-density regions, such as voids, allowed more x-rays to pass through as compared to higher-density regions. X-ray scattering was most pronounced at the interface between distinct materials, such as between the SiC particles and aluminum matrix.

The 3-D images derived from the scattering and absorption data were rendered in shades of gray (i.e., "gray scale"). Even though the gray scale of the particles and aluminum matrix were quite similar, the x-ray scattering rendered the SiC particles clearly visible from the background matrix. To reveal particle structure in greater detail, a unique type of algorithm was applied to the 3-D data set. The algorithm, encoded within the software program Livewire®, was used in a semi-autonomous fashion to search out and identify the boundaries of individual particles appearing in two-dimensional (2-D) slices of the region imaged. A cross-sectional area for a SiC particle was then built up for each 2-D. Approximately 10 such cross-sections, from two perpendicular planes, were needed to construct a full 3-D image of each particle (Fig. 1).

Besides determining particle structure, there was also a need to delineate between voids and cracks. Voids consisted of openings between particles and the matrix, and took on all sorts of shapes; however, cracks were always "slit-like," and consisted of breaks (or fractures) in the matrix and within particles. The researchers found that aspect ratios above 5 indicated cracks, while aspect ratios less than 5 identified voids. Utilizing aspect ratio, the numbers of cracks and voids were then unambiguously tallied.

This research produced several important findings, some unique to this study:

- Damage in the 2080/SiC composite consisted of three main types: particle fracture; particle/matrix debonding; and void growth, occurring mostly near clusters of SiC particles.
- Imaging a sufficiently large number of microstructures via x-ray tomography assured confidence in the conclusions reached about 2080/SiC composite damage.
- Coupling x-ray absorption and refraction with sophisticated data analysis techniques allowed for identification of a variety of structures within the 2080/SiC composite, including SiC particle characterization.
- Void growth and particle fracture were confined to a region within 1 mm of the damage break.
- SiC particles with higher aspect ratios and larger sizes were more susceptible to fracturing when stressed.

Together, the 3-D x-ray tomography, image analysis, and quantitative damage statistics from this research have added significant information our understanding of damage evolution in MMCs. — *Philip Koth*

See: J.J. Williams[1], Z. Flom[1], A.A. Amell[1], N. Chawla[1]*, X. Xiao[2], and F. De Carlo[2], "Damage evolution in SiC particle reinforced Al alloy matrix composites by X-ray synchrotron tomography," Acta Mater. **58**, 6194 (2010). DOI:10.1016/j.actamat.2010.07.039
Author affiliations: [1]Arizona State University, [2]Argonne National Laboratory
Correspondence: *nchawla@asu.edu

A.A.A. acknowledges financial support through a fellowship from the University of Barcelona during her stay at Arizona State University. Use of the Advanced Photon Source, an Office of Science User Facility operated for the U.S. Department of Energy (DOE) Office of Science by Argonne National Laboratory, was supported by the U.S. DOE under Contract No. DE-AC02-06CH11357.

A BETTER UNDERSTANDING OF SIGMA PHASE YIELDS BETTER IRON ALLOYS

The iron-chromium (Fe-Cr) alloy, most commonly used for stainless steel, has been the subject of both practical and scientific interest since at least the mid-1800s, when the French metallurgist Pierre Berthier took note of the alloy's resistance to attack by some acids and suggested that the material could be used in cutlery. Today, the alloy's properties of rust and corrosion resistance, low maintenance, and relatively low cost have made it an indispensable resource with uses ranging from fine wire to the fabled Gateway Arch in St. Louis, Missouri. Fe-Cr is also scientifically useful. It exhibits a variety of interesting physical properties such as magnetism, and can form a solid solution within the whole concentration range while preserving its crystallographic structure. This gives investigators the ability to study the effect of the alloy's composition on a range of physical properties within the same structure and as test different theoretical models and theories. Researchers using an x-ray beamline at the APS have distinguished important characteristics of both the alpha and sigma crystalline phase structures of the $Fe_{52:5}Cr_{47:5}$ iron alloy that forms the basic ingredient of stainless steels. The researchers are confident their conclusions will furnish important data to materials scientists and solid-state physicists as they continue to further investigate iron and chromium alloys.

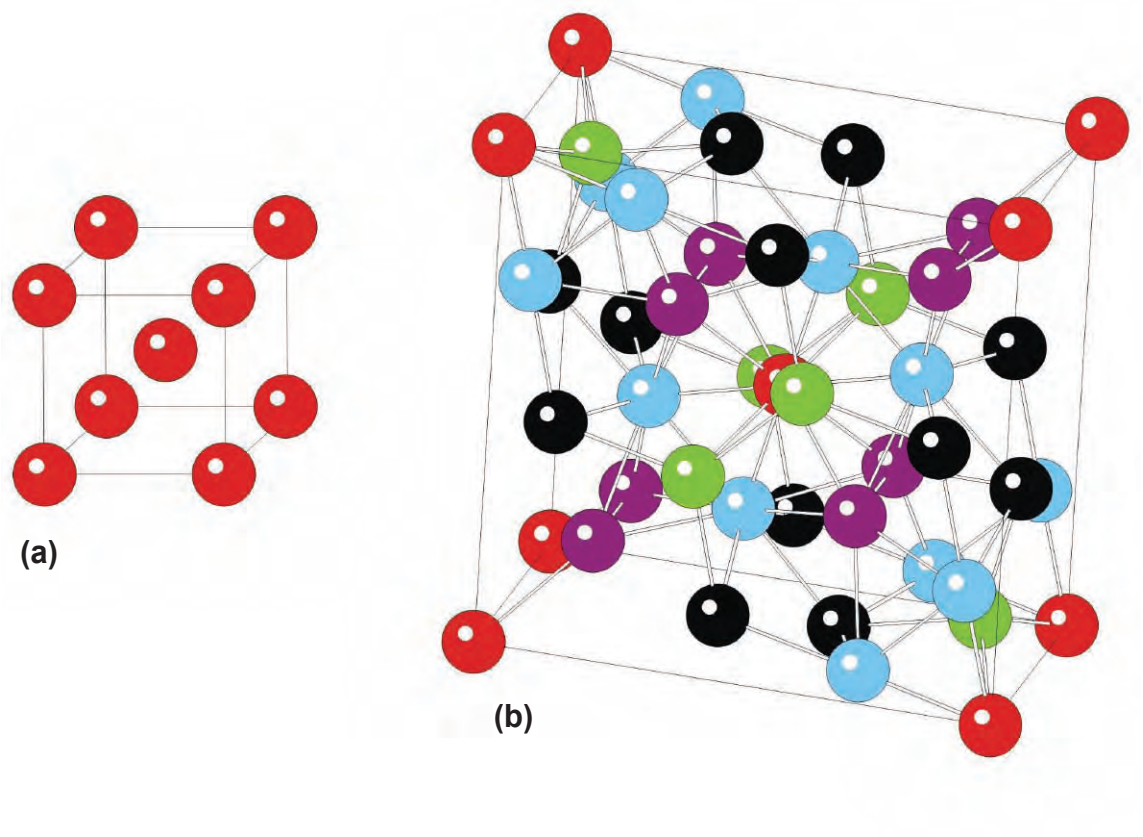

Fig. 1. Crystallographic structure (unit cell) of the (a) alpha phase and (b) sigma phase with five different sublattices.

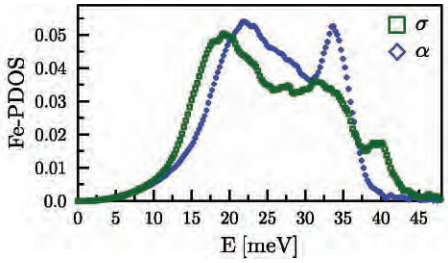

Fig. 2. Fe-partial DOS recorded for the alpha and the sigma phases.

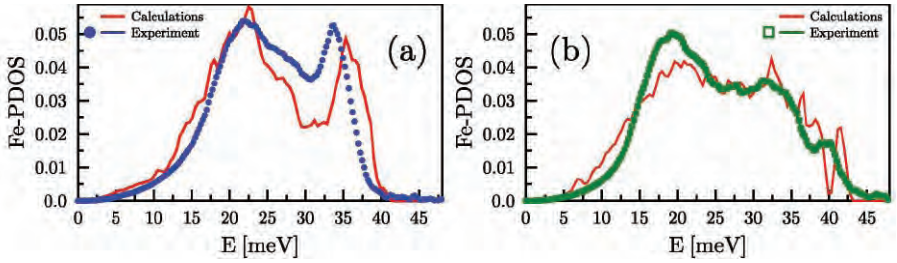

Fig. 3. Comparison between experimental and theoretical PDOS for the (a) alpha and (b) sigma phases.

The research group, from AGH University of Science and Technology, Argonne, the Polish Academy of Sciences, and the Karlsruher Institute of Technology, found that the alpha structure of the $Fe_{52:5}Cr_{47:5}$ alloy is simple (Fig. 1a), while the sigma structure is complex (Fig. 1b) and undesired, as it drastically deteriorates useful properties of the alloys in question. The results reveal significant vibrational differences within the Fe-partial phonon density of states (PDOS) due to the iron alloy's α and σ phases.

Specifically, the researchers' experiments confirmed the theoretical predictions about several key properties of the complex alloy. The vibrational properties of both the alpha and sigma crystalline phases were studied utilizing nuclear resonant inelastic x-ray scattering (NRIXS) at XSD beamline 3-ID by recording the Fe-partial PDOS (Fig. 2). The researchers concentrated on determining the Lamb-Mössbauer factor (f), the kinetic energy per atom (E_k), and the mean force constant (D). They also calculated the vibrational specific heat at constant volume (C_V) and the vibrational entropy (S)—with the phonon density of states—and the Debye temperatures (Θ_D) and the Debye sound velocity (υ_D) – with the values of f and C_V.

In preparation for the experiment, an ingot consisting of super-enriched iron (95% ^{57}Fe) and chromium was melted. The metal stock was cold rolled (below its recrystallization temperature) to a thickness of about 30 µm. Two plates were cut from the ingot, and both were then solution-treated at 1273K for three days. With one plate dedicated for the alpha phase, the other plate was precipitated for seven days into the sigma phase by isothermal annealing at 973K.

Based on their work with the near-equiatomic Fe-Cr alloy, the researchers found excellent agreement between experiment and theory on some key quantities concerning the physical characteristics of the iron-chromium alloy. The researchers also demonstrated—both experimentally and theoretically—significant differences arising from the structural properties of the α and σ phases of the alloy. Their major results showed:

- A statistically significant difference in PDOS between the α and σ phases.
- A similarity between the PDOS obtained for the α phase of the Fe-Cr when compared to that of pure iron with a characteristic peak at about 35 meV.
- An additional high-frequency peak at 40 meV for the PDOS spectrum of the σ phase, which was neither observed in α Fe-Cr nor in pure Fe.
- A wider range of vibrational frequencies for the σ phase relative to that of the α phase due to the downward shift of the low-energy peak as well as to the existence of the additional high-energy peak.
- Good agreement between the calculated and measured PDOS for both phases (Fig. 3).

In addition, for the first time, relevant thermodynamic quantities for a near-equiatomic alloy were obtained without the need for empirical parameters.

These result should provide further understanding of crystal lattice dynamics in a wide variety of alloys with complex structures such as the σ phase in the Fe-Cr alloys. More complete knowledge of this phase (whose precipitation cause severe deterioration of steel properties) may contribute to improve significantly the characteristics of a new generation of stainless steels (a group of corrosion-resistant steel alloys that contain a minimum of 10.5% chromium by mass). These next-generation stainless steels should provide better resistance to high-temperature corrosion and radiation damage, and better toughness, ductility, and welding abilities. These improvements are vital when considering that the Fe-Cr-based steels are regarded as excellent candidates for construction materials within future power plants and advanced fusion and fission reactors, along with the possibly of becoming spallation targets (ejected fragments) inside high-power particle accelerators.

— William Arthur Atkins & Patricia E. Panatier

See: S.M. Dubiel[1]*, J. Cieslak[1], W. Sturhahn[2], P. Piekarz[3], S. Stankov[4], and K. Parlinski[3], "Vibrational Properties of α- and σ-Phase Fe-Cr Alloy," Phys. Rev. Lett. **104**, 155503 (16 April 2010). DOI:10.1103/PhysRevLett.104.155503

Author affiliations: [1]AGH University of Science and Technology, [2]Argonne National Laboratory, [3]Polish Academy of Sciences, [4]Karlsruher Institute of Technology

Correspondence:
*dubiel@novell.ftj.agh.edu.pl

The results reported in this study were partly obtained within the project supported by the Ministry of Science and Higher Education, Warsaw (Grant No. N N202 228837) and Project No. 44/N-COST/2007/0. Use of the Advanced Photon Source, an Office of Science User Facility operated for the U.S. Department of Energy (DOE) Office of Science by Argonne National Laboratory, was supported by the U.S. DOE under Contract No. DE-AC02-06CH11357..

3-ID • XSD • Physics • High-pressure diamond anvil cell, inelastic x-ray scattering, nuclear resonant scattering • 7-27 keV, 14.41-14.42 keV • On-site • Accepting general users

STRENGTH UNDER TENSION: HOW SOME NANOCRYSTALS ADAPT TO STRESS

Although many nanocrystalline materials have great strength, they generally cannot be stretched very much before breaking. But there are exceptions to this rule. By means of x-ray diffraction studies at XSD beamline 1-ID at the APS, scientists have found that the internal structures of nanocrystalline nickel and cobalt respond very differently to tensile stress, explaining why the latter is able to stretch almost three times as much as the former. The discovery offers some insights into how nanocrystalline materials can be made more resilient without losing their strength.

Typical coarse-grained materials, such as ordinary metals, accommodate stress through dislocations in their crystal structures. Imperfections in the atomic lattices can move around, allowing the metal to stretch without breaking — a phenomenon known as strain hardening. In nanocrystalline materials, on the other hand, particularly where grain sizes are as small as a few tens of nanometers, there is little capacity for lattice imperfections to move. These materials tend to show little strain hardening under external stress before the grains start to pull apart, leading to rupture.

Researchers at Lawrence Livermore National Laboratory, Ames Laboratory, and Argonne National Laboratory used an electrodeposition method to synthesize slabs of nanocrystalline nickel and cobalt measuring more than 100 μm thick and centimeters across. They found that although both samples initially showed a similar degree of strain hardening, nickel samples stretched only about 2.7% before breaking, while cobalt could stretch up to 8.4%. Some earlier studies had found comparable results, but the reasons for the difference remained obscure.

To understand what was happening to the internal structures of these materials under stress, the team conducted x-ray diffraction measurements in real time as external forces were applied. The data allowed them to identify many distinct lattice planes in the randomly-oriented grains of the material, and track how the orientation of the planes and the interatomic distances in the planes changed as the samples stretched (Fig.1).

The researchers focused on the change in angles of the lattice planes relative to the loading direction during deformation. For coarse-grained metals, the motion of dislocations through the grains causes rotation of the lattice planes relative to the direction of the applied stress. In the case of the nanocrsytalline nickel, the team saw very modest changes in the orientations of the lattice planes, indicative of nickel's limited ability to accommodate strain. This behavior was very different from the way the same lattice planes respond to stress in coarse-grained nickel, which shows a much greater degree of strain-hardening than its nanocrystalline counterpart.

In nanocrystalline cobalt, by contrast, the lattice planes exhibited large scale rotations as the material stretched. However, by analyzing these changes in comparison with complex models of lattice geometry and distortion, the researchers concluded that nanocrystalline cobalt does not respond to stress through movement of dislocations, but by so-called mechanical twinning. Twins are conjoined crystal lattice regions that share a common plane but have distinct overall orientations; they can also form during normal crystal growth. The formation of twins in nanocrystalline cobalt is a way the grains can respond to stress without fracturing or pulling apart.

Further measurements confirmed this picture. Transmission electron microscope images directly revealed the appearance of twinned structures, which correlated well with the x-ray diffraction data that showed that the cobalt sample developed "texture," meaning that its grains no longer showed random alignment of crystal axes but lined up in a more orderly way as a result of twinning.

Understanding how nanocrystalline cobalt is able to stretch suggests strategies for improving the mechanical properties of other nanocrystalline materials, the scientists say. Doping materials with other chemical elements could alter their stacking fault energies (which influences the extent to which dislocations dissociate) so as to promote twinning or other kinds of imperfections that would allow them to accommodate greater strain without breaking apart. — *David Lindley*

See: Y.M. Wang[1]*, R.T. Ott[2]**, A.V. Hamza[1], M.F. Besser[2], J. Allmer[3], M.J. Kremer[2], "Achieving Large Uniform Tensile Ductility in Nanocrystalline Metals," Phys. Rev. Lett. **105**, 215502-1 (2010). DOI:10.1103/PhysRevLett.105.215502

Author affiliations: [1]Lawrence Livermore National Laboratory, [2]Ames Laboratory, [3]Argonne National Laboratory

Correspondence:
*ymwang@llnl.gov
**rtott@ameslab.gov

This work was performed under the auspices of the U.S. Department of Energy (DOE) (DE-AC52-07NA27344) by Lawrence Livermore National Laboratory. The work at Ames Laboratory was supported by the DOE Office of Basic Energy Sciences, under contract No. (DE-AC02-07CH11358).

1-ID • XSD • Chemistry, materials science, physics • Fluorescence spectroscopy, high-energy x-ray diffraction, pair distribution function, radiography, small-angle x-ray scattering • 50-90 keV, 50-150 keV • On-site • Accepting general users

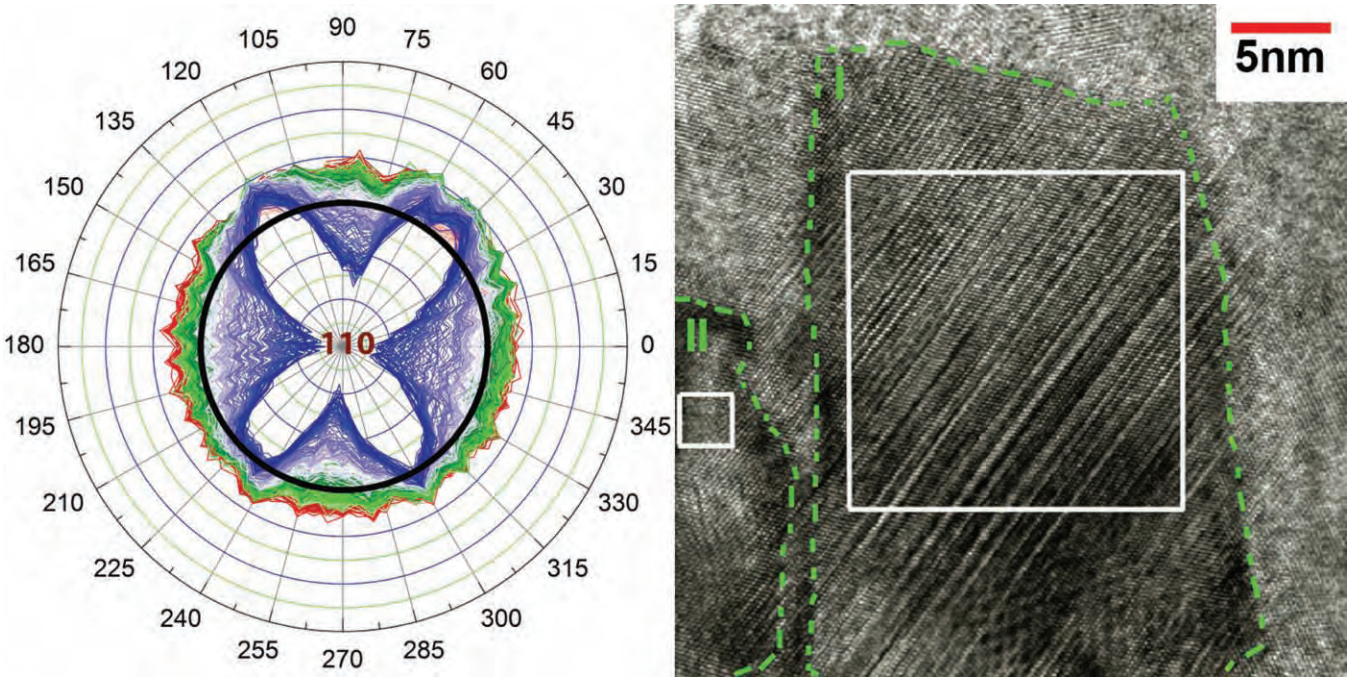

Fig. 1. Strong texture development (left-side plot) as revealed by x-ray diffraction, and high resolution transmission electron microscope image (right-side) of stretched nanocrystalline cobalt showing the lattice within a larger grain (I) has responded to strain by forming twinned crystal structures, while a smaller grain (II) has remained largely unaltered.

Self- and X-ray-Induced Crystallization of Supramolecular Filaments

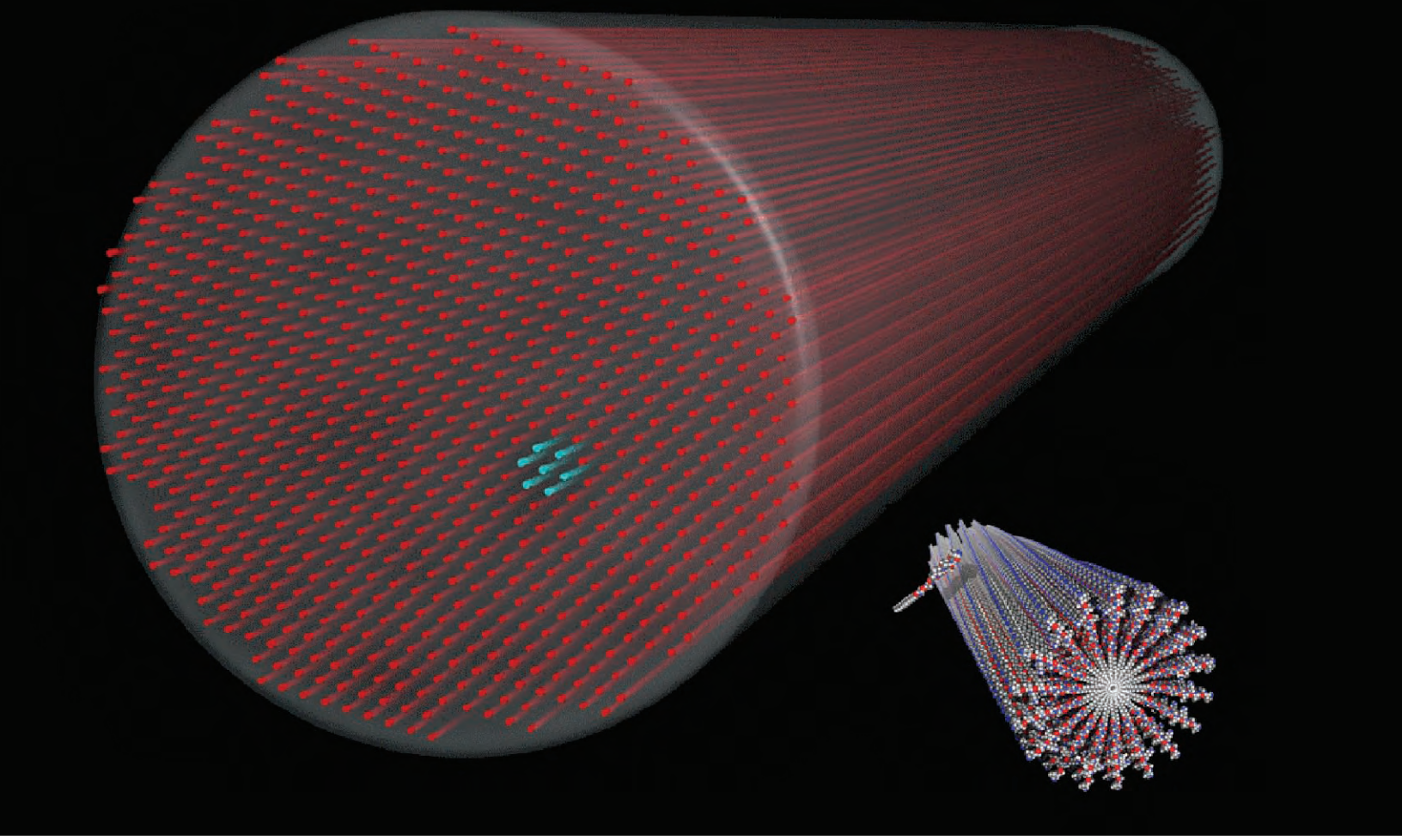

Experiments can sometimes lead to the discovery of completely unanticipated phenomena. Such is the case with the remarkable behavior exhibited by peptide nanostructures (in the form of supramolecular filaments) observed during experiments carried out by researchers from Northwestern University at beamline 5-ID of DND-CAT at the APS. This research could help us understand the organization of nanostructures in biological systems, and may also have applications in controlling the structure of materials

While trying to elucidate the hierarchical organization of peptide nanostructures, the research team discovered that when dispersed in water, those filamentary nanostructures could organize into hexagonally-packed bundles. The researchers were surprised to find that at sufficiently high concentrations in solution, the filaments could spontaneously self-assemble into crystalline structures (the hexagonally-packed bundles, Fig. 1). Even more surprising was the finding that the x-rays used to probe the nanostructures also sometimes triggered filament crystallization. This work may impact our understanding of nanostructures in biological systems and our ability to control the structure of materials.

The filaments used for this research possessed diameters of around 10 nanometers and lengths on the order of tens of micrometers. The filaments were derived from a synthetic molecule containing a short peptide sequence. Peptides are compounds containing two or more amino acids. Here, the peptide sequence consisted of six alanine amino acid molecules

< Fig. 1. A drawing depicting a bundle of 10-nm-diameter peptide filaments positioned in a hexagonal array. Similar phenomena may occur naturally in the cytoskeletons of cells, the cornea of the eye, and other areas of biology. Inset (at lower right) depicts the molecular structure of individual filaments. Image courtesy of S.I. Stupp.

bonded to three glutamic acid molecules—abbreviated Ala6Glu3—which in turn was grafted to an alkyl molecule. The resulting "supramolecules" self-assembled in water to form the filaments.

A sequence of experiments was designed to reveal the arrangement of the filaments dispersed in water. Different aqueous concentrations of the filaments were placed inside tiny 2-mm-diameter quartz capillaries and studied utilizing small-angle x-ray scattering (SAXS) at the DND-CAT beamline. The concentrations ranged from 0.5 to 5 wt%. The SAXS data revealed that all concentrations of filaments aggregated into bundles exhibiting a hexagonal packing (Fig. 1). The organization of the filaments into hexagonally-packed bundles (i.e., crystallization) was quite remarkable. But even more remarkable was the observation that the higher concentration of filaments (2 and 5 wt%) spontaneously crystallized, while the lower-concentration solutions (0.5 and 1 wt%) crystallized only through x-ray exposure.

The crystallization of the filaments, either by self-assembly or by x-ray exposure, constitute phenomena that had not been seen before in other supramolecular systems. In doing the experiments at the APS synchrotron, the team was surprised to find that x-rays could promote crystallization.

A fascinating feature of the x-ray-induced crystallization was the reversibility of the process, which was actually visible. Using the 1-wt%t solution, a cumulative 200 secs of x-ray irradiation turned the initially-transparent solution opaque, indicating crystallization. After x-ray cessation, the solution's opacity slowly decreased until it was clear again within about 40 min, indicating a return to disorder. A follow-up SAXS experiment exposed the solution to a number of 4-sec x-ray bursts. The experimental data showed that the initially-unordered filaments (revealed by the first 4-sec exposure) gradually underwent a change to hexagonally-ordered bundles of filaments as recorded during the last x-ray exposures. When the experiment was repeated two hours later, the SAXS data revealed the filaments were once again disordered; the crystalline structure had disappeared.

The researchers considered whether extraneous factors might have contributed to filament ordering. Intense x-rays can create new chemical compounds within a solution due to ionization, as well as produce subtle heating. However, subsequent tests of the filamentary solutions showed that neither unwanted chemical species, nor thermal effects, had played a part in either the spontaneous or x-ray-triggered crystallizations.

Concerning the basic mechanism responsible for crystallization, the researchers envision that the long-term stability of the crystalline domains is a balance between two opposing tensions: electric charges residing on the filaments (either native or induced by x-ray irradiation) tend to push filamentary bundles apart, while entrapment of filaments within the larger network leads to an inward mechanical compression.

Experimental data revealed that as filament concentration grew, the number of filaments within bundles increased as well, until a critical concentration of filaments resulted in their spontaneous hexagonal arrangement within the bundles (i.e., crystallization). On the other hand, lower filamentary concentrations—unable to spontaneously crystallize—could only do so when x-rays increased the charge density on the filaments' surfaces, thereby changing the balance of interfilament forces in favor of crystallization.

The same mechanism that created their man-made crystalline filamentary networks may well be at work in biological cells, leading the researchers to observe that this research could help us understand the organization of nanostructures in biological systems, and may also have applications in controlling the structure of materials.

— Philip Koth

See: Honggang Cui, E. Thomas Pashuck, Yuri S. Velichko, Steven J. Weigand, Andrew G. Cheetham, Christina J. Newcomb, and Samuel I. Stupp*, "Spontaneous and X-ray–Triggered Crystallization at Long Range in Self-Assembling Filament Networks," Scienc**e 327**, 555 (29 January 2010). DOI:10.1126/science.1182340
Author affiliation: Northwestern University
Correspondence:
*s-stupp@northwestern.edu

This work was supported by the U.S. Department of Energy (DOE) Grant No. DE-FG02-00ER45810. The DND-CAT is supported by E. I. DuPont de Nemours and Company, Dow Chemical Company, and the State of Illinois. Some additional support for this work was obtained from National Institutes of Health National Institute of Dental and Craniofacial Research grant 5R01 DE015920 and National Science Foundation grant DMR-0605427. Use of the Advanced Photon Source, an Office of Science User Facility operated for the U.S. DOE Office of Science by Argonne National Laboratory, was supported by the U.S. DOE under Contract No. DE-AC02-06CH11357.

See also: "Bundling with X-rays," by Cyrus R. Safinya and Youli Li, *Science* Perspectives, *Science* **327**(5965), 529 (29 January 2010). DOI:10.1126/science.1185868

5-ID • DND-CAT • Materials science, polymer science • Powder diffraction, x-ray reflectivity, small-angle x-ray scattering, surface diffraction, wide-angle x-ray scattering, x-ray standing waves, x-ray optics development/techniques • 5-20 keV • On-site • Accepting general users

Deciphering Cholesterol's Position in Cell Membranes

Understanding the structure of cell membranes is necessary for comprehending important processes in cell biology. A new study by researchers from the Illinois Institute of Technology (IIT) and Argonne, using surface liquid x-ray scattering methods at an APS beamline, has illuminated the location and short-range ordering effect of cholesterol in mixed monolayers with phospholipids. The work led the researchers in this study to suggest a new model describing the organization of these layers, which reflects the organization and functioning of cell membranes.

By weight, the plasma membranes surrounding cells are made mostly from a continuous double-layer of phospholipids (two fatty acids attached to a phosphate compound as a head), plus proteins and cholesterol molecules. Cholesterol attracts research attention because it fills a critical role in determining the physicochemical properties of biological membranes. While cholesterol-enriched domains in cell membranes, called lipid rafts, are supposedly involved in a wide variety of cellular activities including protein sorting, signal transduction, and host-pathogen interactions, science still does not understand some basic principles of the formation and function of these domains. Knowledge of the structural organization of cholesterol-lipid membranes could provide new insights into the nature of lipid rafts. Although several models describing the structure of cholesterol-lipid membranes have been proposed, none of them has been directly verified by experiment.

One school of thought believes that cholesterol forms condensed complexes with phospholipids and that these complexes have a fixed ratio of cholesterol to phospholipids that is independent of the overall cholesterol content in the membrane. That would mean that there is only one membrane lipid composition at which the two molecules could mix without forming individual phases. In contrast, other researchers believe that cholesterol forms superlattices—creating highly regular lateral distributions, implying long-range ordering—within the phospholipid bilayer.

In an attempt to resolve the controversy, the researchers from IIT and Argonne performed both grazing incidence x-ray diffraction (GIXD) and x-ray reflectivity experiments on surface monolayers of cholesterol and a phospholipid (1,2-dipalmitoyl-sn-glycero-3-phophocholine, also known as DPPC). The x-ray experiments were conducted at the XSD 9-ID beamline at the APS using a liquid surface diffractometer and a wide range of cholesterol concentrations to account for variations possible within the cell membranes. The researchers tested pure DPPC and cholesterol monolayers as well as mixtures with 13, 25, 46, 70, and 85 mol% of cholesterol, all compressed with a surface pressure of 20 mN/m.

Data from the GIXD studies (Fig. 1) show how the cholesterol and phospholipids are arranged in the plane at different concentrations. At extreme concentrations (below 0.13 and above 0.85 mol% of cholesterol) the diffraction peaks suggest that cholesterol neither forms ordered complexes with DPPC nor participates in any superlattice structures. Mixtures with mole fractions of cholesterol between 0.25 and 0.7 show a broad diffraction peak. This, along with Bragg Rod data, suggests that the molecules form a hexagonal lattice in the liquid-ordered phase with molecular axes oriented normal to the surface. The group believes that this is likely only local ordering involving clusters of 20 to 40 molecules, rather than an indication of superlattice structures. At the different concentrations, a change in the distance between molecules was observed, which contradicts the proposal that organized complexes within the layers have fixed stoichiometry.

Additional x-ray reflectivity data was used to determine the vertical position of cholesterol molecules in the film. As the amount of cholesterol increases, the position of cholesterol changes relative to phospholipids descending into the headgroups region. This, the researchers suggest, may explain some of the phenomena, such as a sharp increase of the chemical activity of the cholesterol at mole

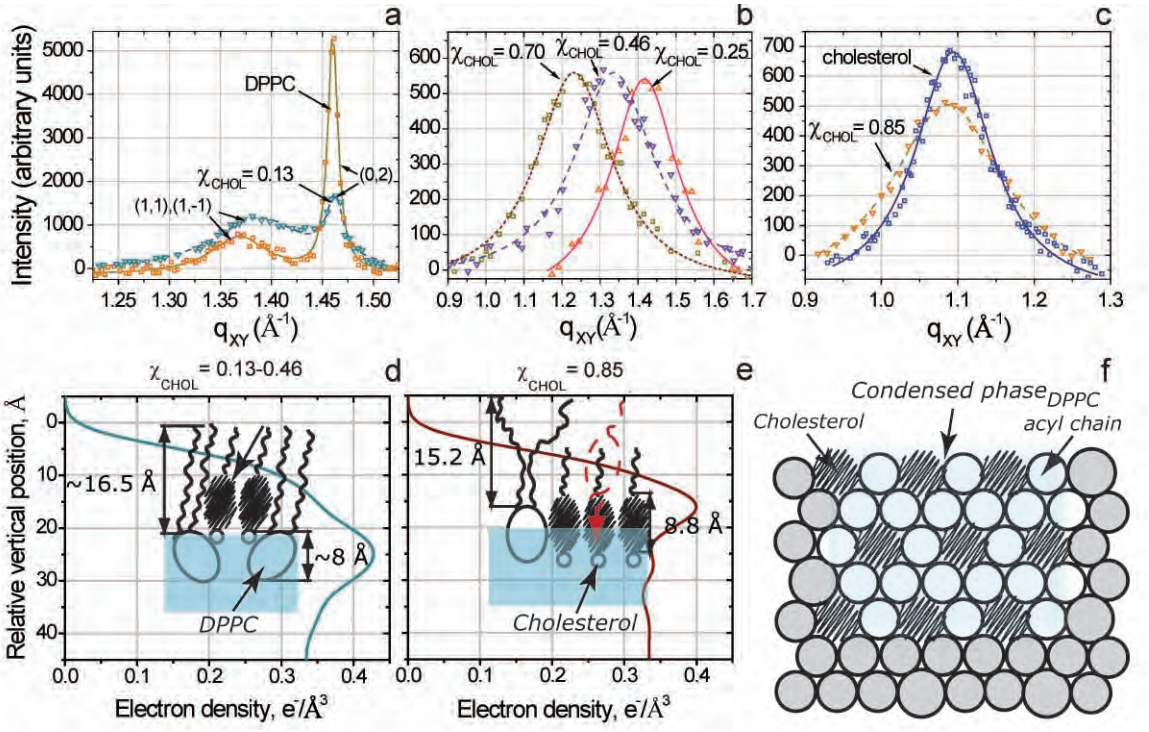

Fig. 1. Grazing incidence x-ray diffraction data: scattering intensity, integrated over q_z range, against scattering vector q_{xy} of (a) pure DPPC and the cholesterol-DPPC mixture with χ_{CHOL} 0.13; (b) cholesterol-DPPC mixture with χ_{CHOL} 0.25, χ_{CHOL} 0.46, and χ_{CHOL} 0.7; (c) pure cholesterol and the cholesterol-DPPC mixture with χ_{CHOL} 0.85. A representative electron density distribution in cholesterol-DPPC mixed monolayer perpendicular to the aqueous interface together with the cartoon schematics of the corresponding out-of-plane molecular arrangement in the mixtures with (d) χ_{CHOL} 0.13–0.46 and (e) χ_{CHOL} 0.85. (f) The cartoon schematics of the in-plane lateral molecular distribution in the mixtures with χ_{CHOL} 0.25–0.7 where the condensed phase is the mixture of cholesterol and DPPC with the stoichiometry identical to that of the film.

fractions of cholesterol around 0.4.

These experiments suggest that the vertical position of cholesterol molecules amid the phospholipids depends on how much cholesterol is in the mix. Furthermore, mixtures of cholesterol and DPPC over a wide range of concentrations act like alloys, with ordering that extends only a few nanometers, and these ordered areas have concentrations that don't vary from the overall stoichiometry of the film.

The researchers present a new elaborate model of sterol-lipid interactions that is consistent with numerous phenomena surrounding cholesterol, such as the condensing effect, liquid-liquid immiscibility, and a steep change in cholesterol's chemical activity at a certain concentration.

— *Yvonne Carts-Powell*

See: Andrey Ivankin[1], Ivan Kuzmenko[2], and David Gidalevitz[1]*, "Cholesterol-Phospholipid Interactions: New Insights from Surface X-Ray Scattering Data," Phys. Rev. Lett. **104**, 108101 (2010). DOI:10.1103/PhysRevLett.104.108101

Author affiliations: [1]Illinois Institute of Technology, [2]Argonne National Laboratory

Correspondence: *gidalevitz@iit.edu

This research was supported by National Institutes of Health R01 AI073892 grant. A. I. was partially supported by the International Centre for Diffraction Data.

Use of the Advanced Photon Source, an Office of Science User Facility operated for the U.S. Department of Energy (DOE) Office of Science by Argonne National Laboratory, was supported by the U.S. DOE under Contract No. DE-AC02-06CH11357.

9-ID • XSD • Materials science, physics • Inelastic x-ray scattering, liquid scattering, resonant inelastic x-ray scattering • 4.5-24 keV, 8.9-30 keV • On-site • Accepting general users

Two Block Copolymers Spring a Spherical Surprise

The long-chain molecules of polymers are arranged in predictable, patterned ways — that's what makes them polymers — but their precise, molecular conformation and intramolecular forces and packing can change according to differing conditions including environment, temperature, and pressure as they undergo phase transitions between order and disorder. The type known as block copolymers tend to be as predictable as the rest, but researchers working at the APS discovered a quite unexpected structure never before seen in block copolymers and previously believed possible only in stainless steel and other similar materials, called a Frank-Kasper σ phase. This work could lead to new insights into quasicrystalline morphology and to practical applications for photonics in fiber optics and optical computing.

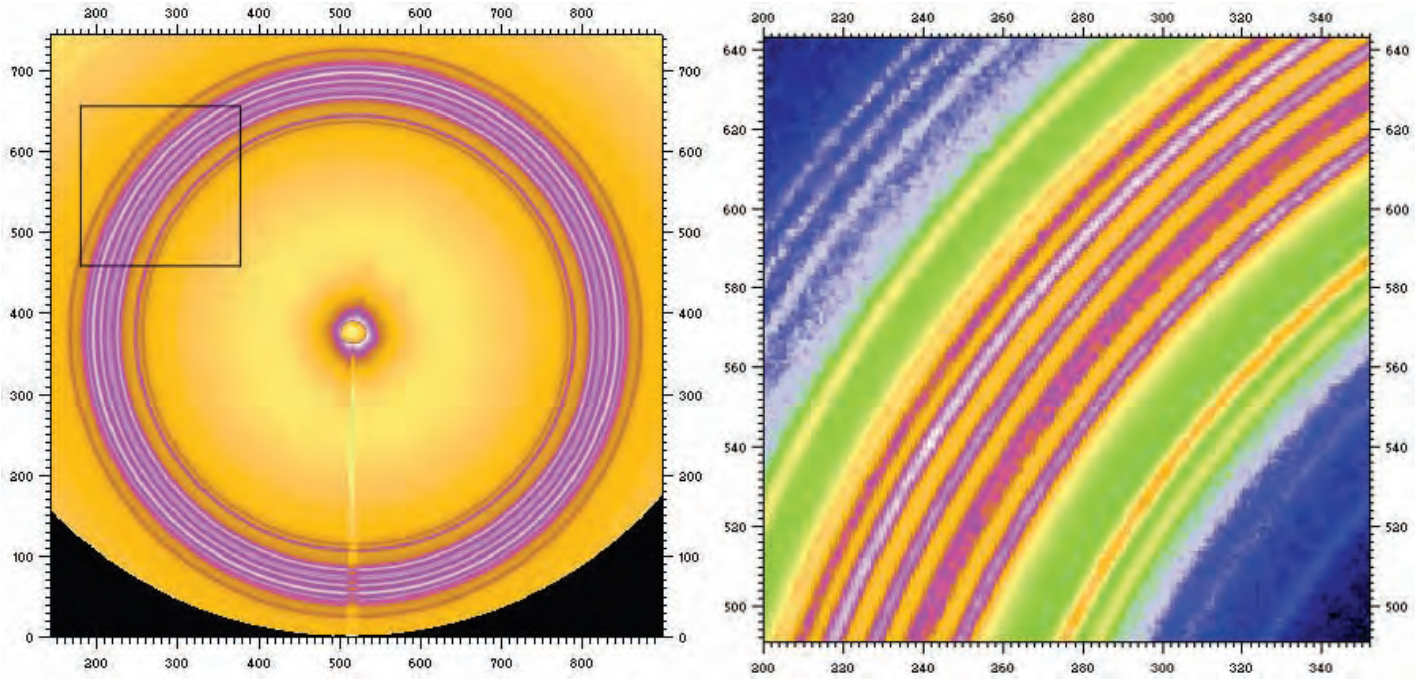

Fig. 1. Small-angle x-ray scattering data obtained at the APS from a block copolymer containing the σ-phase. This page: the left-hand panel shows a two-dimensional diffraction pattern; the region enclosed by the square box is expanded in the right-hand panel, exposing the detailed structure of the diffraction rings. A one-dimensional azimuthal average, intensity versus scattering wavevector q, is plotted in the illustration on the facing page.

Materials scientists from the University of Minnesota conducted small-angle x-ray scattering (SAXS) studies at the DND-CAT 5-ID beamline at the APS. They investigated the structure and mechanical properties of two different block copolymer melts: IL-15, a poly(isoprene-*b*-lactide) (PI-PLA); and SISO-3, a poly(styrene-*b*-isoprene-*b*-styrene-*b*-ethylene oxide), both of which are soft polymeric materials with a variety of potential applications.

Rapid cooling of an IL-15 sample from 70° to 40° C revealed unit cells displaying bcc symmetry under SAXS examination, with PLA spheres forming in a matrix of PI in approximately 30 min. The order-disorder transition (ODT) temperature was identified at 50° C ± 1°. When the IL-15 is rapidly cooled from the ODT temperature to 25° C, however,

the characteristic bcc pattern of scattering peaks gives way over a 24-h period to a highly unusual pattern with at least 48 distinct peaks (Fig. 1). An almost identical phenomenon is observed in SISO-3, leading the investigators to conclude that the same microdomain structure is forming in both materials.

The researchers attempted to define the morphology of the unusual structure using transmission electron microscopy (TEM) studies. Although the IL-15 sample did not easily lend itself to TEM due to its comparative delicacy, the SISO-3 sample could better withstand the necessary microtomy of thin slices and was examined under TEM. This showed a large tetragonal unit cell containing 30 microphase spheres, formed from fused dodecagonal cells, consistent with Rietveld analysis of the SAXS powder pattern of the IL-15. The architecture is clearly that of the σ phase described by Frank and Kasper in alloys formed from spherical particles.

This Frank-Kasper σ phase has never before been observed in a block copolymer crystal, previously occurring naturally only in some forms of uranium and tantalum and seen commonly in various metallic alloys, especially stainless steels. It represents an equilibrium phase resulting from the spherical unit cells of the material attempting to pack themselves into the smallest and most efficient space near the order-disorder transition temperature. Representing a sort of compromise between overcoming this "packing frustration" and reducing the system entropy as much as possible, the Frank-Kasper σ phase unit cell grows from the simpler bcc arrangement to form a large complex structure of 30 microspheres arranged in triangular and square configurations.

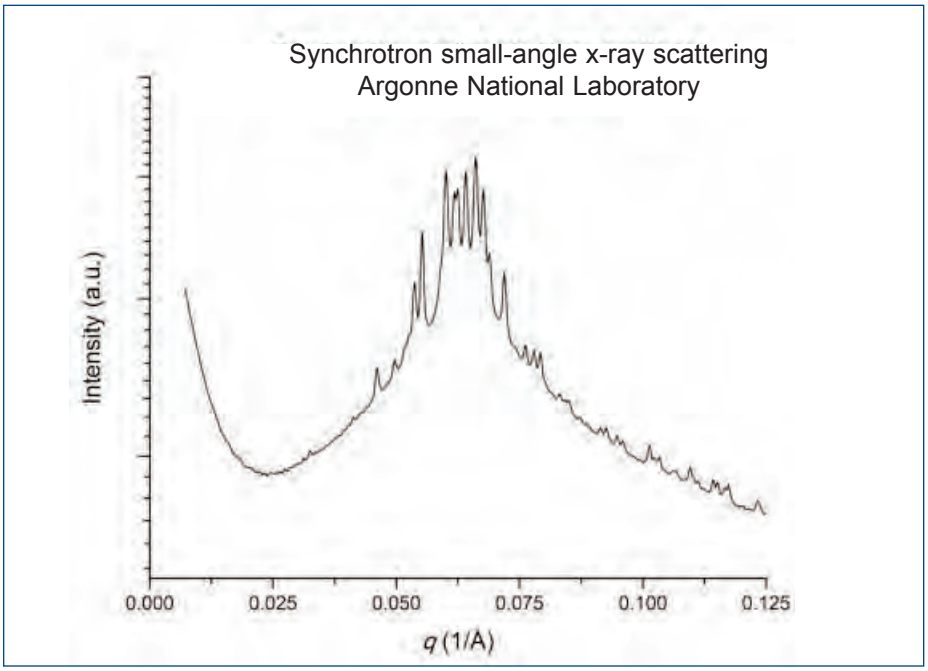

The University of Minnesota researchers note that this huge unit cell structure in the block copolymers is quite similar to quasicrystals, which feature a definable structure but without the repeating periodic order of true crystals. That resemblance offers intriguing prospects that transcend the purely academic interest of finding the Frank-Kasper σ phase in such an unexpected place. The dodecagonal structure of certain quasicrystals is very close to the Frank-Kasper phase observed in the block copolymer melts, which raises the possibility of synthesizing new soft copolymer materials with extremely large unit cells greater than 100 nm in size. Such substances could open the door both to new insights into quasicrystalline morphology and to practical applications for photonics in fiber optics and optical computing. The work also proves that even a field such as polymer physics, which has been extensively and intensively studied for decades, can still offer intriguing surprises in the least expected places. — *Mark Wolverton*

See: Sangwoo Lee, Michael J. Bluemle‡, and Frank S. Bates*, "Discovery of a Frank-Kasper σ Phase in Sphere-Forming Block Copolymer Melts," Science **330**, 349 (15 October 2010). DOI:10.1126/science.1195552
Author affiliation: University of Minnesota. ‡Present address: Ashland, Inc.
Correspondence:
*bates@cems.umn.edu

This work was supported in part (MJB) by the U.S. Department of Energy (DOE), Basic Energy Sciences, Division of Materials Science and Engineering, under Contract No. DEAC05-00OR22725 with UT-Battelle LLC at Oak Ridge National Laboratory, the National Science Foundation through grant DMR-0704192, and the University of Minnesota Materials Research Science and Engineering Center. DND-CAT is supported by E. I. DuPont de Nemours & Company, the Dow Chemical Company, and the State of Illinois. Use of the Advanced Photon Source, an Office of Science User Facility operated for the U.S. DOE Office of Science by Argonne National Laboratory, was supported by the U.S. DOE under Contract No. DE-AC02-06CH11357.

5-ID • DND-CAT • Materials science, polymer science • Powder diffraction, x-ray reflectivity, small-angle x-ray scattering, surface diffraction, wide-angle x-ray scattering, x-ray standing waves, x-ray optics development/techniques • 5-20 keV • On-site • Accepting general users

Not-So-Silly Strings Created from Self-Assembling Gels

Some of the most complex systems in the human body, such as the nervous system and the heart, depend upon intricate, delicate arrangements of cells in arrays of fine fibers. The ways in which these fibers construct themselves from individual cells, and how damage to such networks might be repaired, remain a puzzle. With help from two APS beamlines, a team of materials scientists, biologists, and nanotechnology researchers found a way to induce self-assembling molecules to come together and form two-dimensional filamentous plaques that rupture into nanoscale bundles of fibers, which can be easily aligned over macroscopic distances and serve as an environment to align living cells. This work points the way to new research on macroscopic cell arrays and the possibility of entirely new medical therapies.

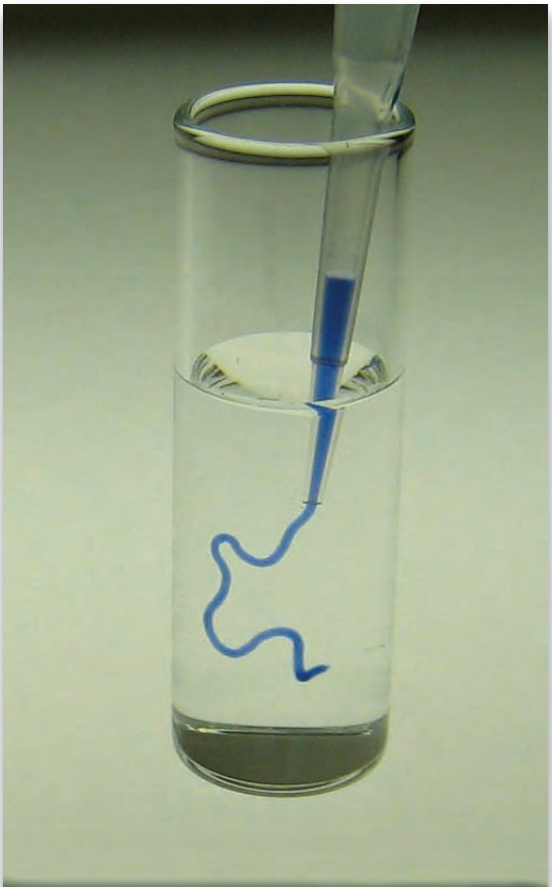

Fig. 1. A peptide amphiphile solution coloured with trypan blue injected into phosphate-buffered saline after heat treatment.

The researchers from Northwestern University studied the structure and development of lamellar plaques in peptide-based solutions at a variety of research facilities, including the DND-CAT Synchrotron Research Center 5-ID beamline and the BioCARS 14-BM-C beamline at the APS. Through the controlled heating and cooling of an aqueous peptide amphiphilic solution, the experimenters were able to form liquid crystals that create long viscoelastic strings from solution containing highly aligned nanofibers that are strong and flexible enough to be manipulated and shaped into various forms (even tied into a knot, Fig. 1). More importantly, they demonstrated that these orientationally ordered strings of nanofibers could be used to form viable wires of aligned living cells. Normally this process requires strong mechanical forces or chemical reactions that are not compatible with living cells.

The team prepared 0.5-1.0wt% peptide amphiphilic solutions and subjected some samples to 80°C for thirty minutes, followed by cooling to 25°C. These solutions showed markedly increased viscosity compared to unheated samples. Adding calcium chloride to the samples caused the formation of a nanofiber domain gel that was highly aligned relative to those formed from unheated solutions.

The heated/cooled solution could be drawn out manually with a pipette through a salty medium to form noodle-like, centimeters-long strings, which displayed birefringence suggesting macroscopic molecular alignment. Scanning electron microscopy and small-angle x-ray scattering (SAXS) examination confirmed well-

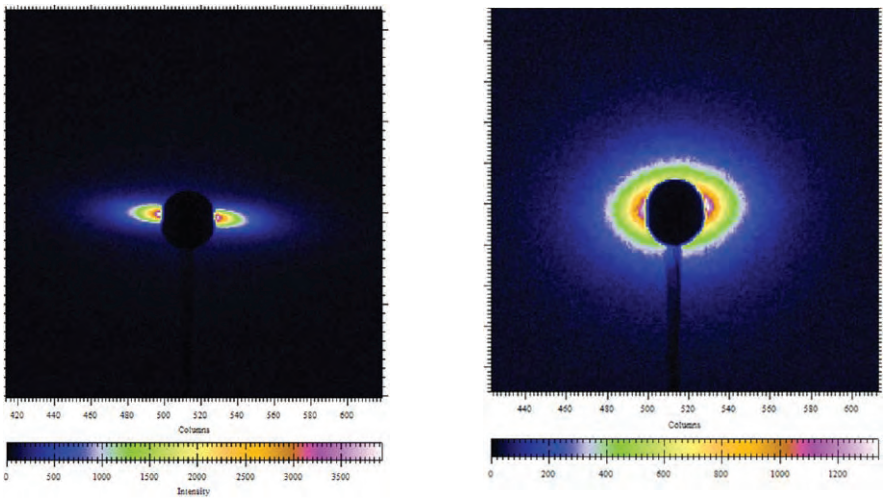

Fig. 2. SAXS of hydrogel strings prepared using peptide amphiphile solutions with (l.) and without (r.) heat treatment.

aligned, long-range structure in these amphiphilic strings, which could only be created from the heated/cooled solution (Fig. 2). Strings drawn from the unheated solution lacked strong internal alignment.

To further explore the mechanisms by which these lamellar plaques and strings were formed, the researchers examined the solutions under heating, using various techniques including transmission electron microscopy, infrared spectroscopy, and SAXS. They found that after heating, small aggregates of nanoscale structures within the solutions formed into thin plaques composed of arrays of aligned filamentous nanofibers. Upon cooling, most of the solution was composed of these aligned nanofibers, broken down from the earlier plaques into bundles of approximately 40 nm in diameter.

After introducing human stem cells into some of the heated/cooled peptide amphiphile solutions, the experimenters repeated the process of manually creating noodle-like strings onto a salty medium. They discovered that the cells within the strings not only remained viable but began to elongate themselves and to connect with each other along the axis of the string. Using heart cells capable of spontaneous electrical activity, the researchers even found that the cells could arrange themselves and propagate electrical signals along the string structure. Other experiments using solutions containing carbon nanotubes also displayed alignment and electrical conductivity. These findings raise the intriguing possibility that similar techniques could be used to create "cellular wires" to repair, restore, or replace the fibers that carry vital electrical signals in the nervous system and heart tissue.

The researchers' discovery of this particular thermal pathway, permitting them to change an isotropic peptide solution into liquid crystals of self-assembling molecules that arrange themselves into plaques that can be manipulated into useful filaments, promises to open up new areas of research into macroscopic cell arrays and ultimately have the potential for important new medical therapies.

— *Mark Wolverton*

See: Shuming Zhang, Megan A. Greenfield, Alvaro Mata‡, Liam C. Palmer, Ronit Bitton, Jason R. Mantei, Conrado Aparicio, Monica Olvera de la Cruz, and Samuel I. Stupp*, "A self-assembly pathway to aligned monodomain gels," Nat. Mater. **9**, 594 (July 2010). DOI: 10.1038/NMAT2778

Author affiliation: Northwestern University. ‡Present address: Nanotechnology Platform, Parc Cientific

Correspondence: *s-stupp@northwestern.edu

This work was supported by the US Department of Energy-Basic Energy Sciences (DOE-BES, DE-FG02-00ER45810, DE-FG02-08ER46539), National Institutes of Health (NIH, 5-R01-EB003806, 5-R01-DE015920, 5-P50-NS054287), National Science Foundation (NSF, DMR-0605427), Department of Homeland Security Fellowship (M.A.G.), Non-Equilibrium Energy Research Center, an Energy Frontier Research Center funded by DOE-BES (award number DE-SC0000989 for L.C.P), Northwestern University's NIH Biotechnology Training Program (pre-doctoral fellowship to J.R.M.), Ben Gurion University of Negev, Israel (post-doctoral fellowship for R.B.), and Generalitat de Catalunya (visiting scholar sponsorship for C.A.) DND-CAT is supported by the E. I. DuPont de Nemours & Company, The Dow Chemical Company, the U.S. NSF through Grant DMR-9304725 and the State of Illinois through the Department of Commerce and the Board of Higher Education Grant IBHE HECA NWU 96. Use of the BioCARS facility was supported by the NIH, National Center for Research Resources, under grant number RR007707. Use of the Advanced Photon Source, an Office of Science User Facility operated for the U.S. DOE Office of Science by Argonne National Laboratory, was supported by the U.S. DOE under Contract No. DE-AC02-06CH11357.

See also: "Regenerative medicine: Noodle gels for cells," Timothy J. Deming, *Nature Materials* News and Views, Nat. Mater. **9**, 535 July (2010).

5-ID • DND-CAT • Materials science, polymer science • Powder diffraction, x-ray reflectivity, small-angle x-ray scattering, surface diffraction, wide-angle x-ray scattering, x-ray standing waves, x-ray optics development/techniques • 5-20 keV • On-site • Accepting general users

14-BM-C • BioCARS • Life sciences • Biohazards at the BSL2/3 level, fiber diffraction, large unit cell crystallography, macromolecular crystallography, subatomic (<0.85 Å) resolution • 8-14.9 keV • On-site • Accepting general users

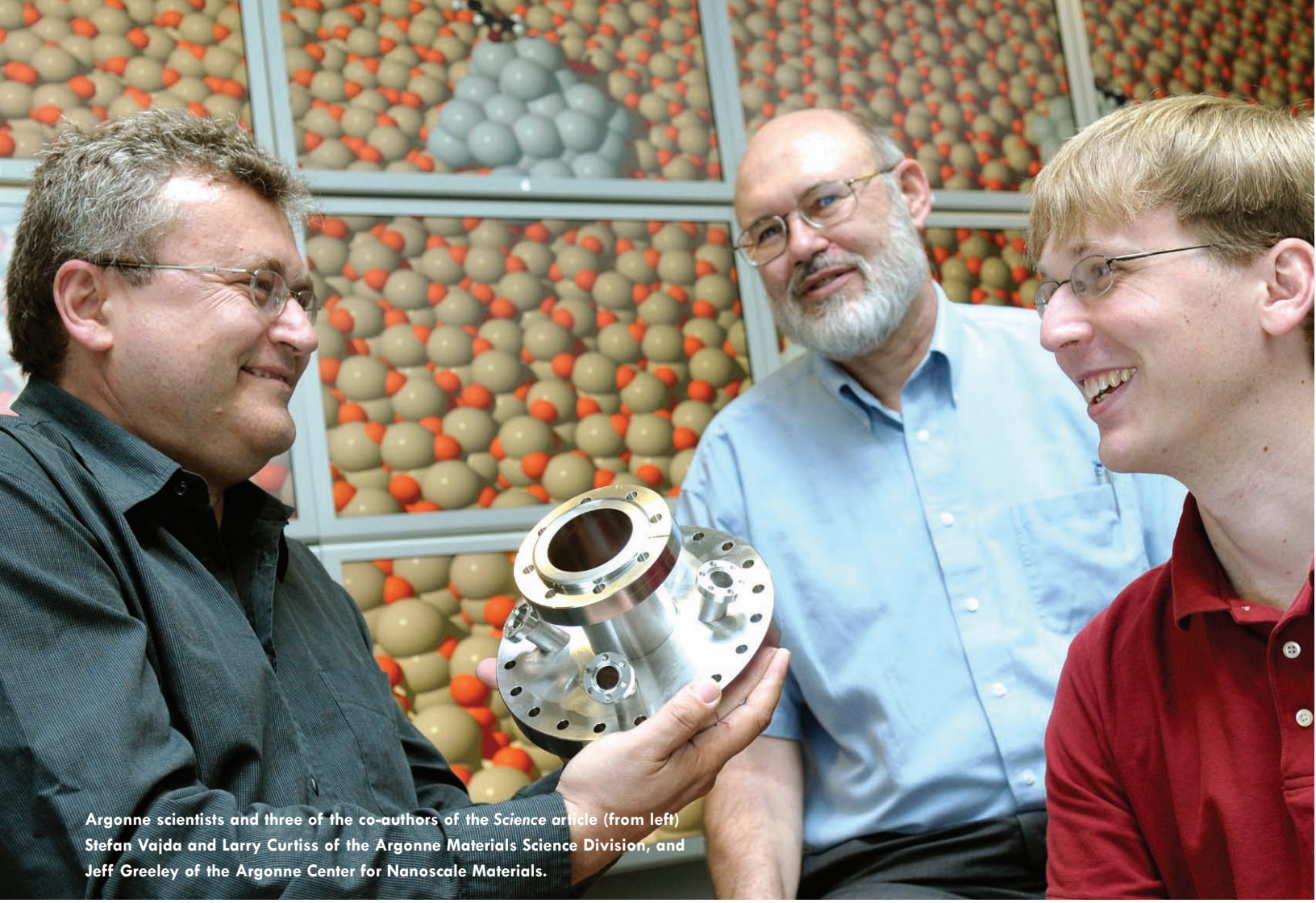

Argonne scientists and three of the co-authors of the *Science* article (from left) Stefan Vajda and Larry Curtiss of the Argonne Materials Science Division, and Jeff Greeley of the Argonne Center for Nanoscale Materials.

Cleaner Industrial Reactions

Propylene oxide is used in the manufacture of various polymers, propylene glycols for paints, in automotive brake fluids, and for household detergents. But the manufacture of propylene oxide requires a great investment of energy and produces large quantities of waste products, including chlorinated and peroxycarboxylic compounds that have to be processed to avoid environmental contamination. Silver nanoclusters, which could be used to catalyze the formation of propylene oxide, were studied by researchers using the XSD beamline 12-ID-C,D at the APS. These novel catalysts could potentially prove to be a much more environmentally friendly and less expensive approach to the manufacture of this important compound.

The researchers from Argonne, Yale University, the University of Illinois at Chicago, and the Fritz-Haber-Institut der Max-Planck-Gesellschaft combined experimental efforts and theoretical analysis to identify a catalyst that not only operates at lower temperatures but bypasses the toxic waste products.

Previous research had focused on large silver particles as catalysts for the conversion of propylene to propylene oxide, but they only showed low selectivity and low conversion rates. Moreover, the reaction generated large volumes of the greenhouse gas carbon dioxide, which counteracts environmental benefits. Other research had shown that gas-phase anionic silver clusters are active in oxidation reactions even at very low temperatures, which led the group in this study to investigatation of the behavior of silver clusters in the solid state. The team found that clusters containing just three silver atoms and larger clusters up to about 3.5 nm across, on an amorphous support, are much more selective.

A problem common to experiments with small metal particles on oxide supports is that of dwindling catalytic performance as the particles stick together, or agglomerate, because of heating during the reac-

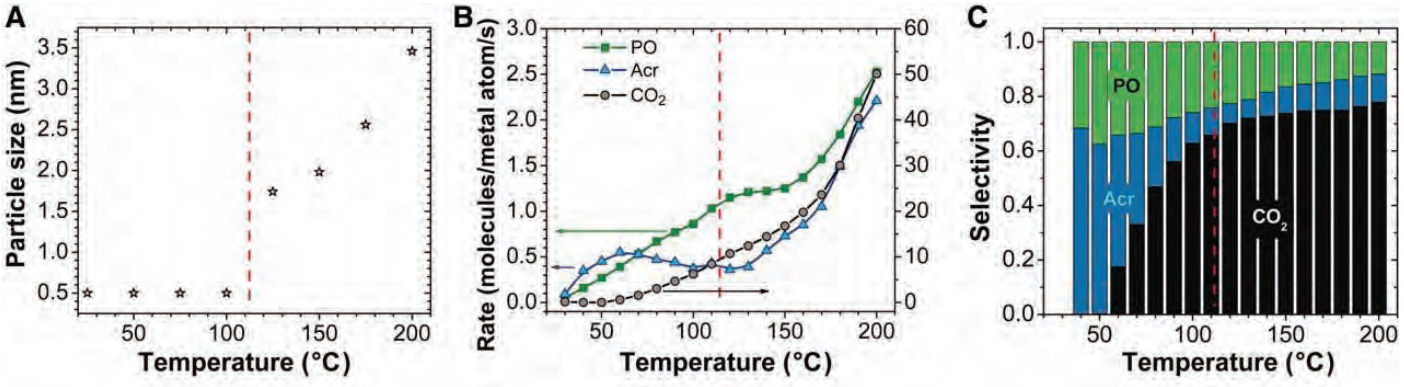

Fig. 1. (A) Temperature-dependent average cluster size from GISAXS. (B) Rate of propylene oxidation toward propylene oxide (PO), acrolein (Acr), and CO_2 per surface silver atom. (C) Selectivity of propylene oxide, acrolein, and CO_2 versus temperature. The vertical dashed lines indicate the temperature at which the sintering of the silver trimers begins. During an additional hour of reaction at 200° C, no change in the size of the aggregates was observed and the turnover rate for propylene oxide decreased to 1.55 s^{-1}, which likely indicates annealing of the newly formed nanostructure. The data shown are results from one run. The estimated uncertainty of GISAXS is ~ ±0.2 nm and ~5% for the turnover rates. Y. Lei et al., Science **328**, 224 (9 April 2010). ttp://www.sciencemag.org/content/328/5975/224.abstract

tion. The team used *in situ* grazing incidence small-angle x-ray scattering (GISAXS) to follow the evolution of size and shape of supported clusters and nanoparticles under reaction conditions and demonstrated that this agglomeration process—referred to as sintering—occurs at temperatures above 110°C and leads to nanoparticles that retain activity up to 200°C, a temperature at which they form 3.5-nm particles. The GISAXS data revealed that no further sintering occurred after this (Fig. 1).

Nevertheless, the nanoparticle aggregates behaved very differently from the subnanometer silver trimers—even under identical reaction conditions—in terms of considerably improved selectivity towards propylene oxide. Moreover, both forms of particle gave a rate of propylene oxide formation much higher than any silver catalyst previously reported. No evidence of nanocatalyst degradation during the 4-h period of the reaction nor any deactivation of the catalyst were observed.

Team also carried out x-ray photoemission spectroscopy (XPS) analysis of the silver samples at BESSY, the Berliner Elektronen speicherring-Gesellschaft für Synchrotron-strahlung in Berlin. An ultrahigh-vacuum x-ray photoemission experiment on the silver trimers and an *in situ* XPS experiment on the nanoparticles showed that the silver atoms are largely in the metallic state during the reaction.

With the experimental data in hand, team members then modeled the process to find out why the very small silver nanoparticles were so much more effective than bulk silver particles. Their density functional theory (DFT) analysis revealed that it is the open shell electronic structure of the silver nanoparticles that endows them with much greater selectivity and activity.

The theoretical aspects of the research also lay bare a possible mechanism in which oxygen is dissociated into two oxygen atoms, one located on the top of the silver trimer, the other at the silver-alumina interface. The atop oxygen atom then hooks up to a propylene molecule to form an oxametallacyle. Subsequently, the oxygen then adds to the double bond and forms a propylene oxide molecule. The oxygen atoms located at the silver-alumina interface participate in the formation of acrolein (another important industrial chemical) and in the combustion of propylene to carbon dioxide.

The DFT study shows that alternative reaction pathways that would otherwise lead to propanal byproducts are unfavorable in terms of the energetics of the process. DFT thus accounts for the high catalytic activity and selectivity of the silver nanoparticles.

— David Bradley

See: Y. Lei[1,2], F. Mehmood[1], S. Lee[1], J. Greeley[1], B. Lee[1], S. Seifert[1], R.E. Winans[1], J.W. Elam[1], R.J. Meyer[2], P.C. Redfern[1], D. Teschner[3], R. Schlögl[3], M.J. Pellin[1], L.A. Curtiss[1]*, and S. Vajda[1,4]**, "Increased Silver Activity for Direct Propylene Epoxidation via Subnanometer Size Effects," Science **328**, 224 (9 April 2010). DOI:10.1126/science.1185200

Author affiliations: [1]Argonne National Laboratory, [2]University of Illinois, Chicago, [3]Fritz-Haber-Institut der Max-Planck-Gesellschaft, [4]Yale University
Correspondence: *curtiss@anl.gov
**vajda@anl.gov

Work at Argonne National Laboratory was supported by the U.S. Department of Energy (DOE), Office of Basic Energy Sciences (Chemical Sciences, Materials Sciences, and Scientific User Facilities), under contract DE-AC-02-06CH11357. Also supported by the American Chemical Society Petroleum Research Fund (Y.L. and R.J.M.) and the U.S. Air Force Office of Scientific Research (S.V.). We acknowledge grants of computer time at the Molecular Science Computing Facility at Pacific Northwest National Laboratory and the Laboratory Computing Resource Center at Argonne National Laboratory. Use of the Advanced Photon Source, an Office of Science User Facility operated for the U.S. DOE Office of Science by Argonne National Laboratory, was supported by the U.S. DOE under Contract No. DE-AC02-06CH11357.

12-ID-C,D • XSD • Chemistry, materials science, physics • Grazing incidence small-angle scattering, small-angle x-ray scattering, surface diffraction, wide-angle x-ray scattering • 4.5-36 keV • On-site • Accepting general users

Revealing the Secrets of Chemical Bath Deposition

X-ray absorption near-edge structure (XANES) spectroscopy is well known as a versatile and powerful technique for examining the microstructure of everything from crystalline solids to amorphous materials, even liquids. Its extreme sensitivity also makes it an ideal tool for probing the kinetics of various chemical reactions *in situ*. Experimenters utilizing the APS have demonstrated a new wrinkle for XANES that opened a window on a poorly-understood technique for deposition of materials. These insights will encourage the development of better-controlled and more precise chemical synthesis techniques for semiconductor and other nanomaterial applications, and are valuable as a demonstration of the extension of XANES spectroscopy into other realms of experimentation.

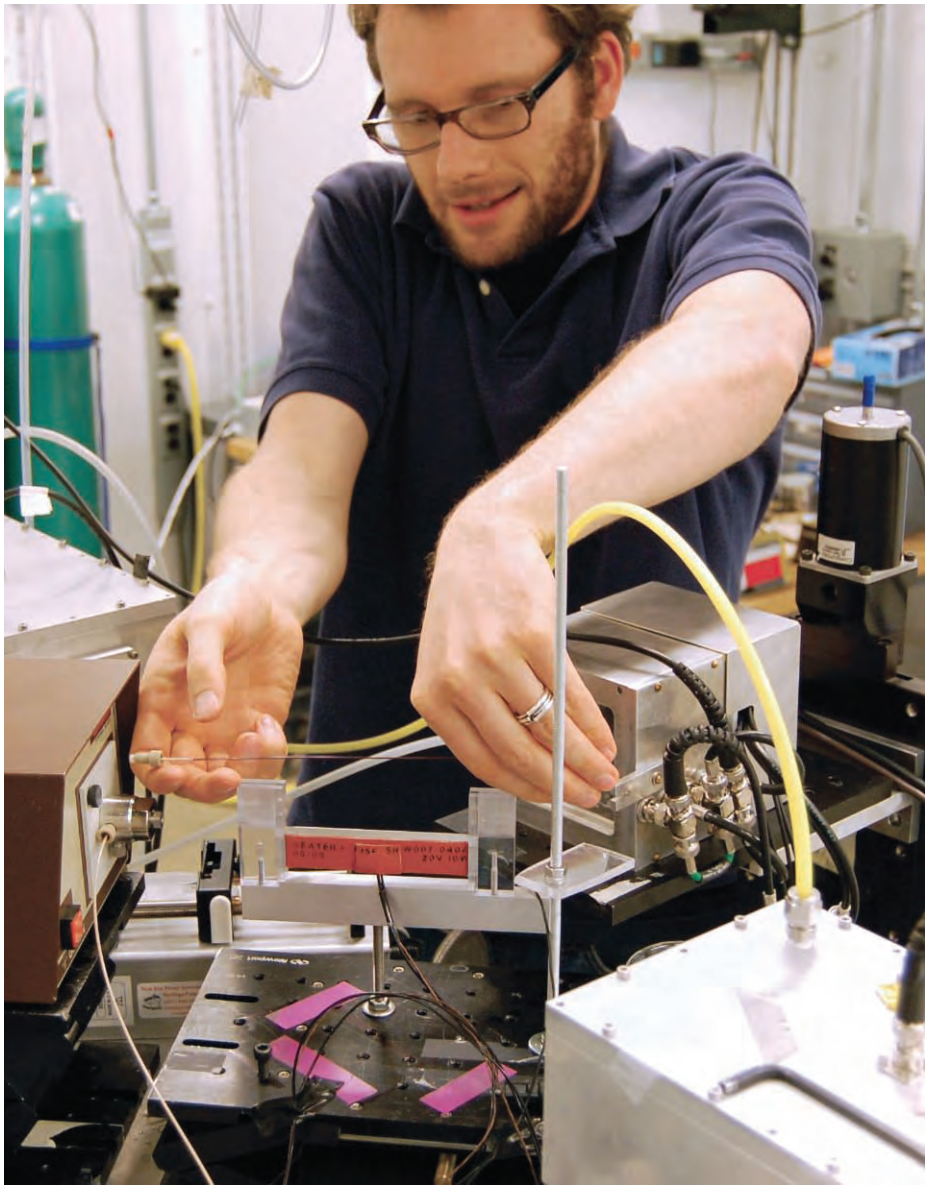

While chemical bath deposition (CBD) is widely used in the laboratory and industry for the creation of thin films and nanostructures for semiconductors and photovoltaics, its actual molecular workings have remained something of a mystery. This has limited its utility, because precise tailoring of CBD products is not possible without a clear understanding and thus control of CBD mechanics. Scientists from Drexel University and the University of Notre Dame have obtained the first detailed look at how CBD operates at the molecular level, using XANES spectroscopy to witness *in situ* the formation of zinc oxide nanowires.

The CBD process begins with a water solution with chemical precursors containing the components from which the desired film structure will be formed. But because the precursor chemical species tend to be very dilute within the solution, identifying and isolating them to monitor their activity during the deposition process has been a daunting challenge because it is difficult to find experimental techniques that will support assessing the different things that must be measured. This has led to some criticism of CBD for being too recipe-based, where it can

< Drexel University Ph.D. student Kevin McPeak, a co-author on the *Chemistry of Materials* article, prepares the microreactor for XANES spectroscopy at the MR-CAT 10-ID beamline. Photo: Matthew Becker, University of Notre Dame.

be difficult to take one set of conditions and say what might happen elsewhere.

The XANES technique proved to be the ideal window into the CBD process. It gives very high sensitivity to allow measurement of species that are very dilute. As a result, the team was able to look at CBD with a degree of accuracy not achieved previously.

The researchers subjected a solution of zinc nitrate and HMTA (hexamethylenetetramine) to different temperatures and pressures inside a custom-built microreactor device to induce ZnO nanowire growth, observing the reactions with XANES spectroscopy at the MR-CAT beamline 10-ID at the APS. A particular advantage of XANES for the current work is that it has good enough time resolution that the reaction could be watched in time. Every minute, the group took a new set of data and looked at the kinetics of the reaction.

One open question the researchers sought to address was the specific role of HMTA in the ZnO CBD process. Previous work had suggested that HMTA might break down into intermediate forms that provided the raw materials for the ZnO film, perhaps even binding to zinc ions in the solution, or that it might act simply as a pH buffer to facilitate the reactions.

This first *in situ* view afforded by the XANES technique demonstrated that HMTA decomposes slowly under heating, releasing hydroxide ions that react with zinc ions in the formation of ZnO. This slow release of hydroxides also has the effect of minimizing ZnO saturation and thus controlling the solution pH. HMTA releases the hydroxide at the appropriate rate, just at the borderline where the zinc oxide is primarily growing on the substrate with minimal precipitation.

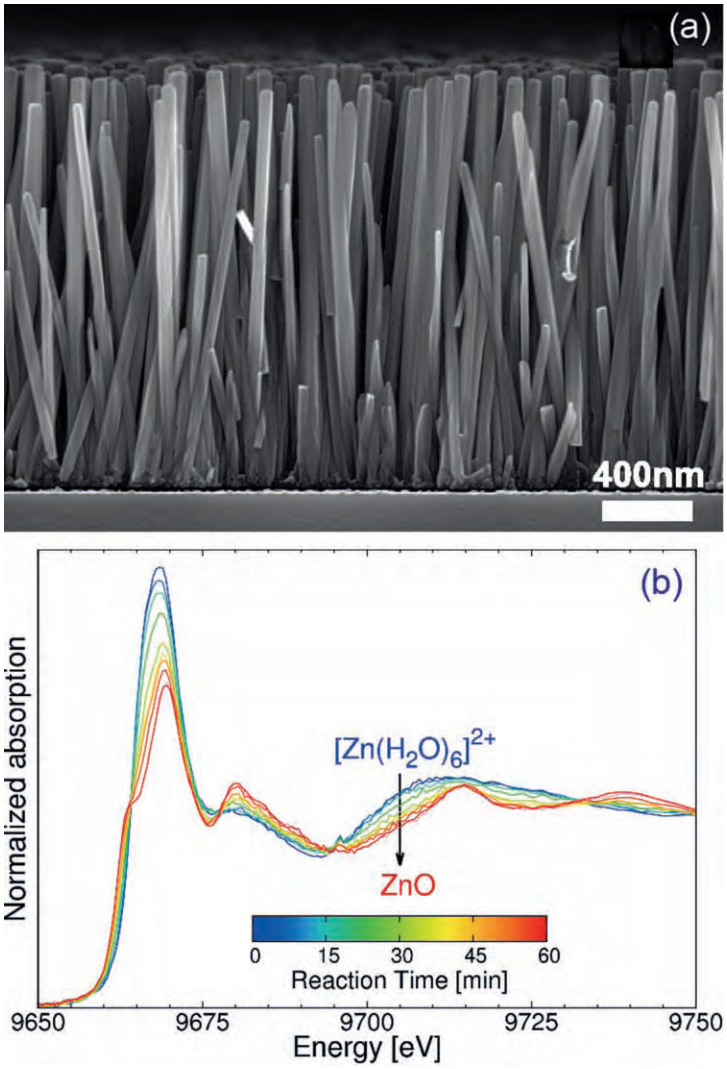

Fig. 1. (a) Scanning electron micrograph of ZnO nanowire array, and (b) *in situ* time-resolved Zn K-edge XANES spectra of ZnO nanowire growth at 90° C showing transition from $Zn(H_2O)_6^{2+}$ to ZnO.

The team observed the growth of ZnO nanowires from zinc nitrate and HMTA precursors at 90° C after two hours, with typical hexagonal cross-sections and diameters of 300-500 nm.

They also employed principal component analysis techniques to obtain quantitative data on the observed species during the CBD process. This showed that the ZnO nanowire growth occurred through direct crystallization from the precursor materials without any long-lived intermediates. The pH buffering provided by the HMTA helps to avoid overabundant precipitation of ZnO in the solution, allowing the controlled growth of the nanowire structures.

These new insights into the mechanisms of CBD will encourage the development of better-controlled and more precise chemical synthesis techniques for semiconductor and other nanomaterial applications.

The work is also valuable as a demonstration of the extension of XANES spectroscopy into other realms. indeed, the group feels that the more widely useful part of the research is actually in the application of XANES spectroscopy to a new type of system. They plan to extend their work to study other CBD chemistries and processes.

— Mark Wolverton

See: Kevin M. McPeak[1], Matthew A. Becker[2], Nathan G. Britton[1], Hasti Majidi[1], Bruce A. Bunker[2], and Jason B. Baxter[1]*, "*In Situ* X-ray Absorption Near-Edge Structure Spectroscopy of ZnO Nanowire Growth During Chemical Bath Deposition," Chem. Mater. **22**, 6162 (2010). DOI:10.1021/cm102155m

Author affiliations: [1]Drexel University, [2]University of Notre Dame

Correspondence: *jbaxter@drexel.edu

MR-CAT operations are supported by the U.S. Department of Energy (DOE) and the MR-CAT member institutions. J.B. acknowledges support from U.S. National Science Foundation through Awards CAREER CBET-0846464 and CMMI-1000111. Use of the Advanced Photon Source, an Office of Science User Facility operated for the U.S. DOE Office of Science by Argonne National Laboratory, was supported by the U.S. DOE under Contract No. DE-AC02-06CH11357.

10-ID • MR-CAT • Chemistry, environmental science, materials science • Diffraction anomalous fine structure, microfluorescence (hard x-ray), small x-ray absorbtion fine structure, x-ray absorption fine structure • 4.3-27 keV, 4.3-32 keV, 15-90 keV • On-site • Accepting general users

CHARGING UP MATERIALS THAT DON'T EXPAND

Most materials expand when heated (with a few exceptions among complex composite materials and specialist alloys), but there are precision engineering applications that could benefit from materials that neither expand nor contract when their temperature changes. Now, an international team has used the XSD x-ray beamline 1-BM at the APS to study the structure of a material that can absorb thermal energy over a wide temperature range without expanding because it consists of a highly flexible framework that contains charged ions trapped in its pores.

Composite materials that do not expand on heating are fairly well known in engineering applications such as optoelectronic devices and telescopes, where precise alignment of components must be maintained and thermal shock avoided, even when temperatures vary. However, because these composites are made from multiple materials with differing coefficients of thermal expansion, they inevitably exhibit internal stresses. A single material with the property of zero thermal expansion (ZTE) would thus be an attractive alternative. Silver oxide and rhenium(VI) oxide display this property over a limited temperature range.

The researchers in this study, from The University of Sydney, the University of Cambridge, and Argonne, investigated tetramethylammonium copper(I) zinc(II) cyanide, which is a flexible but stable framework displaying ZTE (Fig. 1).

Metal cyanides have been investigated as possible ZTE materials for some time. Materials scientists have discovered that varying their precise composition—and the guest molecules that can often reside in host spaces within the porous framework—allows their physical properties to be tuned for different conditions. Unfortunately, the guest molecules in prototypical metal cyanide frameworks are all too keen to leave the host framework and the material either loses its ZTE characteristics or is unstable.

The research team reasoned that finding a way to convert labile guest molecules into trapped prisoners would make a potential ZTE material stable and allow it to retain its properties over a wider temperature range without degradation. They focused on the tetramethylammonium copper(I) zinc(II) cyanide framework, which has the same cristobalite-type structure as single-network cadmium cyanide. The important difference between the copper/zinc material and the cadmium-only framework is that Coulombic forces within the copper/zinc framework prevent the cationic guests from exiting their anionic cages.

The team used synchrotron powder x-ray diffraction on XSD beamline 1-BM at the APS in corroborative conjunction with laboratory single-crystal diffraction studies to monitor the structural changes that occur when the temperature of the mixed metal cyanide is changed. These studies, coupled with computational work using density-functional theory, helped explain why this material has zero thermal expansion at room temperature and over a wide temperature range (200K to 400K). The team explains that the behavior results from a balance between two opposing effects. On the one hand, heat energy causes the framework to flex around the cyanide and copper ions. Just as the ends of a skipping rope are closer together when being used than when pulled taut, this flexibility pulls the metal ions together, resulting in a contraction. On the other hand, the tetramethylammonium ions expand normally with temperature, gradually blocking this effect. This combination results in zero net expansion; and because the guests cannot leave, this property is both stable and reliable.

The team suggests that the trapping of ionic guests within a porous framework could be more generally applicable to the synthesis of ZTE materials, to avoid the problems caused by guest escape from neutral frameworks. — *David Bradley*

See: Anthony E. Phillips[1,2], Gregory J. Halder[1,3], Karena W. Chapman[3], Andrew L. Goodwin[1,2], and Cameron J. Kepert[1]*, "Zero Thermal Expansion in a Flexible, Stable Framework: Tetramethylammonium Copper(I) Zinc(II) Cyanide," J. Am. Chem. Soc. **132**, 10 (2010). DOI:10.1021/ja906895j
Author affiliations: [1]The University of Sydney, [2]University of Cambridge, [3]Argonne National Laboratory
Correspondence:
*c.kepert@chem.usyd.edu.au

This work was supported by ARC Discovery Project Grants DP0664834 and DP0985611 and by the Australian Synchrotron Research Program, which is funded by the Commonwealth of Australia under the Major National Research Facilities Program. Work done at Argonne National Laboratory and use of the Advanced Photon Source, an Office of Science User Facility operated for the U.S. Department of Energy (DOE) Office of Science by Argonne National Laboratory, was supported by the U.S. DOE under Contract No. DE-AC02-06CH11357.

1-BM • XSD • Chemistry, materials science, physics • Powder diffraction • 8-22 keV • On-site • Accepting general users

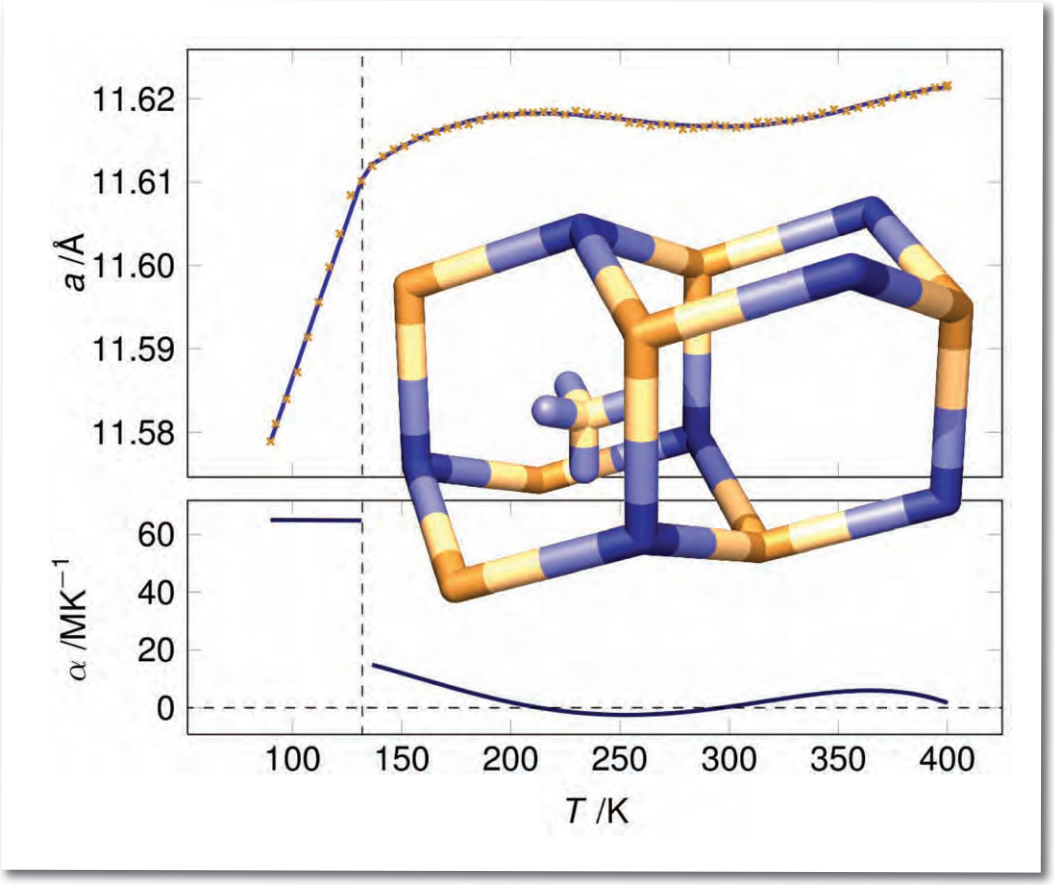

Fig. 1. A single material has the characteristic of ZTE if structural contractions counteract thermal expansion as the temperature rises, as seen in a tetramethylammonium copper(I) zinc(II) cyanide framework studied by the research team.

APS SCIENCE 2002-2009

Back issues of *APS Science* are available in .pdf format (excluding the 2002 issue) at www.aps.anl.gov/Science/Reports/

or in print via a request to: apsinfo@aps.anl.gov.

Elementary! Three-Dimensional Elemental Mapping within a Single Cell

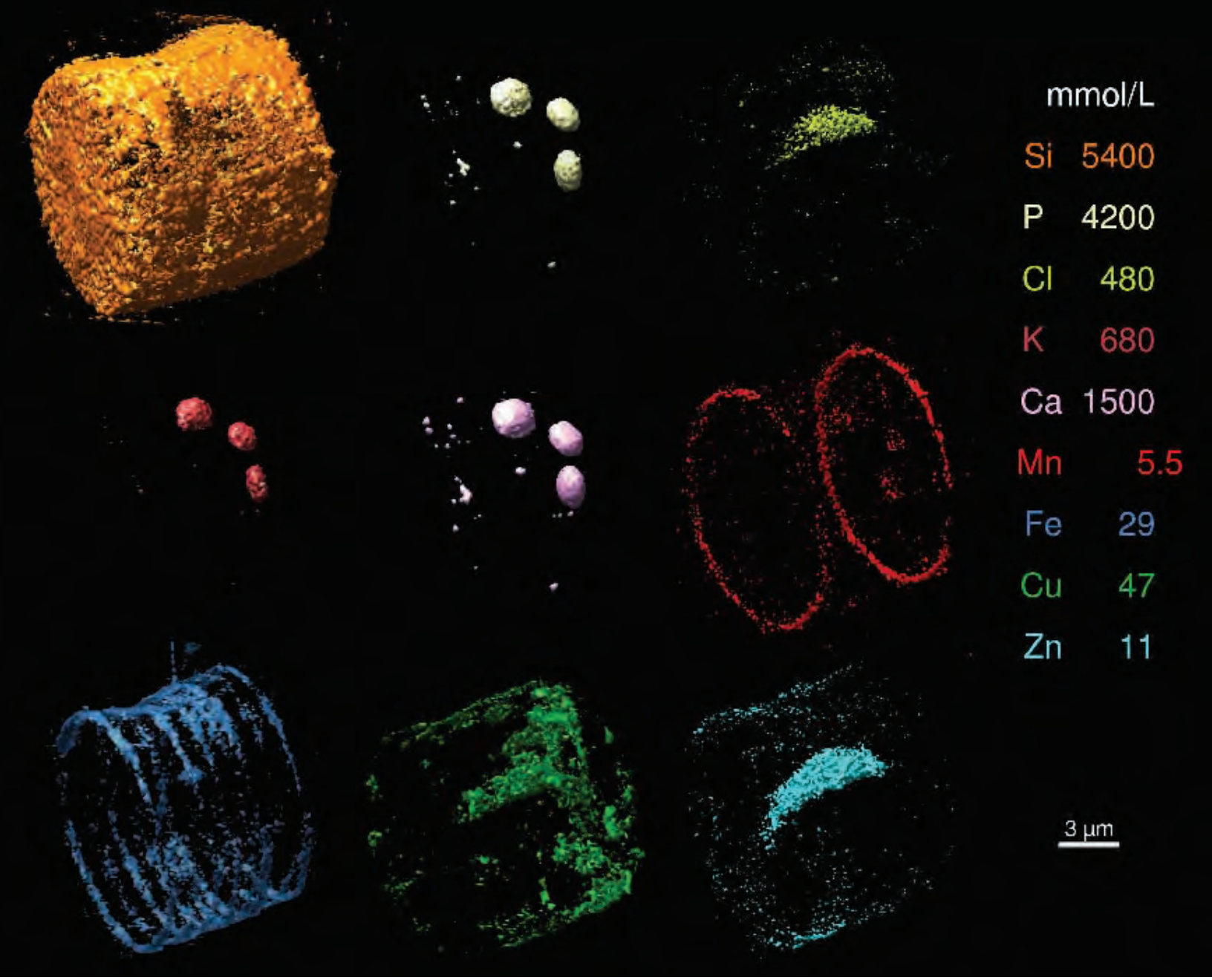

Fig. 1. Three-dimensional maps show the distribution of nine elements in the diatom C. *meneghiniana* revealed by XRF tomography. Silicon dominates the shell of the diatom, which also contains rings of iron and manganese. Calcium, potassium, and phosphorus appear in three distinct organelles, and copper, zinc, and sulfur are associated with a cytoplasmic "pillar" running the length of the shell. From M.D. de Jonge et al., PNAS **107**, (2010). http://www.pnas.org/content/107/36/15676.abstract
A movie of the 3-D elemental distribution of C. *meneghiniana* with a resolution of approximately 400 nm can be viewed at http://tinyurl.com/3nrf36l.

High-resolution, three-dimensional (3-D) cellular images provide a wealth of information for biologists wishing to understand processes at the cellular scale. Determining the identity and location of chemical elements in a biological specimen would be enormously useful for a variety of purposes, from understanding basic biochemistry to learning how organisms take up and recirculate elements from the environment. Although x-ray fluorescence (XRF) is a sensitive probe for chemical elements, using it to obtain 3-D maps of biological specimens has been considered impractical because of the long observation time required, and therefore the high radiation dose imparted to the specimen. Scientists working at the APS have demonstrated 3-D x-ray fluorescence tomography of a whole, single-celled diatom with 400-nm resolution. Their work produced the first compositional make-up of a diatom in such detail and revealed some surprises.

X-ray fluorescence can detect as little as 10^{-18} g of an element (around 10,000 atoms) with a 1-sec measurement, and specimen preparation is simple, greatly reducing artifacts. Other imaging techniques require artificial dyes and contrast agents or exacting specimen preparation, both of which can lead to artifacts in the imaging process. But the sensitivity of XRF means that no dyes or contrast agents are needed, while the penetrating nature of x-rays allows imaging of thick specimens.

XRF tomography XRF requires a huge number of individual measurements. To show that this process is practical, researchers from the Australian Synchrotron, Stony Brook University, the Georgia Institute of Technology, the Bigelow Laboratory for Ocean Sciences in Maine, and Argonne studied the freshwater diatom *Cyclotella meneghiniana*. Droplets of water containing diatoms were deposited on an electron microscopy grid and allowed to dry. The cell walls of diatoms are silicate shells that remain rigid when the cell dries out, making them an excellent subject for this experiment.

At XSD beamline 2-ID-E, a single 10-µm-diameter diatom was guided into an x-ray beam that was focused to a width of 270 nm using a Fresnel zone-plate lens, itself only 160 µm in diameter. The researchers then stepped the specimen across the beam in 150-nm increments in both perpendicular dimensions, recording XRF spectra at each location, to create high-resolution two-dimensional (2-D) images of the diatom's elemental content. After each scan, they rotated the diatom by 6° and were able to obtain data for a total of 24 orientations. The experiment detected 10 elements between silicon and zinc. Combining data from all the 2-D scans allowed the scientists to construct 3-D images of the distribution of these 10 elements in the diatom (Fig. 1 presents 9 of the 10 elements, omitting sulfur).

The 3-D images, the first to show the compositional make-up of a diatom in such detail, contained some surprises. Iron gathers in rings within the roughly cylindrical silica shell, with manganese confined in two rings near the ends of the cylinder. The images also reveal that calcium, phosphorus, and potassium are strongly co-located within three internal organelles. The biological significance of these structures — both the rings and the organelles — is not yet clear, but it seems likely that this cell has been caught in the early stages of cell division, and that the rings and organelles are part of the cell's mechanism for segregating elements for the daughter cells.

While the x-ray data on this single cell took a total of 36 h to obtain, the scientists say that improvements to the experimental method will transform this into a routine and versatile investigative technique. About two-thirds of the measurement time resulted from the lack of automation of the equipment and limitations in detector technology, both of which have existing technological solutions. These and other feasible improvements to the apparatus will reduce the measurement time to as little as 2 to 3 h. — *David Lindley*

See: Martin D. de Jonge[1]*, Christian Holzner[2], Stephen B. Baines[2], Benjamin S. Twining[3], Konstantin Ignatyev[4‡], Julia Diaz[5], Daryl L. Howard[1], Daniel Legnini[4], Antonino Miceli[4], Ian McNulty[4], Chris J. Jacobsen[2‡‡], and Stefan Vogt[4], "Quantitative 3D elemental microtomography of *Cyclotella meneghiniana* at 400-nm resolution," Proc. Natl. Acad. Sci. USA **107**(36), 15676 (September 7, 2010).
DOI:10.1073/pnas.1001469107
Author affiliations: [1]Australian Synchrotron, [2]Stony Brook University, [3]Bigelow Laboratory for Ocean Sciences, [4]Argonne National Laboratory, [5]Georgia Institute of Technology. Present address: ‡University College London; ‡‡Argonne National Laboratory
Correspondence:
*martin.dejonge@synchrotron.org.au

M.D.d.J. acknowledges travel funding provided by the International Synchrotron Access Program (ISAP) managed by the Australian Synchrotron. ISAP is funded by a National Collaborative Research Infrastructure Strategy grant provided by the federal government of Australia. M.D.d.J. was supported under an ARC Discovery Project DP0987422. C.H. was supported by National Institutes of Health Grant 5R21EB006134-02. S.B.B. was supported by National Science Foundation (NSF) Grants OCE 0527059 and OCE 0913080. B.S.T. was supported by NSF Grant OCE 0527062. Use of the Advanced Photon Source, an Office of Science User Facility operated for the U.S. Department of Energy (DOE) Office of Science by Argonne National Laboratory, was supported by the U.S. DOE under Contract No. DE-AC02-06CH11357.

2-ID-E • XSD • Environmental science, life sciences, materials science • Microfluorescence (hard x-ray) • 7-10.5 keV, 11-17 keV • On-site • Accepting general users

How Bovine Dentin Deals with Stress

Teeth are among the strongest and hardest-working parts of human and animal bodies, but they have their weaknesses. Although the main component of a tooth, dentin, features a complex microstructure of ceramic platelets, proteins, and tubular porosity that makes it a tough biomaterial, the tooth is still subject to mechanical stresses making it vulnerable to cracking and breaking. While the mechanical properties of teeth have been widely studied, many unanswered questions remain, such as how stresses are distributed through the different phases of dentin during elastic loading. Researchers utilizing APS x-ray beams have extracted some new information about the composition and stress-tolerance of teeth that could result in better, stronger, and more efficient dental fillings and prosthetics.

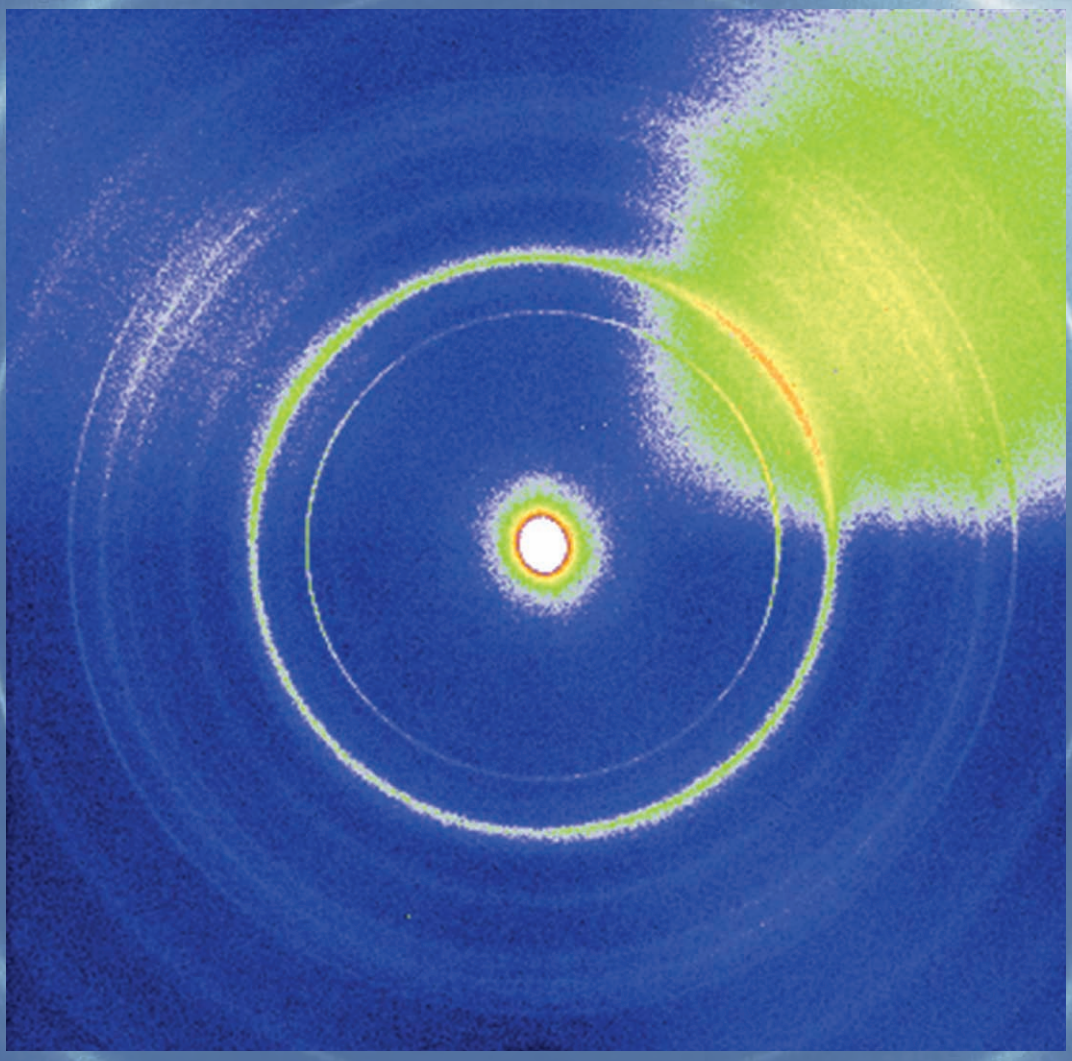

Fig. 1. Main image: Screen print from color fit2D for the dentin WAXS pattern sample. Backgroud: Output from Fit2D (reverse-printed and colorized from the original).

Working at the XSD 1-ID and 2-BM beamlines, the experimenters from Northwestern University and Argonne used a carefully preserved and prepared bovine tooth, which was cut into a sample cross-section and subjected to compressive stresses. They focused their attention in particular on the HAP (hydroxyapatite) platelet phase of dentin and the manner in which stress loads were handled by HAP compared to the proteinaceous collagen matrix phase of dentin. During deformation by stress along the long axis, the sample was examined with wide-angle x-ray scattering (WAXS) measurements in five locations, with a beam wide enough to include both the ITD (intertubular dentin) and PTD (peritubular dentin, Fig. 1). The WAXS studies were followed by micro computed tomography and thermogravimetric analysis (TGA). Inductively coupled plasma mass spectroscopy (ICP-MS) measurements were also performed to determine calcium and phosphorus levels in the sample.

The sample tooth showed pure elastic behavior with a linear stress-displacement curve until finally breaking at a pressure of 107 MPa, with a single branched crack through the full height of the sample. This value is much less than the failure stress levels in previous studies, which were generally reported at 275-300 MPa for human dentin and about 129 MPa for bovine dentin. While the researchers believe this is most likely due to effects resulting from differing sample sizes in the previous experiments, they also observed several other parameters that differed considerably from the typical literature. The present sample showed lower mineralization compared to the reported human dentin levels of 45% HAP, 33% collagen, and 22% water. Similar levels were expected in the bovine dentin, but the sample showed levels of approximately 38.5% HAP, 31% water, and 30.5% collagen. This is likely due to the deciduous nature of the sample tooth.

Perhaps the most surprising finding was that the longitudinal apparent modulus (a measure of how load, and therefore strain, is transferred to a single phase in a composite) of the sample HAP, defined as the applied load divided by the HAP phase strain as determined by x-ray diffraction, was 18 ± 2 GPa, far lower than the expected value for a material of this composition, assuming a Young's modulus value of pure HAP of 114 GPa. Earlier similar experiments using canine teeth and deer antler showed measurements of about 32.8 GPa and 21 GPa, respectively, for the HAP apparent modulus. The study suggests that this could indicate a considerably greater transfer of load from collagen to HAP under stress in bovine dentin compared to other types, resulting from differences in microstructure and composition.

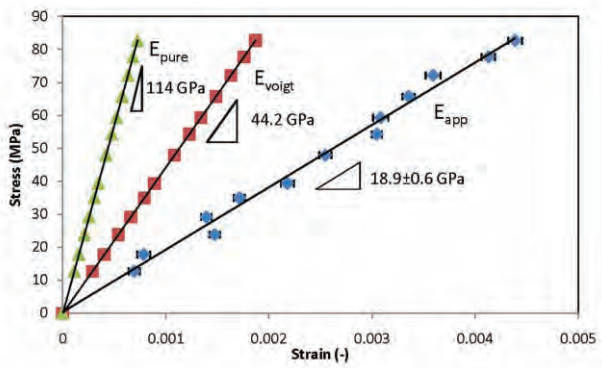

Fig. 1. Plot of the measured HAP apparent t modulus (Eapp) for point 2 on the dentin sample as compared to the minimum HAP apparent modulus (Evoigt) as calculated from the Voigt model using Young's moduli of 114 GPa for pure HAP (Epure) and 1 GPa for pure collagen. The fact that Eapp is lower than the expected minimum modulus suggests that the dentin behavior is more complicated than simply the sum of its parts.

The researchers propose two possible explanations for the marked discrepancy in the apparent elastic modulus of the biological HAP compared to the expected value. While calculations of the apparent modulus assume an even distribution of stress, the x-ray diffraction measurements only sample strain in the HAP platelets closely aligned with the direction of stress, which happen to be preferentially located in areas of stress concentration due to the tubules. Also, the experimenters suggest that the HAP platelets in the dentin of the tooth samples may be considerably less stiff than those of pure bulk HAP, with more amorphous characteristics that are accentuated by the greater interfacial and surface effects that occur on the nanoscale. This decreased HAP stiffness may contribute to the ability of biological dentin to better withstand the great strains it incurs as teeth are used for biting and chewing.

The interesting and unexpected findings of this study raise intriguing prospects for further research and demonstrate that teeth are definitely more than simply the sum of their component parts of HAP and collagen. The unique nature of their biological origins seems to be more important than previously believed, and an improved and more detailed understanding of the complexities involved will lead to better, stronger, and more efficient dental fillings and prosthetics. — *Mark Wolverton*

See: A.C. Deymier-Black[1]*, J.D. Almer[2], S.R. Stock[1], D.R. Haeffner[2], and D.C. Dunand[1], "Synchrotron x-ray diffraction study of load partitioning during elastic deformation of bovine dentin," Acta Biomater. **6**, 2172 (2010).
DOI:10.1016/j.ac bio.2009.11.017
Author affiliations: [1]Northwestern University, [2]Argonne National Laboratory
Correspondence:
*alixdeymier2010@u.northwestern.edu

Partial funding for this research was provided to A.C.D. by a National Defense Science and Engineering Graduate Fellowship from the Department of Defense. Use of the Advanced Photon Source, an Office of Science User Facility operated for the U.S. Department of Energy (DOE) Office of Science by Argonne National Laboratory, was supported by the U.S. DOE under Contract No. DE-AC02-06CH11357.

1-ID • XSD • Chemistry, materials science, physics • Fluorescence spectroscopy, high-energy x-ray diffraction, pair distribution function, radiography, small-angle x-ray scattering • 50-90 keV, 50-150 keV • On-site • Accepting general users

2-BM • XSD • Life sciences, physics • General diffraction, microdiffraction, phase contrast imaging, tomography .5-33 keV, 5-33 keV • On-site • Accepting general users

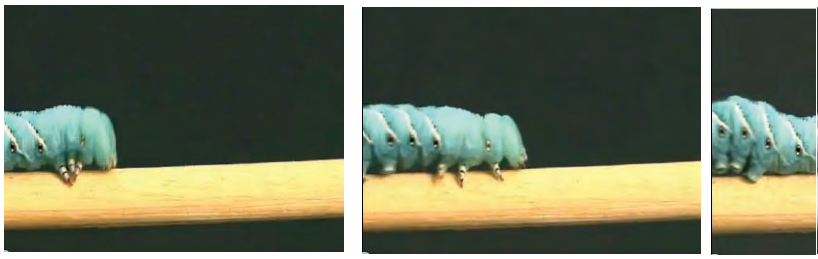

How Caterpillars Crawl

Animals having an open body cavity do not fully constrain their internal tissues when they move, and positional changes of internal tissues and organs during body movements cannot be readily discerned from outside of the body. This complicates modeling of soft-bodied locomotion, because it obscures potentially important changes in the animal's center of mass as a result of internal tissue movements. Researchers used phase-contrast synchrotron x-ray imaging and transmission light microscopy to directly visualize soft-tissue movements inside freely crawling caterpillars, finding evidence for a novel "visceral-locomotory piston" in which the gut moves independently of the body wall and surrounding tissues, unlike any form of legged locomotion previously reported. These results are already contributing to the design and development of deployable, maneuverable, and orientation-independent soft-material robots and may prompt a reexamination of the potential role of soft tissues in the biomechanical performance of animals with stiff skeletons.

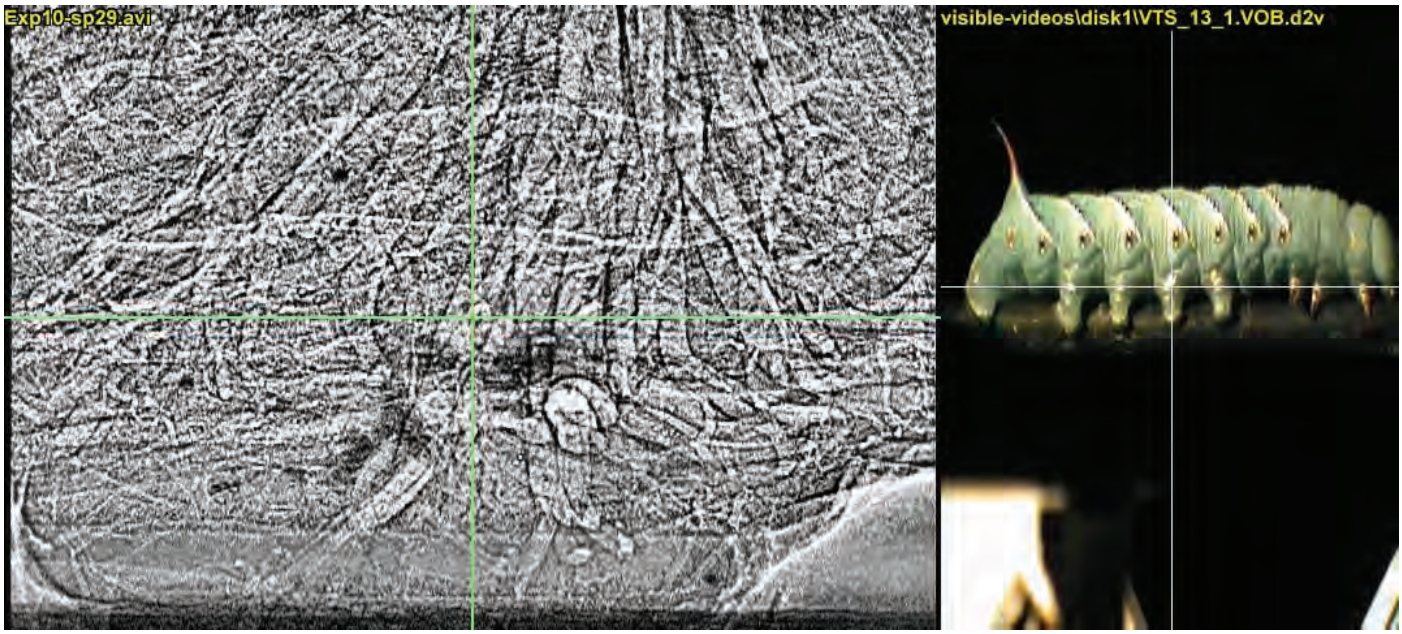

Fig. 1. Freely crawling caterpillars were visualized by means of synchronized x-ray and visible light videos. The x-ray image (left) reveals the highly complex network of tracheae, or air tubes, connecting the caterpillar's musculature and gut to its exterior. Movements of the tracheae could then be compared to external body movements visualized in visible light images (right), revealing gut movements decoupled from the caterpillar's external motion. Image from Trimmer Lab at Tufts University.

Also this and facing page: frames from a Tufts University video, which can be viewed at: http://tinyurl.com/43pxdj2

X-rays generated at the XSD 32-ID beamline of the APS were used by researchers from Tufts University, Virginia Polytechnic Institute and State University, and Argonne to visualize internal tissue movements in freely crawling hawkmoth caterpillars (*Manduca sexta*) by means of a scintillator positioned behind the caterpillars to convert the x-rays to visible light. The researchers quantified the relative timing of gut, body wall, and proleg movements during individual crawls by means of synchronized x-ray and visible light videos (Fig. 1). The most prominent internal features in the x-ray videos were tracheae, which supply all tissues in the body with oxygen and vent carbon dioxide to the outside. These tissues stood out because of the large difference in density at the air-to-tissue interface and the edge-enhancement effects of phase-contrast imaging, making them reliable internal markers. While many tracheae connect to muscles that insert into the body wall, others connect directly to the gut. By simultaneously tracking these differently anchored tracheae, the researchers could determine the timing of movements of the gut and other internal tissues during crawling.

The forward motion of the hawkmoth caterpillar begins at its back end, as its terminal prolegs swing forward before the mid-abdominal prolegs begin to move. The researchers found that the gut also begins sliding forward at the start of this phase, suggesting that the animal's center of mass moves forward before visible translations of the body begin. The midgut typically advances an entire step forward before the body wall has caught up with the gut at the start of the next abdominal proleg stance phase.

To confirm these results throughout the entire gut and to better establish the source of these gut movements, the researchers used transmission light microscopy to analyze gut movements in *Manduca* hatchlings, which are translucent and crawl similarly to their more developed counterparts. Hatchling gut movements correlated with those of the anterior and posterior parts of the animal rather than the body wall, validating x-ray evidence for a gut that is decoupled from the body wall. Additionally, because points within the gut were found to move at different rates relative to each other, the researchers hypothesized that the gut behaves mechanically as a nonlinear elastic structure that translates, shortens, and lengthens within the confines of the body, moved by forces exerted from the anterior and posterior ends of the animal. The gut in *Manduca sexta* is therefore seen as nonelasitically connected to the front and back of the animal and effectively disconnected from much of the remaining propulsive musculature. The researchers conceptualize the *Manduca sexta* caterpillar as a two-body system — consisting of a container and the contained — in which the propulsion of internal tissues is decoupled from the propulsion of the body wall, contributing to the considerable freedom of movement observed in these soft-bodied crawlers.

This gut-sliding arrangement may confer an evolutionary advantage. Because the larval stage of *Manduca* is focused on eating and growing, its body should be structured to permit rapid growth and uninterrupted digestion. By freeing the gut from local perturbations caused by the locomotory compressive wave of crawling, visceral-locomotory pistoning may facilitate a wider expression of movements and behaviors while minimizing mechanical impacts on the digestive system.

These results are already contributing to the design and development of deployable, maneuverable, and orientation-independent soft-material robots and may prompt a reexamination of the potential role of soft tissues in the biomechanical performance of animals with stiff skeletons.

— *Vic Comello*

See: Michael A. Simon[1]*, William A. Woods, Jr.[1], Yevgeniy V. Serebrenik[1], Sharotka M. Simon[1], Linnea I. van Griethuijsen[1], John J. Socha[2], Wah-Keat Lee[3], and Barry A. Trimmer[1], "Visceral-Locomotory Pistoning in Crawling Caterpillars," Curr. Biol. **20**(16), 1458 (2010).
DOI: 10.1016/j.cub.2010.06.059
Author affiliations: [1]Tufts University, [2]Virginia Polytechnic Institute and State University, [3]Argonne National Laboratory
Correspondence:
*michael.simon@tufts.edu

M.A.S., W.A.W., Y.V.S., S.M.S., and L.I.v.G. were funded by a National Science Foundation grant to B.A.T. (IOS 0718537). Use of the Advanced Photon Source, an Office of Science User Facility operated for the U.S. Department of Energy (DOE) Office of Science by Argonne National Laboratory, was supported by the U.S. DOE under Contract No. DE-AC02-06CH11357.

32-ID • XSD • Geoscience, life sciences, materials science • Phase contrast imaging, radiography, tomography, transmission x-ray microscopy • 7-40 keV • On-site • Accepting general users

An Impostor to Treat Debilitating Kidney Stones?

Kidney stones form when salts present in the urine being filtered by the kidneys come out of solution and form tiny crystals. Usually, tiny crystals are no problem and pass down the urinary tract painlessly. However, under certain conditions and in people with a genetic predisposition to a particular type of kidney stone, they can become much larger, sometimes one or two centimeters across, which can cause intense colic-like waves of pain and in some cases be a major risk factor for chronic kidney disease. Now, research, including studies at ChemMatCARS 15-ID beamline, that looks into how the amino acid L-cystine forms crystals might one day lead to a non-surgical treatment for painful and debilitating kidney stones.

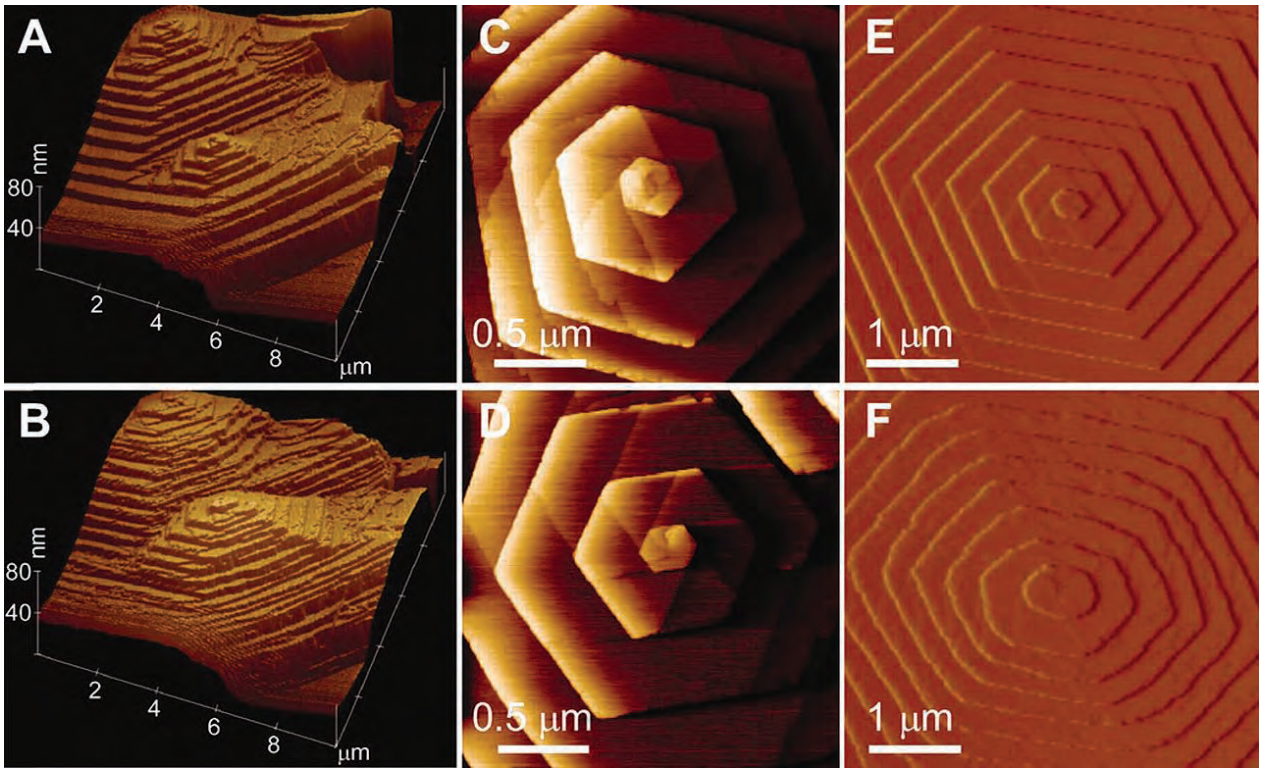

Fig. 1. (A and B) Real-time *in situ* AFM images of a l-cystine crystal, acquired 12 min apart. A pair of hexagonal hillocks generated by two closely spaced dislocations serve as landmarks. (C and D) AFM images of a single dislocation center of (C) l-cystine and (D) d-cystine crystal during growth. (E and F) AFM image of a hexagonal growth hillock on the (001) face of l-cystine (E) before and (F) after addition of L-CDME (5 mg/liter; 0.02 mM), revealing roughening of the {100} steps due to step pinning. Images were acquired in aqueous solutions containing 2 mM l-cystine. Figure this page and next: Jeffrey D. Rimer et al., Science **330** (2010).

Real-time *in situ* movies of crystal growth can be seen at http://tinyurl.com/3pcpzrk

The most problematic form of kidney stones is that in which crystals form from the amino acid L-cystine. These occur in a genetic condition afflicting more than 20,000 people in the U.S. Sufferers often experience much larger kidney stones than seen in people with the more common calcium oxalate monohydrate (COM) type. L-cystine kidney stones often reoccur after surgical removal and are an even greater cause of chronic kidney disease in such patients.

Unfortunately, there are few drugs to prevent cystine kidney stone formation. D-penicillamine, which is a sulfur-containing drug that can react with and bind to L-cystine in solution, prevents crystal formation in some cases but also causes serious adverse effects, including nausea, fever, hypersensitivity, and skin allergies. It also increases the alkalinity of urine, making the urinary tract more susceptible to infection. These sulfur drugs also have an unpleasant, lingering odor that can lead to undesirable body odor and patient non-compliance.

Researchers from New York University, and the Department of Veterans Affairs Medical Center and the Medical College of Wisconsin are hoping to design novel drugs that block the crystallization of L-cystine and circumvent these unwanted side effects. This type of kidney stone forms because there is an excess of L-cystine in the urine. L-cystine is rather poorly soluble in water; in patients who cannot reabsorb L-cystine that has been filtered by the kidneys, concentrations can build up.

The team reasoned that a compound that could bind to the growing crystal surfaces as easily as L-cystine itself might be able to block crystal growth. They used atomic force microscopy and bulk crystallization studies to investigate how two such compounds, L-cystine dimethylester (L-CDME) and L-cystine methylester (L-CME) might work.

In initial studies, the AFM revealed that uninhibited growth of L-cystine crystals occurs through a spiraling process as L-cystine molecules precipitate from solution forming microscopic, hexagonal pyramids (Fig. 1). The inhibitor molecules, also referred to as "impostors," contain an L-cystine group and so can latch on to the edges of the steps of the growing crystal pyramids as if they were normal L-cystine molecules. However, the presence of the "ester" side-chain jutting out from the edge forms a rough inhospitable edge to the step and so prevents further, normal L-cystine molecules from becoming attached, and the crystal can grow no more.

The diffraction studies (Fig. 2) revealed that at a physiological pH slow evaporation leads to the crystallization of L-cystine as hexagonal plates. These were revealed to have large (001) basal surfaces of up to 400-mm width bounded by six equivalent {100} faces. The crystals are typically 10- to 30-mm thick, the team adds. The crystal structure also showed that the L-cystine molecules are arranged in a helix and show hydrogen bonding along the screw axis as well as interactions between sulfur atoms. The data also showed that each flank of the hexagonal hillocks displayed by the crystals have six crystallographically, and therefore chemically, inequivalent ledge sites.

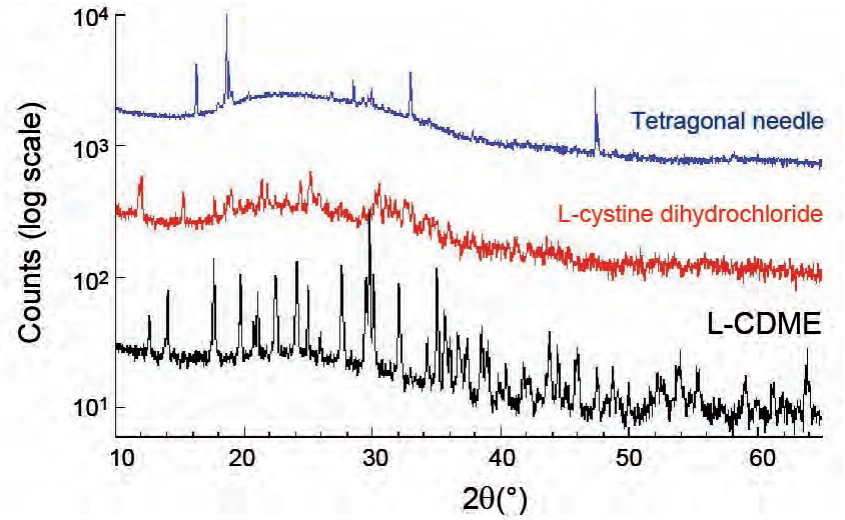

Fig. 2. Comparison of powder x-ray diffraction patterns of L-cystine tetragonal needles, L-cystine dimethyl ester (L-CDME), and L-cystine dihydrochloride. Diffraction was used to verify the absence of these compounds in precipitates of L-cystine obtained by crystallization from aqueous solutions.

The team demonstrated that the reduction in buildup of L-cystine on the nanoscopic crystal edges was directly proportional to the concentration of the impostor molecules in solution. If such impostors can prevent crystallization at the microscopic level, then centimeter-sized kidney stones should never be able to form. The team suggests that L-CDME is the most effective impostor and could function at very low concentrations without the side effects associated with drugs that must react with L-cystine in the body.

A concentration of 2 mg/l would suffice for an adequate therapeutic effect by ensuring that the body can tolerate high levels of L-cystine in solution without the amino acid precipitating out and forming crystals. Published toxicological data on L-CDME suggest that 500 mg/kg of body mass in laboratory rats is the safe dosage limit. The team thus reasoned that a therapeutic dose of 10 to 50 mg per day would most likely be the appropriate therapeutic dose for people with L-cystine kidney stone disease.

This preliminary laboratory research is very much in the early stages and must now be followed by tests in animal models of the disease to demonstrated efficacy in a mammal. Successful results from such tests and positive toxicological testing would allow the work to then move forward to trials in people. — *David Bradley*

See: Jeffrey D. Rimer[1‡], Zhihua An[1], Zina Zhu[1], Michael H. Lee[1], David S. Goldfarb[1], Jeffrey A. Wesson[2], and Michael D. Ward[1*], "Crystal Growth Inhibitors for the Prevention of L-Cystine Kidney Stones Through Molecular Design," Science **330**, 337 (15 October 2010)
Author affiliations: [1]New York University, [2]Department of Veterans Affairs Medical Center and the Medical College of Wisconsin. ‡Present address: University of Houston
Correspondence: *mdw3@nyu.edu

This work was supported primarily by the National Institutes of Health (NIDDKR01-DK068551) and the New York University Molecular Design Institute. The authors also acknowledge support from the Office of Rare Disease Research (1U54DK083908-01). ChemMatCARS is principally supported by the National Science Foundation/U.S. Department of Energy (DOE) (NSF/DOE; CHE-0535644). Use of the Advanced Photon Source, an Office of Science User Facility operated for the U.S. DOE Office of Science by Argonne National Laboratory, was supported by the U.S. DOE under Contract No. DE-AC02-06CH11357.

15-ID • ChemMatCARS • Chemistry, materials science • Anomalous and resonant scattering (hard x-ray), liquid scattering, microdiffraction, single-crystal diffraction, small-angle x-ray scattering, surface diffraction, wide-angle x-ray scattering • 6-32 keV • On-site • Accepting general users

What Makes Butterfly Wings Gleam?

The shimmering hues of some butterfly wings arise not from pigments but from remarkable photonic nanostructures within the scales that adorn the wings' surfaces. The intricate three-dimensional shapes of photonic crystals create colors by selectively reflecting only certain wavelengths. By performing small-angle x-ray scattering studies at XSD beamline 8-ID-I at the APS, researchers have now deduced that the photonic structures in several butterfly wing scales belong to a class of geometrical forms known as "gyroids." A biological mechanism proposed by the researchers that can generate the gyroids may be instructive for scientists trying to synthesize similar photonic crystals in the laboratory.

Light micrograph of the dorsal wing cover scales of the *Parides sesostris* (Papilionidae). Image courtesy of Vinodkumar Saranathan, Yale University. Two animations from this research are available at http://tinyurl.com/3sz2blf. For descriptions, see the supplemental information PDF available at the same location.

Wing scales from five butterfly species belonging to two families, *Parides sesostris, Teinopalpus imperialis* (Papilionidae); and *Callophrys (*formerly *Mitoura) gryneus, Callophrys dumetorum*, and *Cyanophrys herodotus* (Lycaenidae), have long surfaces ridges bridged by cross-ribs, creating windows that allow light into and out of the scales' interiors, where the photonic crystals reside. Previous attempts to characterize the photonic structures using electron micrography have been inconclusive for lack of resolving power, because two-dimensional (2-D) slices reveal only limited information about three-dimensional organization, and because the slices tend to distort under high vacuum.

X-ray diffraction studies allow biological materials to be examined under benign conditions, but because the photonic structures in butterfly wing scales are fairly large, extending more than 300 nm, they will generate diffraction peaks at modest angles. So the team of researchers in this study from Yale University and Argonne chose the small-angle scattering capability available at beamline 8-ID-I to examine single wing scales, 5-10 μm thick, using a 15-μm × 15-μm beam to ensure that each experiment analyzed only a few crystal domains.

The wing scales produced diffraction patterns consisting of peaks or spots distributed irregularly around a number of concentric rings (Fig. 1). The irregular distribution indicated the presence of multiple photonic crystal domains with random orientations. The radii of the rings and the relative intensity of the peaks fit better with a gyroid model of the crystals than with other cubic structures that had been proposed from electron micrography studies. More recent electron micrography work by other researchers had suggested the gyroid structure, but did not precisely characterize it.

The gyroid, a geometrical shape first described in 1970, is a porous structure with a complex, repeating motif in all three directions, consisting of a three-pronged network of curving or "gyrating" channels. Calculations of the expected optical properties of the gyroid shape revealed by the x-ray diffraction pattern obtained at the 8-ID-I beamline agree reasonably well with

the observed properties of the wing scales.

Making such complex shapes in a reliable manner is a tricky task for materials science, but not for butterflies, which appear to have been doing it with relative ease for millions of years. The photonic crystals are made of chitin, a modified extracellular polysaccharide found in insects, shellfish, and many other organisms. Some earlier studies have suggested that cells in developing butterfly wing scales can fold up on themselves in elaborate ways, creating internal spaces in which chitin is deposited. When the cell dies and all the soft organic material disappears, only the hard chitin is left behind. How such a process can generate gyroids has remained unclear.

The team proposes that spontaneous folding of the cell membrane incorporates a second, inner membrane in the cell, the so-called smooth endosplasmic reticulum, to create a double gyroid structure with the cell cytoplasm contained between the two membranes. Protein molecules binding onto the membrane surfaces apparently dictate how the folding proceeds, either through electrostatic interactions or via the physics of bending/curvature (imagine a bulky ball on a flat piece of paper). Chitin then fills the gyroid space formed outside of the cell's membrane, creating a perfect single gyroid that remains when the cell dies.

Double gyroids are easier to make than single gyroids, but single gyroids have more efficient optical properties. Butterflies make the double gyroid template first, then fill in one of the two gyroids and let the rest of the cell die away.

The team posits that, like a modern engineering process, butterflies are employing a complex series of indirect steps to create a final optical device. Mechanisms of this general kind have been used to create complex nanostructures in the lab, but butterflies can make single gyroids at optical size scales, which is much larger than chemists can achieve. A novel aspect of the biological mechanism is that it involves two different membranes with distinct chemical characteristics. Fine-tuning the properties of analogous synthetic membranes could allow for greater versatility in the range of shapes they would fold into.

— David Lindley

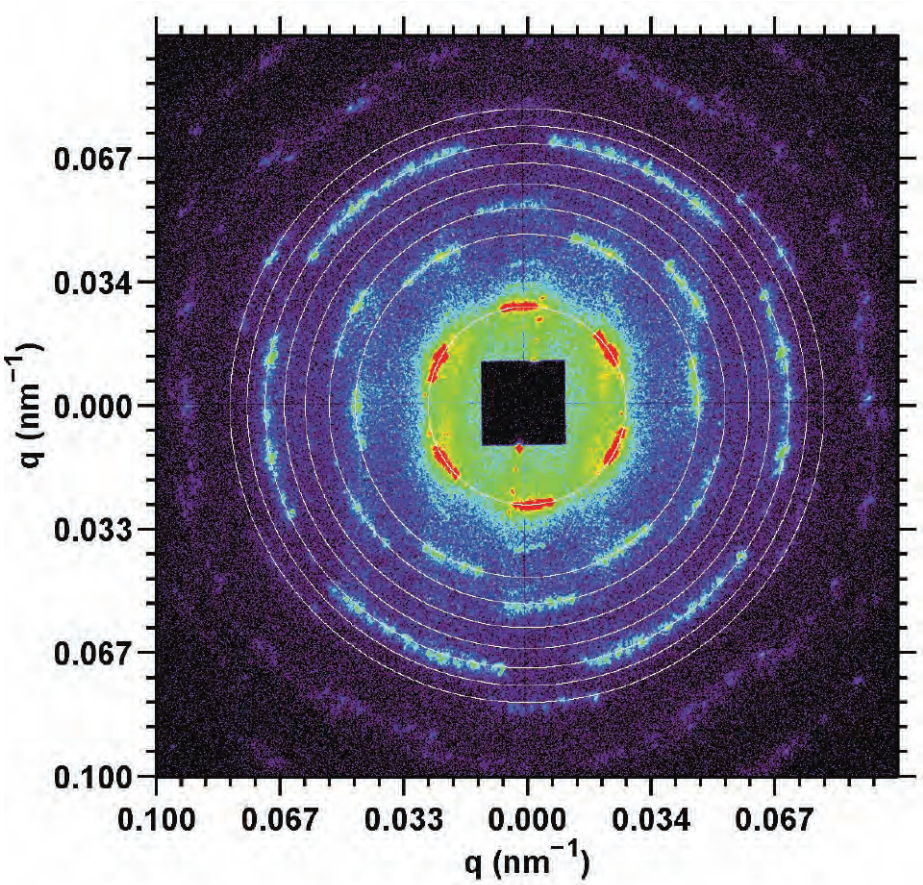

Fig. 1. Representative 2-D SAXS pattern (original image 1340 × 1300 pixels) for *Teinopalpus imperialis*. The false color scale corresponds to the logarithm of the x-ray scattering intensity. The radii of the concentric circles are given by the peak scattering wave vector (q_{max}) times the moduli of the assigned *hkl* indices, where *h*, *k*, and *l* are integers allowed by the single gyroid ($I4_132$) symmetry space group (IUCr International Tables for Crystallography).

See: Vinodkumar Saranathan[1]*, Chinedum O. Osuji[1], Simon G.J. Mochrie[1], Heeso Noh[1], Suresh Narayanan[2], Alec Sandy[2], Eric R. Dufresne[1], and Richard O. Prum[1]**, "Structure, function, and self-assembly of single network gyroid ($I4_132$) photonic crystals in butterfly wing scales," Proc. Natl. Acad. Sci. USA **107**(26), 11676 (June 29, 2010). DOI:10.1073/pnas.0909616107

Author affiliations: [1]Yale University, [2]Argonne National Laboratory

Correspondence:
**Richard.Prum@yale.edu
*vinodkumar.saranathan@yale.edu

This work was supported with seed funding from the Yale National Science Foundation (NSF) Materials Research Science and Engineering Center [Division of Materials Research (DMR) 0520495] and NSF grants to S.G.J.M. (DMR) and R.O.P. (Division of Biological Infrastructure), and Yale University funds to V.S. and R.O.P. Butterfly wing scale specimens were kindly provided by the Yale Peabody Museum of Natural History and the University of Kansas Natural History Museum and Biodiversity Research Center. Use of the Advanced Photon Source, an Office of Science User Facility operated for the U.S. Department of Energy (DOE) Office of Science by Argonne National Laboratory, was supported by the U.S. DOE under Contract No. DE-AC02-06CH11357.

8-ID-I • XSD • Materials science, physics, polymer science • Intensity fluctuation spectroscopy, small-angle x-ray scattering, x-ray photon correlation spectroscopy • 6-12.5 keV, 7.35-7.35 keV, 7.35 keV • On-site • Accepting general users

Packing It In: A New Look at Collagen Fibers

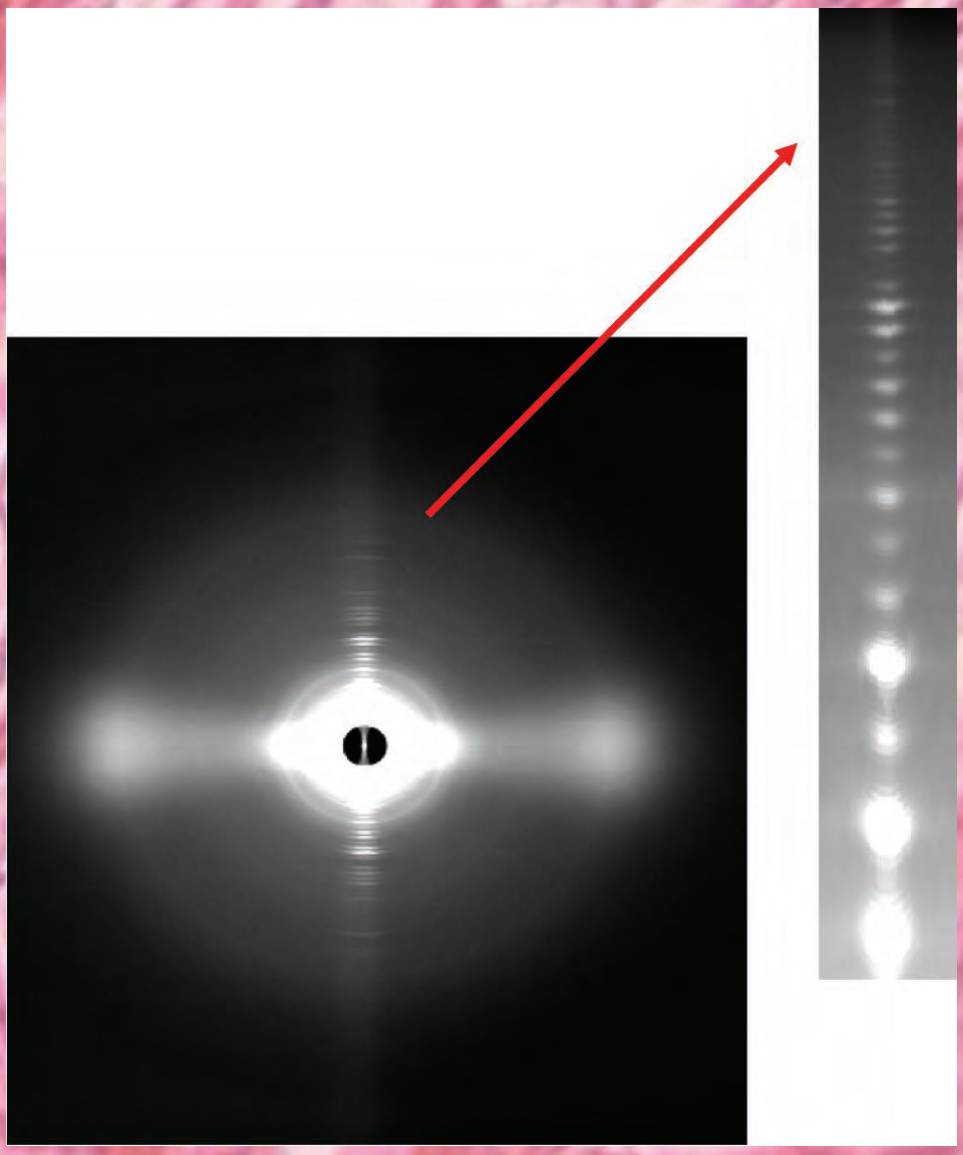

Fig. 1. Left: Medium-wide angle x-ray diffraction pattern of collagen type II fibrils from lamprey notochord. Right: 15-20-Å resolution, as seen in the meridional reflections series. Adapted from O. Antipova and J.R.R.O. Orgel, J. Biol. Chem. **285**(10), 7087 (March 2010).http://www.jbc.org/content/285/10/7087.abstrac.t Background image of collagen fibers courtesy of Andrew Notebaert, Indiana University Bloomington. Source: http://www.indiana.edu/~a215note/virtualscope2/docs/chap2_1.htm, Course A215, "Undergraduate Anatomy." ©2008, The Trustees of Indiana University.

Nature uses collagen everywhere in constructing multicellular animals. There are at least 20 types of collagen, but 80-90% of the collagen in the body consists of types I, II, and III. Collagen type I is used to form skin, tendon, vascular, ligature, organs, bone, dentin, and interstitial tissues. Collagen type II makes up 50% of all cartilage protein, and is essential in normal formation of such structures as cartilage, the vitreous humor of the eye (the clear gel that fills the space between the lens and the retina of the eyeball of humans and other vertebrates), bones, and teeth. To create these structures, collagen molecules are positioned in arrays called fibrils, producing what are known as the D-periodic fibrillar collagens. Though previous work has given some idea of what the D-periodic structure looks like, technical limitations prevented accurate structural studies of collagen type II packing. A research team aided by the Bio-CAT 18-ID beamline and the BioCARS 14-BM-C beamline at the APS has remedied that situation by determining the molecular structure of collagen type II in living tissues. These results mark significant progress in understanding the architectural differences between collagen type I and type II. Using these new data, the study of tissue assembly and degradation, such as in osteo- and rheumatoid arthritis, can take several leaps forward.

The special D-periodic arrangement in fibrillar collagens arises when five fragments from five different collagen molecules are arranged to make one complete collagen molecule. Further packing is accomplished, outside of the cell, when multiple fibrils are combined to form fibril bundles. The fibrils themselves are stabilized by cross-linking between collagen molecules facilitated by groups of specific amino acids known as the telopeptides. If the cross-linking is not performed correctly, the resulting instability of the fibrils and tissue can lead to connective tissue diseases, such as glaucoma and arthritis, and to skin fragility in normal aging.

The researchers from the Illinois Institute of Technology performed their investigations on collagen fibrils from the lamprey fish, which electron microscopy shows to be closely related to mammalian fibrils, even though some details of the larger scale architecture differ. The research group had refined their techniques by studying the structure of Type I collagen and then went on to apply those methods to better understand the structure of the more common Type II collagen.

Their major breakthroughs came in conducting x-ray diffraction experiments on whole tissue samples (Fig. 1). Their resulting data on notochord tissue of adult lampreys give a clear picture of the structure of Type II collagen in living tissues. Collagen Type II was chosen for these studies because it shows marked similarity across species, thus allowing starting inferences about its amino acid sequence and broad application of the structures obtained from this study.

By comparing their newly collected data on collagen type II collagen with their previously collected data on collagen type I, the researchers were able to identify critical differences between the molecular packing of the two types of collagen. Their data led them to conclude that these differences in molecular packing may be due to the specific telopeptide shapes in the two molecules. Such information is critical to understanding tissue assembly.

In collagen Type II there is a well-ordered cross-linking pattern that is different from that found in collagen Type I. The researchers propose that this finding may explain why collagen Type II differs from Type I in both fibril diameter and fibril bundle organization. The Type II molecule has more amino acids available for cross-linking than does the Type I molecule. This could make the Type II molecule more stable and ubiquitous in network-like tissue formation. But the bulkier nature of the telopeptide component in Type II molecules could also inhibit the formation of Type II molecules as large as those observed for collagen type I.

The diligent work of the research team has provided much needed structural and mechanistic data on collagen fibers. Using these new data, the study of tissue assembly and degradation, such as in osteo- and rheumatoid arthritis, has taken several leaps forward. — *Mona Mort*

See: Olga Antipova* and Joseph P.R.O. Orgel*, "*In Situ* D-periodic Molecular Structure of Type II Collagen," J. Biol. Chem. **285**(10), 7087 (March 5, 2010). DOI 10.1074/jbc.M109.060400
Author affiliation: Illinois Institute of Technology
Correspondence: *antiolg@iit.edu
**orgel@iit.edu

Bio-CAT is a National Institutes of Health (NIH)-supported Research Center (RR-08630). Use of the BioCARS Sector 14 was supported by the NIH National Center for Research Resources, under Grant RR-007707. Use of the Advanced Photon Source, an Office of Science User Facility operated for the U.S. Department of Energy (DOE) Office of Science by Argonne National Laboratory, was supported by the U.S. DOE under Contract No. DE-AC02-06CH11357.

14-BM-C • BioCARS • Life sciences • Biohazards at the BSL2/3 level, fiber diffraction, large unit cell crystallography, macromolecular crystallography, subatomic (<0.85 Å) resolution • 8-14.9 keV • On-site • Accepting general users

18-ID • Bio-CAT • Life Sciences • Fiber diffraction, microdiffraction, microfluorescence (hard x-ray), small-angle x-ray scattering, time-resolved x-ray scattering, micro x-ray absorption fine structure • 3.5-35 keV • On-site • Accepting general users

How Compressible is a Protein?

Compressibility is a measure of the physical state of a protein and has been shown to change during the unfolding of various proteins including mitochondrial protein cytochrome c. For this reason, when researchers from Argonne, HASYLAB, and Northeastern University developed a new method for determining protein compressibility, they used cytochrome *c* as a model. Their method involves the use of the inelastic x-ray scattering (IXS) and nuclear resonance vibrational spectroscopy (NRVS) techniques, available on XSD beamline 3-ID end stations C and D at the APS, respectively. This method provides a global measurement of protein compressibility at ambient pressure and gives a more native state result than other methods due to its use of the natural iron-containing heme group associated with the protein. The method is accurate in that it is in agreement with molecular dynamics simulations and will be widely applicable to other materials where compressibility is an important measure of structure or function.

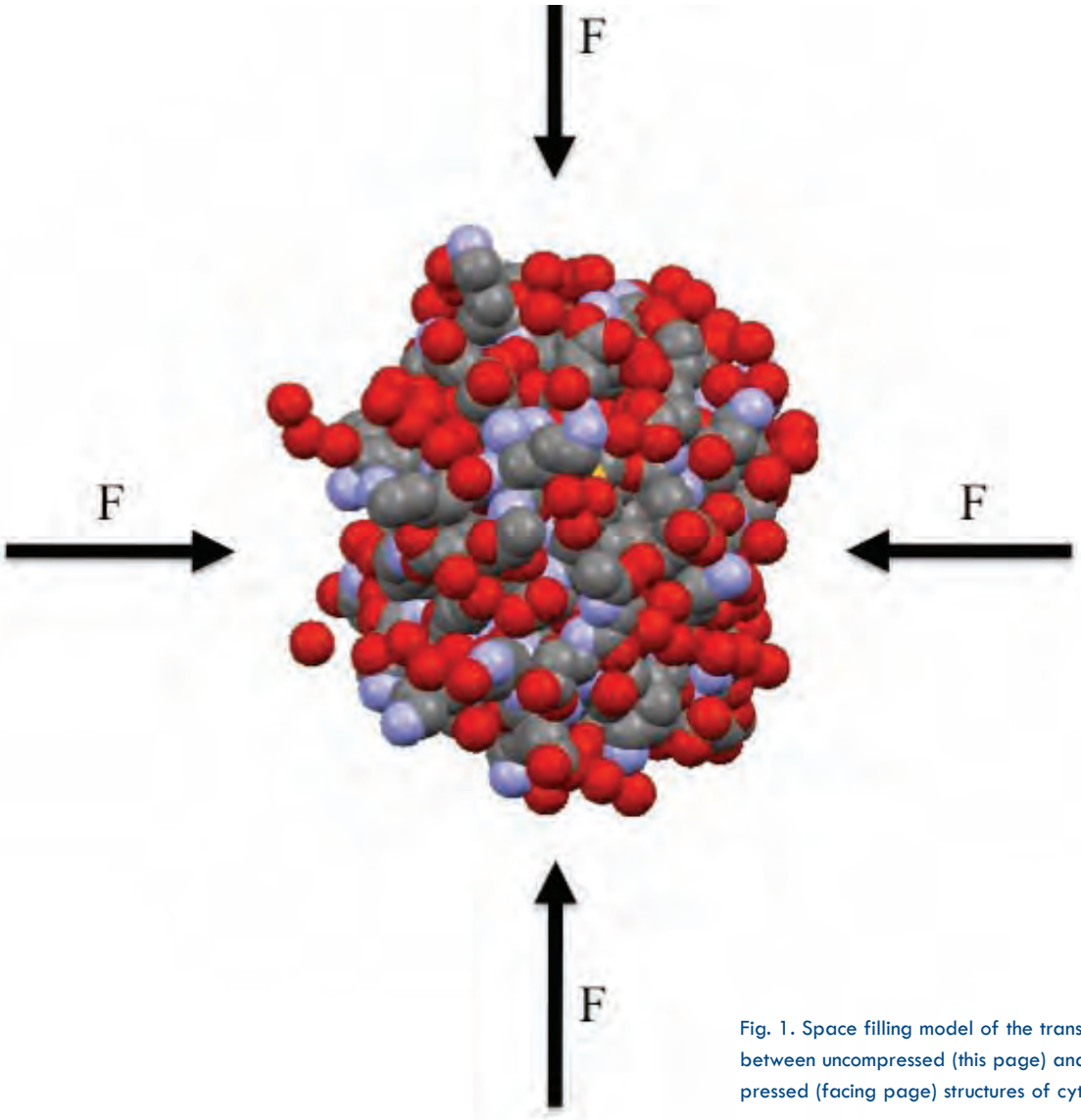

Fig. 1. Space filling model of the transition between uncompressed (this page) and compressed (facing page) structures of cytochrome c.

The method will be widely applicable to other materials where compressibility is an important measure of structure or function.

The role of protein unfolding has only recently come to light as an important factor in the way cells regulate their life and death decisions. Conventional thinking subscribes to the idea that the amino acids in a protein interact in a complex manner to fold the polypeptide chain into a final, stable configuration and that this is the three-dimensional structure that carries out the business of that protein. Now, however, evidence suggests that proteins can adopt different folded or partially unfolded states that are active in various roles. The mitochondrial protein

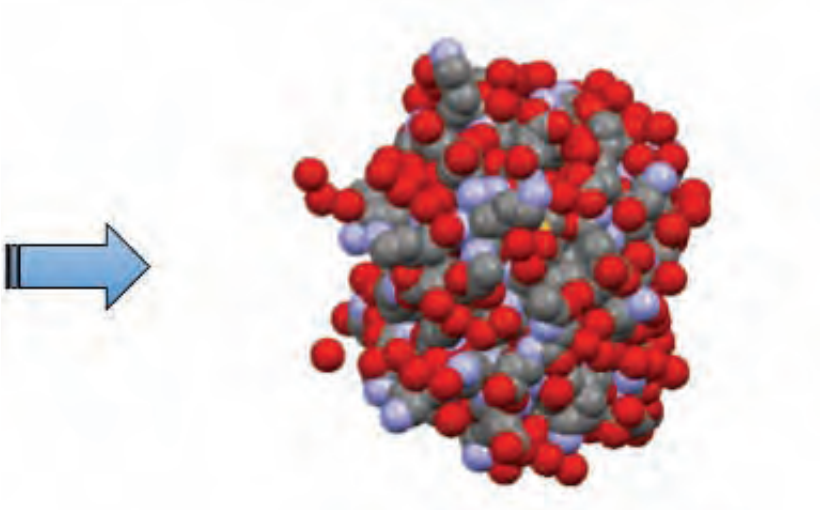

cytochrome *c*, for example, appears to play a role in both electron transport, which generates energy for a living cell, and also in apoptosis, a cell's decision to undergo programmed cell death. These two apparently opposing functions may be mediated by differently folded or partially unfolded states of cytochrome *c* within a cell. Furthermore, in different species, small variations in the structure of cytochrome *c*, seem to be responsible for whether programmed cell death occurs. This suggests that differently folded states may have different activities in cells. Since cytochrome *c*'s compressibility has been shown to change during unfolding, the research team decided it would be a good model for their new compressibility measurement technique.

The strength of the method comes from using both NRVS and IXS to make the compressibility measurements. NRVS reveals the complete vibrational spectrum of a probe nucleus, in this case the targeted nucleus is the heme iron, ^{57}Fe. The vibrations of other atoms in the molecule are ignored by this method. Measurements using the low-energy part of the NRVS spectrum correspond to collective motions from which the Debye sound velocity is determined. Information from the IXS spectrum is used to determine the longitudinal sound velocity of the protein. Together, the Debye sound velocity and the longitudinal sound velocity are used to calculate compressibility of the protein by a series of related equations. From this, changes in the protein's volume and the motion of atoms in the protein can be determined.

Using these techniques, the researchers were able to measure the adiabatic compressibility of hydrated horse heart Fe (III) cytochrome *c* (Fig. 1). Their results show that this method agrees very well with dynamic simulations of compressibility proving the usefulness of the method and its sensitivity. Now that they have shown the method works with proteins, the team will move on to other materials to demonstrate the almost limitless potential of their method. — *Sandy Field*

See: Bogdan M. Leu[1]*, Ahmet Alatas[1], Harald Sinn[2], E. Ercan Alp[1], Ayman H. Said[1], Hasan Yavaş[1], Jiyong Zhao[1], J. Timothy Sage[3], and Wolfgang Sturhahn[1], "Protein elasticity probed with two synchrotron-based techniques," J. Chem. Phys. **132**, 085103 (2010). DOI:10.1063/1.3332585
Author affiliations: [1]Argonne National Laboratory, [2]HASYLAB, [3]Northeastern University
Correspondence: *leu@aps.anl.gov

Support for the NRVS experiments was provided by the National Science Foundation Contract No. PHY-0545787. Use of the Advanced Photon Source, an Office of Science User Facility operated for the U.S. Department of Energy (DOE) Office of Science by Argonne National Laboratory, was supported by the U.S. DOE under Contract No. DE-AC02-06CH11357.

3-ID • XSD • Physics • High-pressure diamond anvil cell, inelastic x-ray scattering, nuclear resonant scattering • 7-27 keV, 14.41-14.42 keV • On-site • Accepting general users

IT'S MAGIC: FOLDING IN RIBOZYMES

The complexity of cellular machinery can be both breathtaking and bewildering. Nowhere does this seem clearer than in the construction of a ribozyme, an RNA enzyme critical to many cellular functions. Starting from the relatively simple one-dimensional RNA molecules, an elaborate time-dependent sequence of folding steps is necessary to produce the fully functioning ribozyme. When this sequence is disrupted and intact ribozymes are not produced, the entire chain of cellular production can be impeded or even brought to a halt. Because such a malfunction would result in a diseased cell, knowing exactly how ribozymes form is critical. The complexity of the folding process has been appreciated for some time, though that same complexity has left important details unknown. New data produced by a research team utilizing the Bio-CAT beamline 18-ID at the APS provide major breakthroughs in understanding ribozyme folding and have produced an elegant model of folding events in a bacterial ribozyme. The new data are widely applicable to knowing what causes ribozyme folding to go right — and wrong — in cells.

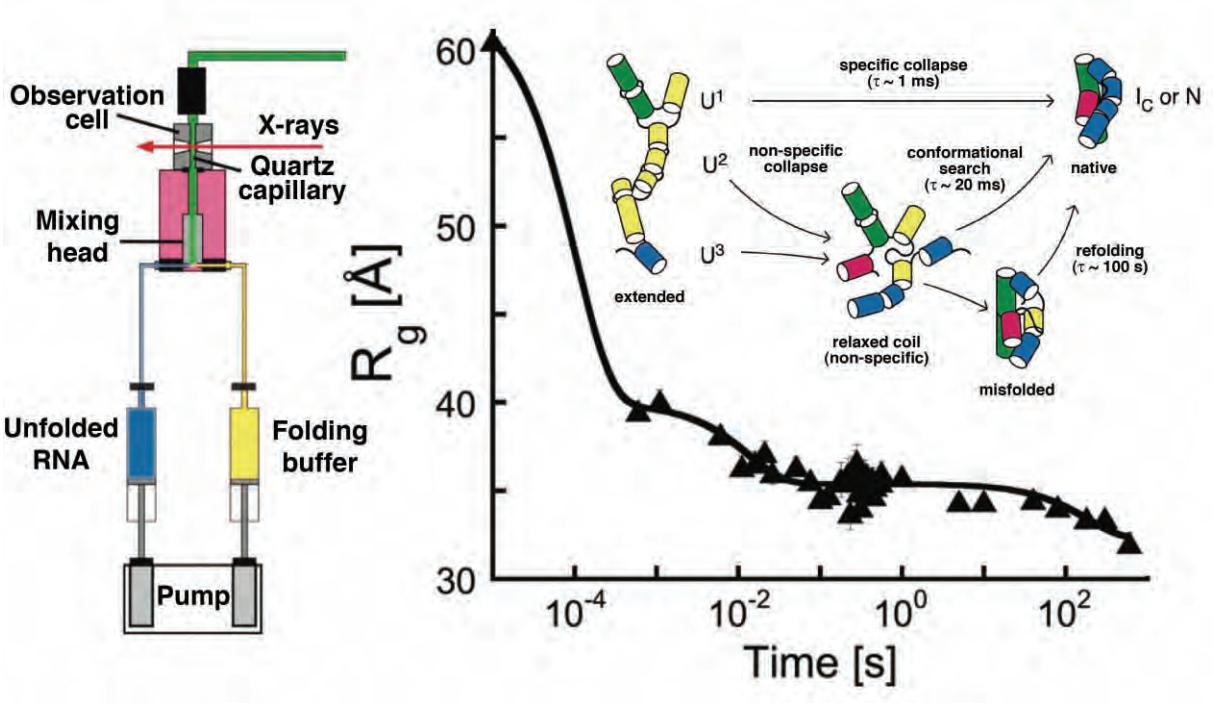

Fig. 1. Left panel: the measurement technique. Right panel: the resulting time-dependent model for ribozyme folding.

The new data are widely applicable to knowing what causes ribozyme folding to go right — and wrong — in cells

The researchers from the University of Maryland, Johns Hopkins University, the National Institute of Standards and Technology, and the Illinois Institute of Technology utilized stopped-flow small-angle x-ray scattering (SAXS) to study how a ribozyme from the bacterium *Azoarcus* folds. The team focused on what is known as collapse transition kinetics — how the RNA molecule reaches its final compact structure.

The structural changes that occur in the RNA are sequence-dependent and ion-dependent. In the first phase of creating the final three-dimensional RNA structure, the phosphate charge is neutralized by cations. Then the unfolded molecules collapse into a compact structure. It is the exact way in which the collapse occurs that determines the structure of the intermediates and how long the collapse takes. The SAXS technique is well suited to this type of event because it can give information of the overall structure — even a very complicated one — as time proceeds.

The research unveiled a complex folding system in the bacterial ribozymes under study (Fig. 1). There are multiple folding pathways that progress at different speeds. The ionic concentration, in the form of magnesium ions, determines how the pathways are separated from one another and affects how quickly the collapse occurs. There is a rapid pathway that collapses the molecules in less than 1 msec, a time span similar to that measured in the catalytic domain of a different type of RNA enzyme but at least ten times shorter than had been reported in a more closely related ribozyme.

The researchers were able to experimentally alter the way in which the folding occured. When the RNA interactions were partly denatured, or weakened, more RNA partitioned into the fast phase of folding. This result suggests that the heterogeneity of the RNA when unfolded is at least partly responsible for the varying folding mechanisms. It also suggests that the slower phases of folding, those that take longer than 1 msec, are produced by a rearrangement of intermediate structures in the folding process.

There is a preferred collapse mechanism and it depends on the magnesium ion concentration and the amount of neutralization it produces. There is, as well, a set of molecular interactions in the unfolded molecule that contributes to the heterogeneity; this results in multiple folding arenas en route to the final folded molecule.

Using their data, the research team was able to construct a model for folding of the ribozyme in which subpopulations fold in one of three ways: rapid triggering of the three-dimensional interactions, non-specific collapse that precedes short-range structural arrangements, or refolding of misfolded structures. The system is best imagined as a folding landscape that can be influenced by weakening interactions along the RNA chain before folding begins. Once folding begins, the magnesium ion concentration has primary influence on how molecules partition on the folding landscape. Thus, electrostatic interactions are of great importance in determining how the final three-dimensional ribozyme is created.

The complexity of the folding system that produces the final functioning ribozyme still seems magical but, thanks to the insights achieved by the research team, the tricks will be a lot easier to understand and reproduce.

— *Mona Mort*

See: Joon Ho Roh[1,2,3]*, Liang Guo[4], J. Duncan Kilburn[2], Robert M. Briber[1]**, Thomas Irving[4], and Sarah A. Woodson[2]***, "Multistage Collapse of a Bacterial Ribozyme Observed by Time-Resolved Small-Angle X-ray Scattering," J. Am. Chem. Soc. **132**, 10148 (2010). DOI:10.1021/ja103867p

Author affiliations: [1]University of Maryland, [2]Johns Hopkins University, [3]National Institute of Standards and Technology, [4]Illinois Institute of Technology

Correspondence:
*rohmio1973@gmail.com
**rbriber@umd.edu
***swoodson@jhu.edu

This work was supported by the National Institute of Standards and Technology and by the National Institutes of Health (NIH) (GM60819 to S.W.). BioCAT is an NIH-supported Research Center RR-08630. Use of the Advanced Photon Source, an Office of Science User Facility operated for the U.S. Department of Energy (DOE) Office of Science by Argonne National Laboratory, was supported by the U.S. DOE under Contract No. DE-AC02-06CH11357.

18-ID • Bio-CAT • Life Sciences • Fiber diffraction, microdiffraction, microfluorescence (hard x-ray), small-angle x-ray scattering, time-resolved x-ray scattering, micro x-ray absorption fine structure • 3.5-35 keV • On-site • Accepting general users

Arsenic and Old Mane

A decades-old mystery has been solved by researchers utilizing the XSD 20-ID and 2-ID-E beamlines at the APS. The world-famous Australian racehorse Phar Lap, dead since 1932, has finally been shown to have been the victim of arsenic poisoning. This work underscores the ability of synchrotron x-ray science to measure minute traces of materials in a wide range of media, which has far-reaching applications in disciplines as diverse as forensics, agriculture, and the life and health sciences to name just a few.

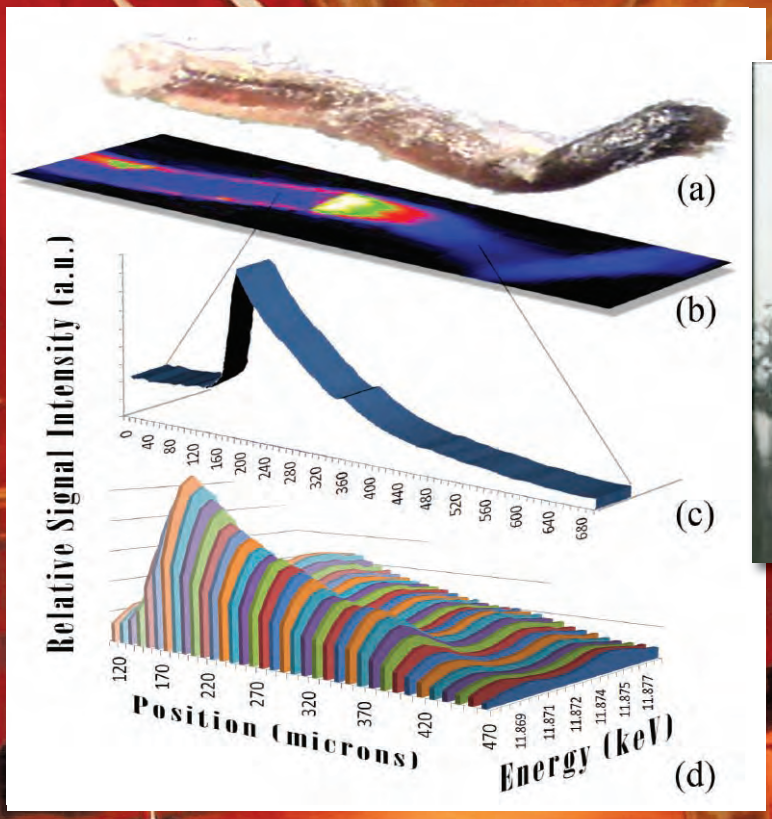

The racehorse Phar Lap looms large in Australians' minds, even though he died nearly 80 years ago. The "Red Terror," as he was known, won 37 of 51 starts. Phar Lap was brought to North America at the age of six, spending three weeks on board an ocean going vessel. He won the era's richest prize, the mile-and-a-quarter Agua Caliente Handicap in Mexico, by two lengths in a course-record time of 2:02 4/5. But just two weeks later he was dead. Phar Lap's death was so sudden, painful, and mysterious that questions about it are still being asked...and answered.

Phar Lap's last hours were spent in California vomiting blood and suffering from severe abdominal pain and fever. Only a few hours after he was discovered ill, Australia's "Wonder Horse" hemorrhaged to death. Autopsies found gastrointestinal inflammation; arsenic poisoning was considered a possibility. Speculation also blamed acute colic or an overdose of arsenic-based tonic, which was given to racehorses to improve performance. In the 1980s a previously unknown form of bacterial gastroenteritis was identified and blamed for the death.

But it was murder that captured the public's imagination. Phar Lap had been the target of a failed shooting in 1930 (he won the Melbourne Cup later that day). In California, U.S. gangsters might have wanted him dead to prevent big losses to their illegal bookmaking. At the time of the autopsy, the arsenic concentration in the horse's organs was thought to be too low. Phar Lap also didn't sufferer from diarrhea, although it is now known that not all victims of arsenic poisoning do.

Could modern analytical techniques be used to solve the mystery? Researchers from Academia Sinica, the University of South Australia, and Museum Victoria, including an expert in hair analysis, sought a solution. Fortunately, the horse's hide was preserved in the Museum Victoria, Australia, and four hairs that had been growing at the time of the horse's death were selected for analysis. (His heart is preserved in the National Museum of Australia, and his skeleton in New Zealand.) Many ingested substances enter into the bloodstream and accumulate in a growing hair, so the scientists hoped that a longitudinal analysis of the hairs would reveal a history of the substances to which the horse was exposed. The team created a longitudinal map of arsenic in the four hairs, utilizing synchrotron x-ray fluorescence microprobe (XRF) along with the ca. 10 x 10 μm, 12-keV beam at 20-ID. Besides low concentrations of arsenic all along the length the hairs, a very high concentration of the poison was found in the subcutaneous region a bit up from the root. Based on the mane hair growth rate, this indicated a spike in arsenic about 30 to 40 hours before Phar Lap's death, and then decay by metabolism or excretion. Arsenic was generally present in much lower concentrations, indicating that the hide had been preserved using an arsenic-based compound.

To find out the source of the arsenic spike, the group again turned to beamline 20-ID and performed x-ray absorption near edge spectroscopy analysis of the arsenic-rich regions and revealed two arsenic species (Fig. 1). The pronounced peak was arsenic glutathione, which was from ingestion. The arsenate peak was smaller but longer lived, indicating that it was a metabolite. The researchers could thus conclude that Phar Lap ingested a large amount of arsenic not long before his death.

Also obtained (utilizing the XSD 2-ID-E beamline at the APS) were micro XRF maps of hair cross-sections microtomed to 1-μm thick from the arsenic-rich region of the hair. These maps show that arsenic is also distributed within the cortex and in the outer root sheath of the hair.

Could the Phar Lap poisoning have been accidental? Arsenite herbicides could have been in his feed, but no other horses in the same barn became ill. Faint traces of arsenic throughout the Phar Lap's hairs indicates that he had received a steady dose of arsenic tonic, but the intensity of the prominent band indicates a large jump in arsenic ingestion.

Although it seems certain that the legendary racehorse was poisoned, history will probably never know who killed Phar Lap. — *Dana Desonie*

< *Far left:* A chemical map along a hair shows the history of that compound in the organism's blood if the compound is there due to ingestion. (a) An optical image of one of the mane hairs that were analyzed (b) An x-ray microprobe image showing the distribution of internal arsenic, (c) The spike in arsenic and its decay, (d) A 2-D XANES map showing arsenic glutathione in front and arsenate in the back. I.M. Kempson and D.A. Henry, Angew. Chem. Int. Ed. **49**, 4237 (2010). ©Wiley-VCH Verlag GmbH & Co. KGaA. Reproduced with permission.
Near left: Frame from a video showing Phar Lap winning the Agua Caluiente, which can be seen at http://tinyurl.com/3mhyovw
Background: Phar Lap's hide on display in the Museum Victoria. Photo: http://travel.webshots.com/photo/2448623210098114439TnzDgp

See: Ivan M. Kempson[1,2]* and Dermot A. Henry[3], "Determination of Arsenic Poisoning and Metabolism in Hair by Synchrotron Radiation: The Case of Phar Lap," Angew. Chem. Int. Ed. **49**, 4237 (2010).
DOI:10.1002/anie.200906594
Author affiliations: [1]Academia Sinica, [2]University of South Australia, [3]Museum Victoria
Correspondence:
*ivan.m.k@hotmail.com

This work was supported by the Victorian Governments' Department of Innovation, Industry and Regional Development, and the Australian Synchrotron Research Program, funded by the Commonwealth of Australia under the MNRFP. Use of the Advanced Photon Source, an Office of Science User Facility operated for the U.S. Department of Energy (DOE) Office of Science by Argonne National Laboratory, was supported by the U.S. DOE under Contract No. DE-AC02-06CH11357.

2-ID-E • XSD • Environmental science, life sciences, materials science • Microfluorescence (hard x-ray) • 7-10.5 keV, 11-17 keV • On-site • Accepting general users

20-ID • XSD • Chemistry, environmental science, geoscience, materials science • Microfluorescence (hard x-ray), small x-ray absorbtion fine structure, surface diffraction, time-resolved x-ray absorption fine structure, x-ray absorption fine structure, x-ray emission spectroscopy, x-ray Raman scattering • 4.3-27 keV, 7-50 keV • On-site • Accepting general users

A Gene Therapy Virus Gets X-ray Treatment

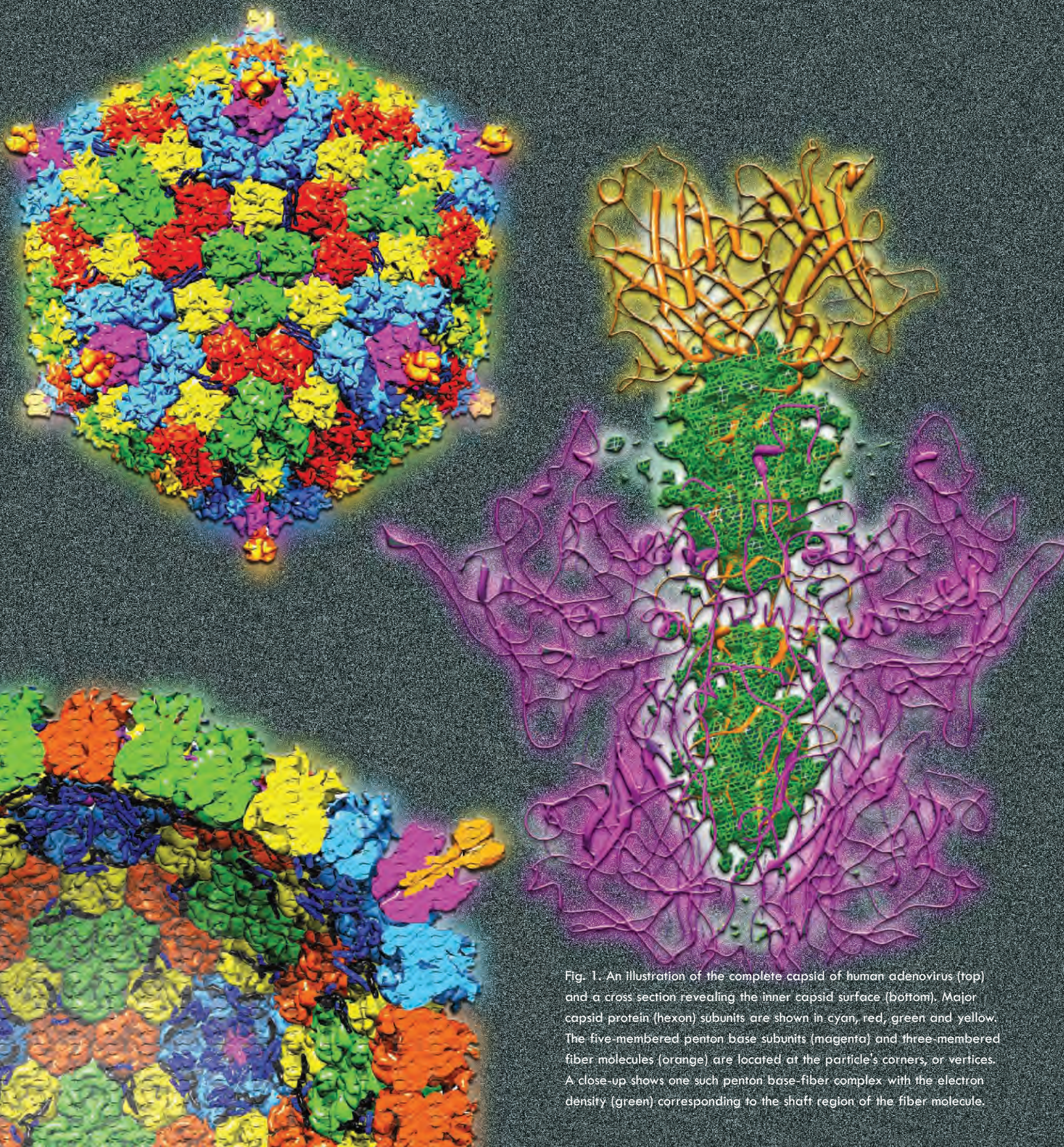

Fig. 1. An illustration of the complete capsid of human adenovirus (top) and a cross section revealing the inner capsid surface (bottom). Major capsid protein (hexon) subunits are shown in cyan, red, green and yellow. The five-membered penton base subunits (magenta) and three-membered fiber molecules (orange) are located at the particle's corners, or vertices. A close-up shows one such penton base-fiber complex with the electron density (green) corresponding to the shaft region of the fiber molecule.

For two decades, scientists have struggled with the challenges presented by engineering human viruses capable of replacing defectives genes with functioning ones — a method known as gene therapy. Researchers studied the human adenovirus, which causes respiratory, eye, and gastrointestinal infections. But detailed information about the biological mechanisms by which adenovirus infects cells hindered the efforts. Now, scientists utilizing two U.S. Department of Energy x-ray research facilities have reported the three-dimensional structure of human adenovirus at atomic resolution, the largest high-resolution structure ever determined, by a factor of two. These results may improve the outcomes of adenovirus gene therapy, which accounts for approximately one quarter of current gene therapy trials, or lead to treatments for adenovirus infections, for which no medications currently exist.

The challenges range from failures of promising clinical trials to reverse cystic fibrosis in the early 1990s to the 1999 death of 18-year-old Jesse Gelsinger, whose body reacted to a live virus designed to correct a genetic defect by mounting a lethal immune response that left his liver unable to metabolize ammonia.

In these well-known cases, researchers had worked with human adenovirus, which causes respiratory, eye, and gastrointestinal infections, but ignorance of the detailed biological mechanisms by which adenovirus infects cells most likely contributed to the failures. Hoping to reverse these trends, scientists from The Scripps Research Institute and the Vanderbilt University Medical Center, using the GM/CA-CAT 23-ID-D beamline at the APS, reported the three-dimensional structure of human adenovirus at atomic resolution, showing the key contacts responsible for holding the virus's individual protein pieces together into a single unit, called a capsid (Fig. 1).

Consisting of some one million amino acids (protein subunits), the adenovirus capsid structure is the largest high-resolution structure ever determined, by a factor of two. The capsid has the structure of an icosahedron, or 20-faceted polygon, and it surrounds a piece of DNA that contains instructions for building new copies of the virus. When exposed to a host cell, the capsid latches onto protein receptors studding the cell and disassembles in such a way that the DNA enters the cell, where it hijacks the machinery responsible for building new proteins and instructs it to make more viruses.

Since Jesse Gelsinger's death, gene therapy researchers have worked with a crippled version of the virus, capable of entering the cell and delivering DNA containing a functioning copy of a human gene, but unable to instruct the cell to make new virus. By understanding the details of how the virus enters the cell, researchers may be able to make the process more efficient and target it to specific tissues in the body such as the heart, lungs, or liver.

Earlier attempts to solve the structure of human adenovirus had failed because of long spoke-like fibers sticking out of the vertices (corners) of the capsid. The research team succeeded in growing a form of the virus with short protruding fibers that was stable enough to form high-quality crystals.

A first round of x-ray studies at the Advanced Light Source at Lawrence Berkeley National Laboratory resolved the crystal to about 10 Å, or roughly the width of several atoms, while a second round of studies at APS achieved a resolution of 3.5 Å.

Of particular interest were the capsid's corners (Fig. 1), where the virus makes contact with the surface of its host cell. Each corner consists of five identical proteins arranged like a donut, one from each adjacent face of the icosahedron. In addition to the corners, the three-dimensional structure showed the positions of the large hexagonal pieces that make up most of the capsid and give it its strength.

The Scripps-Vanderbilt team hopes that future research will uncover how to stop the virus from disassembling – perhaps leading to treatments for adenovirus infection – and to engineer viruses that disassemble in some tissues but not others. If the latter work proves successful, then perhaps the promise of gene therapy will someday be realized.

— JR Minkel

See: Vijay S. Reddy[1]*, S. Kundhavai Natchiar[1], Phoebe L. Stewart[2], and Glen R. Nemerow[1]**," Crystal Structure of Human Adenovirus at 3.5 Å Resolution," Science **329**(5995), 1071 (27 August 2010). DOI: 10.1126/science.1187292

Author affiliations: [1]The Scripps Research Institute, [2]Vanderbilt University Medical Center
Correspondence:
**gnemerow@scripps.edu
*reddyv@scripps.edu

This work was supported by National Institutes of Health grants R01 AI070771 to V.S.R., HL054352 and EY011431 to G.R.N., and AI042929 to P.L.S. GM/CA-CAT has been funded in whole or in part with federal funds from the National Cancer Institute (Y1-CO-1020) and the National Institute of General Medical Science (Y1-GM-1104). Use of the Advanced Photon Source, an Office of Science User Facility operated for the U.S. Department of Energy (DOE) Office of Science by Argonne National Laboratory, was supported by the U.S. DOE under Contract No. DE-AC02-06CH11357.

See also: "Looking Inside Adenovirus," Stephen C. Harrison, Science **329**(5995), 1026 (27 August 2010).

23-ID-D • GM/CA-CAT • Life sciences • Large unit cell crystallography, macromolecular crystallography, microbeam, multi-wavelength anomalous dispersion, single-wavelength anomalous dispersion, subatomic (<0.85 Å) resolution • 5-20 keV • On-site • Accepting general users

Sticking Together: How Cells Do It

Fig. 1. Molecular architecture of the cadherin-catenin cell-cell adhesion complex. The image shows a hypothetical three-dimensional model of the cadherin-catenin complex containing the crystal structure of p120/E-cadherin juxta-membrane domain complex revealed in this study (red; PDB code 3L6X), along with previously determined crystal structures of the C-cadherin ectodomain *trans*-dimer (cyan and blue with Ca^{2+} (brown spheres); PDB code 1L3W) and the β-catenin/E-cadherin catenin-binding domain complex (yellow; PDB codes 1I7W and 1I7X). The background image shows MDCK cells stained for p120.

In order for healthy tissues to form and persist, cells need to come together in carefully calibrated ways. When this adhesion system doesn't work properly, disease including various forms of cancer can result. Malfunction of one set of adhesion proteins, known as cadherin-catenins, has been implicated in lack of adhesion, neurological disease, and some forms of gastric cancer. This important protein complex has been well studied with respect to structure and function, yet important data about how adhesion actually occurred were still missing. Thanks to research carried out at the SBC-CAT 19-BM x-ray beamline at the APS, important structural data on the cadherin-catenin complex are now available. The researchers in this study have constructed models for dynamic and static interactions among critical components of the cadherin-catenin complex. Their work greatly aids our understanding of what happens when cell adhesion does, and does not, function correctly.

The researchers, from the Ontario Cancer Institute; the University of Toronto; and the University of California, San Francisco, studied the cadherin-binding protein p120 catenin (p120), which had previously been shown to be critical for regulating cell-cell adhesion at meeting points called adherens junctions. Much data pointed to p120 as being a kind of gatekeeper for cadherin regulation in vertebrates. The importance of this interaction was implicated by an interesting conservation of structure of the p120-cadherin interaction region across taxa. The p120 catenin associates with the juxta-membrane domain of the cadherin cytoplasmic tail to provide surface stability for cell-cell adhesion. Since loss of E-cadherin expression is a major characteristic of tumor malignancy, studying p120 is one way to further understand tumor metastasis. Recent data had shown that an E-cadherin mutation was linked to hereditary diffuse gastric cancer. Using those results as a starting point, the team asked whether such mutations could be impairing adhesion by disrupting the p120-E-cadherin interaction.

By determining the crystal structure of the p120 catenin when attached to the E-cadherin tail, the researchers were able to glean important insights about how adhesion actually occurs. Their work provided the first examination of the three-dimensional architecture of p120 and, at the same time, revealed fine details about how p120 interacts with cadherin. The data allowed (also for the first time) the visualization of the entire cadherin-catenin complex (Fig. 1). Providing an even more detailed understanding of the interaction, mutational analyses allowed the team to identify which p120 regions were absolutely required for interaction and which were not. Since the interaction complex involves many other binding partners, the data also support creation of hypotheses for future work about how p120 interacts with other associated proteins.

An area of the p120 protein called the "armadillo repeat domain" has binding pockets that are electrostatically and hyrdrophobically complementary to the cadherin's juxta-membrane domain. The interaction is so carefully calibrated that, for both cultured epithelial and neuronal cells, the team was able to disrupt p120 binding by introducing single mutations in the site it uses to bind to both E- and N-cadherins. By performing further analysis with the p120 mutations, the researchers distinguished steps in synapse development as being either N-cadherin dependent or independent.

Using nuclear magnetic resonance studies, the researchers showed that p120 performs its role of stabilizing cadherin-mediated cell-cell adhesion by using both its "static" and "dynamic" binding sites to associate with most of the cadherin juxta-membrane domain. Though the roles of the static and dynamic sites appear to differ, they are both critical for proper functioning of p120. The team was also able to propose a mechanism for cadherin clustering that involves, in an interesting two-way interaction, assembly of p120 that is induced by cadherin's juxta-membrane domain.

The researchers in this study have provided long-sought data on how p120 catenin interacts with cadherins to promote healthy cell-cell adhesion. Questions about how and why cell adhesion malfunctions to create disease will now be much easier to answer. — *Mona Mort*

See: Noboru Ishiyama[1], Seung-Hye Lee[3], Shuang Liu[1], Guang-Yao Li[1], Matthew J. Smith[1], Louis F. Reichardt[3], and Mitsuhiko Ikura[1,2]*, "Dynamic and Static Interactions between p120 Catenin and E-Cadherin Regulate the Stability of Cell-Cell Adhesion," Cell **141**, 117 (April 2, 2010). DOI:10.1016/j.cell.2010.01.017
Author affiliations: [1]Ontario Cancer Institute, [2]University of Toronto, [3]University of California, San Francisco
Correspondence:
*mikura@uhnres.utoronto.ca

This work was supported by the grants from the Canadian Cancer Society (M.I.) and the Simons Foundation (L.F.R.). N.I. is a recipient of a Canadian Institutes of Health Research postdoctoral fellowship. S.-H.L. was supported by a Larry L. Hillblom Foundation fellowship. M.I. holds a Canada Research Chair in Cancer Structural Biology. Use of the Advanced Photon Source, an Office of Science User Facility operated for the U.S. Department of Energy (DOE) Office of Science by Argonne National Laboratory, was supported by the U.S. DOE under Contract No. DE-AC02-06CH11357.

19-BM • SBC-CAT • Life sciences • Multi-wavelength anomalous dispersion, single-wavelength anomalous dispersion, ultra-low-temperature (15K) • 6-13.5 keV • On-site, remote, mail-in • Accepting general users

How Ebola virus Evades the Immune System

The human immune system, which has evolved in the presence of wily immune invaders such as bacteria and viruses, has very specific and effective means of recognizing these intruders and eliminating them before they can cause too much harm. In response, some invaders have developed ways to get around the immune system, sometimes with terrible consequences for the human hosts. One of these is the Ebola virus, which causes an often fatal hemorrhagic fever in humans. Recent studies have suggested that the interferon inhibitory domain (IID) of the Zaire ebolavirus protein VP35 (Fig. 1) is responsible for this evasion through its ability to subvert the immune system's recognition of double stranded (ds) RNA molecules that alert the immune system to viral invasion. Structural studies carried out at the SBC-CAT 19-ID beamline at the APS explain how VP35 binds to dsRNA, which amino acids are important in these interactions, and how this inhibits the immune system. These fundamental details about the way viruses evade the immune system and important information about *ebolavirus* infection can be used to design treatments or vaccines against this virus that is highly pathogenic and a potential tool for bioterrorism.

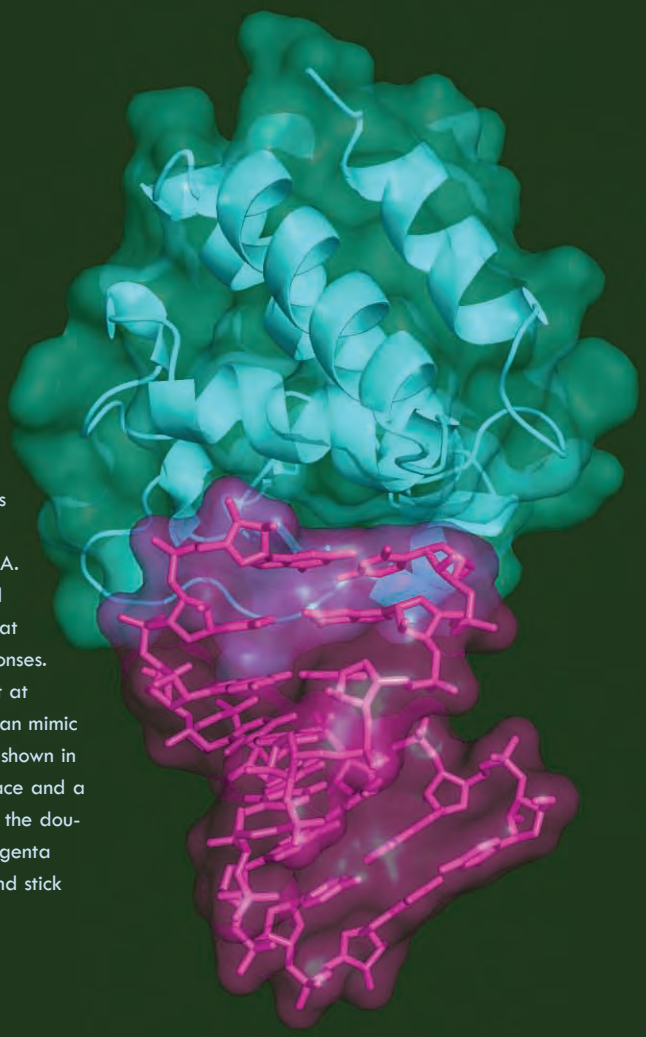

Fig. 1. *Ebolavirus* VP35 protein mimics RNA recognition by cellular RIG-I like receptors. VP35 interferon inhibitory domain forms an "end-cap" that binds at the blunt end of double-stranded RNA. A similar interaction mode is used by cellular RIG-I like receptors that activate host innate immune responses. New structural studies carried out at Sector 19 show that viral VP35 can mimic cellular proteins. VP35 protein is shown in cyan (transparent molecular surface and a cartoon secondary structure) and the double stranded RNA is shown in magenta (transparent molecular surface and stick representation).

As with all important studies, this work was the culmination of many years of work by a number of laboratories. For example, it was already known that VP35 was important for antagonizing the innate immune system, bound to dsRNA, and that a single amino acid change could inhibit VP35's ability to antagonize the immune system. The single amino acid, Arginine(Arg) 312, was then shown to be crucial for dsRNA binding and the structure of VP35, solved in 2009 by this group, showed that Arg 312 was in a region of the protein containing a patch of basic amino acids (Fig. 2). Recent evidence suggested that the host pathway inhibited by Ebola was the RIG-I-like receptor pathway that recognizes dsRNA and activates the production of interferon to alert the immune system. With all of this evidence for the role of dsRNA binding by VP35 in host immune evasion, the group set out to prove how the virus does it.

The structure of the VP35 IID in complex with a short stretch of dsRNA was solved by molecular replacement. This demonstrated conclusively that the central basic region in the β-sheet structure of VP35 IID was important for dsRNA binding. Identification of important amino acids in this region involved in binding to the dsRNA backbone led them to also solve the structures for

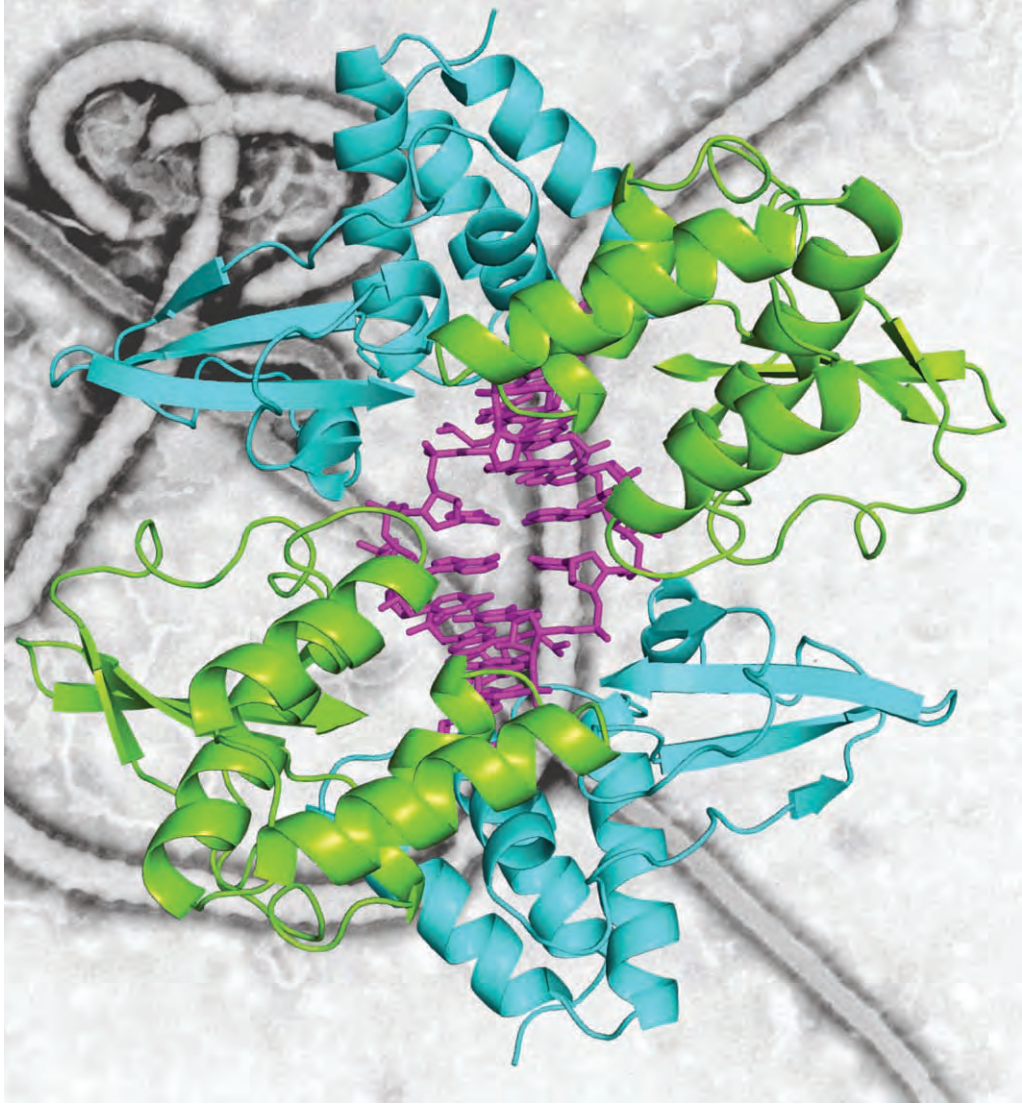

Fig. 2. *Ebolavirus* VP35 is a multifunctional virulence factor. Structure of Zaire Ebolavirus VP35 interferon inhibitory domain bound to double-stranded RNA reveals the structural basis of VP35-mediated immune evasion mechanisms (PBD: 3L25). Background: Transmission electron micrograph of Ebola virus virion. Image source: CDC/Frederick A. Murphy, Public Health Image Library #1833.

mutants of VP35 at two crucial sites, Arg312, and Lysine(Lys) 339. The structures of these two mutants showed that the basic surface of VP35 was not disrupted by the amino acid changes but that electrostatic distribution was changed significantly and this was the basis for disruption of dsRNA binding.

The structure also revealed that the blunt-end of the dsRNA is "capped" by VP35 in a hydrophobic pocket that mimics the binding of blunt-ended dsRNA by the RIG-I-like receptor of the host immune system. Mutation of one of these hydrophobic amino acids, Phenylalanine (Phe) 239, abolished dsRNA binding in RNA binding assays.

Next, the group tested their hypothesis in a cell culture assay for inhibition of immune activation. While the native VP35 was able to suppress immune activation, the mutants of VP35 at sites important for recognizing dsRNA ends and those with mutations in the basic patch important for dsRNA backbone binding were unable to suppress the immune responses. Moreover, the complex structure also identified residues important for protein-protein interactions, which may function through inhibition of signaling events downstream of RIG-I-like receptors, suggesting that VP35 may play a role in dsRNA-independent suppression of immune responses as well.

Further elucidation of these dsRNA-independent mechanisms and exploitation of the knowledge derived here for vaccine and antiviral development will be the topic of future studies.

— Sandy Field

See: Daisy W. Leung[1], Kathleen C. Prins[2], Dominika M. Borek[3], Mina Farahbakhsh[1], JoAnn M. Tufariello[2], Parameshwaran Ramanan[1], Jay C. Nix[4], Luke A. Helgeson[1], Zbyszek Otwinowski[3], Richard B. Honzatko[1], Christopher F. Basler[2], and Gaya K. Amarasinghe[1]*, "Structural basis for dsRNA recognition and interferon antagonism by Ebola VP35," Nat. Struct. Mol. Biol. **17**(2), 165 (February 2010). DOI: 10.1038/nsmb.1765

Author affiliations: [1]Iowa State University, [2]Mount Sinai School of Medicine, [3]University of Texas Southwestern Medical Center, [4]Lawrence Berkeley National Laboratory

Correspondence:
*amarasin@iastate.edu

Use of the Argonne National Laboratory SBC-CAT beamlines at the APS was supported by the U.S. Department of Energy (DOE) under Contract No. DE-AC02-06CH11357. This work is supported by U.S. National Institutes of Health grants (1F32AI084324 to D.W.L., R01GM053163 to Z.O., R01NS010546 to R.B.H., R01AI059536 and AI057158 (Northeast Biodefense Center-Lipkin) to C.F.B. and R01AI081914 to G.K.A.), a Midwest Regional Center of Excellence Developmental grant (U54AI057160-Virgin(PI) to G.K.A.) and the Roy J. Carver Charitable Trust (09-3271 to G.K.A.). Use of the Advanced Photon Source, an Office of Science User Facility operated for the U.S. DOE Office of Science by Argonne National Laboratory, was supported by the U.S. DOE under Contract No. DE-AC02-06CH11357.

19-ID • SBC-CAT • Life sciences • Large unit cell crystallography, macromolecular crystallography, microbeam, multi-wavelength anomalous dispersion, single-wavelength anomalous dispersion, subatomic (<0.85 Å) resolution, ultra-low-temperature (15K) • 6.5-19.5 keV • On-site, remote, mail-in • Accepting general users

NATURE AS ARCHITECT: BUILDING CELLULAR COMPARTMENTS

Keeping the good and pitching out the bad is one activity that makes cells run efficiently. And if the substances deemed unwanted or toxic can't be thrown out immediately, they can be put into "compartments" for degradation or later ejection. Understanding how cells build such compartments is critical to knowing how toxic substances are metabolized before they damage important components of the cell — a situation that could lead to disease. A team of researchers, with the help of the NE-CAT beamline 24-ID-C at the APS, has obtained a much clearer picture of the structure and assembly of a bacterial cellular compartment.

Much is already known about how viruses build their breathtakingly beautiful outer structures. Now, recent studies on bacterial cells have revealed internal compartments that bear an architectural resemblance to viral coats. Like virus coats, the shells of these bacterial compartments have been shown to be composed of proteins, but knowledge of which proteins and how they are assembled is still badly needed.

The researchers from the University of California, Los Angeles focused on proteinaceous microcompartments in the bacterium *Escherichia coli*. These compartments are also known as organelles to indicate their status as little organs. As organelles, the compartments carry out specific functions, such as metabolism of volatile or toxic substances, in a semi-autonomous state from the rest of the cell. The researchers chose to study the ethanolamine utilization (Eut) microcompartment because it had been shown to metabolize ethanolamine without releasing the toxin acetaldehyde into the cell. The presence of microcompartment organelles in bacteria is especially significant, as organelles are generally thought of as being present only in eukaryotic cells, such as plants and animals.

The team studied the proteins that make up the shell of the microcompartment, known as bacterial microcompartment (BMC) proteins, because the correct assembly of the shell is critical to proper functioning of the compartment in its metabolism of ethanolamine. In addition, this particular ethanolamine-metabolizing organelle has been shown to be present and active in many other types of bacteria, such as *Salmonella*.

The researchers have now unveiled the three-dimensional (3-D) crystal structures of the BMC proteins from *E. coli*: EutS, EutL, EutK, and EutM. The four Eut proteins are closely related and have similar 3-D folds but they differ in important ways that explain their specific functions in the microcompartment. One example of differing function is the EutL protein, which undergoes a change in shape that allows it to facilitate molecular transport through the shell protein pores (Fig. 1). Another example is the EutK protein, which has a structure suggesting binding of a nucleic acid component.

By studying the structures of the shell proteins and then comparing those structures to closely related proteins in *Salmonella*, in which functional studies had already been conducted, the research team proposed a mechanism for assembly of the shell of the microcompartment. Much like the geometric beauty found in virus coats, the assembled shells of three (EutS, EutL, EutM) of the BMC proteins take on a hexameric shape, which is repeated in a pleasing symmetry. The EutK protein does not form hexamers in solution, suggesting that it exists as a mixed hexamer in the cell, and it also has an extra domain that is probably related to its proposed nucleic-acid binding role. That the Eut compartment shell could bind nucleic acid gives it a functional similarity to viral shells, which take up viral DNA.

This research team has shown that the shell of the bacterial microcompartment is complex and actively involved in the metabolic function of the organelle, in this case metabolism of ethanolamine in such a way as to prevent its byproducts from becoming toxic to the cell. What might have been considered a simple cellular inclusion is, on careful inspection, a complex organelle. The work shows how form and function are related in a critical manner for proper metabolic functioning in cells. — *Mona Mort*

See: Shiho Tanaka, Michael R. Sawaya, and Todd O. Yeates*, "Structure and Mechanisms of a Protein-Based Organelle in *Escherichia coli*," Science **327**, 81 (1 January 2010). DOI:10.1126/science.1179513
Author affiliation: University of California, Los Angeles
Correspondence:
*yeates@mbi.ucla.edu

This work was supported by the Biological and Environmental Research program of the U.S. Department of Energy (DOE) Office of Science and by NSF grant MCB-0843065. Use of the Advanced Photon Source, an Office of Science User Facility operated for the U.S. DOE Office of Science by Argonne National Laboratory, was supported by the U.S. DOE under Contract No. DE-AC02-06CH11357.

See also: "Some Enzymes Just Need a Space of Their Own," by Sebyung Kang and Trevor Douglas, *Science* Perspectives, Science **327**(5961), 42 (1 January 2010). DOI: 10.1126/science.1184318

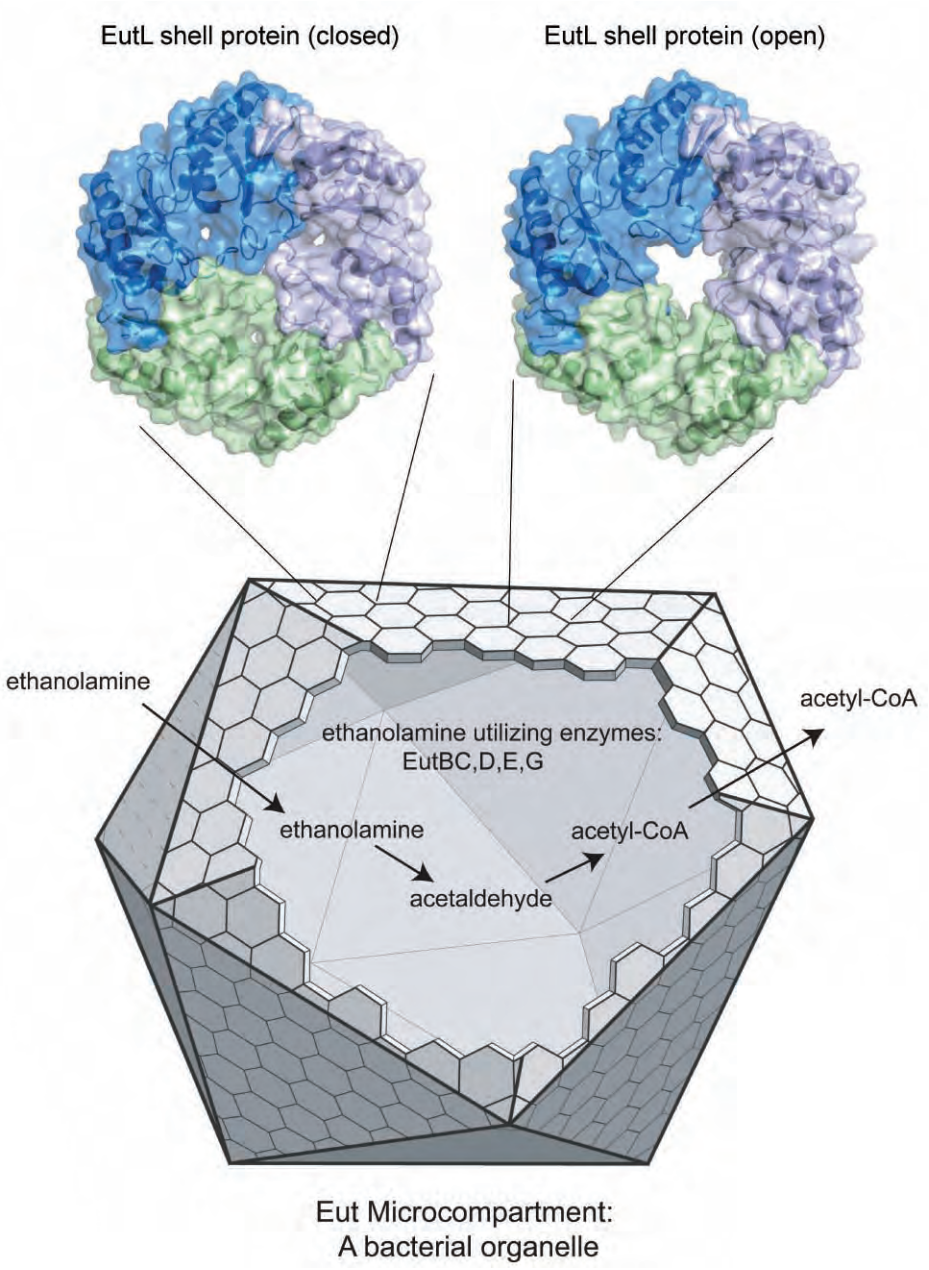

Fig. 1. Upper: The EutL shell protein in both closed and open conformations. Lower: The assembled Eut microcompartment showing the metabolic pathway for degradation of ethanolamine. Image courtesy of Todd Yeates, UCLA.

24-ID-C • NE-CAT • Life science • Macromolecular crystallography, microbeam, single-crystal diffraction, microdiffraction, single-wavelength anomalous dispersion • 6.5-23 keV • On-site • Accepting general users

The Machinery of Movement in Bacteria

Some bacteria are mobile — they can use a hair-like structure called a "flagellum" to gracefully make their way from point A to point B. The cellular machinery that makes up the flagellum and its motor is incredibly complex and awe-inspiring. Understanding this flagellar machinery is important not only for knowing about the biology of bacteria but also to gain a better understanding of bacteria that may be involved in human disease. Now, researchers utilizing x-ray beamlines at the APS and the European Synchrotron Radiation Facility have determined several important new pieces of information about the functioning of the flagellar motor.

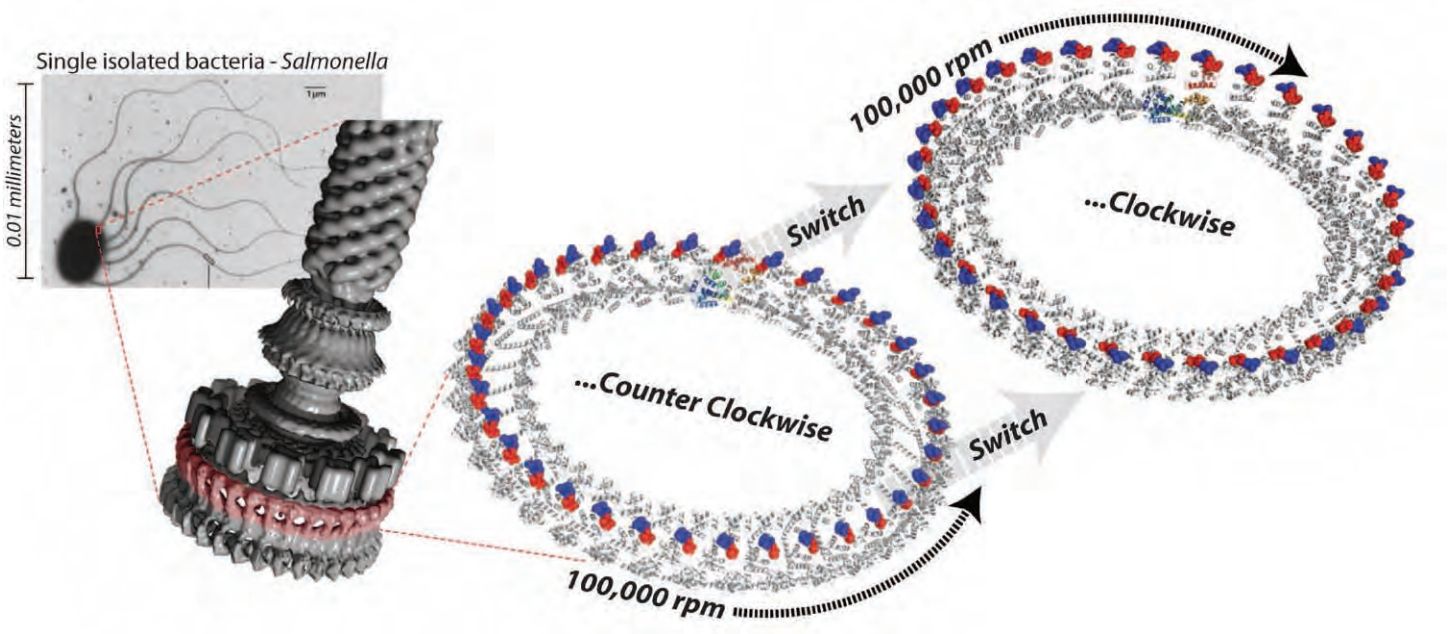

Fig. 1. The bacterial flagellar switching mechanism.

The flagellar motor is no lightweight. Rather, it is strong enough to propel the flagellum at hundreds of revolutions per second through dense liquids. Previous studies had shown that a switch in the motor's direction of rotation could determine if the bacterium continued to move smoothly or began to tumble when changing trajectory. But the molecular details of exactly how this switch operated were unknown. Using the BioCARS 14-ID and GM/CA-CAT 23-ID-D beamlines at the APS, and the European Synchrotron Radiation Facility beamline ID14-1, a research team from the Victor Chang Cardiac Research Institute, the MRC Laboratory of Molecular Biology, and the University of New South Wales has solved the mystery.

The researchers unveiled the molecular structure of the switch protein, shown how this protein changes shape to account for the rotational changes, and identified structural changes that are necessary for formation of the torque ring in the motor. Their data show what an exquisite piece of molecular engineering the bacterial rotational motor really is and add fine detail to current models of flagellar motors.

The flagellar filaments studied by the researchers are powered by an electrochemical gradient of cations across the cytoplasmic membrane (Fig. 1). This gradient generates torque that turns the flagellum in an anti-clockwise direction. To change direction, the rotation switches to clockwise, a change mediated by a sophisticated switching system. The main player in this switching mechanism is a protein called "FliG," which is involved in generating torque by forming a ring in the flagellar motor via interaction with another protein that forms cation-channels. FliG had been shown to be necessary for an intact flagellar motor. Though changes in the shape of FliG were thought to trigger switching, the structural and mechanistic details were missing. The research team set out to discover these details by determining the molecular structure of the full-length FliG protein (from *Aquifex aeolicus*) and then identifying how the FliG protein changed shape and formed a torque ring. The protein has three distinct regions, or domains, that are connected by two helices.

To understand the importance of the FliG shape changes, the researchers mapped mutations that were known to influence the flagellar motor's direction of rotation. These mutations clustered into three regions of the protein, suggesting three important areas of activity with respect to shape changes. One critical finding from these studies is that the closed conformation of the FliG protein is present during the default anticlockwise rotation and that the switch to clockwise rotation is accompanied by a change in FliG to its open conformation. Movement of FliG into its open conformation may involve dissociation in a certain loop domain and explain why nearly all mutations at that loop can bias the rotation direction.

The research team used their data to model the FliG ring and found that its diameter corresponded well to the ring in the flagellar motor where the switch resides. In addition, the model provides evidence for a reversal of electrostatic charges that accompanies the rotational switching of the flagellum's motor.

By carefully collecting new data and adding their findings to what was understood (or surmised) about the role of FliG in the rotational switching mechanism of bacterial flagella, the researchers have unraveled the inner workings of this fine piece of cellular machinery. Their model fits remarkably well with what was already known about the flagellar motor and, most important, smoothly moves our understanding of the switching mechanism many turns in the right direction.

— Mona Mort

See: Lawrence K. Lee[1], Michael A. Ginsburg[1], Claudia Crovace[2], Mhairi Donohoe[1], and Daniela Stock[1,3]*, "Structure of the torque ring of the flagellar motor and the molecular basis for rotational switching," Nature **466**, 966 (19 August 2010). DOI:10.1038/nature09300

Author affiliations: [1]The Victor Chang Cardiac Research Institute, [2]MRC Laboratory of Molecular Biology, [3]University of New South Wales
Correspondence:
*d.stock@victorchang.edu.au

Use of the BioCARS beamline was supported by the National Institutes of Health, National Center for ResearchResources (grant RR007707). GM/CA-CAT is funded in whole or in part with federal funds from the National Cancer Institute (Y1-CO-1020) and the National Institute of General Medical Science (Y1-GM-1104). This work was supported by the Australian Synchrotron Research Program of the Australian Nuclear Science Technology Organization. D.S. was initially funded by an MRC Career development award (UK) and C.C. by an MRC predoctoral fellowship (UK). Use of the Advanced Photon Source, an Office of Science User Facility operated for the U.S. Department of Energy Office of Science by Argonne National Laboratory, was supported by the U.S. DOE under Contract No. DE-AC02-06CH11357.

Go to http://tinyurl.com/3hflzh7 to view six animations derived from this study (see supplementary info; QuickTime required).

14-ID • BioCARS • Life sciences • Biohazards at the BSL2/3 level, Laue crystallography, macromolecular crystallography, time-resolved x-ray scattering, wide-angle x-ray scattering • 7-20 keV • On-site • Accepting general users

23-ID-D • GM/CA-CAT • Life sciences • Large unit cell crystallography, macromolecular crystallography, microbeam, multi-wavelength anomalous dispersion, single-wavelength anomalous dispersion, subatomic (<0.85 Å) resolution • 5-20 keV • On-site • Accepting general users

Size Doesn't Matter for Cytochrome P450

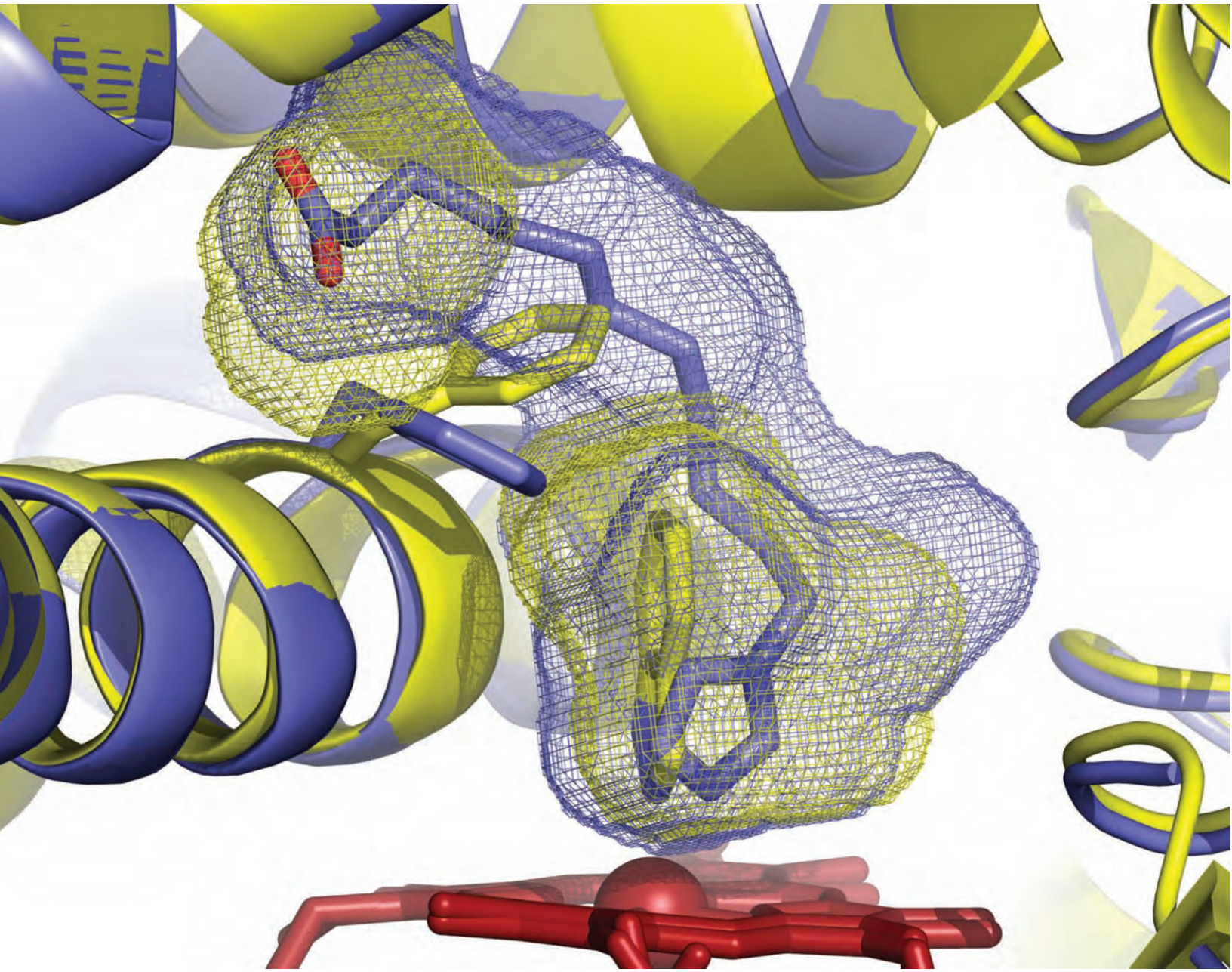

Fig. 1. When CYP2E1 (yellow ribbons) binds indazole (yellow sticks), it binds above the heme prosthetic group (red sticks) in a small enclosed active site (yellow mesh) separated from another small adjacent void (yellow mesh) by Phe298 (yellow sticks). However, when CYP2E1 binds an imidazolyl fatty acid analog (blue sticks), the overall backbone structure of the enzyme (blue ribbons) doesn't change, but Phe298 (blue sticks) rotates to merge the two indazole structure voids into one continuous cavity (blue mesh) to accommodate the fatty acid compound.

The cytochrome P450 (CYP) superfamily is responsible for the metabolism of many normal cellular compounds as well as foreign compounds such as drugs. In humans, nine members of this superfamily of enzymes are estimated to process up to 75% of pharmaceutical compounds, making them an important focus of clinical medicine. The CYP enzyme 2E1(CYP2E1) oxidizes more than 70 compounds, ranging from small-molecule drugs such as acetaminophen to larger molecules such as the long-chain fatty acid arachidonic acid, an important cellular signaling molecule. Previous work determined the structure of CYP2E1 in the presence of small-molecule substrates, but how the active site might also accommodate the long fatty acid substrates was unclear. To answer this question, a research team utilizing two U.S. Department of Energy x-ray light sources built on previous work by solving the co-crystal structures of CYP2E1 with three fatty acid analogs of varying chain length. This study provides new insights into the mechanism of action of this important class of enzymes.

One challenge faced by the researchers — from The University of Kansas and IMCA-CAT — in determining the structure of the enzyme bound to a fatty acid was to identify an appropriate fatty acid to co-crystallize with CYP2E1. Fatty acids consist of a head group of an acid at one end and a long hydrocarbon tail. The latter makes them relatively water-insoluble and difficult to work with under crystallization conditions that require millimolar concentrations of protein in an aqueous solution. In this case, addition of a carbon-nitrogen-containing ring called imidazole to the last carbon in the fatty acid tail increased the solubility, as well as causing an absorbance change that could be used to monitor ligand binding to the protein. Finally, imidazole addition encouraged the fatty acid analogs to bind in a single orientation corresponding to the major fatty acid metabolite observed experimentally. This is helpful because fatty acid ligands can bind CYP2E1 in multiple orientations, which are difficult to resolve with x-ray crystallography.

These substrate analogs, imidazole-containing fatty acid chains of 8, 10, and 12 carbons in length, were co-crystallized with CYP2E1 and their structures solved to 2.9 Å-, 2.7 Å-, and 3.1-Å resolution, respectively. The 10-carbon analog was solved at the IMCA-CAT 17-BM beamline at the APS; the 8- and 12-carbon analogs were solved at beamline 9-2 at the Stanford Synchrotron Radiation Light Source.

This work reveals the nature of a CYP2E1 active site that is dramatically expanded to accommodate these molecules. Furthermore, the binding mode is unlike that observed in other fatty acid-binding cytochrome P450 molecules. The structures all had the basic CYP fold and were overall very similar to the previous CYP2E1 structure, but the active site itself reveals dramatic changes when long chain fatty acids are bound. In the small molecule structure, the size of the active site was 190 $Å^3$, but when bound to fatty acids, the active site was more than doubled to 420 $Å^3$ for the 8-carbon compound, 440 $Å^3$ for the 10, and 473 $Å^3$ for the 12-carbon compound. This striking change in active site architecture is not the result of large scale changes in the structure of the enzyme but rather the rotation of a single amino acid, phenylalanine 298, which moves to merge the previously-identified small active site with an adjacent void between nearby helices in the protein (Fig. 1).

Studies on this enzyme have revealed a third, substantially different, active site topology when an inhibitor is bound. These remarkable changes in active site shape and volume are determined by the substrate that is present and make the prediction of drug substrate metabolism very difficult. For this reason, the researchers plan to solve additional structures of the enzyme with other substrates bound in order to understand its ability to oxidize 70+ different substrates. — *Sandy Field*

See: Patrick R. Porubsky[1], Kevin P. Battaile[2], and Emily E. Scott[1]*, "Human Cytochrome P450 2E1 Structures with Fatty Acid Analogs Reveal a Previously Unobserved Binding Mode," J. Biol. Chem. **285**(29), 22282 (July 16, 2010). DOI:10.1074/jbc.M110.109017

Author affiliations: [1]The University of Kansas, [2]Industrial Macromolecular Crystallography Association Collaborative Access Team

Correspondence: *eescott@ku.edu

Crystals were grown using the facilities of the Protein Structure Laboratory core facility at the University of Kansas (supported by National Institutes of Health Grant RR017708). The Stanford Synchrotron Radiation Laboratory is a national user facility operated by Stanford University on behalf of the U.S. Department of Energy Office of Basic Energy Sciences. Use of the IMCA-CAT beamline 17-BM was supported by the companies of the Industrial Macromolecular Crystallography Association through a contract with the Center for Advanced Radiation Sources at the University of Chicago. Use of the Advanced Photon Source, an Office of Science User Facility operated for the U.S. Department of Energy Office of Science by Argonne National Laboratory, was supported by the U.S. DOE under Contract No. DE-AC02-06CH11357.

17-BM • IMCA-CAT • Life sciences • Macromolecular crystallography, multi-wavelength anomalous dispersion, single-wavelength anomalous dispersion • 7.5 keV-14 keV • On-site, remote, mail-in • Accepting general users

Anatomy of a Viral Hijacking

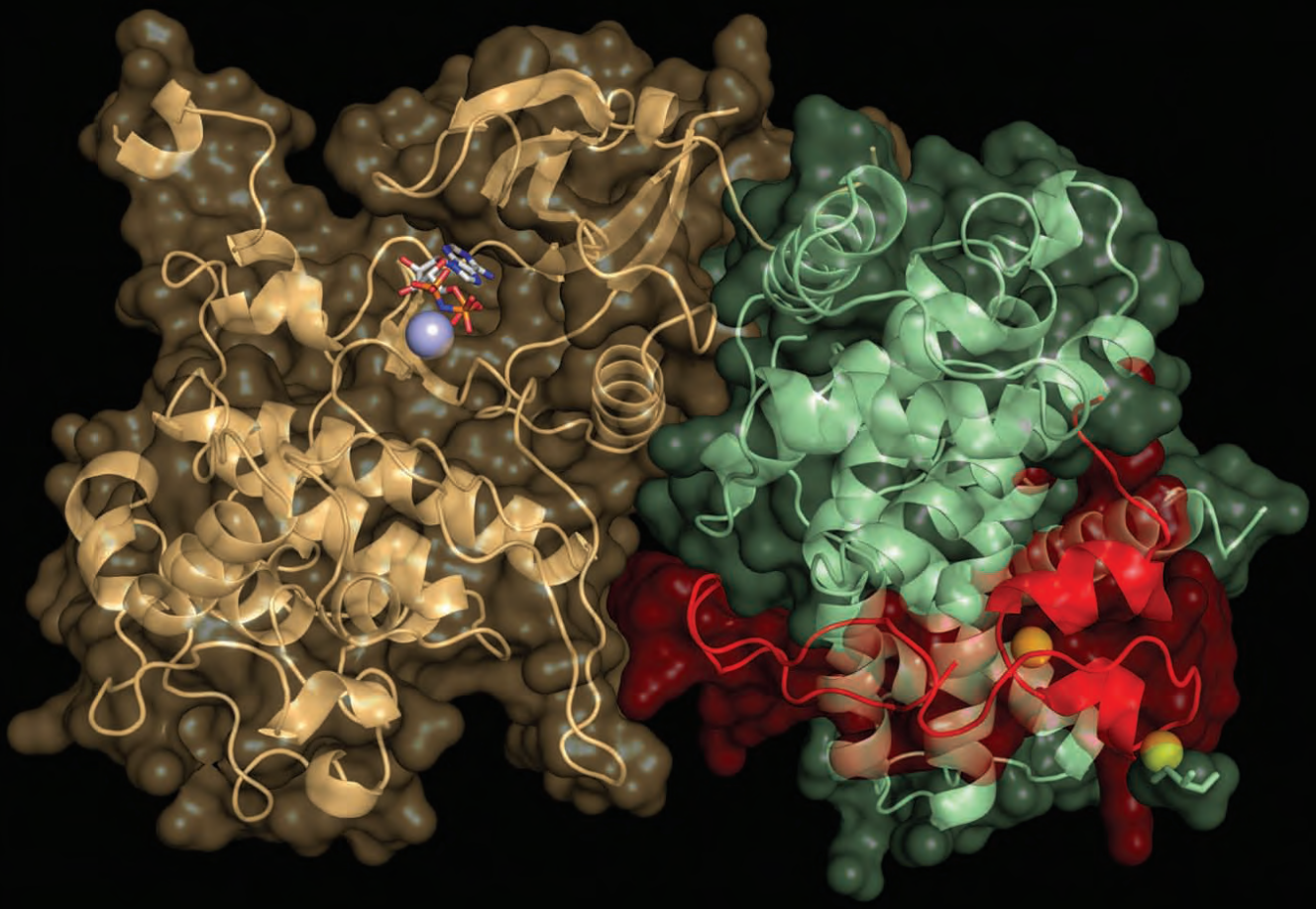

Fig. 1. Overall view of Tat•P-TEFb•ATP complex. The subunits are represented as cartoons and transparent surfaces. HIV Tat is red and Cdk9 and Cyclin T1 subunits of P-TEFb are in light orange and pale green, respectively. The ATP molecule and a bound magnesium ion are shown as sticks and a light blue ball. The Tat-bound zinc ions are shown as yellow balls. The figure was prepared with PyMOL.

Viruses are not capable of self-replication and they carry only a few genes essential to their infection cycle. They must take over their host's cellular machinery in order to transcribe their genes and translate them into proteins. These proteins are then used to build new viral particles that can spread to other cells. For the human immunodeficiency virus (HIV) this is achieved by hijacking a cellular transcription elongation factor called P-TEFb using the viral protein HIV-1 Tat. The intimate details of this hostile takeover have now been elucidated by researchers from the University of Nebraska Medical Center and the University of Iowa, who solved the structure of the P-TEFb•Tat complex utilizing the NE-CAT 24-ID-C and 24-ID-E x-ray beamlines. The work shows that Tat induces significant structural changes in P-TEFb and provides an opportunity for the design of targeted drugs that disrupt the complex and inhibit HIV replication but do not affect normal cellular functions.

Although drugs have been developed to treat HIV infection, drug resistance is common because of the rapid development of new strains of the virus that no longer respond to the drugs. Most current HIV therapies inhibit viral enzymes, but it might also be possible to block the interactions between viral proteins and host proteins that are hijacked as part of the infection process. One such interaction is that between the viral protein Tat and the positive elongation factor P-TEFb. P-TEFb functions in cells to regulate the activity of RNA polymerase II in the generation of mRNA. It consists of a cyclin-dependent kinase (Cdk9) and a cyclin subunit, cyclin T1. It is normally maintained in an inactive state by the protein HEXIM and, when activated, binds to genes and promotes transcription. However, when P-TEFb is bound to HIV Tat, it is recruited to promote the transcription of HIV genes and support HIV infection instead.

Tat proteins maintain a flexible structure and do not have much secondary structure when not bound to their target. Once bound, HIV Tat devotes a large proportion (37%) of its folded surface to interactions with P-TEFb, mainly through interactions with the cyclin T1 subunit (88%). Comparison of the structure of P-TEFb alone to that of P-TEFb•Tat revealed that HIV Tat induces significant conformational changes in P-TEFb that alter the surface that normally interacts with its inhibitor, HEXIM, as well as the substrate binding surface of its kinase subunit. This explains observations that the phosphorylation profile of the P-TEFb•Tat complex is different from that of P-TEFb alone. Alteration of the HEXIM binding surface suggests that Tat induces changes in P-TEFb that weaken HEXIM's inhibitory effect and facilitate P-TEFb extraction by HIV Tat.

In addition to increasing our understanding of the mechanism that HIV uses to take over cellular transcription for its own ends, this work provides a possible means for blocking this takeover. Comparison of sequence alignment data and the P-TEFb•Tat structure shows that HIV Tat amino acids that are crucial to P-TEFb binding are the most conserved and that those which are exposed on the protein surface are the least essential. This is important information for drug design projects that will be most effective if they target conserved amino acids that facilitate the binding interaction. Also, due to the fact that the structure of P-TEFb is very different when bound to HIV Tat, it might be possible to exploit these differences in order to design new drugs that could interfere with the interactions between P-TEFb and HIV Tat but would not inhibit normal gene transcription. This will be crucial to finding an effective treatment that can overcome the rapid evolution of HIV without harmful side effects. In fact, the research team will explore the structure of the P-TEFb•Tat complex for the design of a new generation of inhibitors called "Conditionally Anchored Smart Inhibitors," or CASIs, which will become active and inhibit P-TEFb only when it is "infected" with HIV Tat. — *Sandy Field*

See: Tahir H. Tahirov[1]*, Nigar D. Babayeva[1], Katayoun Varzavand[2], Jeffrey J. Cooper[2], Stanley C. Sedore[2], and David H. Price[2], "Crystal structure of HIV-1 Tat complexed with human P-TEFb," Nature **465**, 747 (10 June 2010). DOI:10.1038/nature09131

Author affiliations: [1]University of Nebraska Medical Center, [2]University of Iowa

Correspopndence:
*ttahirov@unmc.edu

This work is supported by the National Institutes of Health (NIH) grants GM35500 and AI074392 to D.H.P., by Nebraska Department of Health and Human Services grant LB506, and in part by NIH grant GM082923 to T.H.T. The Northeastern Collaborative Access Team beamlines are supported by award RR-15301 from the National Center for Research Resources at the NIH. Use of the Advanced Photon Source, an Office of Science User Facility operated for the U.S. Department of Energy Office of Science by Argonne National Laboratory, was supported by the U.S. DOE under Contract No. DE-AC02-06CH11357.

24-ID-C • NE-CAT • Life science • Macromolecular crystallography, microbeam, single-crystal diffraction, microdiffraction, single-wavelength anomalous dispersion • 6.5-23 keV • On-site • Accepting general users

24-ID-E • NE-CAT • Life science • Macromolecular crystallography, microbeam, microdiffraction, single-crystal diffraction, single-wavelength anomalous dispersion • 12.68 keV, 13.74 keV • On-site • Accepting general users

Stalking the Structure of Drug-Pumping Proteins

The family of proteins known as multidrug and toxic compound extrusion (MATE) functions in the cell to help export toxins and substrates. As part of a larger class of proteins, these proteins also participate in the development of resistance to multiple antibiotics (multiple drug resistance [MDR]) in bacteria and mammals. MATE transporters are the only remaining class of MDR transporters whose structure has not been determined. With the use of x-ray crystallography at the GM/CA-CAT beamline 23-ID-D at the APS, researchers determined the structure of the MATE transporter NorM from the bacterium *Vibrio cholerae*. The findings reveal that the structure of the MATE transporter is unlike that of any other protein class involved in MDR. This work promises to contribute significantly to the understanding of the processes involved in drug resistance.

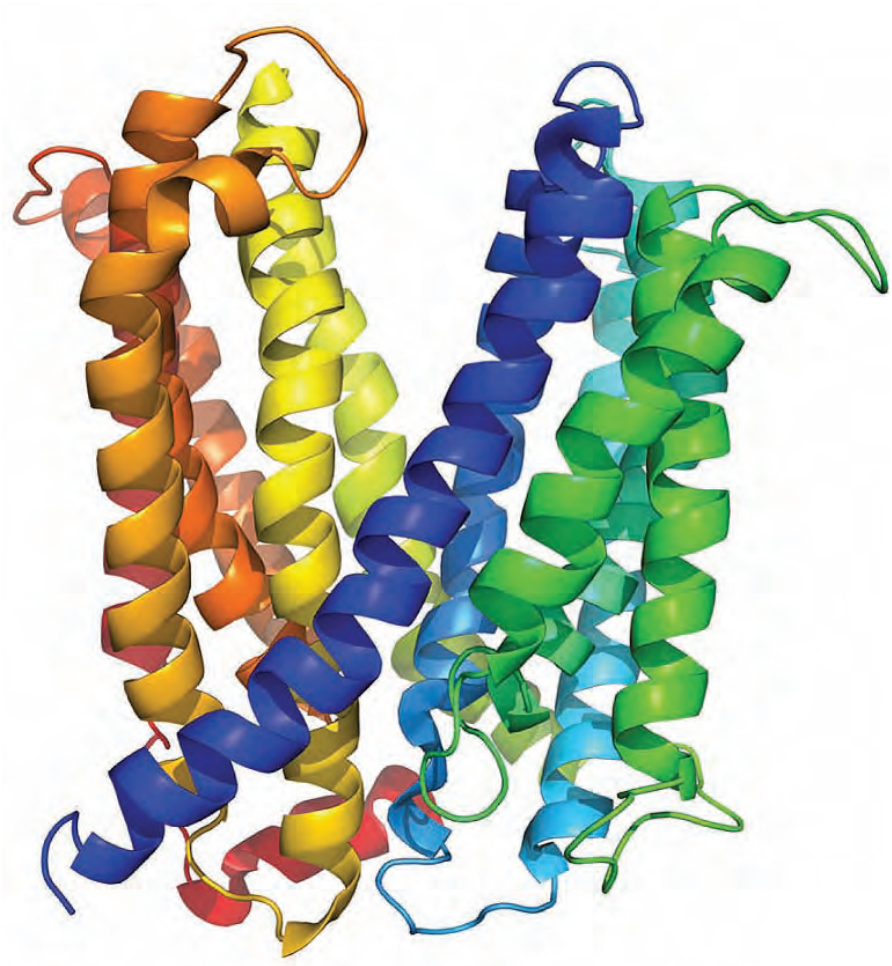

Fig. 1. Front view of the NorM model, showing the extracellular (top) and cytoplasmic (bottom) sides, with the molecule colored by a raindow gradient from the N terminus (blue) to the C terminus (red). Xiao He et al., Nature **467**, 991 (21 October 2010). ©2010 Macmillan Publishers Limited. All rights reserved.

MATE transporters function by coupling to hydrogen-ion or sodium-ion gradients across the membrane to drive substrate export. But the way in which they do this is not completely understood. Multiple forms of MATE proteins are present throughout all life forms and share about 40% protein sequence similarity, suggesting that the structure and transport function has been conserved throughout evolution.

To further characterize the function of MATE transporters, investigators from The Scripps Research Instiutute determined two x-ray structures of the MATE protein NorM from *V. cholerae*. The researchers found that the structure of the NorM protein had a topology distinct from all other MDR transporter families; it is also the last known MDR transporter family to be elucidated using x-ray crystallography. MATE transporters, as well as some other MDR transporters families, have drug-binding sites that bind many different types of drugs and are composed of membrane-spanning spiral-like protein segments within the cell membrane. The researchers propose that substrates may be directly expelled from the inner to the outer membrane leaflet through portals positioned within the cell membrane, a feature that may be common for MATE and other MDR transporter families. They also found that the protein structure forms a V-shaped conformation, a molecular scaffold important for the transport of various types of substrates.

Understanding the structure, and therefore the function of the MATE proteins, may be especially important from a medical standpoint; in mammals these proteins export a several different types of drug and waste molecules in the liver and

"Proteins" cont'd on page 83

A New Order in Purine Metabolism

The enzyme xanthine oxidase plays a central role within cells by helping to break down purine molecules, some of which contribute to the structure of DNA and RNA. With the use of x-ray crystallography at the LRL-CAT 31-ID beamline at the APS, researchers from the University of California, Riverside, and The Ohio State University revealed some of the intricacies of how xanthine oxidase breaks down purines. The findings provide new insights into how xanthine oxidase acts on its substrate hypoxanthine to produce an end product uric acid, with a finding that goes against a previously accepted mechanism.

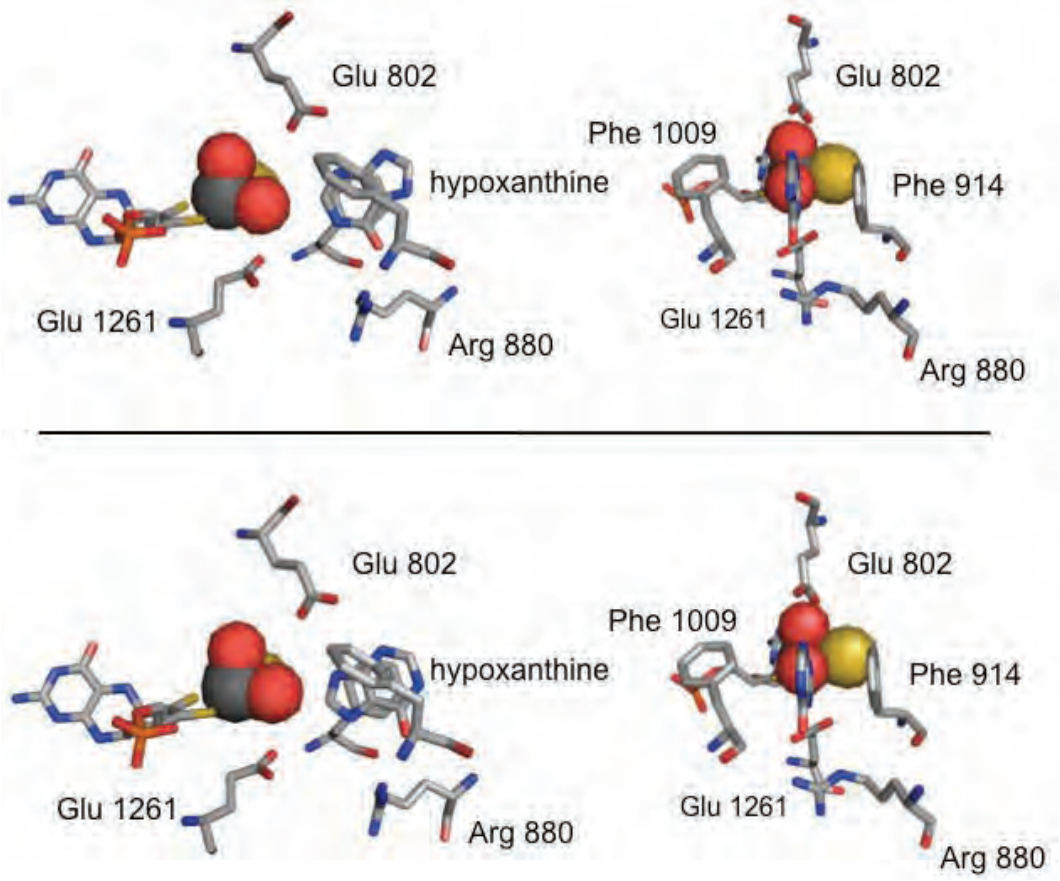

Fig. 1. Structure of the substrate hypoxanthine bound in the active site in two alternate orientations. Top: The catalytically relevant orientation with C-2 of the purine substrate oriented toward the active site molybdenum center. Bottom: A dead-end complex with the C-8 position of substrate oriented toward the molybdenum center. For each orientation, view on the righthand side is rotated clockwise approximately 90° about the vertical from that on the left. Catalytically relevant residues are indicated.

Xanthine oxidase catalyzes the oxidation of hypoxanthine to xanthine, and then acts on xanthine to form uric acid. Uric acid is important from a medical standpoint because, when present at high levels in serum, it can lead to a type of arthritis known as gout as well as to the formation of kidney stones. Proper substrate orientation is essential when an enzyme catalyzes a reaction so that molecules can be aligned, and therefore enzymatic reactions require the least energy. It has long been recognized that the oxidation of hypoxanthine to uric acid happens in a sequential process: xanthine oxidase first catalyzes the addition of an oxygen group at the second carbon of hypoxanthine — forming xanthine — and then, by the addition of a second oxygen group, further converts xanthine to uric acid.

This study suggests that while hypoxanthine can bind in a way that leads to 6,8-dihydroxypurine, the x-ray crystallography carried out at LRL-CAT shows that minimal amounts of 6,8-dihydroxypurine accumulate during the course of the reaction. This observation is accounted for by the intrinsically lower reactivity of the C-8 position of hypoxanthine toward hydroxylation (which would result in 6,8-dihydroxypurine) relative to its C-2

"Metabolism" cont'd on page 83

Fat Biochemistry Clarified

How cells metabolize fats is a subject of primary interest to biochemists and medical scientists. Normal fat metabolism keeps cells healthy while abnormal metabolism can lead to disease. Recent research linking cholesterol to arterial disease suggests that the relationships are much more complicated than previously thought. At this point, any new knowledge about the metabolism of fats is eagerly welcomed. Although much is already known about how receptors in the cell's nucleus bind fats, there are many questions left unanswered. One set of these questions revolves around a receptor called RORγ, known as an "orphan receptor" because it was difficult to figure out what it was actually binding. A research team set out to determine whether RORγ really was involved in fat metabolism, as had been previously suggested. The team collected structural data with the help of the LS-CAT 21-ID-F beamline at the APS and discovered an important link between fat metabolism and RORγ. Their work rescues RORγ from its orphan status and contributes important new insights to our overall understanding of how cells process fats.

Fig. 1. Ribbon representation of the structure of RORγ ligand binding domain complexed with 22(R)-hydroxycholesterol. RORγ is colored in red and the SRC2-2 co-activator motif is in yellow. The bound ligand is shown in stick representation with carbon and oxygen atoms depicted in green and red, respectively.

The researchers from Xiamen University and the University of Pittsburgh studied the retinoic-acid related orphan receptor γ (RORγ), which belongs to a family of nuclear receptors that are important in development, lung inflammation, circadian rhythms, and lipid metabolism. Although other members of this receptor family were well characterized with respect to their roles, RORγ remained an orphan because it could not be linked with certainty to binding of any particular molecules. The importance of RORγ was strongly implicated by observations that it was prevalent in liver and adipose tissue as well as in skeletal muscles.

One of the interesting aspects of RORγ biochemistry was that the receptor seemed to be always active, thus implying its importance to the cell. Yet RORγ was one of the few nuclear receptors with an unknown structure because the structure could not be determined until it was known exactly what RORγ was binding.

To solve the mystery of RORγ, the researchers framed a central question: Could cholesterol, or its hydroxycholesterol derivatives, activate RORγ? To answer this question, the research team first used biochemical assays to show that RORγ was involved with hydroxycholesterols, which activated its ability to bring in co-activators. This evidence clearly showed that human RORγ was important to fat metabolism. The researchers then went on to solve the crystal structure of the RORγ binding region when attached to hydroxycholesterols (Fig. 1). They tested various hydroxycholesterols and found that all of them took on a shape that suggested binding activity. To further prove a connection between RORγ and hydroxycholesterols, the researchers examined mutations that hinder the binding activity of hydroxycholesterols. Such mutations also eliminated active RORγ, which is usually always active in the cell.

The research team was also able to show that RORγ was capable of recruiting co-activators that resulted in necessary genes being turned on, with subsequent production of proteins necessary to fat metabolism. This process involved what

"Biochemistry" cont'd on facing page

"Proteins" cont'd from page 80

kidney. The export of drugs in turn can influence the plasma concentrations of these drugs. For example, in the case of metformin, used to treat type 2 diabetes, the export of metformin by the MATE proteins in the kidney contributes to the decreased efficacy of metformin in certain patients. Likewise, in bacteria, MATE transporters can pump out antibiotics from the cell. For example, this has been shown to occur in some strains of methicillin-resistant *Staphylococcus aureus* when treated with tigecycline, a new glycylcycline-class antibiotic originally developed to overcome methicillin-resistant and vancomycin-resistant *S. aureus*. Preventing the export of tigecycline by bacterial MATE transporters may therefore help make tigecycline more effective as an antibiotic. Given the involvement of MATE proteins in drug resistance, the current work may therefore contribute significantly to the understanding of these processes. — *Emma Hitt*

See: Xiao He, Paul Szewczyk, Andrey Karyakin, Mariah Evin, Wen-Xu Hong, Qinghai Zhang, and Geoffrey Chang*, "Structure of a cation-bound multidrug and toxic compound extrusion transporter," Nature **467**, 991 (21 October 2010). DOI:10.1038/nature09408
Author affiliation: The Scripps Research Institute
Correspondence: *gchang@scripps.edu

This work was supported by grants from the National Institutes of Health (GM70480 to G.C., and GM73197 to Q.Z.), the Beckman Foundation and the Skaggs Chemical Biology Foundation. Use of the Advanced Photon Source, an Office of Science User Facility operated for the U.S. Department of Energy (DOE) Office of Science by Argonne National Laboratory, was supported by the U.S. DOE under Contract No. DE-AC02-06CH11357.

23-ID-D • GM/CA-CAT • Life sciences • Large unit cell crystallography, macromolecular crystallography, microbeam, multi-wavelength anomalous dispersion, single-wavelength anomalous dispersion, subatomic (<0.85 Å) resolution • 5-20 keV • On-site • Accepting general users

"Metabolism" cont'd from page 81

position (which would result in xanthine). Interestingly, the current study finds that 6,8-dihydroxypurine, which was long thought not to be a substrate for xanthine oxidase, can also be converted into uric acid by the enzyme.

To elucidate the current findings, the researchers formed crystal structures of xanthine oxidase in complex with different substrates to show that the substrates are able to assume alternate positions within the active site of the enzyme. The substrate orientations differ in that either the C-2 or C-8 position of substrate is oriented toward the center of the enzyme, indicating that addition of an oxygen group to hypoxanthine at C-8 prior to C-2 should be feasible--an observation which goes against currently accepted thinking. However, the researchers, by showing the crystal structure of xanthine oxidase, also helped to define several reasons to explain why an oxygen group would be more likely to be added to hypoxanthine at C-2 rather than C-8. — *Emma Hitt*

See: Hongnan Cao[1], James M. Pauff[1,2], and Russ Hille[1]*, "Substrate Orientation and Catalytic Specificity in the Action of Xanthine Oxidase. The sequential hydroxylation of hypoxanthine to uric acid," J. Biol. Chem. **285**(36), 28044 (September 3, 2010). DOI:10.1074/jbc.M110. 128561
Author affiliations: [1]University of California, Riverside, [2]The Ohio State University
Correspondence: *russ.hille@ucr.edu

This work was supported in part by the United States Department of Energy (DOE) Office of Science, under Contract DE-AC02-06CH11357 and by Eli Lilly & Company. Use of the Advanced Photon Source, an Office of Science User Facility operated for the U.S. DOE Office of Science by Argonne National Laboratory, was supported by the U.S. DOE under Contract No. DE-AC02-06CH11357.

31-ID • LRL-CAT • Life sciences • Fiber diffraction, macromolecular crystallography, single-crystal diffraction, single-wavelength anomalous dispersion • 4.7-28 keV • Mail-in • Accepting general users

"Biochemistry" cont'd from page 82

is known as a charge clamp, which was further studied to provide an even more detailed model of what RORγ is up to in cells.

Taken together, the data collected by the research team point to a strong relationship between the cell's hydroxycholesterols and RORγ activity. The researchers showed that hydroxycholesterols bind, with high affinity, to what was previously known as the orphan receptor RORγ, and that hydroxycholesterols regulate the activity of RORγ. The prevalence of RORγ in cells can now be explained by the prevalence of hydroxycholesterols. The data also suggest that the hydroxycholesterols may even become part of the RORγ structure, further strengthening the argument for a relationship between the two. The results point to the role of RORγ as a nuclear receptor that is closely monitoring the ratio and balance of hydroxycholesterols in cells.

Thanks to this work, RORγ is an orphan no longer. What RORγ binds — and why — can now be added to our understanding and will enable further study of fat metabolism in cells.

— *Mona Mort*

See: Lihua Jin[1], Dariusz Martynowski[2], Songyang Zheng[2], Taira Wada[2], Wen Xie[2], and Yong Li[2]*, "Structural Basis for Hydroxycholesterols as Natural Ligands of Orphan Nuclear Receptor RORγ," Mol. Endocrinol. **24**(5), 923 (May 2010). DOI:10.121 0/me.2009-0507
Author affiliations: [1]Xiamen University, [2]University of Pittsburgh
Correspondence: *yol21@pitt.edu

This work was supported by the National Institutes of Health Grant DK081757, an award from the American Heart Association, grants from the Science Planning Program of Fujian Province (2009J1010), and 111 Project (B06016). Use of the Advanced Photon Source, an Office of Science User Facility operated for the U.S. Department of Energy (DOE) Office of Science by Argonne National Laboratory, was supported by the U.S. DOE under Contract No. DE-AC02-06CH11357.

21-ID-F • Life sciences • Macromolecular crystallography • 12.7 keV • On-site • Accepting general users

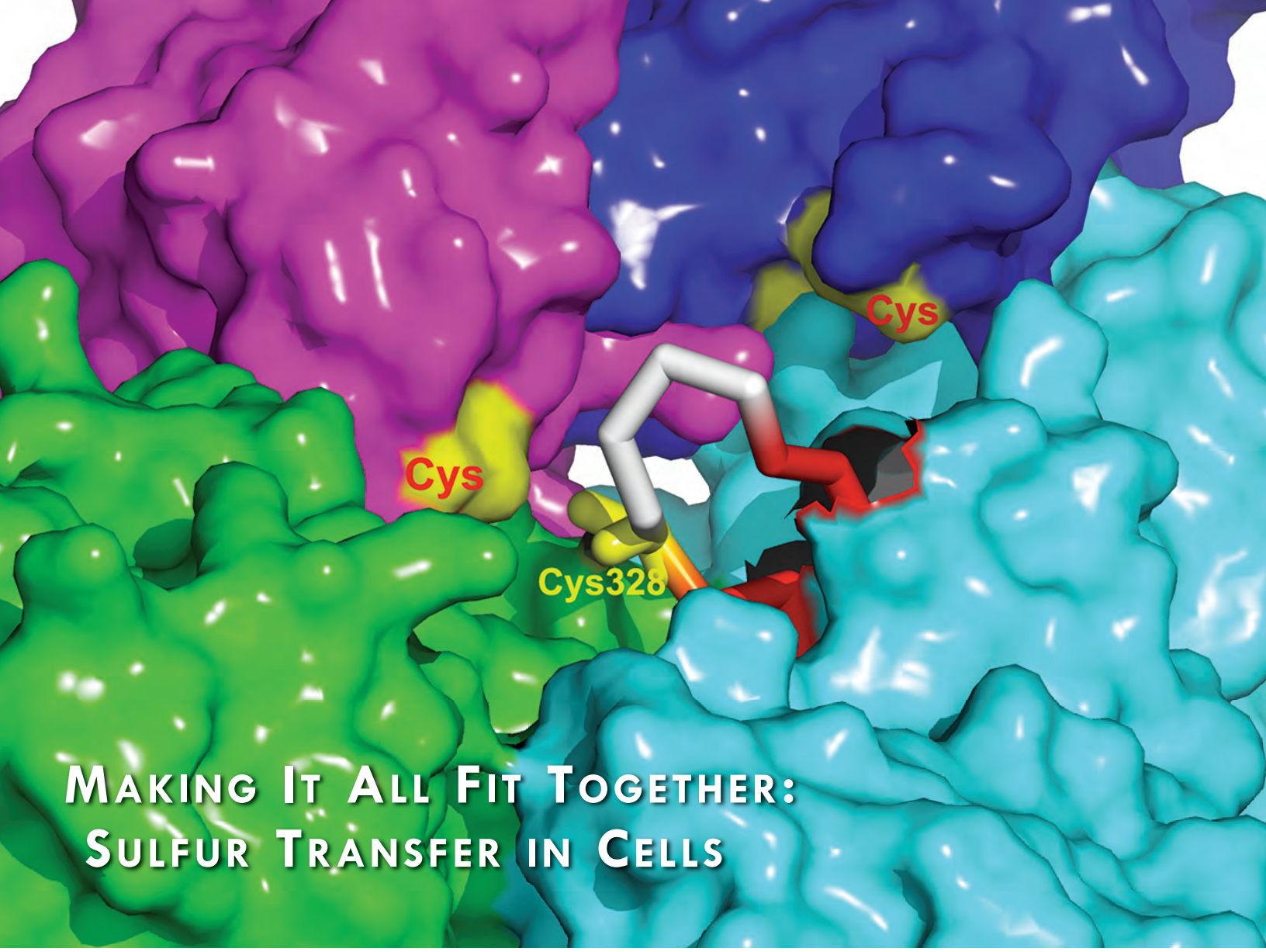

Making It All Fit Together: Sulfur Transfer in Cells

Sulfur is everywhere necessary in the biochemistry of cells; it is involved in building proteins, vitamins, and RNA. Wondrously complex and sophisticated molecular mechanisms exist for making sure that sulfur is in the right place at the right time. Moving sulfur around cells is not a simple process — it requires many transfers of sulfur (as persulfide) among many proteins. The good news is that the mechanisms and the protein complexes appear to be much the same across species, so that characterizing the molecules in one taxonomic group can give a good idea of what is happening in other seemingly unrelated groups. Protein crystallographers have assembled extensive structural information about the proteins involved in these processes, but little was known about how these proteins communicate to transfer the sulfur. Now a research team has broken the code, utilizing the LRL-CAT 31-ID beamline at the APS and the Canadian Macromolecular Crystallography Facility (CMCF) 08ID beamline at the Canadian Light Source.

< Fig. 1. The composite image, showing the surface representation of the complex of IscS dimer (cyan and green) with bound TusA (magenta) and IscU (blue). The cysteine residues on TusA and IscU that accept persulfide from Cys328 of IscS are painted yellow. TusA and IscU can dock to IscS only one at the time due to potential steric clashes. The IscS loop (red) containing Cys328 (yellow) is partially disordered in our crystals and the disordered part (painted gray) was modeled in one of many possible conformations.

One of the proteins involved in assembling bacterial iron-sulfur clusters (*isc*), is also involved in general-purpose assembly and in transferring sulfur to cofactors and tRNA. A master enzyme called cysteine desulfurase (IscS) initiates the process. The IcsS enzyme is widely distributed, found in humans and in *E. coli*, and also highly conserved—it seems to have changed little as it spread through the kingdoms of life. This enzyme is versatile. It is responsible for starting sulfur trafficking within the cell and for delivering sulfur to many different intracellular pathways. IscS is also involved in a network of interactions with other proteins. While there is a wealth of information about the structure of IscS and its fellow network proteins, still missing was accurate information on how IscS was able to communicate with and deliver sulfur to such a wide variety of different partners. Answering these questions requires structural information on how IscS interacts with its binding partners.

The researchers determined the crystal structures for IscS bound to IscU, which is a scaffold protein for iron-sulfur cluster assembly, and for IscS bound to TusA, which is the first member of a sulfur relay leading to sulfur incorporation in several tRNA molecules. These data provide the first glimpses into different modes of binding and sulfur transfer. The researchers used extensive mutational analysis to map the IscS surface with respect to binding sites of partner proteins and to the biochemical and functional roles of certain amino acids of IscS and TusA.

The fine detail provided by the team's results shows that the IscS dimer interacts with partner proteins through a large and well-conserved surface that is centered on a flexible loop containing the active site Cys328 (Fig. 1). IscS extracts sulfur from the amino acid cysteine substrate, converting it to alanine, and attaches it to Cys328. From there the sulfur is delivered to an acceptor protein. The structural data suggest that the acceptor proteins approach the cysteine site from different directions and that some of the plasticity exhibited by IscS is due to a long loop containing the cysteine site. This loop appears to be integral to the ability of IscS to transfer sulfur to a variety of acceptor proteins. While the sulfur acceptors can bind only one at a time to IscS, other proteins that were studied (frataxin and IscX) can form a three-way complex with IscU and IscS. The data are also consistent with frataxin's involvement as an iron donor for IscU to form iron-sulfur clusters.

By describing in atomic detail how IscS binds to two different proteins (IscU and TusA), the research team has provided much needed detail on iron-sulfur cluster formation (IscU) and how sulfur is delivered for tRNA modification (TusA). These very important cellular processes are now much more clearly understood, as is the IscS binding site, thanks to the team's careful mutation studies. — *Mona Mort*

See: Rong Shi[1], Ariane Proteau[1], Magda Villarroya[2], Ismaïl Moukadiri[2], Linhua Zhang[3], Jean-François Trempe[1], Allan Matte[3], M. Eugenia Armengod[2], and Miroslaw Cygler[1,3]*, "Structural Basis for Fe–S Cluster Assembly and tRNA Thiolation Mediated by IscS Protein–Protein Interactions," PLoS Biology **8**(4), e1000354 (April 2010). DOI:10.1371/journal.pbio.1000354.s009

Author affiliations: [1]McGill University, [2]Centro de Investigación Príncipe Felipe, [3]Biotechnology Research Institute

Correspondence:
*mirek.cygler@bri.nrc.ca

This work was funded by Canadian Institutes of Health Research grant GSP-48370 to MC and AM and Ministerio de Ciencia e Innovacion and Generalidad Velenciana (grants BFU2007-66509, ACOMP/2009/348 and AP-079/09 to MEA). Use of the LRL-CAT beamline facilities was provided by Eli Lilly & Company, which operates the facility. The CMCF is supported by CFI, NSERC, and CIHR. Use of the Advanced Photon Source, an Office of Science User Facility operated for the U.S. Department of Energy (DOE) Office of Science by Argonne National Laboratory, was supported by the U.S. DOE under Contract No. DE-AC02-06CH11357.

See also: "Multiple Sulfur Acceptors Dock at IscS," by Kira Heller, *PLoS Biol* **8**(4): e1000353.

31-ID • LRL-CAT • Life sciences • Fiber diffraction, macromolecular crystallography, single-crystal diffraction, single-wavelength anomalous dispersion • 4.7-28 keV • Mail-in • Accepting general users

HOW A DNA POLYMERASE PREVENTS SKIN CANCER MUTATIONS

Ultraviolet radiation damages DNA in a way that normally stops the cell's reproductive machinery in its tracks, resulting in genetic mutations. There is one cellular enzyme capable of bypassing these damaged bits of DNA and leading to correct DNA synthesis, and a recent study explains how it does so. With the high-brightness x-rays from four beamlines at the APS, researchers solved a series of three-dimensional (3-D) crystal structures of DNA polymerase η (or Polη) synthesizing a new strand of DNA from a damaged strand. Their findings show that the enzyme acts as a molecular splint, stabilizing the structure of the damaged DNA to make it resemble that of normal DNA.

The structure of DNA is a double helix, similar to a spiral staircase. Each stair is made of two pieces, or nucleotide bases, one from each DNA strand. When ultraviolet light strikes DNA, it can catalyze a chemical reaction in which two adjacent pyrimidine bases from the same strand join together in what is called a cyclobutane pyrimidine dimer (CPD; see Fig. 1), creating a bulge in one strand of the double helix. Most of the known human DNA polymerases—the enzymes that take one strand of DNA and synthesize a matching strand from it—cannot process CPDs. Instead the polymerase simply falls off of the DNA strand it is reading from (called the template strand), and many of the specialized Y-family DNA polymerases may attempt to extend the nascent DNA strand by inserting the wrong nucleotides.

Polη is the only human polymerase capable of replicating DNA from a CPD lesion without introducing a mutation in the process. Previous studied had revealed the 3-D structure of Polη from yeast but did not show how the polymerase does its job. To solve this problem, researchers, from the National Institutes of Health (NIH), Zhejiang University, Osaka University, the University of Sussex, and Gakushuin University crystallized human Polη mixed with each of four short pieces of double helix containing a CPD. Utilizing the SER-CAT 22-ID and 22-BM beamlines, and the GM/CA-CAT 23-ID-B and 23-ID-D beamlines, all at the APS, they obtained the 3-D structures of the crystallized molecules.

The group found that Polη keeps the damaged DNA straight and rigid thanks to a strongly positively charged surface that binds the DNA and holds it in place. Like other polymerases, the structure resembles a hand with two outstretched fingers and a thumb, which grasp the DNA. A slight shift of the protein's "finger" and "little finger" domains relative to those of many Y-family DNA polymerases enlarges Polη's active site (the part of the enzyme that catalyzes a chemical reaction), giving it room to hold both nucleotide bases making up the CPD (Fig. 1).

Together the four separate structures demonstrated how a CPD moves through the polymerase's active site. Each structure represented a step in the reaction wherein Polη recognizes the CPD and extends the primer opposite and beyond it with the correct nucleotides. Once the reaction is finished, Polη appears to lose most of its weak chemical bonds with the template strand of DNA, which suggests that Polη falls off after processing a CPD. This would make sense, as replicative polymerases with high accuracy and efficiency could then pick up where it left off.

The structures also reveal the biological underpinnings of the disease xeroderma pigmentosum, the variant form of which is caused by mutations in the Polη gene. The disease is characterized by an elevated risk of skin cancer caused by ultraviolet radiation in sunlight. The researchers matched five known Polη mutations to points in the structure where the interruption of a chemical bond would disrupt the enzyme's ability to synthesize DNA.

— JR Minkel

See: Christian Biertümpfel[1], Ye Zhao[1,2], Yuji Kondo[3], Santiago Ramón-Maiques[1‡], Mark Gregory[1], Jae Young Lee[1‡‡], Chikahide Masutani[3], Alan R. Lehmann[4], Fumio Hanaoka[3,5*], and Wei Yang[1**], "Structure and mechanism of human DNA polymerase η," Nature **465**, 1044 (24 June 2010). DOI:10.1038/nature09196

Author affiliations: [1]National Institutes of Health, [2]Zhejiang University, [3]Osaka University, [4]University of Sussex, [5]Gakushuin University. Present address: ‡Spanish National Cancer Research Centre, ‡‡Dongguk University-Seoul

Correspondence:
**wei.yang@nih.gov
*fumio.hanaoka@gakushuin.ac.jp

The research was funded by the intramural research program of NIDDK, NIH; and grants from the Ministry of Education, Culture, Sports, Science, and Technology of Japan. Y.Z. is the recipient of a Chinese Ministry of Education scholarship and joint PhD student in NIH-Zhejiang University Graduate Partnership Program. S.R.-M. received a fellowship from the Human Frontiers Science Program. Use of the Advanced Photon Source, an Office of Science User Facility operated for the U.S. Department of Energy (DOE) Office of Science by Argonne National Laboratory, was supported by the U.S. DOE under Contract No. DE-AC02-06CH11357.

22-BM • SER-CAT • Life sciences • Macromolecular crystallography • 8-20 keV • On-site • Accepting general users

22-ID • SER-CAT • Life sciences • Macromolecular crystallography, multi-wavelength anomalous dispersion • 6-15 keV • On-site • Accepting general users

23-ID-B & 23-ID-D • GM/CA-CAT • Life sciences • Large unit cell crystallography, macromolecular crystallography, microbeam, multi-wavelength anomalous dispersion, single-wavelength anomalous dispersion, subatomic (<0.85 Å) resolution • 3.5-20 keV (23-ID-B),5-20 keV (23-ID-D) • On-site (23-ID-B & 23-ID-D), remote (23-ID-B) • Accepting general users

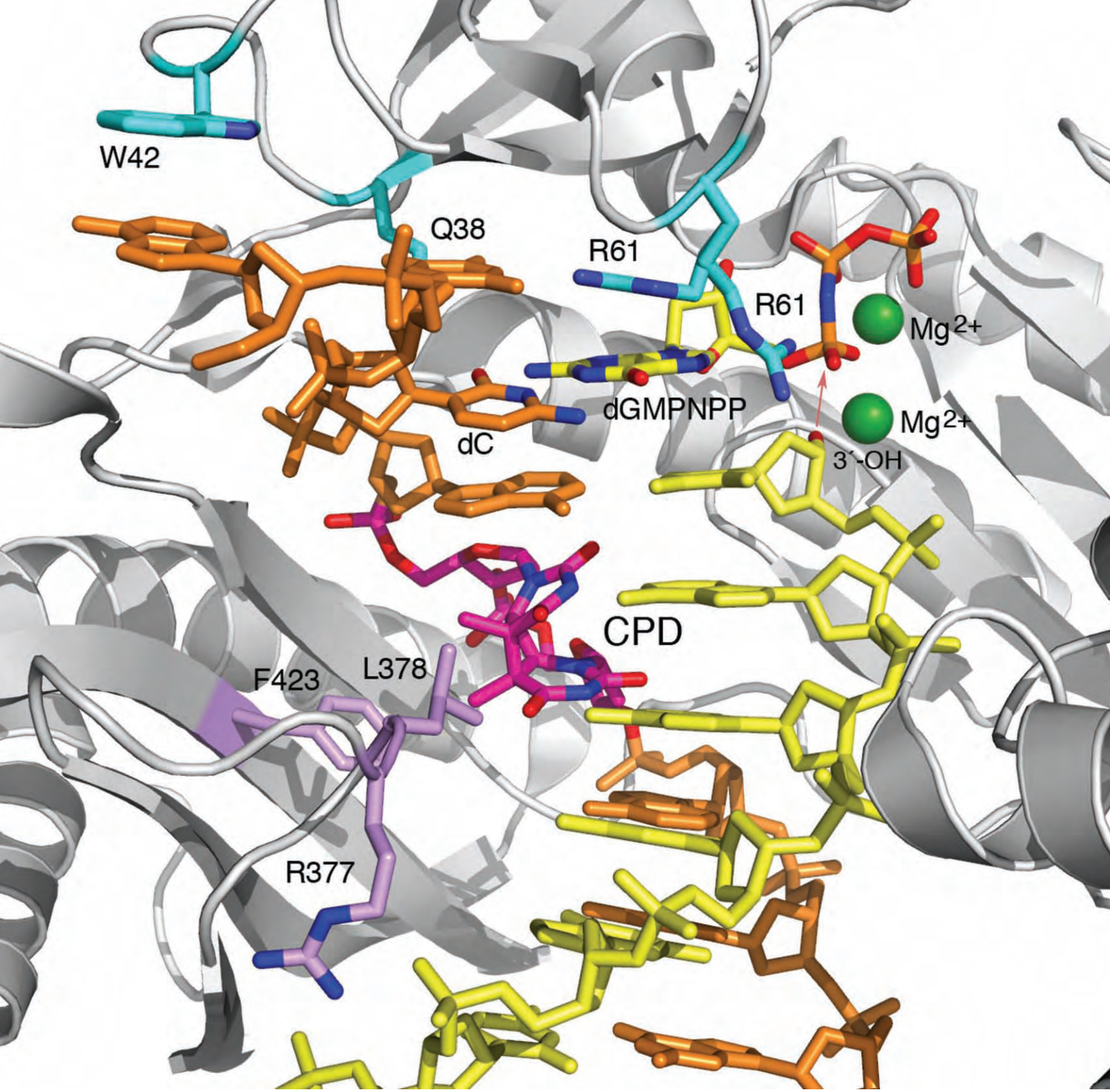

Fig. 1. Structure of human Polη complexed with a short stretch of DNA containing a cyclobutane pyrimidine dimer (CPD; magenta), which will lead to a genetic mutation if not corrected. The DNA template strand is shown in orange and the primer strand (the piece of DNA Polη will add to) is in yellow. Amino acids bonding with the incoming nucleotide base and the template strand are highlighted in cyan. Amino acids bonding with the CPD lesion and the primer strand are shown in light purple. Two metal ions required for catalysis are shown as green spheres.

HOW ENZYMES HANDLE REACTIVE MOLECULES

DNA and RNA are the critical materials upon which life is based, serving as a template for the production of proteins within a cell. Thanks to experiments carried out at three beamlines at the APS, researchers from Northwestern University and the Massachusetts Institute of Technology have revealed some of the intricacies whereby an enzyme called ribonucleotide reductase (RNR) changes the building blocks of RNA into the building blocks of DNA. The findings provide new insights into how reactive small molecules can be channeled within complex enzyme systems and could lead to new approaches to fighting pathogenic bacteria.

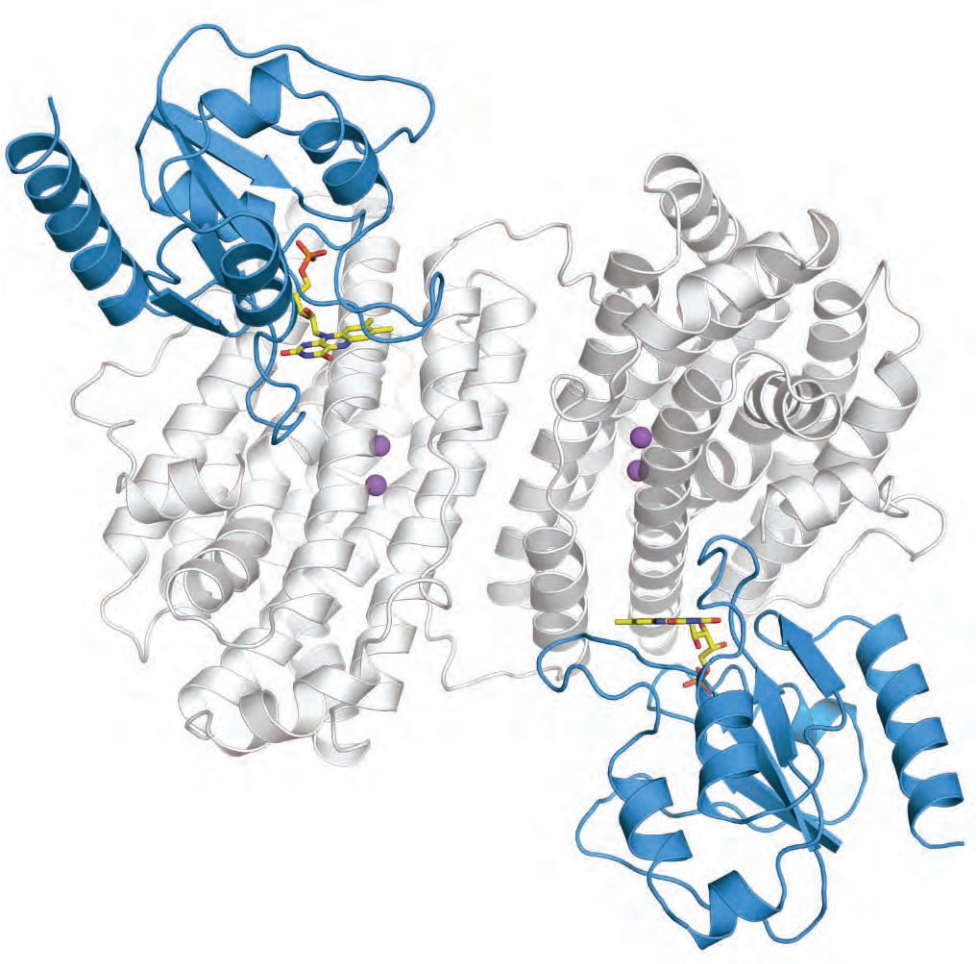

Fig. 1. The complex between NrdF (gray) and NrdI (blue). The manganese ions bound to NrdF are shown as purple spheres, and the NrdI flavin molecule that reacts with oxygen is shown in yellow.

RNRs are enzymes within the cell that enable nucleotides to be made into deoxynucleotides. Nucleotides and deoxynucleotides are building blocks of RNA and DNA, respectively. RNRs, therefore, play an essential role in the synthesis and repair of DNA, a process central to the life of all organisms. The bacterium *Escherichia coli* contains two types of class I RNRs, Ia and Ib, that can function under aerobic growth conditions. The class Ia RNR uses an iron-based cofactor and supplies deoxynucleotides during normal growth conditions. The class Ib RNR is essential for deoxynucleotide production in many pathogenic bacteria, but in *E. coli*, it is expressed under growth conditions of limited iron availability and of oxidative stress.

Recently, it has become clear that the *E. coli* class Ib RNR uses a different type of cofactor involving manganese—rather than an iron cofactor—inside the cell. Studies on the *E. coli* class Ib RNR metal-binding subunit, NrdF, demonstrated that it requires a second protein, NrdI, to make this manganese-based cofactor [1]. NrdI is a protein that reacts with O_2 and generates the oxidant necessary for active site assembly in manganese-loaded NrdF.

To find out more about how NrdI helps activate the class Ib RNR in *E. coli*, the researchers in this study utilized LS-CAT beamlines 21-ID-D and 21-ID-F, and GM/CA-CAT beamline 23-ID-B, to determine the crystal structure of manganese-loaded NrdF in complex with NrdI (Fig. 1). The structure revealed a channel (Fig. 2) between the two proteins that would allow the oxidant generated by NrdI to travel to the manganese site in NrdF without being released into the cellular environment.

This work provides substantial insight into the mechanism by which the class Ib RNR becomes functional in *E. coli* and why NrdI is required for this process. Because NrdI is likely required for activation of the class Ib RNRs of many pathogens, such as the bacteria that cause tuberculosis and anthrax, insight into how these essential enzymes are activated inside the cell could lead to new approaches to combat these deadly diseases.

— Emma Hitt

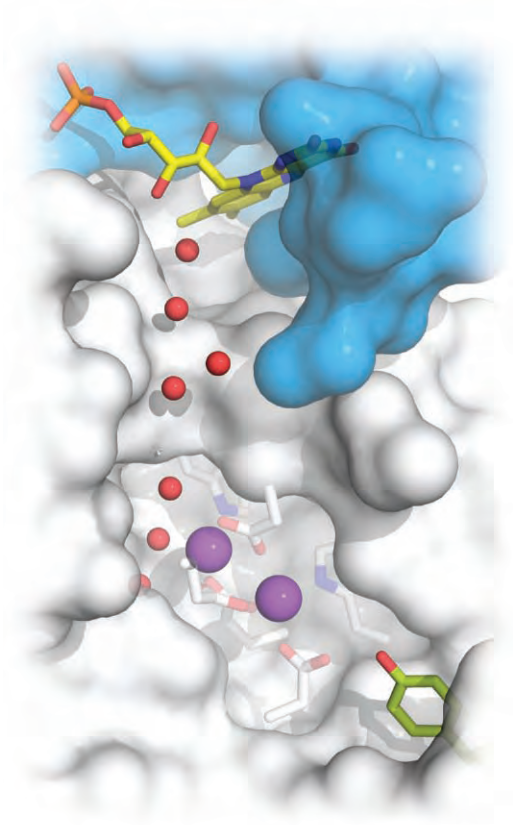

Fig. 2. An enlarged and cut-away view of the NrdI-NrdF complex showing the channel of water molecules (red spheres) connecting the site of production of the oxidant in NrdI with the metal site in NrdF.

Reference

[1] Joseph A. Cotruvo, Jr. and JoAnne Stubbe, "An Active Dimanganese(III)-Tyrosyl Radical Cofactor in Escherichia coli Class Ib Ribonucleotide Reductase," Biochem. **49**(6), 1297 (2010).

See: Amie K. Boal[1], Joseph A. Cotruvo, Jr.[2], JoAnne Stubbe[2]*, and Amy C. Rosenzweig[1]**, "Structural Basis for Activation of Class Ib Ribonucleotide Reductase," Science **329**(5998), 1526 (17 September 2010).
DOI:10.1126/science.1190187

Author affiliations: [1]Northwestern University, [2]Massachusetts Institute of Technology
Correspondence:
*stubbe@mit.edu
**amyr@northwestern.edu

This work was supported by National Institutes of Health grants GM58518 (A. C. R.) and GM81393 (J. S.) and a National Defense Science and Engineering Graduate Fellowship (J. A. C.). Use of LS-CAT at Sector 21 was supported by the Michigan Economic Development Corporation and the Michigan Technology Tri-Corridor (Grant 085P1000817). Some data were collected at GM/CA-CAT, which has been funded in whole or in part with Federal funds from the National Cancer Institute (Y1-CO-1020) and the National Institute of General Medical Science (Y1-GM-1104). Use of the Advanced Photon Source, an Office of Science User Facility operated for the U.S. Department of Energy (DOE) Office of Science by Argonne National Laboratory, was supported by the U.S. DOE under Contract No. DE-AC02-06CH11357.

See also: "A Never-Ending Story," by Britt-Marie Sjöberg, *Science* Perspectives, Science **329**(5998), 1475 (17 September 2010).
DOI: 10.1126/science.1196347

21-ID-D • LS-CAT • Life sciences • Macromolecular crystallography • 6.5-20 keV • On-site • Accepting general users

21-ID-F • Life sciences • Macromolecular crystallography • 12.7 keV • On-site • Accepting general users

23-ID-B • GM/CA-CAT • Life sciences • Large unit cell crystallography, macromolecular crystallography, microbeam, multi-wavelength anomalous dispersion, single-wavelength anomalous dispersion, subatomic (<0.85 Å) resolution • 3.5-20 keV • Remote • Accepting general users

Dynamic Insights into the Way Cells Engulf

In the process called endocytosis, cells ingest or engulf molecules that would not otherwise be able to pass through the cell membrane. An important form of endocytosis involves the protein clathrin, which facilitates the formation of membrane vesicles (bubble-like membranous structures that store and transport cellular products, and digest metabolic wastes within the cell) at the inner cell surface. The self-polymerizing clathrin scaffold helps in deforming the cell membrane as it coats the cytoplasmic surface of the developing vesicle. Before the new vesicle can be completely brought into the cell, the membrane connecting the vesicle to the cell surface must be pinched off. This process is facilitated by an enzyme called dynamin, but the fundamental workings of dynamin were unclear. Researchers used x-ray crystallography at an APS beamline to investigate the structure and function of dynamin, revealing new insights into the catalytic machinery of this enzyme and how it participates in endocytosis.

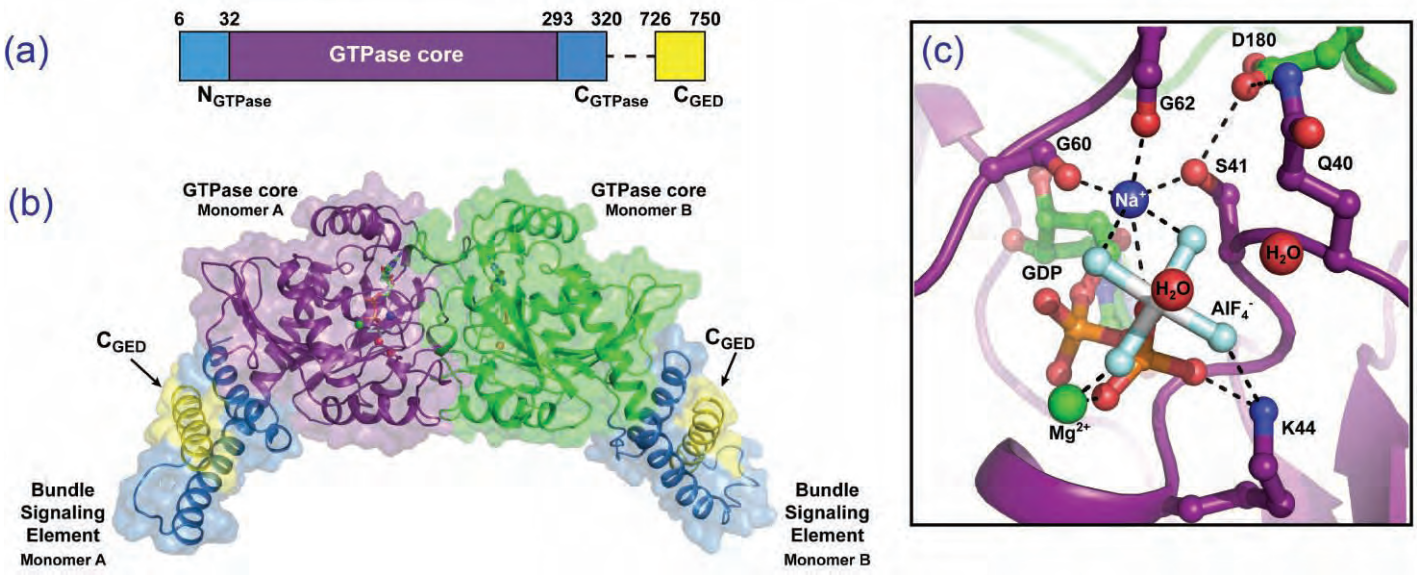

Fig. 1. Structure of a minimal GTPase-GED fusion (GG) reveals dynamin's catalytic machinery. (a) The design of GG connects the N-terminal G domain of human dynamin 1 (purple) to the C-terminal fragment of its distal GTPase effector domain (C_{GED}, yellow) via a flexible linker (dashed line). Regions of the G domain (N_{GTPase} and C_{GTPase}) that directly interact with C_{GED} and form part of the bundle signaling element are colored blue. (b) Structure of the GDP.AlF_4^--stabilized GG dimer (long axis crystal form, PDB: 2X2e). Structural elements are labeled and colored as in (a). The G domain core from the second monomer is colored green. (c) GG active site. Key catalytic side chains [Q40 and S41in monomer (A) and D180 in monomer (B)] and important main chain atoms are shown as sticks. Catalytic and bridging waters are shown as red spheres while GDP and AlF_4^- are depicted as sticks. Dashed lines indicate hydrogen-bonding interactions. G domain dimerization optimally positions the catalytic machinery, resulting in a >100-fold stimulation of dynamin's basal GTPase activity. A catalytic arginine finger that is essential for the activation of small G proteins is markedly absent from the GG active site. Occupying its place is a bound sodium ion (blue sphere), which in conjunction with the bound magnesium ion (green sphere) and the K44 side chain, compensates for the developing negative charge around the β- and γ–phosphates in the transition state.

These findings provide further insight into the mechanisms underlying dynamin-catalyzed membrane fission and the important process of endocytosis

During clathrin-mediated endocytosis, a clathrin-coated pit forming at the cell's membrane ultimately engulfs a molecule and brings it inside the cell. The process is assisted by a set of cytoplasmic proteins, including dynamin. Specifically, dynamin catalyzes a process in endocytosis called fission, the point at which the clathrin-coated vesicle pinches off and becomes free to journey inside the cell. The way in which dynamin functions in fission is incompletely understood. Dynamin is an atypical GTPase, one of a large family of enzymes that bind and split up a molecule called guanosine triphosphate (GTP). In the case of dynamin, the splitting of GTP is what provides the energy needed for it functions during endocytosis. It is known that dynamin molecules have a tendency to form oligomers and ultimately assemble into multiple-unit helical arrays on membranes. It is this helical assembly that stimulates the catalytic GTP-splitting activity of dynamin. However, many of the mechanisms of underlying dynamin's activity are unknown and its catalytic machinery has not been identified.

Dynamin is known to consist of five subdomains: 1) the G domain, a catalytic subunit that binds and splits up GTP; 2) another area involved in the oligomerization of dynamin molecules; 3) a domain involved in interacting with the plasma membrane; 4) a segment known as the GTPase effector domain (GED), which is also involved in self-assembly, and 5) and another domain that mediates interactions with other proteins. In an earlier study, it was determined that two of these five subdomains, the G domain and the GED region, 1) and 4) as described above, might associate with each other during endocytosis.

To explore this concept further, the researchers in this study, from the Scripps Research Institute and the National Institutes of Health, created a fusion protein consisting of these two subdomains joined together by a flexible linker region. Using x-ray crystallography at SER-CAT 22-ID beamline at the APS, the researchers were able to ascertain more about the structure of and infer new information about dynamin's catalytic machinery. They were also able to explain how the splitting of GTP is stimulated by the dimerization of the GTPase domains, and compared human dynamin molecules with rat dynamin molecules to further assess the structural changes that trigger the aggregation of dynamin and stimulate its catalytic activity.

These findings provide further insight into the mechanisms underlying dynamin-catalyzed membrane fission and more about the important process of endocytosis in general.

— Emma Hitt

See: Joshua S. Chappie[1,2], Sharmistha Acharya[2], Marilyn Leonard[2], Sandra L. Schmid[2]*, and Fred Dyda[1]**, "G domain dimerization controls dynamin's assembly-stimulated GTPase activity," Nature **465**(27), 435 (May 2010). DOI:10.1038/nature09032

Author affiliations: [1]National institutes of Health, [2]The Scripps Research Institute

Correspondence:
*slschmid@scripps.edu
**dyda@helix.nih.gov

This work was supported by National Institutes of Health (NIH) grants GM42455 and MH61345 (to S.L.S.) and the Intramural Program of the National Institute of Diabetes and Digestive and Kidney Diseases (NIDDK) of the NIH. J.S.C. was supported by a Ruth Kirschstein individual predoctoral fellowship from the National Institute of Mental Health (MH081419) and by a postdoctoral Intramural Research Training Award from NIDDK. Use of the Advanced Photon Source, an Office of Science User Facility operated for the U.S. Department of Energy (DOE) Office of Science by Argonne National Laboratory, was supported by the U.S. DOE under Contract No. DE-AC02-06CH11357.

22-ID • SER-CAT • Life sciences • Macromolecular crystallography, multi-wavelength anomalous dispersion • 6-15 keV • On-site • Accepting general users

Where and When to Leave the Cell

In cells that have a nucleus, proteins are sent to various destinations by a complex sorting and delivery system. This involves transport in small membranous vesicles that move from one intracellular membrane to the next. The vesicles bud from the departure membrane and then fuse with the destination membrane, depositing their contents. This system requires highly coordinated and specific addressing of vesicles involving complexes of proteins at both ends of the journey. In yeast, a complex that regulates the targeting of vesicles to the plasma membrane for extracellular delivery of proteins, a process known as exocytosis, has been identified. The structure of one of these proteins, Sec3 (Fig. 1), was recently solved at IMCA-CAT beamline 17-BM at the APS. The structure reveals important information about how Sec3 acts as a coincidence detector for exocytosis and identifies a new subtype of pleckstrin homology (PH) domain and new proteins that share this new domain, information that will be instrumental in uncovering their functions.

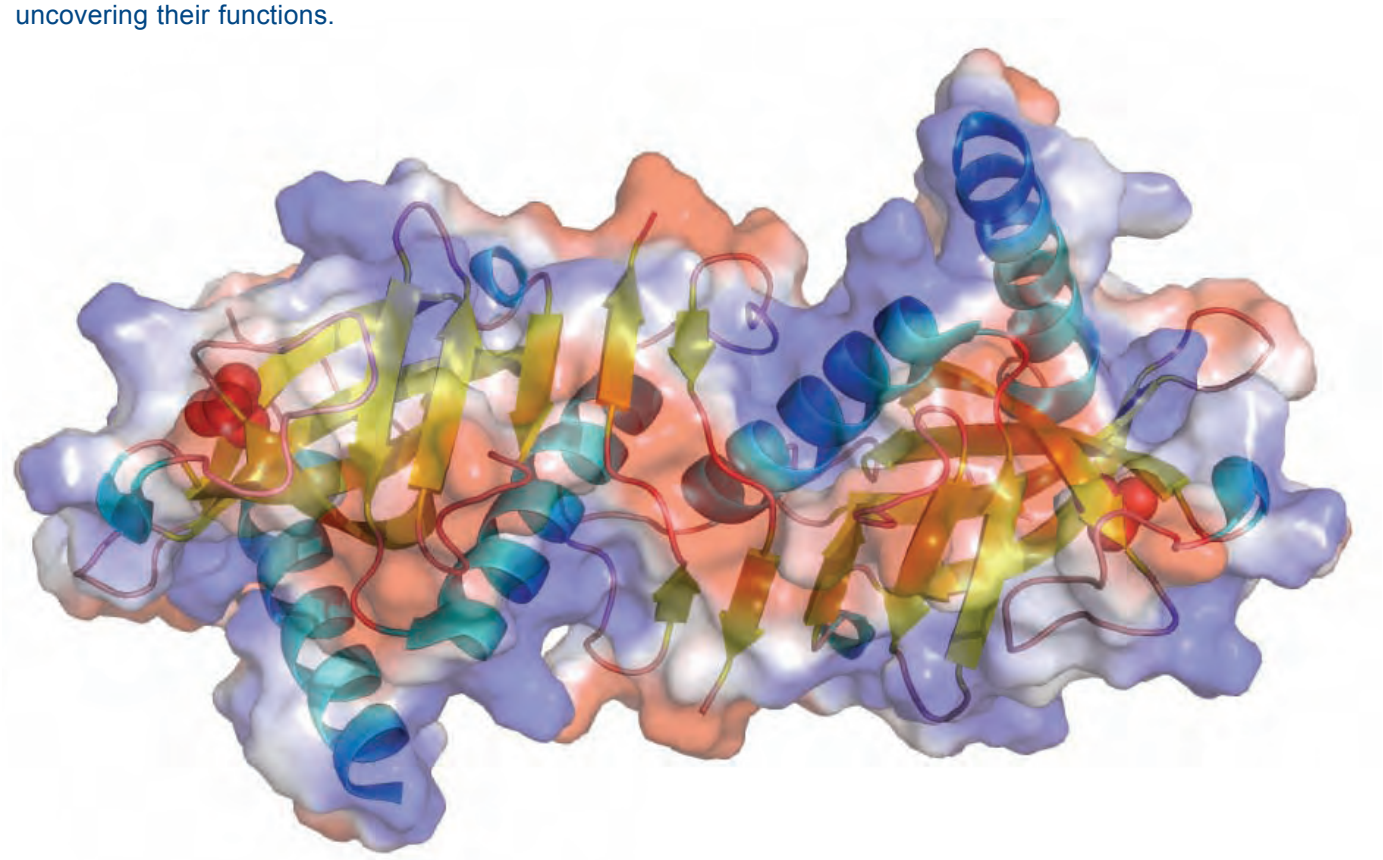

Fig. 1. Structure of the Sec3 PH-domain dimer. The view is down the pseudo two-fold axis of the dimer. A transparent electrostatic surface representation (positively charged: blue; negatively charged: red) is shown along with a ribbon diagram of the structure (helices: cyan; strands: yellow; loops: firebrick). The phosphate groups bound in the phospholipid-binding pockets are shown as red spheres.

This finding provides a new paradigm for understanding the function of PH domain-containing proteins

What is a coincidence detector? This is a term used for proteins that detect the presence of more than one molecule and perform a function when both are present at a specific location. This task is crucial for coordination of exocytosis which requires the formation of a complex of proteins at the cell membrane at a specific time. The team was interested in the N-terminal section of the Sec3 protein because it had been identified as important in vesicle targeting and exocytosis, and had been shown to bind to phospholipids of the plasma membrane and small G proteins that regulate spatiotemporal control of the process.

Their first task was to crystallize the protein. After some trial and error, they were able to get crystals for a segment of Sec3 from amino acid 71 to 241 that contained the regions of interest. There were four copies of the Sec3 segment in the asymmetric unit and, surprisingly, these seemed to comprise two dimeric units mediated through β-sheet interactions in the C-terminal part of the protein fragment. Although dimerization had not been detected by other methods, the presence of two dimeric units in the crystal structure suggested the possibility of dimeric association of Sec3 at the plasma membrane where a high local concentration might favor such interactions.

After the team solved the structure of the Sec3 protein fragment to a resolution of 2Å, their analysis revealed that Sec3 formed part of a new subfamily of PH domains, a fold that is relatively abundant but whose presence in Sec3 was unsuspected. Searching of the database for sequence similarity revealed a number of proteins with homology to this new domain subtype that were not previously suspected to have PH domains. In particular, a protein with a known function in exocytosis called amisyn. This finding provides a new paradigm for greater understanding of the function of PH domain-containing proteins and will be important in discovering the functions of other proteins like amisyn.

Examination of the conserved region of the PH domain revealed possible phospholipid contact points, coinciding with the presence of a bound phosphate ion in the structure, which enabled the team to make mutations at those positions and determine their importance to exocytosis in secretion assays in yeast. Although they were unable to co-crystallize Sec3 in the presence of phospholipids, they were able to determine that the amino acids they identified in the structure were important in Sec3 function in exocytosis. This work, combined with earlier work that showed that this N-terminal region binds to small G proteins, shows that Sec3 mediates interactions between membrane phospholipids and G proteins to act as a coincidence detector. This has also been shown for a growing number of other PH domain-containing proteins and represents an important new paradigm for vesicle trafficking.

The team plans to follow up on their discovery of a new type of PH domain by determining whether the other exocytosis protein identified by this study, amisyn, also acts as a coincidence detector. — *Sandy Field*

See: Kyuwon Baek, Andreas Knödler, Sung Haeng Lee‡, Xiaoyu Zhang, Kelly Orlando, Jian Zhang, Trevor J. Foskett, Wei Guo*, and Roberto Dominguez**, "Structure-Function Study of the N-terminal Domain of Exocyst Subunit Sec3," J. Biol. Chem. **285**(14), 10424 (April 2, 2010). DOI:10.1074/jbc.M109.096966
Author affiliation: University of Pennsylvania. ‡Present address: Chosun University School of Medicine
Correspondence:
*guowei@sas.upenn.edu
**droberto@mail.med.upenn.edu

This work was supported, in whole or in part, by National Institutes of Health Grants R01-GM073791 (to R. D.) and R01-GM64690 (to W. G.). Use of the IMCA-CAT beamline was supported by the Industrial Macromolecular Crystallography Association through a contract with Hauptman-Woodward Medical Research Institute. Use of the Advanced Photon Source, an Office of Science User Facility operated for the U.S. Department of Energy (DOE) Office of Science by Argonne National Laboratory, was supported by the U.S. DOE under Contract No. DE-AC02-06CH11357.

17-BM IMCA-CAT • Life sciences • Macromolecular crystallography, multi-wavelength anomalous dispersion, single-wavelength anomalous dispersion • 7.5-14 keV • On-site, remote, mail-in • Accepting general users

WATCHING MYOGLOBIN CHANGE IN REAL TIME

X-ray crystallography provides valuable information about proteins and their molecular interactions. But this technique produces static structures of molecules, while proteins in their native state are actually active, moving in solution, changing conformation as they catalyze reactions and bind to different molecules. Researchers from the National Institutes of Health (NIH) and The University of Chicago, working at the BioCARS facility at the APS, have met this limitation head-on by developing a time-resolved x-ray scattering diffractometer that can detect changes in protein scattering patterns in solution, providing researchers with a new, sensitive method for studies of protein structure, function, and dynamics.

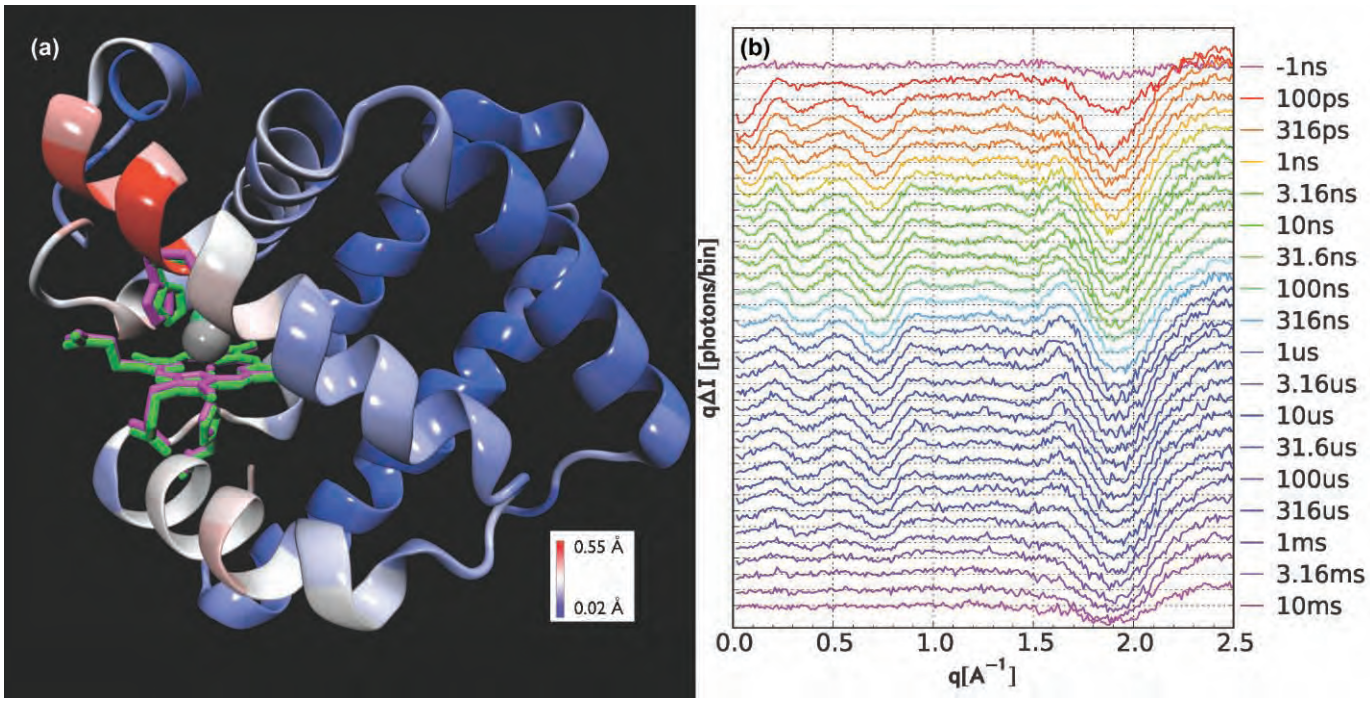

Fig. 1. (a) Structural differences between MbCO and Mb. The heme and nearby histidines are rendered as licorice for both MbCO (magenta) and Mb (green). The back bone is rendered as ribbon and color coded according to the rmsd between these two structures, the global mean of which is less than 0.2 Å. (b) Time-resolved SAXS/WAXS differences. For clarity, the curves are offset from one another and color-coded according to the five states found along the reaction pathway.

X-ray crystallography reveals details about protein structure down to the atomic level. The relative position of each amino acid can be identified and its role in secondary structures such as α-helices and β-sheets can be determined. This technique has provided science with invaluable information about proteins and their molecular interactions, but it has one drawback: It produces static structures of molecules constrained by crystal packing forces. Proteins in their native state are active, moving in solution, changing conformation as they catalyze reactions and bind to different molecules. Spectroscopic techniques can measure changes of proteins in solution but they rely on indirect information from a chromophore and do not detect global structural changes.

In an effort to overcome these limitations, the researchers from the NIH and The University of Chicago have developed a timeresolved x-ray scattering diffractometer that uses small-angle x-ray scattering (SAXS) and wide-angle x-ray scattering (WAXS) to detect changes in protein scattering patterns in solution. This diffractometer, developed on the BioCARS 14-ID beamline at the APS, can probe protein structural changes in solution on short timescales of 100 ps and provides researchers with a new, sensitive method for studies of proteins.

The first step was to develop a high-dynamic-range diffractometer capable of simultaneous coverage of the SAXS and WAXS scattering regions. This was done by positioning the x-ray detector close enough to the sample to access the WAXS region up to q = 2.5 $Å^{-1}$, and making the beamstop diameter small enough to access the SAXS region down to q = 0.02 $Å^{-1}$. For testing the system, the research team chose the muscle protein myoglobin, about which much is already known. Myoglobin binds reversibly to oxygen and carbon monoxide (CO) and the crystal structures of myoglobin with CO bound and unbound have been solved. However, the changes they reveal are subtle, with only very small differences between them. The team set out to test their new diffractometer on myoglobin because they could generate a conformational change with a flash of laser light. This does not require any mixing procedures and thus allows for measurements to be made very quickly upon activation of the conformational change. In the case of myoglobin, a flash of light on myoglobin bound to CO will cause the CO molecule to release. To achieve time resolution as short as 100 ps, these experiments required the ability to isolate a single bunch of x-rays from the APS 24-bunch mode with a mechanical chopper, a feat made possible thanks to a recently completed major upgrade of the BioCARS 14-ID beamline. The unprecedented time-resolved capabilities achieved by this upgrade resulted from a partnership involving BioCARS, NIH/National Institute of Diabetes and Digestive and Kidney Diseases (NIDDK), and the APS (see "100-ps Time-Resolved Crystallography at BioCARS," *APS Science 2008*, p. 89 (ANL-08/24 Argonne National Laboratory, May 2009).

After accounting for factors such as the temperature change generated by the absorbed laser light, solvent and helium chamber contributions, protein scattering patterns can be determined. Measurements made on myoglobin using this system showed x-ray scattering differences recorded over times of 100 ps to 10 ms to be rich in structural information. The SAXS data, which are sensitive to the size and shape of the protein, showed a sudden >22 $Å^3$ expansion in the volume of the protein followed by a relaxation 10 ns later to a volume 2 $Å^3$ greater than myoglobin bound to CO before the flash of light. The WAXS data provide higher resolution information, and the combination of SAXS and WAXS data show the subsequent escape of the CO molecule as the conformation of myoglobin changes.

This striking example of the use of a diffractometer that can capture SAXS and WAXS scattering information at the same time on a very small time scale will provide researchers with a valuable new tool for studies of protein structure, function, and dynamics.

— Sandy Field

See: Hyun Sun Cho[1], Naranbaatar Dashdorj[1], Friedrich Schotte[1], Timothy Graber[2], Robert Henning[2], and Philip Anfinrud[1], "Protein structural dynamics in solution unveiled via 100-ps time-resolved x-ray scattering," Proc. Natl. Acad. Sci. USA **107**(16), 7281 (April 20, 2010).
DOI:10.1073/pnas.1002951107
Author affiliations: [1]National Institutes of Health, [1]The University of Chicago
Correspondence: *anfinrud@nih.gov

This research was supported in part by the Intramural Research Program of the NIH/NIDDK. Use of the BioCARS 14- ID beamline was supported by the National Institutes of Health, National Center for Research Resources, under Grant RR007707. Use of the Advanced Photon Source, an Office of Science User Facility operated for the U.S. Department of Energy (DOE) Office of Science by Argonne National Laboratory, was supported by the U.S. DOE under Contract No. DE-AC02-06CH11357.

14-ID • BioCARS • Life sciences • Biohazards at the BSL2/3 level, Laue crystallography, macromolecular crystallography, time-resolved x-ray scattering, wide-angle x-ray scattering • 7-20 keV • On-site • Accepting general users

A Beneficial Transformation of Uranium in Groundwater

Uranium is an all-too-common groundwater contaminant found at nuclear sites in the U.S. and worldwide. The advantages of bioremediation for removing contaminants from difficult-to-access environments, such as groundwater systems, are many. But to be sure that bioremediation is effective, the impact of biogeochemical processes on contaminant speciation must be understood. Research at the MR-CAT 10-ID beamline at the APS shows that the reduction of highly mobile aqueous hexavalent uranium (UVI) to insoluble tetravelent uranium (UIV) under oxygen-deficient conditions by the addition of an electron donor, or by modifying the environment to promote bacterial growth (biostimulation) can bring the uranium concentration in groundwater to below the U.S. Environmental Protection Agency maximum allowed level for drinking water.

10-ID • MR-CAT • Chemistry, environmental science, materials science • Diffraction anomalous fine structure, microfluorescence (hard x-ray), small x-ray absorbtion fine structure, x-ray absorption fine structure • 4.3-27 keV, 4.3-32 keV, 15-90 keV • On-site • Accepting general users

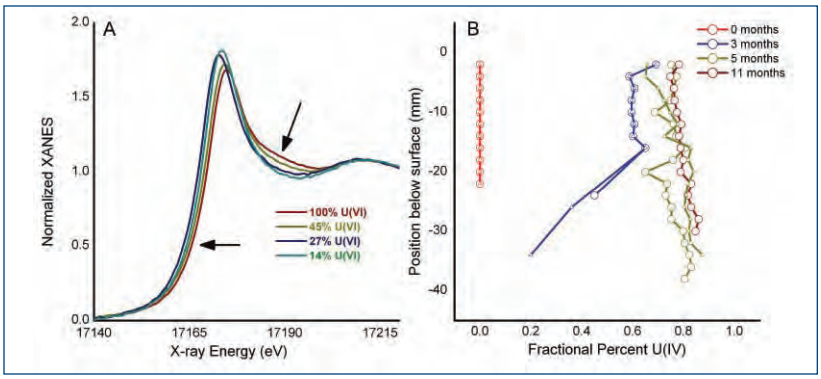

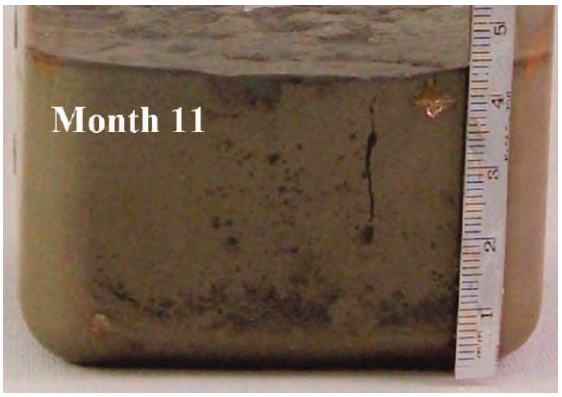

Fig. 1. Photograph (right) of microcosm at T11 and (above) U L_3-edge XANES spectra for microcosm 1 (O) and microcosm 2 (△) as the microcosms aged from T0 to T11. (A) Evolution of the U spectra, with percentage of U^{VI} (based on linear combination fitting), with the remainder as U^{IV}. Arrows point in the direction of more U(IV). (B) Percentage of U^{IV} (based on linear combination fitting of the XANES spectra), with depth below the groundwater-sediment interface at 0 mm. Uncertainty is approximately 10%. (Figures this page ©2010 American Chemical Society)

The reduction of U^{VI} to U^{IV} occurred by two processes: Initial U^{VI} complexed by C- and P-containing ligands was transformed to U^{IV} in uraninite and associated with Fe-containing ligands, while Fe^{III} and sulfate was reduced by microbes.

Monitoring the spatial and temporal changes in the biogeochemistry of a sediment requires an analytical technique that does not disturb the sample. In this study, the researchers from Argonne, Stanford University, Michigan State University, and Oak Ridge National Laboratory (ORNL) monitored uranium, iron, and the microbial community in a sediment and groundwater sample from well FW026 at the Y-12 National Security Complex in Oak Ridge, Tennessee. A 1 mm × 1 mm x-ray beam was used to probe the sediment depth profile for uranium and iron valence state and speciation within static microcosms, allowing analyses in sediment columns without disturbing them. X-ray fluorescence is used to map the distribution of U within the microcosm. Uranium x-ray absorption near edge structure measurements revealed two processes transforming U^{VI} to U^{IV} (Fig. 1). Extended x-ray absorption fine structure measurements determined the speciation of the uranium during transformation.

Analyses began five days after creating the microcosms (Time 0 (T0)) at the MR-CAT beamline. Samples were analyzed again at 3 months (T3), 5 months (T5), and 11 months (T11). Changes in biogeochemistry mirrored visual changes within the sample. At T0 the entire sediment was a uniform yellow-tan with only U^{VI} present. By T3, bioreduction had turned the top layer and several regions within the sediment black. U^{IV} totaled 75% of uranium in the topmost layer and decreased at greater depths. At T5 and T11 the U^{IV} concentration of 80% ± 10% was distributed evenly. Iron reduction, like uranium reduction, began at the top and progressed down the sediment profile. The uranium species changed, from U^{VI} in monodentate P ligands (U^{VI}-P) and bidentate C ligands (U^{VI}-C) at T0 to uranium associated with iron and with U^{IV} in the form of uraninite by T11.

The relative abundances of different bacterial phylogenetic groups revealed that the maximum phylogenetic diversity and most even relative abundances were at T0. Aqueous sulfate was completely consumed by T5, after which the population of sulfate-reducing bacteria decreased. Bacterial groups not dependent on sulfate then increased and were dominant at T11. Not all bacterial groups tracked the changes in electron donor and acceptor abundances, suggesting that other factors affected microbe abundances, including differences in sediment chemistry, and biological factors such as competition and commensalism between species and predation by viruses.

In the year-long experiment, U^{IV} only reached 82%. The authors speculate that the remaining U^{VI} is unavailable for reduction because it is sequestered within the sediments. Since the sediments have been exposed to the uranium-contaminated groundwater at ORNL for over 50 years, the sediments have had time to incorporate uranium into their internal structure. To be sure that this method of bioremediation will be effective, researchers must determine that this U^{VI} is stable and will remain sequestered under other geochemical conditions. — *Dana Desonie*

See: Shelly D. Kelly[1‡*], Wei-Min Wu[2], Fan Yang[3], Craig S. Criddle[2], Terence L. Marsh[3], Edward J. O'Loughlin[1], Bruce Ravel[1‡‡], David Watson[4], Philip M. Jardine[4], and Kenneth M. Kemner[1], "Uranium Transformations in Static Microcosms," Environ. Sci. Technol. **44**, 236 (2010). DOI:10.1021/es902191s

Author affiliations: [1]Argonne National Laboratory, [2]Stanford University, [3]Michigan State University, [4]Oak Ridge National Laboratory. Present addres.: ‡EXAFS Analysis, ‡‡Brookhaven National Laboratory/National Institute of Standards and Technology
Correspondence:
*dr.sdkelly@gmail.com

This work was supported under contract DE-AC02-06CH11357 by the U.S. Department of Energy (DOE) Office of Science, Office of Biological and Environmental Research, Environmental Remediation Sciences Program. MR-CAT operations are supported by the DOE and the MR-CAT member institutions. Use of the Advanced Photon Source, an Office of Science User Facility operated for the U.S. DOE Office of Science by Argonne National Laboratory, was supported by the U.S. DOE under Contract No. DE-AC02-06CH11357.

THE PUSH AND PULL OF PLANT VIRUSES

New insights have been obtained into the way a seemingly simple plant virus, the turnip crinkle virus (TCV), goes about replicating in infected cells. This new information comes to us via solution nuclear magnetic resonance spectroscopy (NMR) and small/wide angle x-ray scattering (SAXS/WAXS) studies carried out with a novel methodology at two APS x-ray beamlines. The findings build on earlier work but provide a clearer understanding of RNA genetics and can explain the paradox of how RNA translation and protein synthesis operate in parallel even though they pull the machinery — the enzymes and ribosome — of the host cell in different directions. The work may have implications for coping with crop-plant viral diseases.

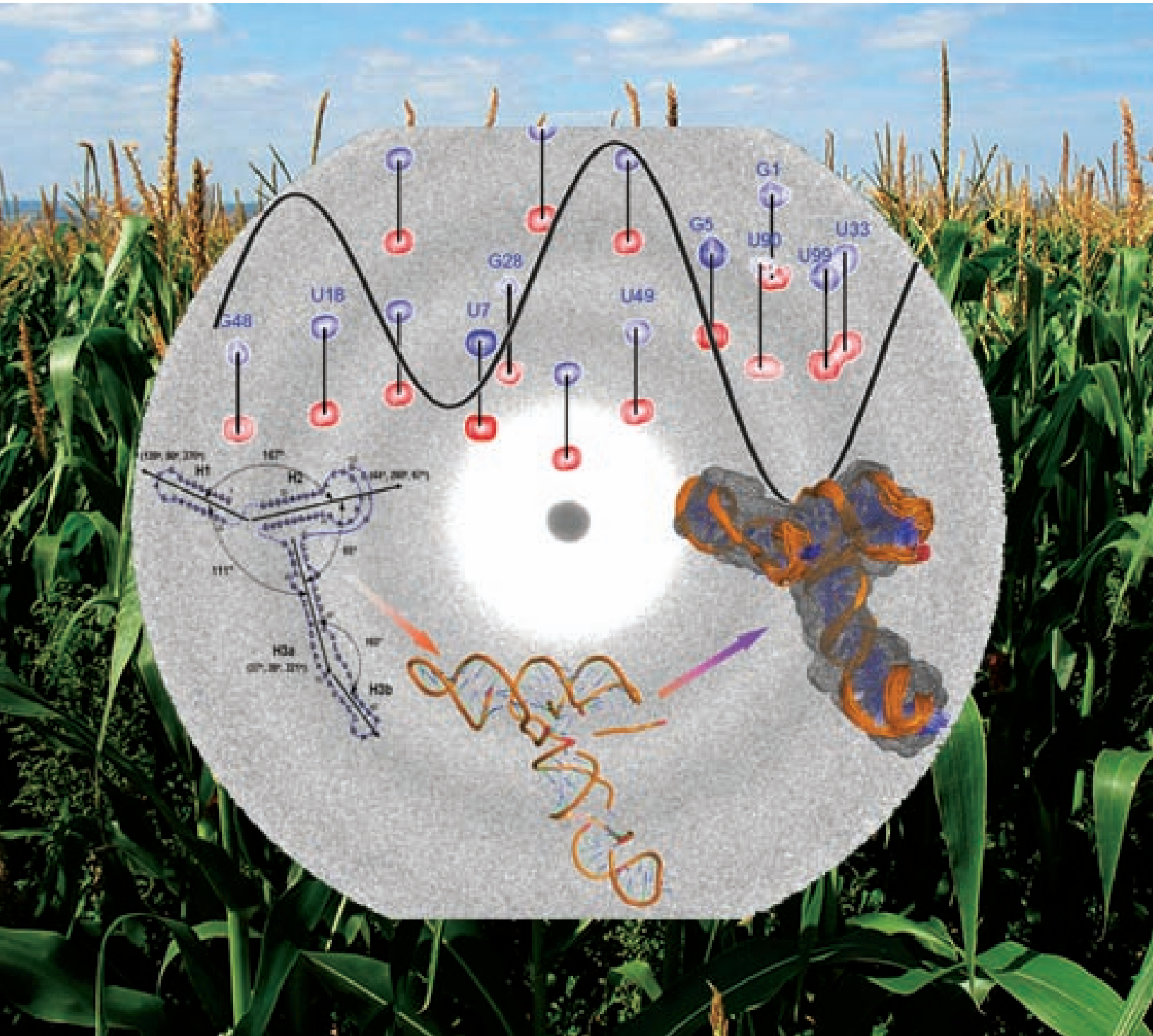

The turnip crinkle virus has just 4054 bases in its genetic code, making it among the smallest and simplest of the single-component RNA viruses that infect plants. Moreover, sub-viral strands of TCV's RNA can use the enzyme polymerase to replicate without the rest of the virus being involved. So molecular biologists find this virus useful as templates for genetic studies of replication and recombination.

TCV also uses several structural elements of messenger RNA to make translation of its genetic code more efficient. This allows it to replicate rapidly in the infected host plant without being subjected to the host cell self-defense system. Some of these structural elements also work together to trigger translation and boost efficiency. Now, researchers from the National Cancer Institute at Frederick, Johns Hopkins University, Argonne, the University of Maryland College Park, and the National Institutes of Health have obtained the three-dimensiona (3-D)l solution structure of one such structural element: a ribosome-binding element in TCV. The researchers developed a novel method that allowed them to combine the benefits of SAXS/WAXS with nuclear magnetic resonance imaging (Fig. 1). The SAXS/WAXS experiments were performed at XSD beamline 12-ID-C,D and the Bio-CAT beamline 18-ID at the APS.

TCV lacks the known translational enhancers, the so-called 5' cap and the 3' poly(A) tail, which are normally used for starting protein synthesis in animals, plants, and fungi. As such, understanding how translation is initiated and enhanced to make TCV infectious to host plants seemingly relies on the structural element located in the region after the protein synthesis stop signal (stop codon). This region is called the 3′ untranslated region (3' UTR). This structural element helps the virus to hijack the host plant's protein factory, the ribosome, and use it to replicate the viral proteins without hindrance from the plant's self-defense mechanisms. One of the problems facing researchers trying to understand the underlying molecular biology is that the two key processes, translation and replication, seem to be mutually exclusive as they operate in the opposite direction, one synthesizing RNA, the other proteins.

The 3' UTR in TCV has a cap-independent translation element (CITE), within which is a ribosome-binding structural element (RBSE). It is this section that hijacks the large subunit of the host ribosome to make viral proteins. There is a large symmetric loop within the RBSE, which plays a key role in coordinating translation and replication. The structure determination achived by the researchers in this study offers the global structure of this loop, the 102-nucleotide RBSE RNA. The structure reveals that it shares almost every structural feature with transfer RNA (tRNA) in solution, as if the 102-nt RBSE were a large cousin of tRNA. There are two hairpins, H1 and H2, linked by a 7-nucleotide unit, which resembles to the variation loop in tRNA even in its sequence, H3, and is accessible to interactions with the ribosome.

This new global structure provides an insight into how the unit can bind to the ribosome and might explain how the system can switch between replication and protein production by revealing that H1 and H2 work together in translation but independently of H3, which is involved in protein synthesis through ribosome binding.

This is the first experimental determination of a functional element in the 3' UTR of RNA from any organism and could open up research into viral infectivity that has implications beyond this simple plant virus. The researchers feel that the key to the success of the study were the SAXS/WAXS experiments performed at APS. — *David Bradley*

< Fig. 1. A new method (G2G, "Global measurements to Global structure") has been developed for structure determination of large RNAs in solution using residual dipolar coupling (RDC) from NMR measurements, represented by the blue and red contour linked by black lines with residue labels; and SAXS/WAXS measurements, represented by gray co-centered circular rings in the background. The black "wave" is the RDC-structural periodicity correlation curve that was used to extract the orientation of the RNA duplexes. At the lower left is a two-dimensional (2-D) drawing of the topology of the 102-nt RNA. The low-center model is a rendering of the 2-D drawing of the topology in 3-D space; at the lower right is the refined 3-D ensemble of the 102-nt RNA structures that were restrained with RDC and SAXS data. (For a detailed description of the G2G method, see J. Mol. Biol. 393, 717 [2009]. Cornfield photo courtesy of Sam Mugraby, Photos8.com, www.photos8.com.)

See: Xiaobing Zuo[1], Jinbu Wang[1], Ping Yu[1], Dan Eyler[2], Huan Xu[1‡], Mary R. Starich[1], David M. Tiede[3], Anne E. Simon[4], Wojciech Kasprzak[1], Charles D. Schwieters[5], Bruce A. Shapiro[1], and Yun-Xing Wang[1]*, "Solution structure of the cap-independent translational enhancer and ribosome-binding element in the 30 UTR of turnip crinkle virus," Proc. Natl. Acad. Sci. USA **107**(4), 1385 (January 26, 2010). DOI: 10.1073/pnas.0908140107

Author affiliations: [1]National Cancer Institute at Frederick, [2]Johns Hopkins University, [3]Argonne National Laboratory, [4]University of Maryland College Park, [5]National Institutes of Health. ‡Present address: Fudan University

Correspondence:
*wangyunx@mail.nih.gov

This research was supported (in part) by the Intramural Research Program of the National Institutes of Health (NIH), National Cancer Institute, Center for Cancer Research to B.A.S. and Y-X.W.; by the Intramural Research Program of the NIH, the CIT Intramural Research Program to C.D.S, and U.S. Public Health Service (GM 061515-05A2/G120CD) to A.E.S. This publication has been funded in whole or in part with federal funds from the National Cancer Institute (NIH), under grant HHSN2612008 00001E to W.K. and P.Y. Work at Argonne National Laboratory (DMT) and use of the Advanced Photon Source, an Office of Science User Facility operated for the U.S. Department of Energy (DOE) Office of Science by Argonne National Laboratory, was supported by the U.S. DOE under Contract No. DE-AC02-06CH11357. Bio-CAT is an NIH-supported Research Center RR-08630.

12-ID-C,D • XSD • Chemistry, materials science, physics • Grazing incidence small-angle scattering, small-angle x-ray scattering, surface diffraction, wide-angle x-ray scattering • 4.5-36 keV • On-site • Accepting general users

18-ID • Bio-CAT • Life sciences • Fiber diffraction, microdiffraction, microfluorescence (hard x-ray), small-angle x-ray scattering, time-resolved x-ray scattering, micro x-ray absorption fine structure • 3.5-35 keV • On-site • Accepting general users

The Spin State of Iron in Perovskite at Lower Mantle Pressures

Earth's mantle is composed of magnesium-silicate minerals that contain iron in two different oxidation states, Fe^{2+} and Fe^{3+}. A series of experiments carried out at three APS x-ray beamlines show that when Fe^{3+} substitutes for silicon (Si) in perovskite (Pv), Fe^{3+} undergoes a spin transition in the mid- to lower-mantle resulting in an increase in the bulk modulus without an increase in density. Seismic studies can use this and other changes in physical properties of Fe^{3+} as a seismic probe to understand the origin of some lower mantle properties, such as the presence of oceanic crust, within the lower mantle.

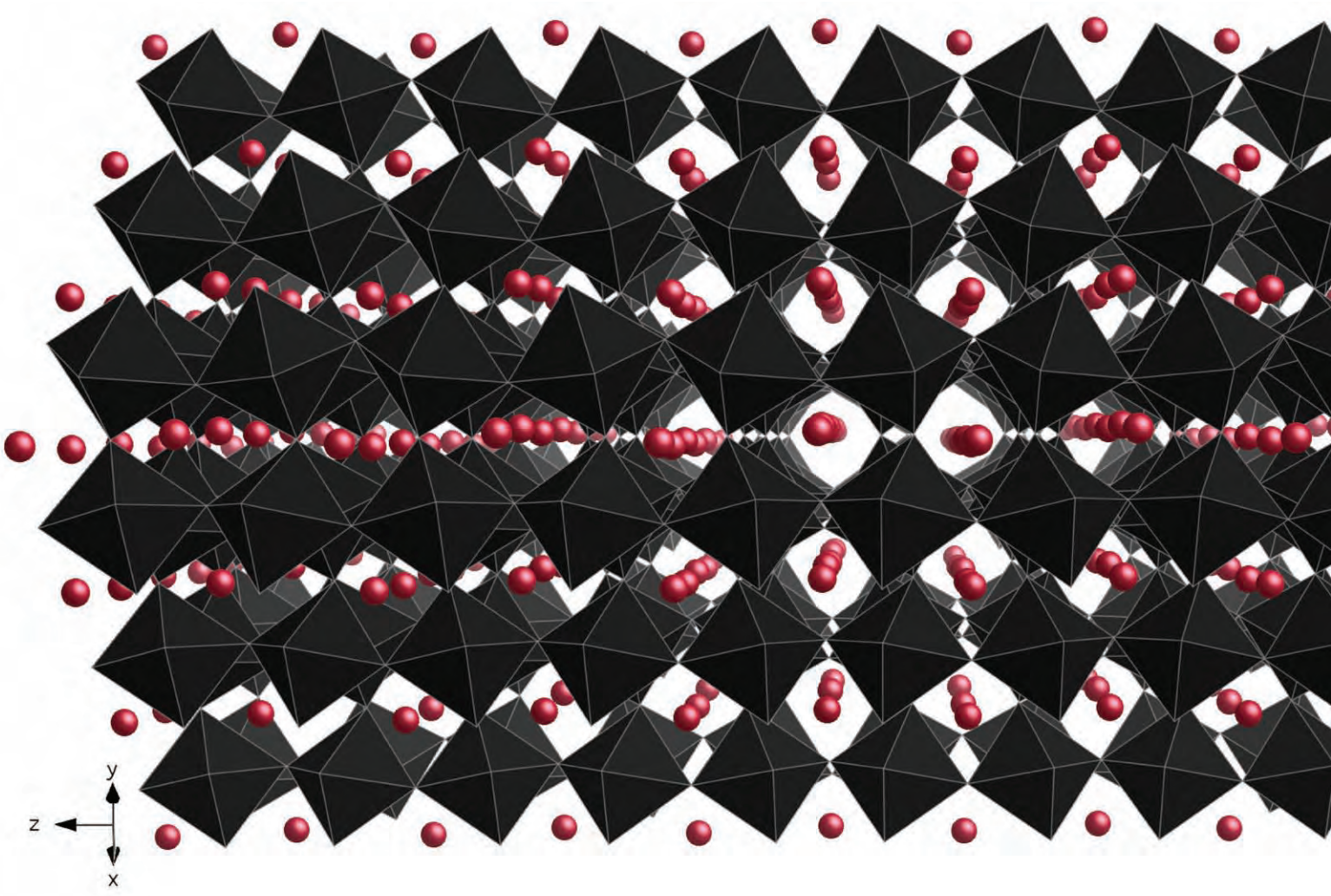

Fig. 1. The crystal structure of $MgSiO_3$ perovskite, spacegroup Pbnm. Magnesium atoms are shown as red spheres (A site), while the black octahedra contain silicon atoms at the center (B site) with oxygen atoms at the corners. The study found that ferric iron entered into the A and B sites in approximately equal proportions; above ~55 GPa, all ferric iron in the B site was found to be low spin.

Magnesium silicate-perovskite ($MgSiO_3$ Pv) is stable over a large depth range in the lower mantle. Aluminum and iron may substitute for Mg and/or Si in perovskite (Fig. 1). Due to the effect of pressure, iron may exist as both Fe^{2+} and Fe^{3+} even under the highly reducing conditions of the lower mantle. The presence of Fe^{3+} may alter the properties of Pv because Fe^{3+} is more likely to transition from high spin to low spin, which would, for example, increase electrical conductivity and control radiative conductivity.

To investigate the spin state of ferric iron in $MgSiO_3$–Pv and its effect on the properties of Pv, researchers from MIT, the Carnegie Institution of Washington, Lawrence Livermore National Laboratory, and The University of Chicago carried out the first laser-heated diamond anvil cell analysis of a Pv synthesized with all iron as Fe^{3+}. The researchers took full advantage of the diverse high-pressure techniques available at the APS to study the spin state of Fe^{3+} and its effects on physical properties: synchrotron Mössbauer spectroscopy at XSD beamline 3-ID, x-ray emission spectroscopy at the HP-CAT 16-ID-D beamline, and angle dispersive x-ray diffraction at the GSECARS 13-ID and HP-CAT 16-ID-D beamlines.

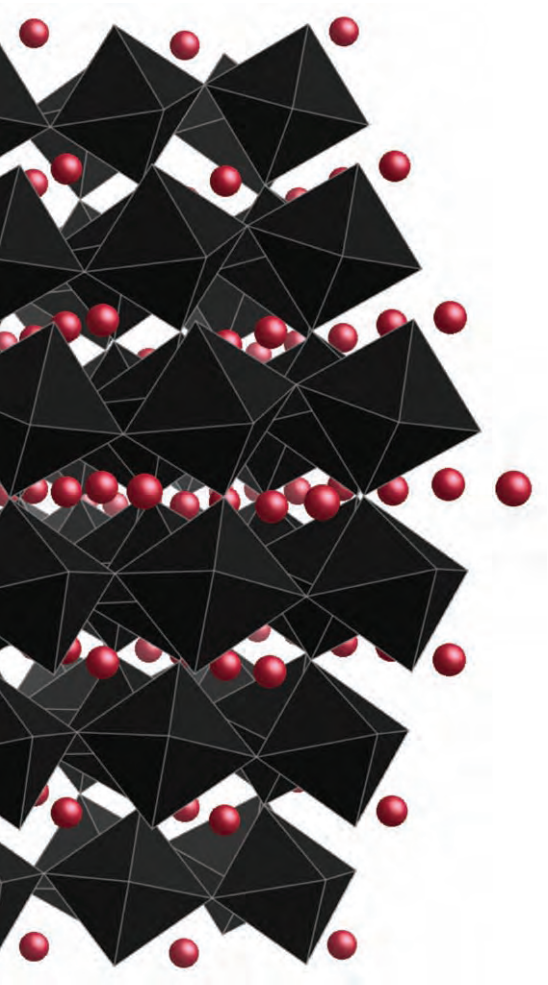

The team found that Fe^{3+} substitutes for Mg and Si about equally. With increasing pressure, Fe^{3+} in the Si site undergoes a gradual spin-pairing transition from high spin to low spin up to 55 GPa. The Fe^{3+} in the Mg site remains high spin. This results in a change in compressibility with no change in density.

The unusual change found in Fe^{3+}-bearing perovskite may provide a new seismic probe sensitive to the oxidation state of iron in Pv. A number of seismic studies have shown that oceanic crust can be transported deep into the mantle through subduction processes around the Circum-Pacific and other regions. Oceanic crust has a very distinct composition from the bulk mantle, notably elevated amounts of aluminum. It has been shown that aluminum enhances the fraction of Fe^{3+} in Pv. Therefore, it can be postulated that Pv in oceanic crust in the lower mantle may contain higher amounts of Fe^{3+}.

According to this study, the elevated amount of Fe^{3+} in oceanic crust would make this material elastically distinct from the surrounding mantle. Seismologists can combine their imaging tools with these new results to answer some important questions in geophysics, such as how deep subducting slab materials reach in the mantle, and where the slab materials would ultimately be deposited. These are very important questions in geophysics because oceanic crust material contains much greater concentrations of heat producing elements and distinct isotopes which geochemists have used to unravel the evolution of Earth's mantle. — *Dana Desonie*

See: Krystle Catalli[1]*, Sang-Heon Shim[1], Vitali B. Prakapenka[2], Jiyong Zhao[3], Wolfgang Sturhahn[3], Paul Chow[4], Yuming Xiao[4], Haozhe Liu[4], Hyunchae Cynn[5], and William J. Evans[5], "Spin state of ferric iron in $MgSiO_3$ perovskite and its effect on elastic properties," Earth Planet. Sci. Lett. **289**, 68 (2010). DOI:10.1016/j.epsl.2009.10.029

Author affiliations: [1]Massachusetts Institute of Technology, [2]The University of Chicago, [3]Argonne National Laboratory, [4]Carnegie Institution of Washington, [5]Lawrence Livermore National Laboratory

Correspondence: *krystle@mit.edu

GSECARS is supported by the National Science Foundation (NSF), Department of Energy (DOE), and the State of Illinois. Portions of this work performed at HP-CAT were supported by DOE, NSF, and the W. M. Keck Foundation. Use of XSD beamline 3-ID was partially supported by the Consortium for Materials Properties Research in Earth Sciences. K.C. is supported by the DOE National Nuclear Security Administration Stewardship Science Graduate Fellowship. This work is supported by NSF to S.H.S. (EAR0738655). Use of the Advanced Photon Source, an Office of Science User Facility operated for the U.S. DOE Office of Science by Argonne National Laboratory, was supported by the U.S. DOE under Contract No. DE-AC02-06CH11357.

3-ID • XSD • Physics • High-pressure diamond anvil cell, inelastic x-ray scattering, nuclear resonant scattering • 7-27 keV, 14.41-14.42 keV • On-site • Accepting general users

13-ID • GSECARS • Environmental science, geoscience • High-pressure diamond anvil cell, high-pressure multi-anvil press, inelastic x-ray scattering, microdiffraction, microfluorescence (hard x-ray), small x-ray absorbtion fine structure, x-ray absorption fine structure • 4-45 keV • On-site • Accepting general users

16-ID-D • HP-CAT • Materials science • High-pressure diamond anvil cell, inelastic x-ray scattering (1-eV resolution), nuclear resonant scattering, x-ray emission spectroscopy, x-ray raman scattering • 6-25 keV • On-site • Accepting general users

First Look at the 3-D Surface and Interface Structure of Goethite in Contact with Water

As we seek to understand how toxic materials move through the ground, we must understand the chemical and physical details of how such materials interact with the molecules in soil and ground water. One such close relationship is between an iron oxide mineral known as goethite (α-FeOOH). Goethite is found globally but is particularly abundant in water-rich delta areas in South Asia — a geographic region that also sees an excess of arsenic-related health problems. Iron oxides are responsible for the transport of arsenic, as well as other toxic materials such as lead and mercury. Understanding how goethite reacts with arsenic can enhance models of how the toxic element is transported and released throughout this and other areas. By revealing new information about the interface of goethite and water, researchers using the APS have replaced educated assumptions with facts that will help us understand the movement of toxins from soil to groundwater, and point toward potential remediations.

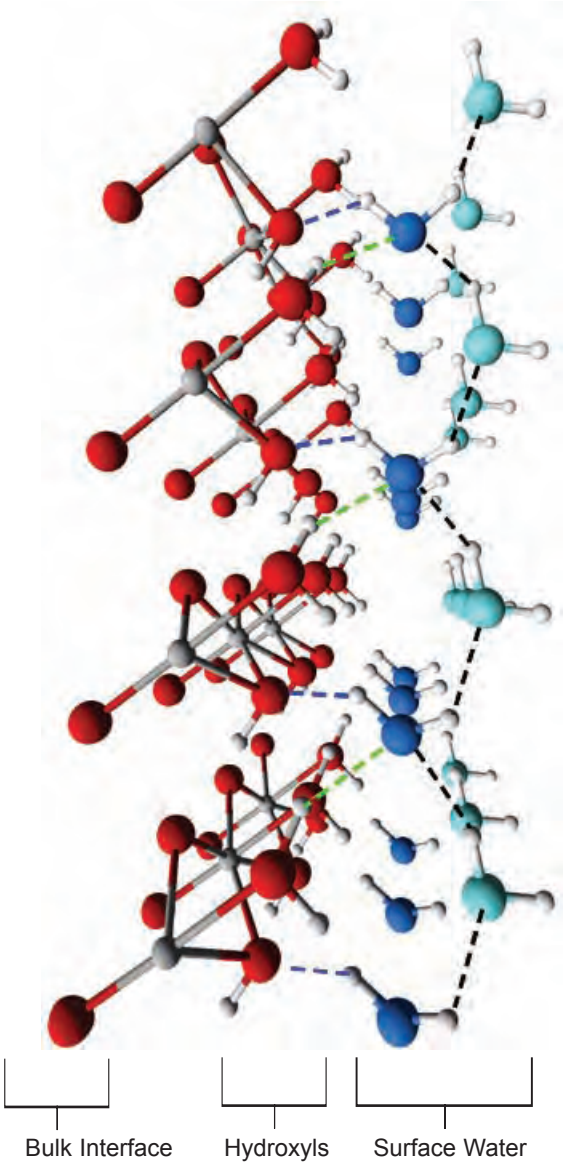

Fig. 1. Three-dimensional view of the interface structural model of hydrated goethite. Dashed lines show the hydrogen bonding between the terminal hydroxyls of the goethite, the first water layer, and the second water layer. The different colors correspond to different hydrogen bond lengths: green = 2.0 Å, black = 1.9 Å, and blue = 1.7 Å.

These results will aid in predicting whether arsenic is likely to stay in the soil or make its way to groundwater

Carrying out surface x-ray diffraction experiments at the GSECARS 13-ID beamline at the APS provided researchers from The University of Chicago, Lawrence Berkeley National Laboratory, and the University of Alaska Fairbanks with the first three-dimensional surface structure of goethite with a water interface and predicted the hydroxyl structures of the surface oxygen atoms, which are the most important and vulnerable areas for reactions and bonding with outside elements.

The team began with a single natural goethite sample with crystals up to a millimeter in size that they then cleaved into hundreds of small chips, resulting in some 10 high-quality crystals with near atomically smooth cleaved surfaces. For this study they used a chip that had a 1mm by 1 mm surface and a thickness of 0.2 mm.

The surface x-ray diffraction study was carried out while the sample was in a water saturated helium environment at standard temperature and pressures. The specific x-ray technique used was a type known as crystal truncation rod analysis. This technique is particularly sensitive to studies of a crystal's surface and interface and it can be applied to *in situ* conditions. Such sensitivity is only possible due to the high-brightness x-ray beams from third-generation synchrotron radiation sources such as the APS, and this three-dimensional description of goethite's surface is one of the first ever done (Fig. 1). Previous studies have provided some information of how water reacts with certain surfaces, but only in one dimension and with little detail.

For the goethite sample in water at a neutral pH, the team found the surface terminated in Fe-OOH molecules. They then predicted the hydrogen bonding at the surface and thus mapped out the way water is ordered on the surface. Namely, the interface with the water is two water molecules, two hydroxyls (oxygen and hydrogen) and then the goethite surface, also written as (($H_2$0)-($H_2$0)-OHv-OH-Fe-O-O-Fe). There are two types of termination hydroxyls: a bidentate hydroxo group and a monodentate aquo group. The researchers went on to apply bond-valence constraints to the terminal hydroxyls and predicted a plausible dipole orientation as well.

Previous studies using goethite as a model environment sorbent have had to incorporate assumptions about surface chemistry, sorbate binding, and the magnitude of binding constants. These new results provide structural details to fill in such assumptions with quantitative information. Such details, in turn, aid in understanding how the surface interacts and bonds with various toxic elements, which can help predict whether something like arsenic is more likely to stay in the soil or make its way to the groundwater. In addition, such understanding opens the door to remediation possibilities. — *Karen Fox*

See: Sanjit K. Ghose[1,2*], Glenn A. Waychunas[2], Thomas P. Trainor[3], and Peter J. Eng[1], "Hydrated goethite (α-FeOOH) (1 0 0) interface structure: Ordered water and surface functional groups," Geochim. Cosmochim. Acta **74**, 1943 (2010). DOI:10.1016/j.gca.2009.12.015

Author affiliations: [1]The University of Chicago, [2]Lawrence Berkeley National Laboratory, [3]University of Alaska Fairbanks

Correspondence: *sghose@bnl.gov

This research was supported by the National Science Foundation (NSF)-Nanoscale Interdisciplinary Research Team (NSF-0404400) and NSF- Environmental Molecular Science Institute (NSF-0431425) Grants; and the Director, Office of Science, Office of Basic Energy Sciences, Division of Chemical Sciences, Geosciences, and Biosciences, of the U.S. Department of Energy (DOE) under Contract No. DE-AC02-05CH11231. GSECARS is supported by the NSF–Earth Sciences EAR-0622171 and the DOE–Geosciences DE-FG02-94ER14466. Use of the Advanced Photon Source, an Office of Science User Facility operated for the U.S. DOE Office of Science by Argonne National Laboratory, was supported by the U.S. DOE under Contract No. DE-AC02-06CH11357.

13-ID • GSECARS • Environmental science, geoscience • High-pressure diamond anvil cell, high-pressure multi-anvil press, inelastic x-ray scattering, microdiffraction, microfluorescence (hard x-ray), small x-ray absorbtion fine structure, x-ray absorption fine structure • 4-45 keV • On-site • Accepting general users

In or Out: Setting a Trap for Radioactive Iodine

Nuclear power plants produce a host of radioactive isotopes as by-products. One such radioisotope is Iodine-129 (^{129}I). With a half-life of nearly 16 million years, the ^{129}I produced by nuclear power plants will be sticking around for a long time. Because iodine plays a role in human metabolism, radioactive ^{129}I is especially dangerous if it escapes into the environment. Researchers utilizing the APS have uncovered new information that might lead to improved long-term storage of Iodine-129.

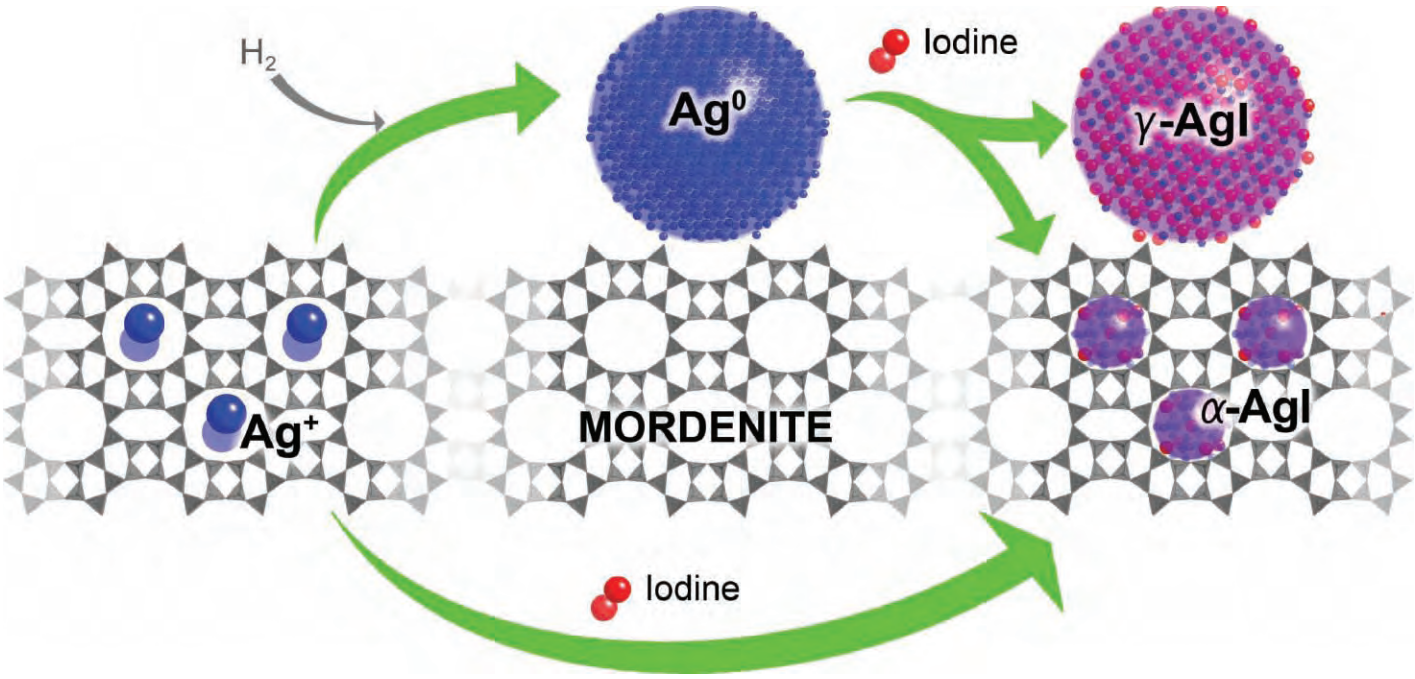

Fig. 1. Porous mordenite is illustrated in the middle portion of the figure. Tiny particles of ionic silver (Ag^+) are attached to the mordenite, as depicted by the three small blue spheres. Today's standard approach to capturing radioactive iodine begins with the reduction of the Ag^+ particles using hydrogen gas, resulting in neutral silver (Ag0—the large blue sphere at top center) embedded within the mordenite. When exposed to iodine gas (the tiny red spheres) the silver-laden mordenite forms different crystalline phases of silver iodide—depicted by the larger gamma phase (γ-AgI) particles upon the mordenite's surface, and the smaller alpha phase (α-AgI) confined within its pores.

For decades the nuclear industry has employed silver particles embedded within a mineral matrix to capture radioactive iodine gas. The silver and iodine combine to form silver iodide (AgI) nanocrystals. The researchers in this study, from Argonne and Sandia National Laboratories, wanted to learn more about the microscopic structure of the AgI formed from iodine capture. To accomplish their goal they employed highly-intense x-rays produced at XSD beamline 11-ID-B of the APS to probe mineral samples containing silver iodide particles.

For this study, , the group prepared powdered samples of a commercially produced mineral analog called mordenite, a type of zeolite. Zeolites encompass an array of porous minerals used extensively by industry as catalysts, molecular filters, and—of particular importance here—in radioactive waste remediation.

Mordenite laced with silver has long been used to capture radioactive iodine, but no one had been able to decipher the details of the capture mechanism on the molecular scale. To uncover those molecular details, the group turned to a technique called pair distribution function (PDF) analysis. The PDF experiment is conceptually very similar to x-ray powder diffraction. Used in laboratories all over the world, x-ray powder diffraction can analyze that materials possess crystalline structure, but exist as jumbles of smaller particles; for instance, the hundreds of crystalline grains found in a teaspoon of salt. In powder diffraction, x-rays travelling through a sample produce a

This research shows the importance of studying materials on the molecular and atomic scales so as to optimize their desirable characteristics

distinctive pattern used to deduce the underlying crystalline structure(s).

For these particular materials, PDF is superior to standard powder diffraction techniques. Unlike powder diffraction, which analyzes only the position and intensity of the peaks in the pattern, PDF analyzes all the scattering, including diffuse scattering features in the so-called background. PDF provides information about the different interatomic distances within the material regardless of sample crystallinity or homogeneity. The APS provides ideal conditions to carry out the PDF technique because and the 11-ID-B beamline is the only dedicated PDF beamline in the U.S.

A total of four samples of silver-laced mordenite were examined using PDF (Fig. 1). Two of the samples held a mordenite-and-silver combination (the silver can bind to iodine). But the silver in those two mordenite samples differed: one held ionic silver (Ag^+), meaning that the silver atoms donated electrons to other types of atoms in the mineral. The other mordenite-and-silver sample was treated with heated hydrogen gas so that the silver was converted (or reduced) from the ionic form to the neutral (or pure metallic) form, called Ag^0.

The other two samples were identical to the first two, except that they were exposed to iodine gas, resulting in AgI nanocrystal formation within the mordenite. By subtracting-out the x-ray data from the samples lacking iodine, a differential PDF (denoted d-PDF) produced detailed molecular-scale information of the AgI particles themselves (i.e., excluding the mordenite matrix).

In nuclear waste remediation, radioactive iodine is trapped by mordenite impregnated with neutral silver (Ag^0) particles. The PDF data showed that after exposure to gaseous iodine, the Ag^0–and-mordenite sample formed AgI nanocrystals within the mordenite, as expected.

But two sizes of nanoparticles were revealed, each possessing its own crystalline phase, or form. The smaller alpha crystalline phase of silver iodide (α-AgI) was trapped within the tiny pores of the mordenite and possessed sub-nanometer dimensions. By contrast, the larger gamma crystalline phase of silver iodide (γ-AgI) lay upon the mordenite's surface. These findings shed new light on how silver iodide particles exist within mordenite in present-day nuclear waste treatment.

What struck the researchers was the quite unexpected finding that the AgI nanoparticles found in the Ag^+ (ionic silver)-impregnated sample all possessed sub-nanometer dimensions, and were confined within the mordenite's pores. The researchers hypothesize that this new finding may provide an improved method for radioactive iodine capture and retention if a way can be found to permanently trap the toxic AgI within the mordenite's pores.

This research shows the importance of studying materials on the molecular and atomic scales so as to optimize their desirable characteristics.

— Philip Koth

See: Karena W. Chapman[1]*, Peter J. Chupas[1], and Tina M. Nenoff[2], "Radioactive Iodine Capture in Silver-Containing Mordenites through Nanoscale Silver Iodide Formation," J. Am. Chem. Soc. **132**, 8897 (2010). DOI: 10.1021/ja103110y

Author affiliations: [1]Argonne National Laboratory, [2]Sandia National Laboratories

Correspondence:
*chapmank@aps.anl.gov

Work performed at Argonne and use of the Advanced Photon Source, an Office of Science User Facility operated for the U.S. Department of Energy (DOE) Office of Science by Argonne National Laboratory, was supported by the U.S. DOE under Contract No. DE-AC02-06CH11357. Work performed at Sandia is supported by the U.S. Department of Energy, Office of Nuclear Energy, Fuel Cycle R&D, Separations and Waste Forms Campaign. Sandia is a multiprogram laboratory operated by Sandia Corporation, a Lockheed Martin Company, for the U.S. DOE's National Nuclear Security Administration under Contract No. DE-AC04-94AL85000.

11-ID-B • XSD • Chemistry, environmental science, materials science • Pair distribution function • 58-60 keV, 90-91 keV • On-site • Accepting general users

El Dorado in the Lab: 3-D Imaging of Nanoporous Gold

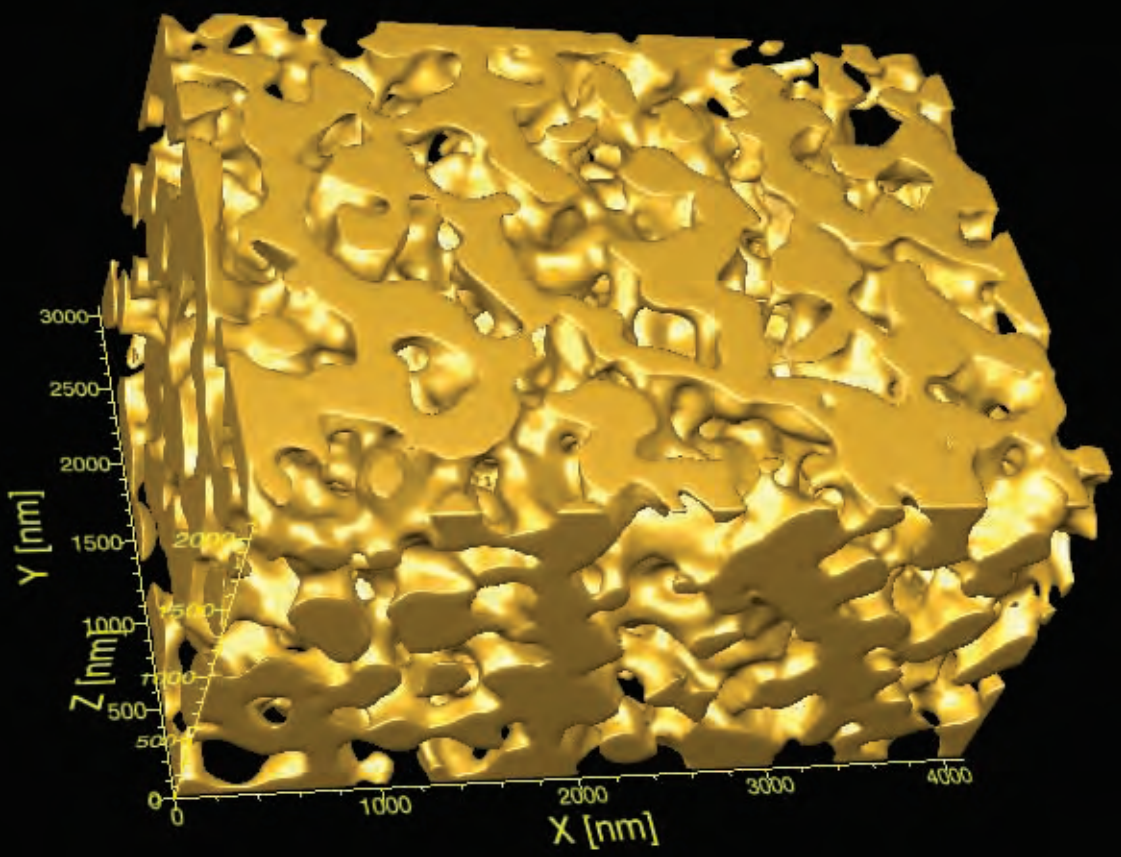

Although the alchemists never managed to transform lead into gold, materials scientists are now capable of producing a useful form of the precious metal from a common alloy of silver and gold. Fabrication of nanoporous gold is not new; thin films are routinely created and analyzed in the lab. But the ability to examine in three dimensions the morphological and topological properties of thicker segments of nanoporous gold coarsened by annealing has remained elusive. Now, a study by researchers using an APS x-ray beamline offers a new understanding of coarsened nanoporous gold, a material with promising applications as catalysts, biomedical sensors, and drug delivery devices.

Using transmission x-ray microscopy (TXM) at XSD beamline 32-ID at the APS, the team of researchers from Northwestern University and the Argonne and Brookhaven national laboratories made nanotomographic measurements of a 10-μm nanoporous gold wire created by dealloying a gold/silver alloy and annealing the porous gold structure.

Images were captured by a technique similar to a computerized axial tomography scan. Multiple two-dimensional slices taken at a sequence of angles over time are reconstructed using a common algorithm—filtered-back-projection—to create a three-dimensional (3-D) reconstruction of the specimen (Fig. 1), which was analyzed to determine its morphological and topographical features.

The specimen was obtained by casting a silver/gold alloy wire 50 μm in diameter, with a gold content of 30% and a monocrystalline structure, through a thin Pyrex tube. The alloy that protruded from a fracture point in the tube was treated with nitric acid to leach the silver out and create a wire with gold ligaments interspersed with nanometer sized chambers of air, somewhat like a sponge. The gold wire was then milled using focused ion beam-scanning electron microscopy (FIB-SEM) into a cylinder that measured 10-μm in diameter and 20-μm tall. Coarsening was achieved by annealing the tip of the wire at 400° C for 30 min.

< Fig. 1. A 3-D reconstruction of a nanoporous gold sample, annealed at 400° C for 30 min, imaged at XSD beamline 32-ID utilizing TXM.

The use of TXM represents an improvement over electron-based tomographic techniques used to examine thin films of nanoporous gold because the electrons cannot penetrate the depths of thicker film. Thin films can also be analyzed using FIB-SEM, but those scans are destructive and cannot be used to observe the evolution of the structure over time. The non-destructive synchrotron x-ray sources of TXM offer resolution at a scale of 30 nm and also capture images as thick as tens of microns.

A small sample 2 × 3 × 4 μm in volume was obtained from the coarsened wire tip for analysis of topology and morphology (Fig. 1). Interfacial shape distribution of the annealed specimen revealed a wide range of curvatures unlike those found in other bicontinuous structures coarsened using a bulk diffusion method. Other mechanisms for coarsening include evaporation/condensation or surface diffusion, which are likely responsible for the broadening of the curvature distribution of the interfaces in this sample.

Upon visual inspection, the surface structure of the 3-D reconstructed sample appeared to be isotropic, or uniform in all directions. Calculation of the surface normal distribution, however, revealed an anisotropic texture which cannot be due to grain effects because of the monocrystalline structure of the nanoporous gold. Rather, the dealloying or annealing process likely altered the alignment and orientation of the closely packed planes along the interfaces between the gold and air pockets. The finding of anisotropy in the surface morphology has important implications for the properties and functions of nanoporous gold.

This study represents a step forward in understanding the basic characteristics of coarsened nanoporous gold, a material with promising applications as catalysts, biomedical sensors, and drug delivery devices.

— Elise LeQuire

See: Yu-chen Karen Chen[1,2]*, Yong S. Chu[3], JaeMock Yi[2], Ian McNulty[2], Qun Shen[3], Peter W. Voorhees[1], and David C. Dunand[1], "Morphological and topological analysis of coarsened nanoporous gold by x-ray nanotomography," Appl. Phys. Lett. **96**, 043122 (2010). DOI:10.1063/1.3285175

Author affiliations: [1]Northwestern University, [2]Argonne National Laboratory, [3]Brookhaven National Laboratory

Correspondence:
*yuchenchen2010@u.northwestern.edu

Use of the Advanced Photon Source, an Office of Science User Facility operated for the U.S. Department of Energy (DOE) Office of Science by Argonne National Laboratory, was supported by the U.S. DOE under Contract No. DE-AC02-06CH11357.

32-ID • XSD • Geoscience, life sciences, materials science • Phase contrast imaging, radiography, tomography, transmission x-ray microscopy • 7-40 keV • On-site • Accepting general users

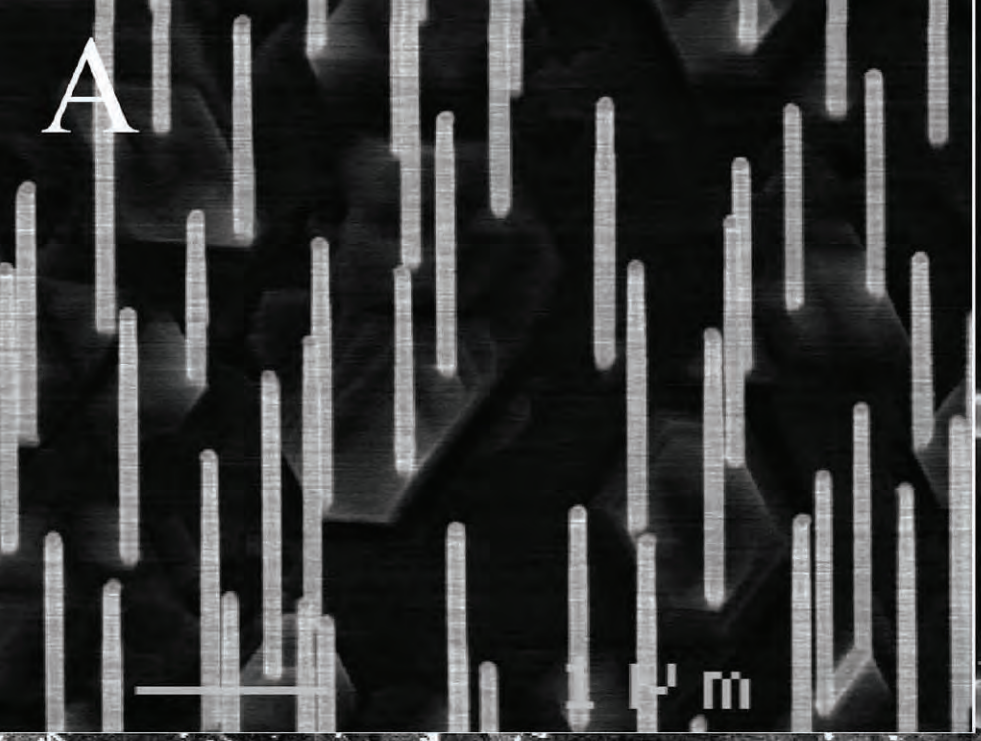

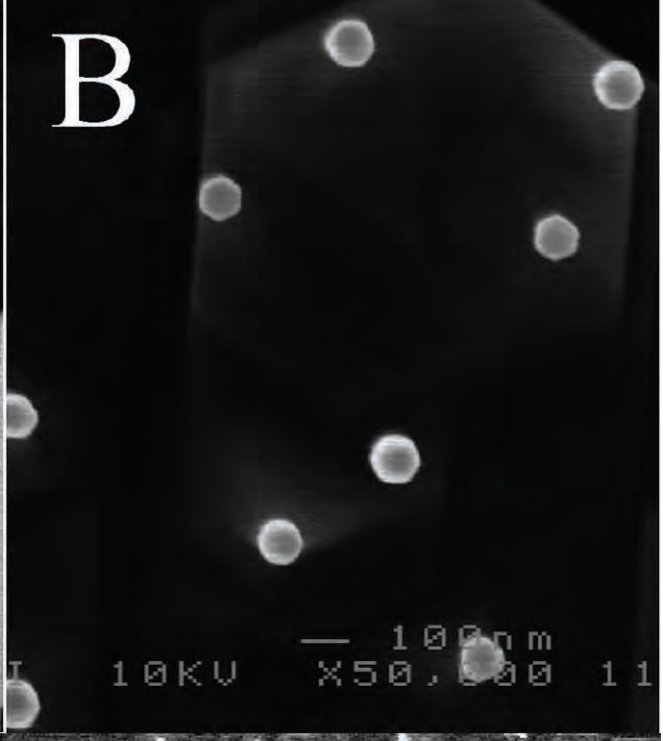

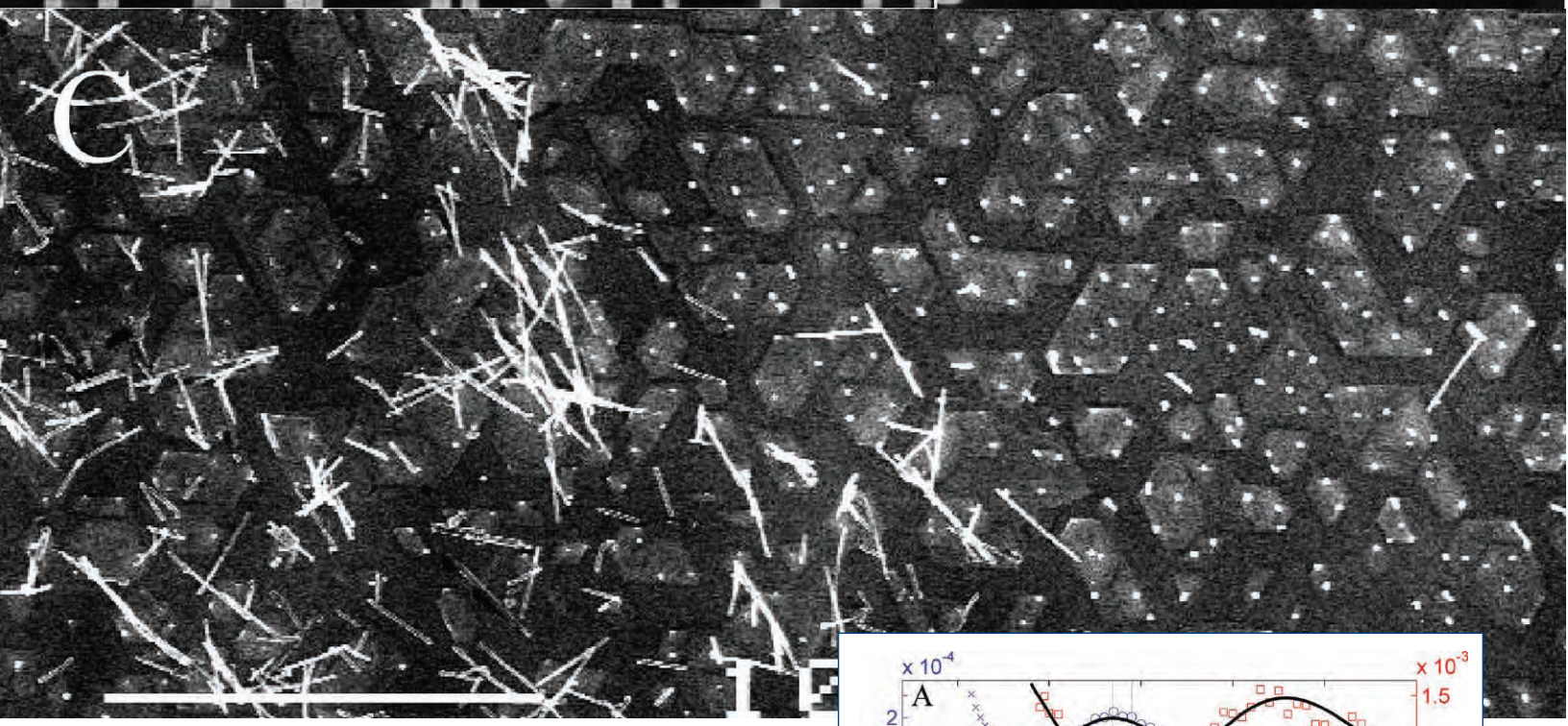

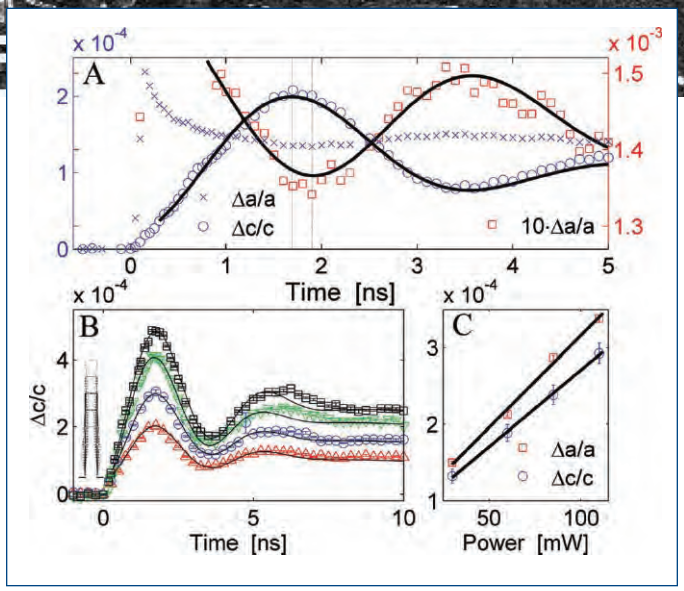

Main image: Scanning electron microscope images of InAs nanowires seen at an angle of 20° (A) and showing the hexagonal facets from a top view (B). The lower image (C) shows a region of wires broken at high laser power. *Inset at right:* Extensional mode. (A) Relative change in lattice constants a (crosses) and c (circles) as a function of time. as measured by time-resolved x-ray diffraction. The motion in the axial lattice constant a has also been amplified 10 times (squares, right y axis) for easier comparison. The vertical lines serve as guides to the eye for the phase shift in the first extrema. The solid lines are fit to the data. (B) Relative change in the axial lattice constant c at powers of 30 (triangles), 60 (circles), 85 (down-pointing triangles), and 110 mW (squares) including fits to the data. (C) Average extension as a function of power.

MAKING NANOWIRES SHIMMY AND SHAKE

One can tell a lot about someone by the way they move: Gracefulness or clumsiness can sometimes be clues to someone's personality and behavior. The same is true of inanimate objects, although we usually have to shake them, push them, or otherwise interact with them to see how they respond. That is true both on the macro level, where, for example we might jostle a table to test its sturdiness, and on the nanolevel, where structures can be nudged by more subtle means to see how they respond. Now experimenters have set nanowires in motion with laser pulses to study their structure and mechanical properties using x-ray diffraction techniques at the XSD 7-ID beamline at the APS and beamline ID09b at the European Synchrotron Radiation Facility (ESRF). Directly quantifying and observing acoustic oscillations in nanowire structures enhances the exploration of basic research questions in nanoscience and has important implications for the design of the many practical applications for which nanowires are ideally suited, such as various types of sensors and detectors.

A team of researchers from the Niels Bohr Institute at the University of Copenhagen and from the ESRF grew InAs nanowires on an InAs substrate, then subjected the samples to a femtosecond laser pulse. Using time-resolved x-ray diffraction and optical reflectivity techniques, they achieved direct measurements of three different acoustic oscillations in the structure of the InAs nanowire.

Much effort has gone in to studying and measuring acoustic vibrations (also called coherent acoustic phonons) in nanowires because they provide an easy and convenient means to characterize the structure and mechanical behavior of the wires and even of other nanostructures. Techniques including scanning electron microscopy, Raman spectroscopy, scattering interferometry, and other optical and electron microscopy tools have been used, but at best are able to provide only approximate models based on continuum elasticity theory. The present work with synchrotron x-ray diffraction and optical reflectivity, however, provides much greater detail and precision than has been possible with any of the alternative techniques.

The experiments were conducted in two phases. In both cases, a Ti:sapphire laser pulse was used to create acoustic phonons in the nanowires, which were then studied either by obtaining Bragg diffraction peaks from the forest of nanowires, or by optical reflectivity measurements using a second laser as a probe. As the nanowire lattice responded to the laser excitation, the researchers could isolate three distinct acoustic eigenmodes: a "breathing" oscillation in the radial direction; a extensional motion in the longitudinal axis of the nanowire; and a bending mode between the free and fixed ends of the wire. Optical reflectivity and x-ray diffraction measurements allowed the frequencies and amplitudes of the breathing and extensional eigenmodes to be determined. These were found to be in excellent agreement with mathematical predictions from continuum elasticity theory, but also demonstrated that there is a slight delay between the axial and radial oscillations, and that in general the interaction and overlapping between the different oscillatory modes needs to be taken into account in order to fully explain their mechanics.

The breathing and extensional modes are followed by bending of the nanowire in the laser scattering plane, again in good agreement with theoretical calculations. The researchers believe that while the first two acoustic eigenmodes begin with excitation of electron-hole pairs that lead to acoustic phonons, the bending mode is the result of strain waves from the uneven heating of the wire. The speed of sound in the InAs nanowires is identical to that in bulk cubic crystal InAs, but the nanowires display anisotropic thermal expansion.

This newly refined capacity to directly quantify and observe acoustic oscillations in nanowire structures obviously enhances the exploration of basic research questions in nanoscience. But it also has important implications for the design of the many practical applications for which nanowires are ideally suited, such as various types of sensors and detectors. It can provide a double-barreled benefit, because precisely measuring acoustic oscillations could help determine nanoscale geometries and mechanics, while certain types of nanostructures can be used to study the formation and behavior of acoustic phonons. As with many other things, the experiments show that when it comes to nanowires, it's all in the way they move. — *Mark Wolverton*

See: Simon O. Mariager[1]*, Dmitry Khakhulin[1], Henrik T. Lemke[1], Kasper S. Kjær[1], Laurent Guerin[2], Laura Nuccio[1], Claus B. Sørensen[1], Martin M. Nielsen[1], and Robert Feidenhans[1]**, "Direct Observation of Acoustic Oscillations in InAs Nanowires," Nano Lett. **10**, 2461 (2010). DOI:10.1021/nl100798y
Author affiliations: [1]University of Copenhagen, [2]European Synchrotron Radiation Facility
Correspondence: *som@fys.ku.dk and **robert@fys.ku.dk

The work was supported by the Danish Natural Science Council through DANSCATT and by the Danish National Science Foundation. OE and the MR-CAT member institutions. Use of the Advanced Photon Source, an Office of Science User Facility operated for the U.S. Department of Energy (DOE) Office of Science by Argonne National Laboratory, was supported by the U.S. DOE under Contract No. DE-AC02-06CH11357.

7-ID • XSD • Atomic physics, chemistry, materials science • Phase contrast imaging, time-resolved x-ray absorption fine structure, time-resolved x-ray scattering • 6-21 keV • On-site • Accepting general users

SEEING STRAIN IN A SINGLE NANOSCALE STRUCTURE

Determining the properties of nano-sized structures is vitally important to research scientists, not least because discovering the unique characteristics of these structures could lead to improved optics, electronics, or super-strong building materials. Because the properties of nanostructures are typically quite different than those of bulk amounts of the same material, researchers are compelled to probe these incredibly tiny structures to uncover their unique properties. In this research, carried out at the XSD 34-ID beamline at the APS, the strain (the internal forces between atoms) within a zinc oxide (ZnO) nanorod was determined. Previous efforts, using techniques such as transmission electron microscopy, had only measured nanorod strain in one dimension. But the scientists involved in this research experimentally determined the strain in all three dimensions within a ZnO nanorod. These techniques could conceivably be used to determine critical properties of nanoscale semiconductors for future electronic devices as well as advances in materials for energy storage.

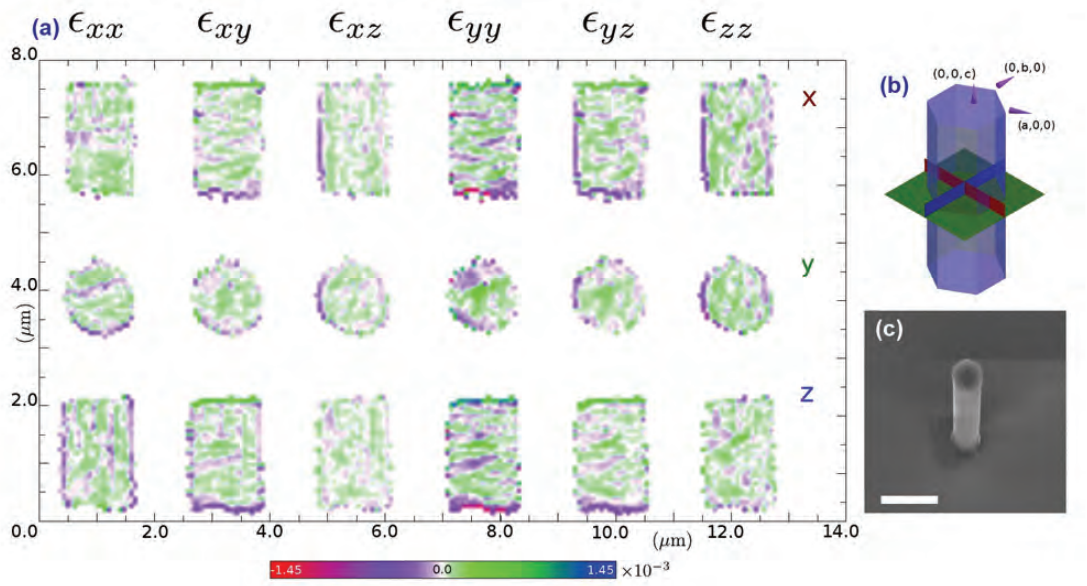

Fig. 1. (a) Two-dimensional slices of the six independent components of the strain tensor. Components are taken along the three Cartesian axes according to (b). Regions of compressive (negative) strain are observed near the (100) surfaces of the crystal and at the interface with the Si substrate. A strained layer approximately 200-nm in width near the surface and along the length of the rod (y axis) is visible in all tensor components except the ϵ_{yy} component. This implies that the strain is uniform along the length of the rod and is attributed to absorption of oxygen at the surface during sample preparation. (b) Diagrammatic representation of a single ZnO rod showing the three crystallographic orientations. The three planes from which slices of the phase map are taken are also shown (color coded). (c) Scanning electron micrograph of the single ZnO rod used in x-ray measurements standing on a Si substrate with its c axis approximately normal to the surface. Scale bar: 2 μm.

The zinc oxide nanorods created for this research were formed on a flat silicon substrate. Nanorod formation involved a multi-step process beginning with the vaporization of a zinc-containing powder at high temperatures in the presence of a gaseous argon/oxygen mixture, followed by condensation of the vapor upon the silicon substrate. The resulting crystalline ZnO nanorods formed hexagonal prisms. Lengths of the hexagonal nanorods ranged from between 2 μm to 4 μm, with widths of between 1 μm and 2 μm.

Individual ZnO nanorods could be moved from their original silicon substrate to a new one using a tiny needle-shaped manipulator arm. One particular nanorod was chosen for the x-ray diffraction measurements, and was placed on-end atop a new silicon substrate. The nanorod and substrate were heated to 750° C for 16 h in the presence of pure oxygen gas. The resulting 50-nm-thick silicon oxide layer "glued" the nanorod to its transplanted silicon substrate. After the oxidation process was finished, the nanorod was imaged resting upon the silicon substrate using a scanning electron microscope, as shown in Fig. 1c.

Passing the x-ray beam from 34-ID through a double-crystal monochromator filtered out all but a narrow range of x-rays with wavelengths centered on 1.42 Å.

The silicon substrate upon which the nanorod was mounted could be rotated through an entire revolution. As the nanorod was incrementally rotated, the coherent x-ray beam diffracted through its crystalline structure. At certain angular positions, Bragg peaks were produced by the diffracted x-rays. At each incremental rotation of the nanorod during this experiment, planar (two-dimensional) slices of the diffraction pattern were acquired by a charge-coupled device.

Coherent x-rays (as used in this experiment) that are diffracted from a perfectly crystalline nanorod remain in phase coherence. Deviation from perfect crystalline order in the ZnO nanorod (due to, for instance, strain) caused a phase shift of the reflected x-rays. The researchers applied various algorithms to the diffraction data sets that were collected in order to "undo" (i.e., reconstruct) those x-ray phase shifts. From the reconstructed x-ray data, the three-dimensional strain within the nanorod could be calculated. Strain within the nanorod is represented by mathematical quantities called "tensors," otherwise known as strain tensors (Fig. 1a).

The capability to determine the strain distribution within nanostructures, such as the ZnO nanorod examined here, is extremely important because any strain present will influence various properties of the nanorod, such as its electrical or optical characteristics.

The importance of these results has both contemporary and long-term ramifications. The most immediate and practical impact is that the strain within a nanocrystal was experimentally deciphered in three dimensions, opening the door to determining the three-dimensional strain in other nanostructures using similar methods; that is, through the use of highly-intense, coherent x-rays produced at the APS and other synchrotron facilities.

In the longer term, the capability to resolve three-dimensional strain in nanostructures has profound implications for future technological applications. The researchers speculate that their techniques could be applied to measuring important properties of nanoscale semiconductors that hold considerable promise for future electronic devices. Three-dimensional strain mapping of nanostructures could also lead to improvements in materials used for energy storage, and in the characterization of the strain gradients at semiconductor dopant sites.

— Philip Koth

See: Marcus C. Newton[1]*‡, Steven J. Leake[1], Ross Harder[2], and Ian K. Robinson[1,3], "Three-dimensional imaging of strain in a single ZnO nanorod," Nat. Mater. **9**(2), 120 (February 2010). DOI: 10.1038/NMAT2607

Author affiliations: [1]University College London, [2]Argonne National Laboratory, [3]Diamond Light Source ‡Present address: University of Surrey

Correspondence:
*Marcus.Newton@ucl.ac.uk or
*m.newton@physics.org

This work was supported by Engineering and Physical Sciences Research Council Grant EP/D052939/1 and a European Research Council FP7 "advanced grant." Beamline 34-ID was built with funds from the U.S. National Science Foundation under Grant DMR-9724294. and operated by the US Department of Energy (DOE), Office of Science, Office of Basic Energy Sciences, under Contract DE-AC02-06CH11357. Use of the Advanced Photon Source, an Office of Science User Facility operated for the U.S. DOE Office of Science by Argonne National Laboratory, was supported by the U.S. DOE under Contract No. DE-AC02-06CH11357.

34-ID • XSD • Materials science, physics • Coherent x-ray scattering, microdiffraction • 5-15 keV, 7-25 keV • On-site • Accepting general users

DNA-MEDIATED ASSEMBLY OF ANISOTROPIC GOLD NANOPARTICLES

The physical and chemical properties of nanomaterials are often very different from their bulk counterparts, and both the size and shape of a nanoparticle change its inherent properties and basic behavior. Researchers have shown that spherical nanostructures can be assembled into ordered structures by chemically attaching short DNA strands to gold nanoparticles, and subsequently using programmable DNA recognition interactions to form extended superlattices. The same team of researchers has extended this methodology to incorporate four different morphologies of anisotropic gold nanoparticles: rods, triangular prisms, rhombic dodecahedra, and octahedra (Fig. 1). Small-angle x-ray scattering (SAXS) performed at the DND-CAT beamline 5-ID at the APS determined the crystallographic structure, lattice parameters, and crystal domain sizes of the assembled materials. The characteristics revealed by this work point to the possibility of creating designer materials with applications in new optical sensors, plasmonic-based computing technologies, and molecular detectors.

Interestingly, the shape of the nanoparticles being ordered was shown to significantly affect their assembly behavior, as each nanoparticle type directed the formation of a different superlattice whose crystallographic symmetry was dictated by the shape of the individual particle building blocks. In addition, transmission electron micrographs (TEM) of crystals embedded in a resin were used to confirm the findings of the SAXS experiments. The advantage of using synchrotron-based SAXS in probing the colloidal samples used in this study is that it does not require removal of the superlattices from aqueous suspension, which would significantly alter their structure. SAXS has been used previously by this team of researchers from Northwestern University and Argonne, to provide visible evidence of both the final assembled structure, as well as the assembly process of forming ordered superlattices.

Unlike previous assemblies made from spherical nanoparticles, which exhibit identical DNA binding interactions in all directions, particles with shape anisotropy demonstrate directional bonding interactions. The DNA strands used to assemble these particles have “sticky ends” that are presented at a programmable distance off of the particle surface; lattices are formed when these sticky ends hybridize to the sticky ends of adjacent particles. Such structures exhibit increasing stability as the number of DNA sticky ends interactions increases. As one would expect, different particle shapes exhibit different amounts of DNA interactions depending on how these particles are aligned relative to one another.

For one-dimensional (1-D) nanorods, which are longer than they are wide or deep, the maximum number of sticky end interactions is obtained when the rods aligned themselves with their long axes parallel to one another. This results in ordered two-dimensional (2-D) superlattices with a closely packed hexagonal configuration. Extremely thin, 2-D, triangular nanoprisms, which have up to 140 nm triangular edges and a thickness of only ~7 nm, arrange themselves in a columnar fashion, forming 1-D stacks. Rhombic dodecahedra, a complex shape that has twelve identical faces, form ordered lattices where each particle has twelve nearest neighbors, and the faces of adjacent particles are aligned parallel to one another. In each of these cases, the different facets of the nanoparticles are aligned such that the DNA interactions between adjacent particles are maximized. Octahedral particles exhibit unique behavior that depends on both the shape of the particle and the length of the DNA strands used to assemble them. Using different lengths of DNA to assemble the particles, ranging from ~15 to ~45 to ~90 nm, the crystals formed either a disordered lattice, a body-centered-cubic lattice, or a face-centered-cubic lattice, respectively. This was attributed to the increasing flexibility of longer DNA strands. For DNA that was very rigid, the sticky ends were found to conform to the anisotropy of the nanoparticle, with densest regions of DNA being found at positions perpendicular to the flat octahedral faces. For very long DNA, this anisotropy was lost, and the resulting superlattice structure demonstrated that the sticky ends were placed around the particle in essentially a spherical arrangement.

The shape of the nanoparticle building blocks and the length and flexibility of the DNA strands play complementary roles in determining the crystallographic symmetry of these assembled nanoconjugate materials. These characteristics add to the tunability of the ordered structures and point to the possibility of creating designer materials with potential applications in new generations of optical sensors, plasmonic-based computing technologies, and molecular detectors.

— Elise LeQuire

See: Matthew R. Jones[1], Robert J. Macfarlane[2], Byeongdu Lee[2], Jian Zhang[1], Kaylie L. Young[1], Andrew J. Senesi[1], and Chad A. Mirkin[1]*, “DNA-nanoparticle superlattices formed from anisotropic building blocks,” Nat. Mater. **9**, 913 (November 2010). DOI:10.1038/NMAT2870

Author affiliations: [1]Northwestern University, [2]Argonne National Laboratory

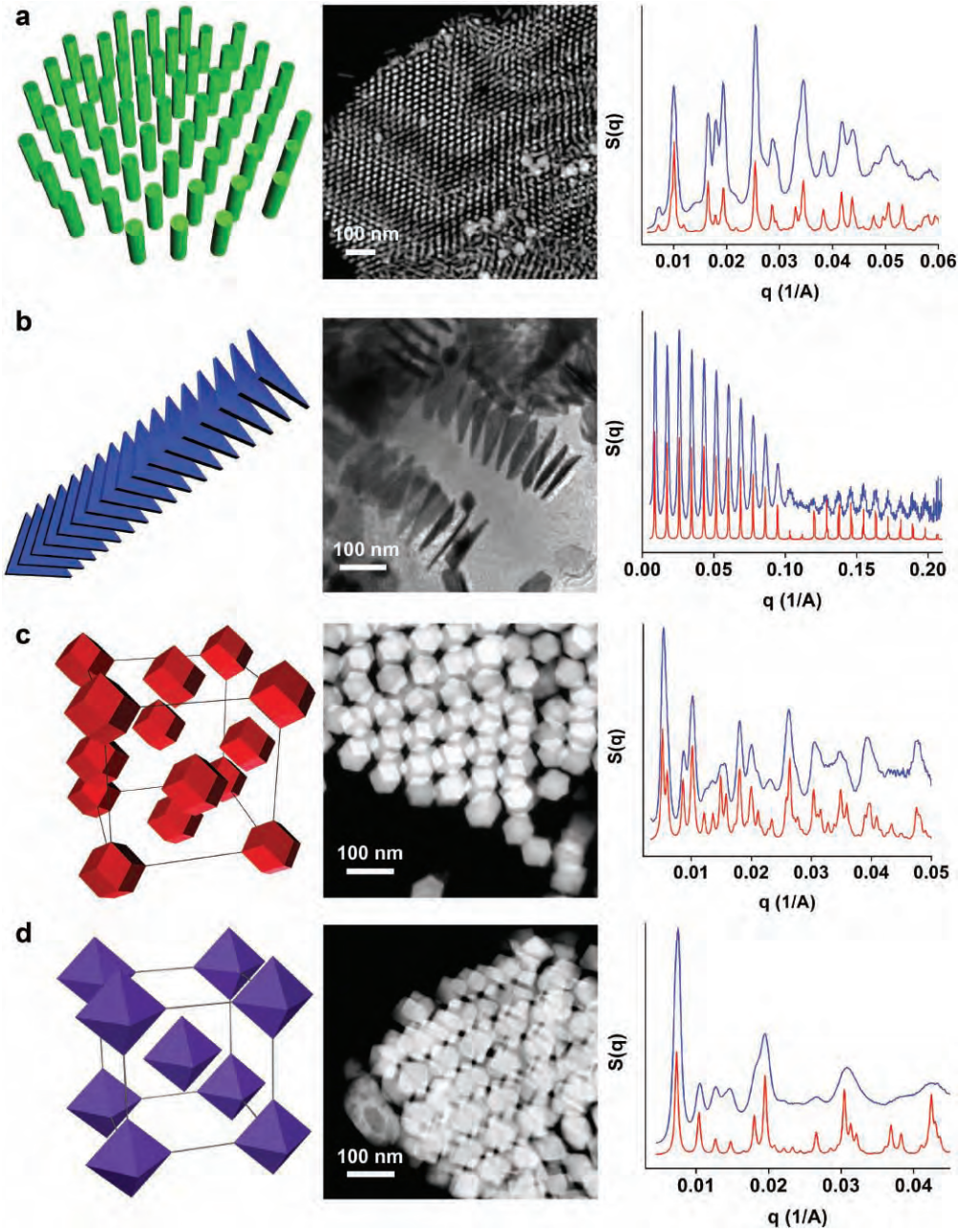

Fig. 1. Anisotropic gold nanoparticles dictate the symmetry and dimensionality of the assembled superlattices that they compose. From left to right: schematic illustration, TEM image, and SAXS pattern of nanoparticle superlattices composed of (a) rods, (b) triangular prisms, (c) rhombic dodecahedra, and (d) octahedra. Experimental SAXS patterns are shown in blue while simulated patterns are shown in red.

Correspondence:
*chadnano@northwestern.edu

See also: Sung Yong Park et al., "DNA-programmable nanoparticle crystallization," Nature **451,** 553 (31 January 2008). Robert J. Macfarlane et al. "Assembly and Organization Processes in DNA-Directed Colloidal Crystallization," Proc. Natl. Acad. Sci. USA **106**(26), 10493 (May 2009).

C.A.M. acknowledges the National Science Foundation (NSF)-Nanoscale Science & Engineering Center and the Air Force Office of Scientific Research for grant support, and the U.S. Department of Energy (DOE) Award No. DE-SC0000989 for support through the Northwestern University Nonequilibrium Energy Research Center. He is also grateful for a National Security Science and Engineering Faculty Fellowship from the Department of Defense. M.R.J. acknowledges Northwestern University for a Ryan Fellowship and the NSF for a Graduate Research Fellowship. R.J.M. acknowledges Northwestern University for a Ryan Fellowship. K.L.Y. acknowledges the NSF and the National Defense Science and Engineering Graduate Fellowship program for Graduate Research Fellowships. DND-CAT is supported by E.I. DuPont de Nemours & Co., The Dow Chemical Company, and the State of Illinois. Use of the Advanced Photon Source, an Office of Science User Facility operated for the U.S. DOE Office of Science by Argonne National Laboratory, was supported by the U.S. DOE under Contract No. DE-AC02-06CH11357.

5-ID • DND-CAT • Materials science, polymer science • Powder diffraction, x-ray reflectivity, small-angle x-ray scattering, surface diffraction, wide-angle x-ray scattering, x-ray standing waves, x-ray optics development/techniques • 5-20 keV • On-site • Accepting general users

THE STRUCTURAL EVOLUTION OF 2-D NANOCRYSTAL SUPERLATTICES

Scientists are striving to use nanocrystals as building blocks to make macroscopic artificial crystals, also known as nanocrystal superlattices (NCSs). In particular, two-dimensional (2-D) NCSs hold great promise for advances in electronic, photonic, and magnetic devices. Many of these applications require nanocrystals to be in a perfect single-crystal phase with long-range order and limited defects so that individual particles can be digitally addressed. The direct characterization of 2-D NCSs has been lacking, partially due to the experimental difficulty of driving nanocrystals into forming perfect 2-D crystalline lattices and the lack of *in situ* probes to precisely determine the superlattice structure. In research carried out at XSD beamline 8-ID-E of the APS, a self-assembling 2-D NCS was probed in real time while it evolved through various ordered states as the highly intense x-rays from the APS allowed the research team to follow the structural evolution of the NCS superlattice.

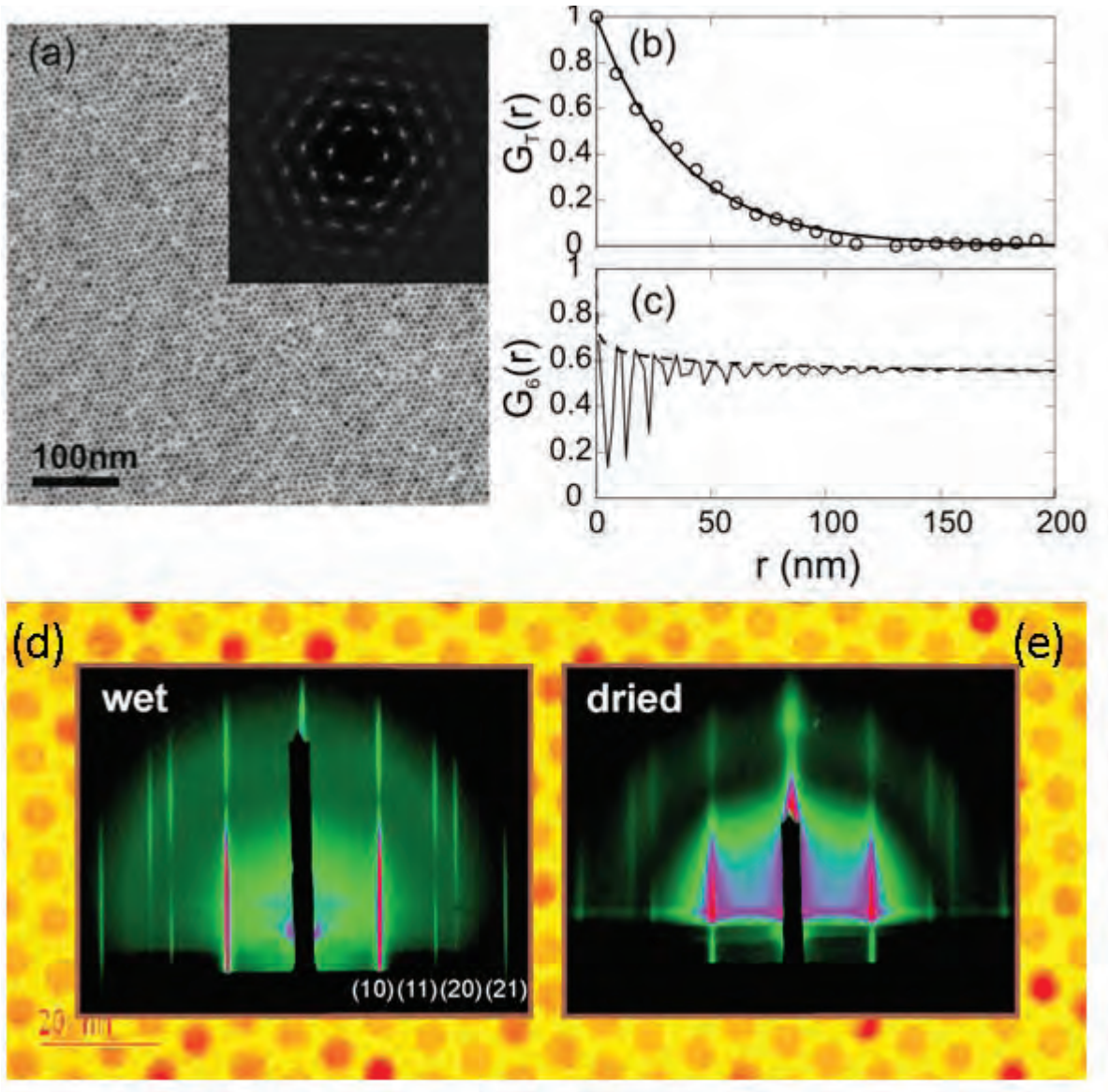

The 2-D superlattice investigated in this research was formed from gold nanocrystals dispersed in toluene. The nanocrystal-in-toluene solution formed a droplet held atop a substrate of silicon nitride. As the solvent evaporated, the gold nanocrystals spontaneously self-assembled to form a 2-D superlattice at the air/liquid interface.

The measurements were carried out by a team of Argonne researchers using highly collimated and monochromatic x-rays (photon energy of 7.35 keV) and grazing-incidence small-angle x-ray scattering (GISAXS) at beamline 8-ID-E. The silicon nitride substrate holding the colloidal suspension of nanocrystals was tilted a 0.3° with respect to the incoming x-ray beam; the x-rays that grazed off the colloidal droplet formed a scattering pattern that was captured by an x-ray charge-coupled device (CCD) detector.

The ordering within many different kinds of 2-D crystals is predicted by the Kosterlitz-Thouless-Halperin-Nelson-Young (KTHNY) theoretical model. KTHNY theory accurately predicts both the long-range orientational ordering that 2-D crystals exhibit and their inherent quasi-long-range positional ordering. The researcher team applied the KTHNY theoretical framework to the GISAXS measurements made of the colloidal nanocrystal sample.

As soon as x-ray scattering was carried out on the colloidal sample, the Bragg peaks occurring within the resulting x-ray diffraction pattern indicated an ordered state. The high measuring resolution afforded by the collimated x-ray beam from 8-ID-E generated diffraction peak shapes that could have only been measured previously by complex scanning methods and a long scanning time. The measurement carried out at 8-ID-E with the CCD detector yielded detailed diffraction patterns in a matter of a few seconds.

Quantitative analysis of the diffraction line shapes resulting from the GISAXS measurements (Fig. 1) revealed that the NCSs were indeed in a crystalline phase at the liquid/air interface of the droplet according to the KTHNY theory. As time progressed, the toluene solvent continued to slowly evaporate. The researchers observed that the spacing between crystalline lattices, which was found to be around 7.7 nm, was more or less constant for periods of up to several hours, if the experimental condition was well controlled.

After the colloidal sample completely dried out, the nanocrystal domains had lost their long-range positional ordering, but retained an orientational ordering. The loss of long-range positional ordering meant that the sample was no longer in a perfect crystal phase as defined by KTHNY theory, but had instead entered a hexatic phase somewhere between that of a crystalline phase, and an isotropic (i.e., no preferred ordering) liquid phase.

One particularly important point is that the GISAXS measurements carried out at the APS were able to directly probe the structural transition at the air/liquid interface, something that other techniques, such as scanning probe microscopes and transmission electron microscopy, cannot accomplish.

The finding of structural evolution during superlattice formation is critical to an understanding of the complexity during bottom-up and template-guided self-assembling processes, which will help in the design of future nanoparticle supelattice-based devices.

— Philip Koth

See: Zhang Jiang, Xiao-Min Lin, Michael Sprung, Suresh Narayanan, and Jin Wang*, "Capturing the Crystalline Phase of Two-Dimensional Nanocrystal Superlattices in Action," Nano Lett. **10**, 799 (2010). DOI:10.1021/nl9029048

Author affiliation: Argonne National Laboratory
Correspondence: zjiang@aps.anl.gov

Use of the Advanced Photon Source, an Office of Science User Facility operated for the U.S. Department of Energy (DOE) Office of Science by Argonne National Laboratory, and the Center for Nanoscale Materials at Argonne National Laboratory was supported by the U.S. DOE, Office of Science, Office of Basic Energy Sciences, under Contract No. DE-AC02-06CH11357.

< Fig. 1. Although the TEM image and its Fourier transform of a dried nanocrystal superlattice (a) showed visually good orders, the positional and orientational correlation functions, $G_T(r)$ (b) and $G_6(r)$ (c), respectively, revealed only a short-range positional order and a quasi long-range orientational order, characteristics of hexatic phase. *In situ* high-resolution x-ray scattering patterns of nanocrystal superlattices before and after the solvent evaporation is finished are shown in (d) and (e), respectively. When the sample is still "wet," the analysis of the 2-D diffraction lines (10), (11), (20), and (21) showed that the lattice domains are in a crystalline phase (d). The scattering pattern from a dried sample confirms that the domains had tranformed into a disordered phase (e).

8-ID-E • XSD • Materials science, physics, polymer science • Grazing incidence small-angle scattering, intensity fluctuation spectroscopy, x-ray photon correlation spectroscopy, x-ray reflectivity • 7.35 keV, 12 keV • On-site • Accepting general users

Discovering New Talents for Diamond

Diamond exhibits a unique combination of superlative physical qualities such as high mechanical hardness, high thermal conductivity, high radiation hardness, and low thermal expansion, etc. Accordingly, diamond is in great demand for an ever-increasing number of technological applications. Researchers using the XSD 30-ID beamline at the APS and beamline X19C of the National Synchrotron Light Source have discovered that synthetic diamond crystals exhibit a very high degree of perfection. These results open vistas for entirely new, highly advanced technology applications of diamonds and new opportunities in x-ray optics, in particular the realization of new, fully coherent x-ray sources, such as x-ray free-electron laser oscillators (XFELOs).

Recently, diamond crystals were identified as being indispensable for the realization of next-generation, fully coherent hard x-ray sources such as XFELOs, that have the potential for unprecedented average brightness along with record narrow spectral bandwidths. Diamonds are considered a most promising material for high-reflectance Bragg crystal mirrors of the XFELO optical cavities. There are two major reasons for this.

First, theory predicts that even at normal incidence the reflectivity of x-rays from diamond should approach 100%, under the Bragg diffraction condition. However, a priori it was not clear whether the remarkably high reflectivity of diamond crystals predicted in theory could be achieved in practice. And if the theory predictions are correct, is the quality of the presently available diamond crystals sufficiently high for practical use, e.g., for the XFELO mirrors?

Second, the outstanding thermo-mechanical properties of diamonds, such as record high thermal conductivity and low thermal expansion, are crucial to ensure stability of the x-ray cavity under the thermal load of the intense XFELO radiation. Thermal expansion of diamond at room temperature, though much smaller compared to other crystals, is not sufficiently small to guarantee the required stability. Does it become small enough at low temperatures? Surprisingly, the answer was not known. Thermal expansion of diamond at low temperatures has been an unresolved problem in solid state physics, due primarily to deficient measurement accuracy. In particular, it has been unclear how small the thermal expansion was below 100K. It was also not clear if diamond exhibits negative thermal expansion like Si, Ge, and other semiconductors with a diamond structure.

Researchers from the Argonne and Brookhaven national laboratories utilized the 30-ID beamline to discover that synthetic diamond crystals exhibit a very high degree of perfection. Almost-theoretical values were measured for the reflectivity and spectral width in Bragg diffraction at normal incidence to the reflecting atomic planes for hard x-rays with a photon energy of E

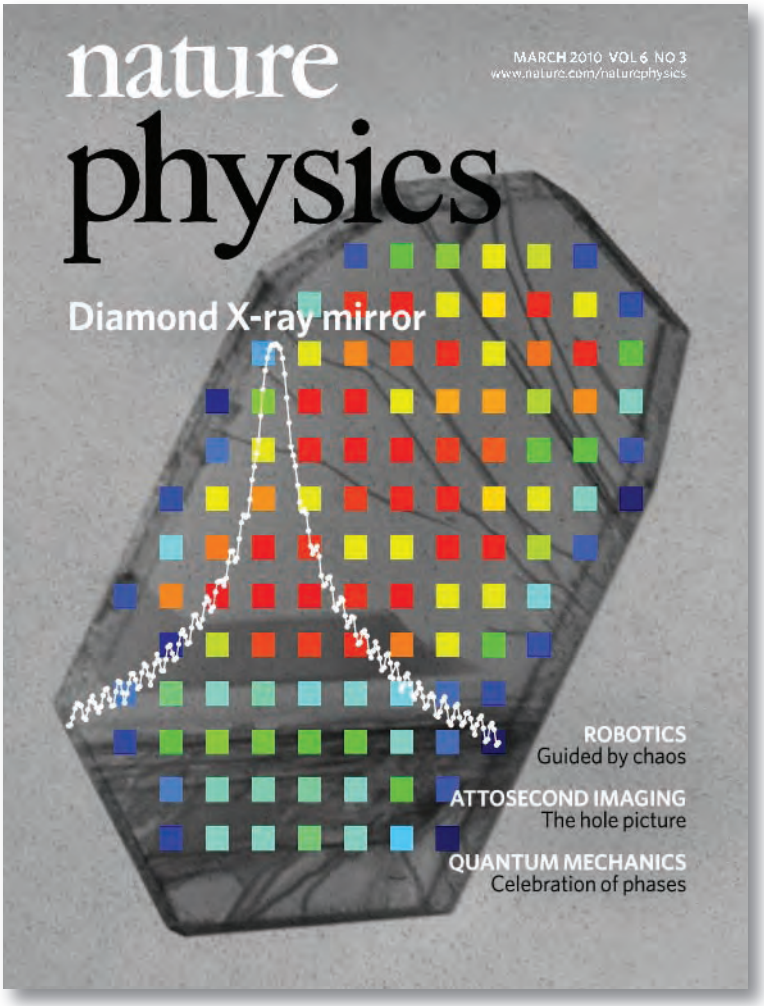

Fig. 1. X-ray topogram with superimposed reflectivity color map and reflectivity curve of a diamond crystal, on the cover of *Nature Physics* Vol. 6, No. 3 in which the article appears.

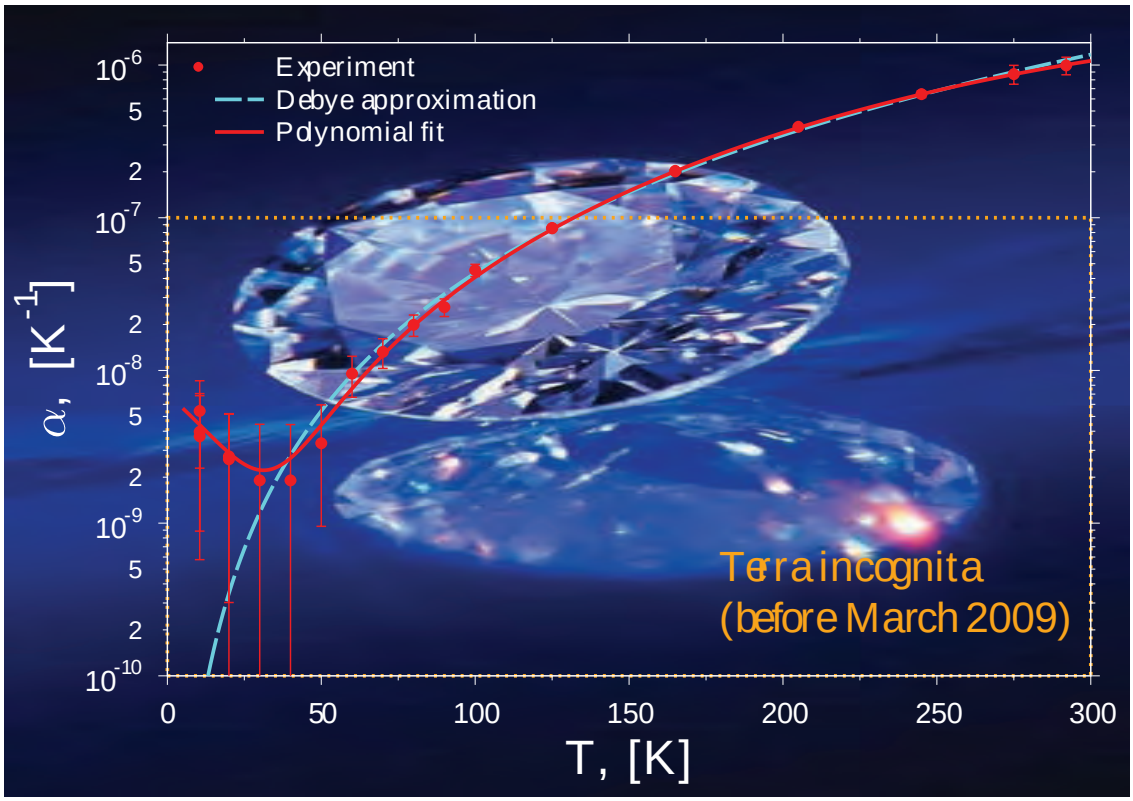

Fig. 2. Temperature dependence of the thermal expansion in diamond.

= 24 keV. The reflectivity is significantly higher than that of Si crystals under similar conditions. (Synchrotron white-beam topography [Fig. 1] was applied at beamline X19C of the National Synchrotron Light Source to preselect the diamond crystal with the lowest density of defects.)

In another experiment performed at the same APS beamline, a two-order-of-magnitude improvement in the measurement accuracy of thermal expansion of diamonds has been achieved, as compared to previous studies. The researchers measured an extremely small value of thermal expansion of diamond: ~2 x $10^{-9}K^{-1}$ at temperatures around 40K (Fig. 2). The ability to measure such a small variation of the crystal lattice is equivalent to measuring a variation of the Earth's radius with an accuracy of a few millimeters. Only positive values of the thermal expansion coefficient were observed in diamond. Therefore, unlike Si or Ge, diamond has no negative thermal expansion.

The results of these studies go beyond solving critical outstanding problems related to the basic physical properties of diamonds. The demonstrated high reflectivity and the extremely small thermal expansion at low temperatures of diamond crystals open up vistas for entirely new, highly advanced technology applications of diamonds and new opportunities in x-ray optics, in particular. These results could greatly assist the realization of fully coherent x-ray sources, such as x-ray free-electron laser oscillators.

— *Yuri Shvyd'ko*

See: Yuri V. Shvyd'ko[1]*, Stanislav Stoupin[1]**, Alessandro Cunsolo[1,2], Ayman H. Said[1], and Xianrong Huang[2], "High-reflectivity high-resolution X-ray crystal optics with diamond," Nat. Phys. **6**(3) 196 (2010). DOI:10.1038/NPHYS1506
Author affiliations: [1]Argonne National Laboratory, [2]Brookhaven National Laboratory
Correspondence:
*shvydko@aps.anl.gov
**sstoupin@aps.anl.gov

This work and use of the Advanced Photon Source, an Office of Science User Facility operated for the U.S. Department of Energy (DOE) Office of Science by Argonne National Laboratory, was supported by the U.S. DOE under Contract No. DE-AC02-06CH11357.

References

K.-J. Kim, Yu. Shvyd'ko, and S. Reiche, "A Proposal for an X-Ray Free-Electron Laser Oscillator with an Energy-Recovery Linac," Phys. Rev. Lett. **100**, 244802 (2008).
S. Stoupin and Yu. Shvyd'ko, "Thermal Expansion of Diamond at Low Temperatures," Phys. Rev. Lett. **104**, 085901 (2010).
K.-J. Kim and Yu. Shvyd'ko, "Tunable optical cavity for an x-ray free-electron-laser oscillator," Phys. Rev. ST Accel. Beams **12**, 030703(2009).

See also: Nature Physics News and Views, "X-ray optics: Diamond brilliance," by Stephen M. Durbin and Roberto Colella, Nat. Phys. **6**, 163 (2010). DOI:10.1038/nphys1610

30-ID • XSD • Materials science, physics • Inelastic x-ray scattering • 5-14 keV, 5-30 keV, 23.7-29.7 keV• On-site • Accepting general users

A New Binary Quasicrystal Makes Its Debut

Researchers at the Ames Laboratory and Iowa State University recently discovered stable binary icosahedral quasicrystals in a scandium-zinc alloy created in growth solution. With only slight variations in growth conditions, they were able to identify two different morphologies, producing quasicrystal grains with both pentagonal dodecahedron (PD) and rhombic triacontahedron (RT) shapes, which were defined and studied under high-energy x-ray diffraction at XSD beamline 6-ID-D of the APS. This work opens new possibilities for study of this fascinating structural phenomenon. A more complete understanding of their unique properties and the conditions that lead to their formation and stability will lead to a deeper understanding of the nature and potential of these novel materials.

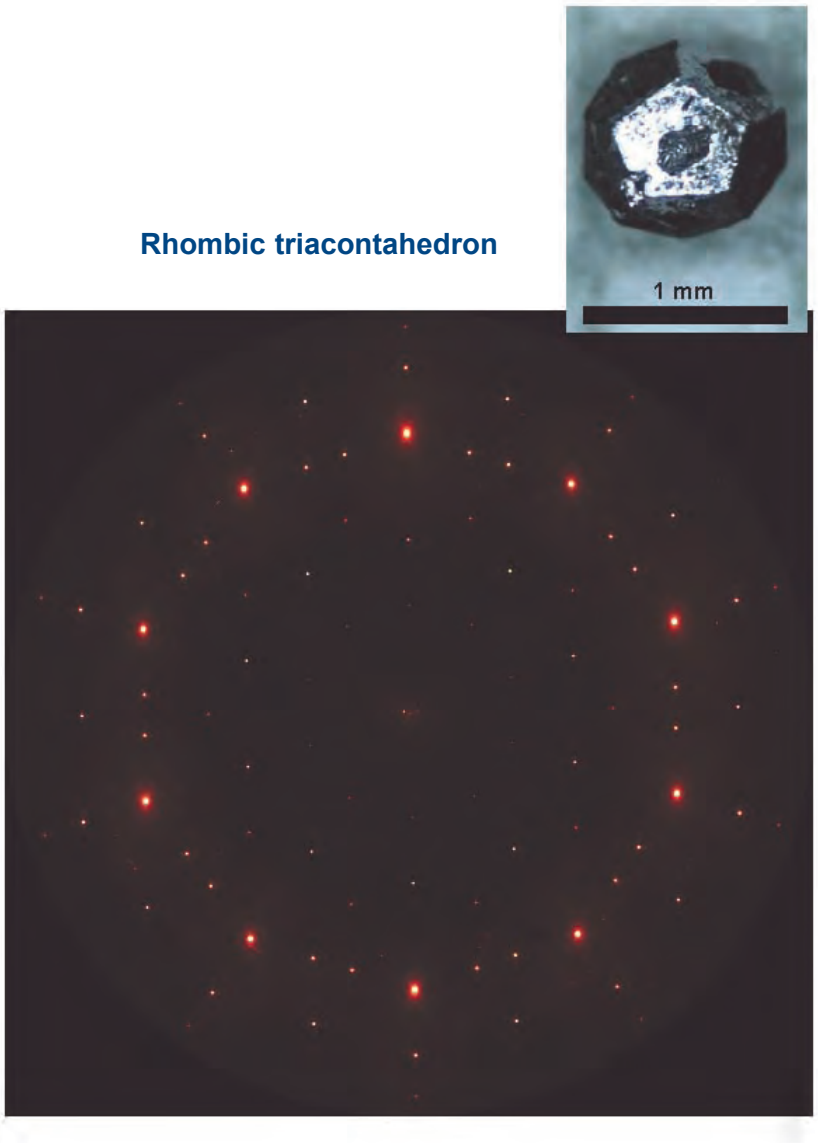

Fig. 1. The growth morphology of the pentagonal dodecahedral (this page) and rhombic tricontahedral (facing page) grains of the $Sc_{12}Zn_{88}$ icosahedral quasicrystals are shown along with high-energy x-ray diffraction patterns taken with the incident beam parallel to the 5-fold axis of each sample.

The term "quasicrystal" is actually shorthand for "quasiperiodic crystal," generally characterized by two features in their diffraction patterns: Whereas the well-known conventional crystal systems display periodic arrays of diffraction spots, quasicrystals manifest an aperiodic spacing of diffraction peaks along a given direction; and quasicrystals exhibit rotational symmetries that are forbidden for conventional periodic crystals, including 5-fold, 10-fold, and 12-fold rotation axes.

When they were first discovered in the 1980s, quasicrystals were thought to be generally unstable, reverting to periodic crystalline alloys upon heat treatment. But soon, many stable quasicrystal forms were found. Stable quasicrystals have been seen in a wide variety of ternary and quaternary metallic alloys, but finding one in a binary alloy is far more difficult. A decade ago, a stable icosahedral phase was found in Cd-Yb and Cd-Ca alloys, but that was all — until now.

The Ames experimenters were studying the phase diagram of the Sc-Zn alloy system, creating samples through a routine solution growth process when, much to their surprise, they found the i-$Sc_{12}Zn_{88}$ quasicrystals among the sample material they produced. After confirming that the quasicrystal grains were composed solely of Sc and Zn and ruling out the presence of a third element that could have produced a ternary alloy, the researchers characterized the grains in detail. They found grains characterized by icosahedral morphologies with shapes of either pentagonal dodecahedron (PD) or rhombic triacontahedron (RT) configurations.

High-energy x-ray diffraction studies at the APS clearly demonstrated the icosahedral structure of both types of faceted grains, as shown in Fig. 1. These patterns were recorded on beamline 6-ID-D using 120-keV x-rays and an area detector as the sample was rocked through small angles about the two axes perpendicular to the inci-

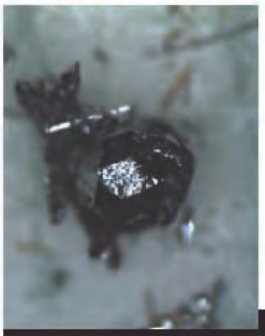

Pentagonal dodecahedron

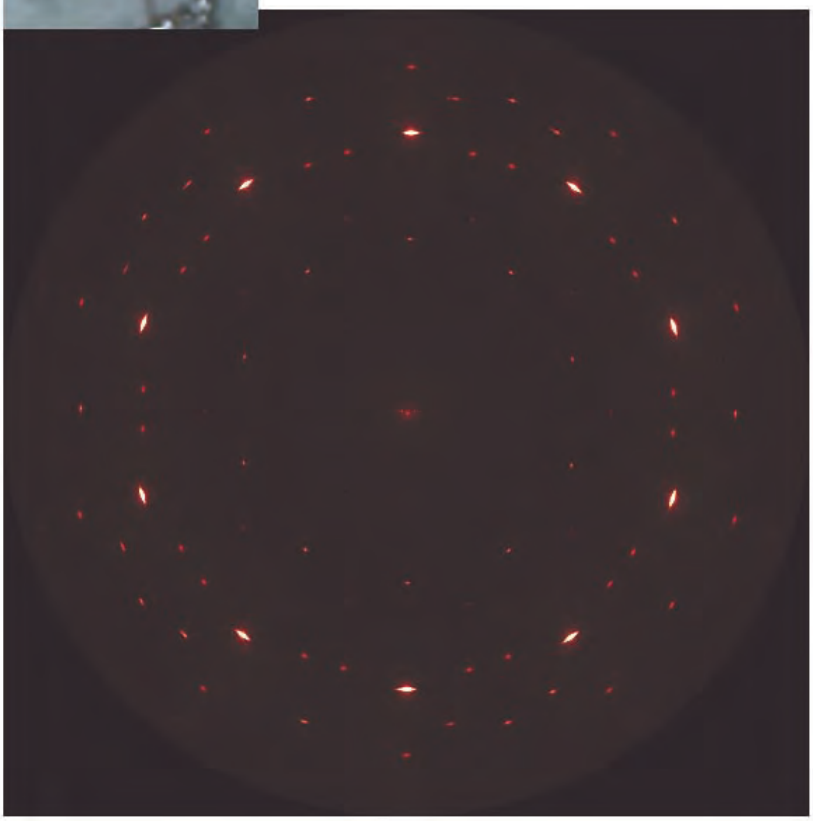

dent beam direction. For both the RT and PD grains, the diffraction peaks could be fully indexed by a P-type icosahedral phase, although some differences in the degree of structural order were detected between the RT and PD morphologies. Forming during the cooling phase of the solution growth process, the resulting shape of the quasicrystal appears to depend somewhat on the concentration of each element present in the starting compositions. Nevertheless, both the PD and RT grains are quite stable over a broad temperature range.

The experimenters speculate that one reason this particular icosahedral quasicrystal phase was not discovered earlier is that the exposed liquidus line for primary solidification of $Sc_{12}Zn_{88}$ is very limited. It is possible that previous experiments may have actually created the binary icosahedral phase, which then escaped detection as the material underwent further phase transitions. The researchers point out that this also implies that there could be many other binary quasicrystalline alloys that remain to be discovered by future experiments with related alloy systems.

Whether more binary quasicrystals are found next year, next decade, or never, the discovery of the $Sc_{12}Zn_{88}$ quasicrystal opens new possibilities for the study of this fascinating structural phenomenon. Although practical uses for such materials are still speculative, a more complete understanding of their unique properties and the conditions that lead to their formation and stability may bring such applications closer to reality. — *Mark Wolverton*

See: P.C. Canfield[1,2*], M.L. Caudle[2], C.-S. Ho[1‡], A. Kreyssig[1,2], S. Nandi[1,2], M.G. Kim[1,2], X. Lin[1,2], A. Kracher[1], K.W. Dennis[1], R.W. McCallum[1,2], and A.I. Goldman[1,2**], "Solution growth of a binary icosahedral quasicrystal of $Sc_{12}Zn_{88}$," Phys. Rev B **81**, 020201R (2010).
DOI:10.1103/PhysRevB.81.020201
Author affiliations: [1]Ames Laboratory, [2]Iowa State University ‡Present address: University of California, Berkeley
Correspondence:
*canfield@ameslab.gov,
**goldman@ameslab.gov

Work at the Ames Laboratory was supported by the U.S. Department of Energy, Basic Energy Sciences, under Contract No. DE-AC02-07CH11358.

6-ID-D • XSD • Materials science, physics • High-energy x-ray diffraction, magnetic x-ray scattering, pair distribution function, powder diffraction • 26.4-52.6 keV, 49.5-100.5 keV, 66.5-132.3 keV • On-site • Accepting general users

Pressuring Hydrogen and Xenon Into a New Form

If a true "hydrogen economy" based on nonpolluting energy sources such as fuel cells for cars is going to become a viable reality, we will need to develop inexpensive and efficient ways to store hydrogen and keep it readily available. One possibility is to "trap" hydrogen using weak chemical forces in molecular compounds. Recently, a group of scientists working at the APS took a major step in that direction. Although xenon is one of the noble elements that does not generally react or combine with others, the experimenters found that under special high-pressure conditions, xenon and hydrogen molecules could be made to bond in a surprisingly stable structure held together by van der Waals forces. This unexpected stability may provide the pathway to an entirely new family of hydrogen-rich compounds in temperature and pressure regimes that have yet to be fully explored or exploited.

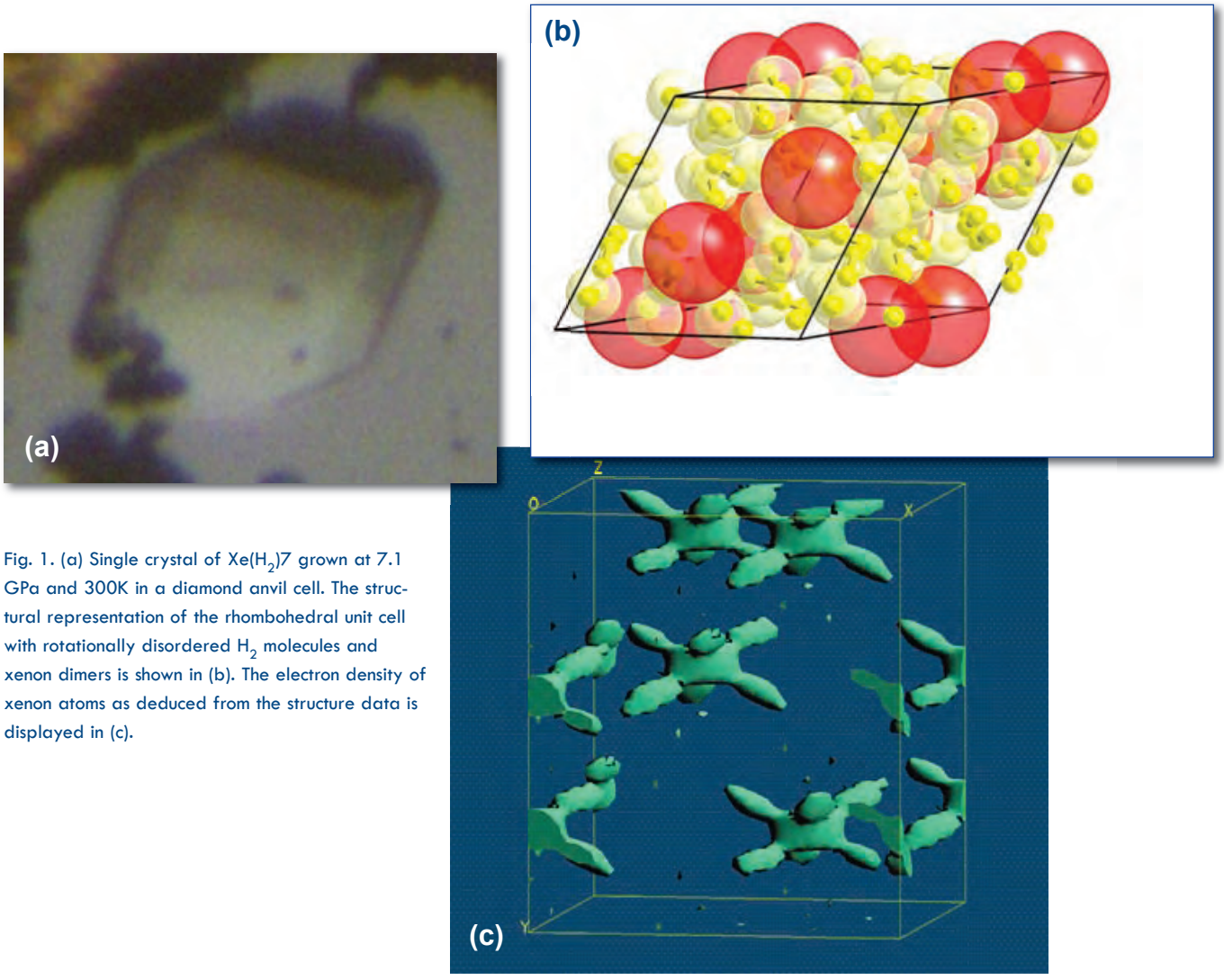

Fig. 1. (a) Single crystal of $Xe(H_2)7$ grown at 7.1 GPa and 300K in a diamond anvil cell. The structural representation of the rhombohedral unit cell with rotationally disordered H_2 molecules and xenon dimers is shown in (b). The electron density of xenon atoms as deduced from the structure data is displayed in (c).

Researchers from the Carnegie Institute of Washington, The University of Chicago, and Argonne loaded a series of H_2-Xe gas mixtures into diamond anvil cells and proceeded to grow single crystals under various pressures and temperatures. They examined the crystal structure of the resulting material using synchrotron x-ray diffraction at the HP-CAT 16-BM-B and16-BM-D beamlines at the APS. Raman and infrared spectroscopy were also employed to gather spectroscopic data that was used to construct starting structural models.

As the gas mixture reached a pressure of 4.1 GPa, the experimenters observed a xenon-rich solid beginning to form. Additional transitions could be seen at 4.4, 4.9, and 5.4 GPa, which were identified to be induced by stoichiometric changes. The data obtained was of very high quality and could be used to determine the xenon sublattice from direct methods. The structure revealed the presence of two distinct Xe-Xe distances, with the Xe atoms in each unit cell arranging themselves into an array of three Xe-Xe dimers along the *c* axis. At 4.9 GPa, the Xe dimers are separated by 4.915 Å, while the Xe-Xe distance within each dimer measures 3.875 Å. This latter distance is comparable both to that seen with neutral dimers in the gas phase and in the solid fcc phase of pure Xe at room temperature and at 5 GPa. These distances and the Xe sublattice were stable across transitions up to 7.1 GPa, implying that the stoichiometric transitions the researchers observed resulted from the changes of hydrogen coordination into the structure.

Electron density maps provided clues to the compound's stability. The lowest-pressure structure revealed distortion in the normally spherical electron density of xenon. The placement of the hydrogen molecules in the xenon sublattice along these directions not only minimized the structural refinement parameter, but also accounted for the spectroscopic signatures observed. At pressures as high as 2.6 Mbars, the compound was stable while no evidence for metallization of the hydrogen sublattice was observed. This implies that the electron density increases in the interstitial space rather than along the Xe-H_2 bond at higher pressures. These observations constitute the first direct evidence for the origin of stability of this class of molecular solids and can be explained as due to the depopulation of a Xe_2 unit orbital and a gradual transition from van der Waals to covalent bonding with the formation of ionic Xe_2 with pressure.

Single-crystal oscillation photographs were obtained at HP-CAT beamline 16-ID-B to further investigate the stability and compressibility of the compound. While xenon itself would be too expensive for practical use, the current work is the first time hydrogen and xenon have been combined in a stable form. More importantly, however, it provides the first experimental evidence of how such unique compounds can be made, and opens new possibilities for the development of hydrogen storage methods. The unexpected stability of the xenon-hydrogen compound created in this experiment indicates that these techniques may provide the pathway to the discovery of an entirely new family of hydrogen-rich compounds in temperature and pressure regimes that have yet to be fully explored and exploited.

— Mark Wolverton

See: Maddury Somayazulu[1]*, Przemyslaw Dera[2], Alexander F. Goncharov[1], Stephen A. Gramsch[1], Peter Liermann[1], Wenge Yang[1], Zhenxian Liu[1], Ho-kwang Mao[1], and Russell J. Hemley[1], "Pressure-induced bonding and compound formation in xenon–hydrogen solids," Nat. Chem. **2**, 50 (January 2010). DOI:10.1038/NCHEM.445

Author affiliations: [1]Carnegie Institution of Washington, [2]The University of Chicago

Correspondence: *zulu@gl.ciw.edu

This work was supported by DOE-BES (DE-FG02-06ER46280), DOE-NNSA (CDAC), NSF-DMR (DMR-0805056), NSF-EAR (COMPRES) and the Balzan Foundation. Use of the Advanced Photon Source, an Office of Science User Facility operated for the U.S. Department of Energy (DOE) Office of Science by Argonne National Laboratory, was supported by the U.S. DOE under Contract No. DE-AC02-06CH11357.

16-BM-B • HP-CAT • Chemistry, geoscience, materials science, physics • Energy dispersive x-ray diffraction, high-pressure diamond anvil cell, white laue single-crystal diffraction • 10-120 keV • On-site • Accepting general users

16-BM-D • HP-CAT • Chemistry, geoscience, materials science, physics • High-pressure diamond anvil cell, powder angular dispersive x-ray diffraction, single-crystal diffraction, x-ray absorption near-edge structure • 6-70 keV • On-site • Accepting general users

16-ID-B • HP-CAT • Chemistry, materials science, geoscience, physics • High-pressure diamond anvil cell, microdiffraction, single-crystal diffraction • 24-35 keV • On-site • Accepting general users

< Co-authors Wenge Yang (left) and Lin Wang of the Carnegie Institution of Washington, shown in an HP-CAT research station at the APS with the diamond anvil cell and x-ray instrumentation used to probe the PDF of the sample at high applied pressures at room temperature.

When Size Matters: Yttrium Oxide Breaking Down under Pressure

Sometimes size does matter, such as when certain nanomaterials exhibit different behaviors under varying extreme conditions. An example is yttrium oxide (Y_2O_3), a compound employed in industrial coatings and many other applications, including nanotechnology. But as with many materials, the qualities and stabilities of yttrium oxide on the nanoscale can vary greatly from those of the bulk material, so a thorough understanding of those differences and how they work is crucial. A team of researchers working at the APS has discovered that Y_2O_3 in nanometer-sized particles undergoes a definite phase transition under pressure that results in characteristics quite different from bulk Y_2O_3, a finding with important implications for the use of yttrium oxide as a nanomaterial. Similar transitions have been observed in silicon dioxide and other bulk materials, but the exact mechanism of the amorphization process remained elusive.

Led by HPSynC (the joint consortium of the Geophysical Laboratory at the Carnegie Institution of Washington, or CIW, and the APS), the research team from CIW, Argonne, Stanford University, Jilin University, Xiangtan University, Stanford University, and the SLAC National Accelerator Laboratory examined yttrium oxide samples with grain sizes ranging from 5 nm to 1 μm. After transmission electron microscopy revealed the same crystal structure in all of the samples under ambient conditions, the team subjected the crystals to high pressures utilizing diamond anvil cells with transmitting media of He and silicone and a variety of *in situ* high-pressure techniques, including x-ray diffraction, Raman spectroscopy, and high-energy pair distribution analysis, at the HP-CAT 16-ID-B and 16-BM-D beamlines and XSD beamline 11-ID-C at the APS.

The 16-nm, particle-sized material demonstrates increased stability compared to bulk Y_2O_3, with the cubic phase persisting up to 24.8 GPa (approximately 12.8-GPa greater than in the bulk material). As

pressure was increased to above 24.8 GPa, disorder began to appear, eventually yielding to a completely amorphous state above 30 GPa. The larger-grained 21-nm material, however, behaved considerably differently, maintaining its cubic structure up to 14 GPa, then undergoing a transition to the hexagonal phase up to 32.7 GPa. Meanwhile, micron-sized material transformed from cubic to the hexagonal phase at 12 GPa, which persisted to the highest pressures measured. This demonstrates that yttrium oxide nanoparticles have a critical size above which they behave like the bulk Y_2O_3, but become amorphized below that size. Raman spectroscopy confirms the amorphized state of the samples subjected to high pressure.

To further characterize this observed dependence of particle size on structural stability under pressure, high-energy pair distribution function (PDF) measurements were performed on 16-nm-sized samples. Using this technique, the team could identify differences of atom-to-atom linkage (Fig. 1). Because the distance between each pair of atoms in the structure can be determined by the position of peaks in the PDF data, shifts in those peaks represent changes in the atomic bonding length, while a complete disappearance of peaks indicates breakdown of the original linkage. Under increasing pressures, the connectivity of the YO_6 octohedra in the cubic Y_2O_3 phase begins to break down, while the links between the edges shared by neighboring octahedra remain intact. Finally, at ~29 GPa and beyond, long-range ordering disappears and amorphization is completely dominant.

This work represents the first PDF measurement of this size-dependent amorphization mechanism. The observed size effect explains the greater stability under pressure: While grain sizes of 21 nm and above transform from a cubic to hexagonal phase under pressure, the smaller-grained Y_2O_3 maintains the cubic phase for a longer period before amorphization sets in.

The research team plans to continue their work studying both Y_2O_3 and other materials, examining how various nanomaterial and bulk compounds with differing particle sizes behave under extreme conditions. Their findings will have direct implications regarding the manufacture and versatility of nanomaterials for various applications. As the current work demonstrates, the high-energy PDF measurement technique adds an important new tool to the experimental toolbox, presenting a new way to look at the disordering mechanism of nanomaterials.

— Mark Wolverton

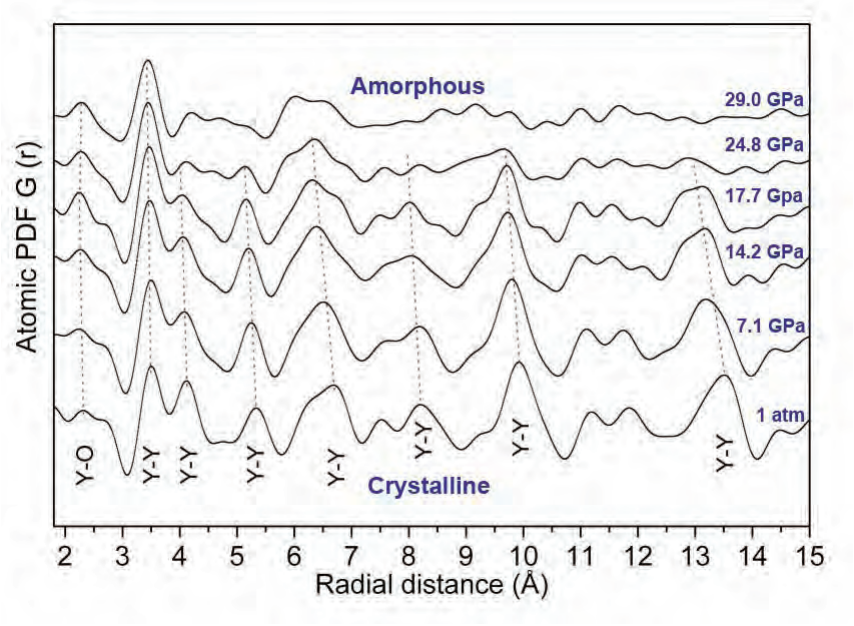

Fig. 1. Pair distribution function (PDF) of 16-nm-sized Y_2O_3 at high pressures.

See: Lin Wang[1,2*], Wenge Yang[1], Yang Ding[1], Yang Ren[3], Siguo Xiao[4], Bingbing Liu[2], Stanislav V. Sinogeikin[1], Yue Meng[1], David J. Gosztola[3], Guoyin Shen[1], Russell J. Hemley[1], Wendy L. Mao[5,6], and Ho-kwang Mao[1], "Size-Dependent Amorphization of Nanoscale Y_2O_3 at High Pressure," Phys. Rev. Lett. **105**, 095701 (27 August 2010). DOI:10.1103/PhysRevLett.105.095701

Author affiliations: [1]Carnegie Institution of Washington, [2]Jilin University, [3]Argonne National Laboratory, [4]Xiangtan University, [5]Stanford University, [6]SLAC National Accelerator Laboratory

Correspondence:
*wanglin@aps.anl.gov

The research was supported by the U.S. National Science Foundation (NSF) (MRI-0821584 and EAR-0810255), and the International Balzan Foundation. HPSynC is supported as part of EFree, an Energy Frontier Research Center funded by the U.S. Department of Energy (DOE), Office of Science, Office of Basic Energy Sciences (BES) under Grant Number DE-SC0001057. HP-CAT is supported by CIW, the Carnegie/DOE Alliance Center, the University of Nevada Las Vegas, and Lawrence Livermore National Laboratory through funding from the DOE National Nuclear Security Administration, DOE-BES, and NSF. The work was conducted at the APS, the Electron Microscopy Center for Materials Research, and the Center for Nanoscale Materials at Argonne under Contract No. DE-AC02-06CH11357. This work was also partially supported by the NSF of China (10979001), the National Basic Research Program of China (2005CB724400). Use of the Advanced Photon Source, an Office of Science User Facility operated for the U.S. DOE Office of Science by Argonne National Laboratory, was supported by the U.S. DOE under Contract No. DE-AC02-06CH11357.

11-ID-C • XSD • Materials science, geoscience, physics, chemistry • Diffuse x-ray scattering, high-energy x-ray diffraction, pair distribution function • 115 keV • On-site • Accepting general users

16-BM-D • HP-CAT • Chemistry, geoscience, materials science, physics • Energy dispersive x-ray diffraction, high-pressure diamond anvil cell, white Laue single crystal-diffraction • 10-120 keV • On-site • Accepting general users

16-ID-B • HP-CAT • Chemistry, materials science, geoscience, physics • High-pressure diamond anvil cell, microdiffraction, single-crystal diffraction • 24-35 keV • On-site • Accepting general users

Squeezing Information from Materials under Extreme Pressure

By compressing tiny amounts of material between two diamond anvils, scientists have for more than three decades been able to achieve pressures of over 1 million atmospheres. The physical changes and phase transitions that occur under such pressures test theories of solid-state physics and shed light on conditions in planetary interiors. But to gain useful information from highly compressed samples, researchers need probes that resolve fine details of the materials' structure. A team of scientists used nanoscale x-ray beams at the APS to resolve, on a scale of 250 nm, different elements in a mixture of metals, and to obtain diffraction patterns of similarly-sized single crystals in a powder. Such techniques make it feasible to perform measurements at even higher pressures, using smaller diamond anvil cells.

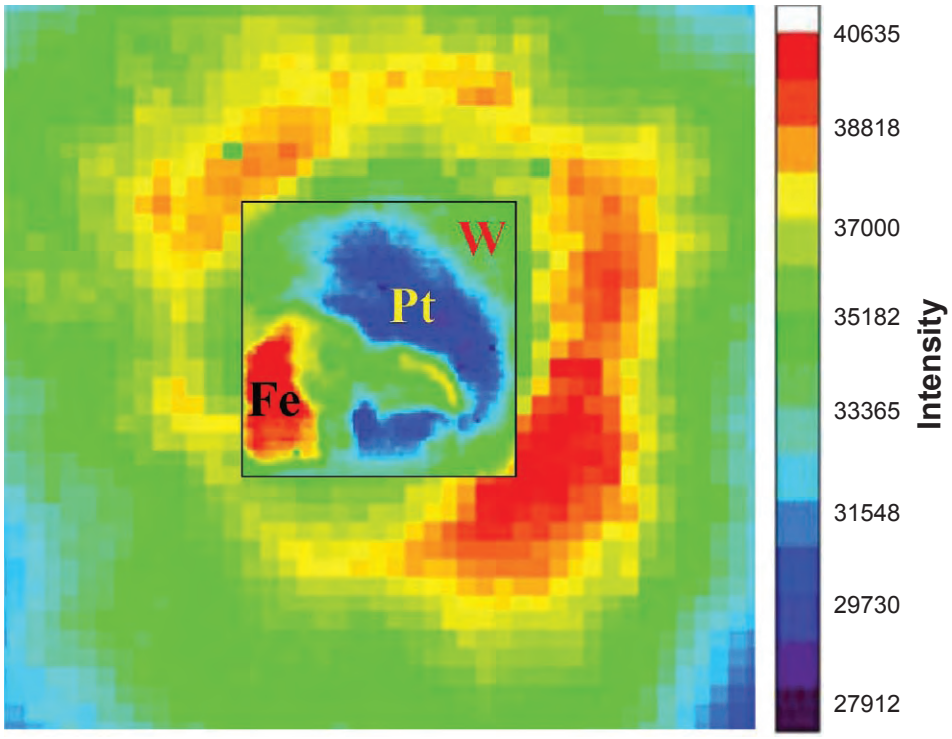

Fig. 1. Measurement of x-ray transmission (red highest, blue lowest) through a mixture of iron, platinum, and tungsten compressed to 282 GPa. The outer image, 40 μm x 40 μm, is resolved into 1-μm pixels, and shows only the roughly circular boundary of the diamond face compressing the sample. The inner portion, 15 μm x 15 μm, is resolved into 250-nm pixels, and clearly shows distinct regions of the three metals.

The devices used to create enormously high pressures pose problems for investigations of the compressed samples. Light passes through the diamonds that squeeze the materials, but the resolution of optical measurements can be no better than several hundred nanometers, a typical light wavelength. Electron microscopes have much better resolution, but because they must operate in a vacuum cannot work in conjunction with extreme pressure apparatus.

The short wavelengths of x-rays offer the potential for high-resolution studies, but the x-ray beams at dedicated high-pressure synchrotron beamlines are a few micrometers across. Because no conventional lens operates in the x-ray regime, making beams narrower is difficult. In recent years, however, a number of synchrotron sources, including the APS, have been able to make available x-ray beams with widths of hundreds of nanometers. These can be produced either using Kirkpatrick-Baez mirrors or Fresnel zone plates.

A team of researchers from Argonne, the Carnegie Institution of Washington, National Cheng Kung University, and Stanford University used narrow x-ray beams at two XSD beamlines at the APS to probe a mixture of iron, platinum, and tungsten compressed in diamond anvil

The researchers think it is realistic to get useful data from experiments at terapascal pressures, an order of magnitude higher than achieved to date

cell to pressures up to 2.82 million atm. It took about two years of working closely with scientists at APS nanodiffraction beamlines 34-ID and 2-ID-D to optimize the experimental setup with the diamond anvil cell apparatus so that measurements could be performed. At beamline 34-ID, Kirkpatrick-Baez mirrors produce a beam 600-nm across, while at beamline 2-ID-D, zone plates produce a beam 250-nm across. For comparison, the scientists also made measurements on the HP-CAT high-pressure beamline 16-ID-B at the APS, where the focusing beam size is approximately 5-μm across.

To make the samples, the researchers loaded a mixture of iron and platinum into a 10-μm hole drilled into a sheet of tungsten. They then squeezed the sheet between two diamond anvils with faces measuring 18 μm across. Figure 1 shows a transmission map of x-rays through the sample, obtained by stepping the 250-nm beam across it in 1-μm increments (outer part) or 250-nm increments (central inset). In the inset, the high resolution clearly shows how the three different metals are distributed. Similar results a sample that had already been identified as being predominantly one metal or another yielded distinct x-ray diffraction patterns characteristic of those elements. In contrast, the 5-μm beam produced the same diffraction pattern, including features corresponding to all of the metals, no matter where the beam was focused.

In another set of experiments, the researchers compressed a perovskite mineral, $(Mg_{0.6}Fe_{0.4})SiO_3$, to 142 GPa, forcing it into a different crystal structure, known as postperovskite, that has thus far been only partly characterized. Diffraction measurements using the 5-μm beam produced a complex pattern created by the numerous small crystallites of postperovskite in the crushed sample. But the 250-nm beam produced a much simpler diffraction pattern, from which the scientists concluded that the beam was intersecting a single nanocrystal with a size similar to the beam width. The ability to pick out and study single crystals in a complex sample allows more precise determination of crystal structure.

The success of these techniques for high resolution x-ray studies of materials under extreme pressures makes it feasible to go to still higher pressures, using smaller diamond faces. Ultimately, these researchers think it is realistic to get useful data from experiments at terapascal pressures, an order of magnitude higher than has been achieved to date.

— David Lindley

See: Lin Wang[1], Yang Ding[1], Wenge Yang[1], Wenjun Liu[2], Zhonghou Cai[2], Jennifer Kung[3], Jinfu Shu[1], Russell J. Hemley[1]*, Wendy L. Mao[4,5], and Ho-Kwang Mao[1], "Nanoprobe measurements of materials at megabar pressures," Proc. Natl. Acad. Sci. USA **107**, 6140 (2010). DOI:10.1073/pnas.1001141107

Author affiliations: [1]Carnegie Institution of Washington, [2]Argonne National Laboratory, [3]National Cheng Kung University, [4]Stanford University, [5]Stanford Linear Accelerator Laboratory

Correspondence: *hemley@gl.ciw.edu

HPSynC is supported as part of EFree, an Energy Frontier Research Center funded by the U.S. Department of Energy (DOE), Office of Science, Office of Basic Energy Sciences under Award DE-SC0001057. Use of the HP-CAT facility was supported by the Department of Energy, Office of Basic Energy Sciences, the Department of Energy, National Nuclear Security Administration (Carnegie/Department of Energy Alliance Center), and the National Science Foundation. Research of L.W. was supported by National Science Foundation Grants MRI-0821584 and EAR-0810255 and the International Balzan Foundation. W.L.M. is supported through the National Science Foundation Geophysics Grant EAR-0738873. Use of the Advanced Photon Source, an Office of Science User Facility operated for the U.S. DOE Office of Science by Argonne National Laboratory, was supported by the U.S. DOE under Contract No. DE-AC02-06CH11357.

2-ID-D • XSD • Life science, materials science, environmental science • Microfluorescence (hard x-ray), microdiffraction, micro x-ray absorption fine structure • 5-30 keV • On-site • Accept-ing general users

16-ID-B • HP-CAT • Chemistry, materials science, geoscience, physics • High-pressure diamond anvil cell, microdiffraction, single-crystal diffraction • 24-35 keV • On-site • Accepting general users

34-ID • XSD • Materials science, physics • Coherent x-ray scattering, microdiffraction • 5-15 keV, 7-25 keV • On-site • Accepting general users

Extending Resonant X-ray Diffraction to High Energies

Our understanding of how complex materials are tailored at the atomic level continues to be driven by novel analytical techniques. Among these is resonant high-energy x-ray diffraction (XRD), which provides an element-specific snapshot of the way atoms are arranged inside materials having topological and/or chemical disorder. Until recently, such snapshots were overcrowded by the inherently large number of atomic coordination spheres appearing in the atomic pair distribution functions (PDFs) yielded by traditional XRD. But, thanks to optimized high-energy x-ray optics on XSD beamline 1-ID at the APS, researchers have shown that coordination spheres related to a particular atomic species can be "highlighted" and others "dimmed" by exploiting high-energy *K*-shell resonances, thereby revealing the atomic arrangement in materials with both excellent spatial resolution and elemental specificity. This work paves the way to a greater understanding of the properties of many types of complex materials with a wide range of potential applications.

The technique of resonant XRD uses sharp changes in the atomic x-ray scattering factor near the characteristic *K*-absorption edge of an element to isolate the scattering associated with that particular type of atom. This yields information qualitatively similar to extended x-ray absorption fine structure (EXAFS) spectroscopy in that the data reflects only correlations involving the element whose absorption edge is probed. Unlike EXAFS, resonant high-energy XRD is capable of revealing correlations over very long interatomic distances. Resonant XRD entails measuring two diffraction data sets close to but below the absorption edge of an atomic species, taking the difference between these two data sets, and Fourier transforming the difference into a quantity called the differential atomic PDF. Achieving excellent spatial resolution and elemental specificity over very long interatomic distances involves probing the high-energy *K*-shell electrons of elements having relatively high atomic number (*Z*). In general, good quality differential atomic PDFs can be obtained for any material that contains elements with a *K*-absorption edge of 20 keV or higher.

To demonstrate the feasibility of this nontraditional experimental approach, the researchers from Central Michigan University and Argonne probed the *K*-absorption edge of gold (Au) atoms (~81 keV) in chemically ordered and disordered bulk Cu_3Au alloys. The resulting Au-differential PDFs showed very good sensitivity to the different ways Au atoms are known to occupy the sites of otherwise identical cubic lattices of those materials, confirming the feasibility of the high-energy resonant XRD approach. The technique was then applied to more complex materials—a PtPd nanosized alloy and core-shell nanosized (~2–4 nm) PtPd particles developed for catalytic applications—by probing the K-absorption edge of platinum (Pt) (~78 keV). The resulting Pt-differential atomic PDFs revealed that Pt atoms in the nanosized alloy and core-shell PtPd particles exhibit a great deal of structural diversity, reflecting the different ways Pt and palladium (Pd) assemble at the nanoscale (Fig. 1). In particular, the core and shell of the nanoparticles were found to be structurally incoherent in respect to each other, something that has never been expected to take place in nanoparticles based on face-centered cubic metals. The resonant XRD-based results agreed with those of high-angle-annular-dark-field scanning transmission electron microscopy (HAADF-STEM) experiments, but went beyond the mostly qualitative picture yielded by imaging techniques by providing a firm, quantitative basis for rigorous modeling of the three-dimensional atomic ordering in the nanoparticles. Such models are a critical prerequisite to understanding the nanoparticles' properties, particularly when catalytic applications are involved. Nanosized materials based on Au and Pt are also being explored for high magnetic-density recording, bioimaging, and drug delivery. These research areas can also benefit significantly from high-energy resonant XRD experiments involving differential atomic PDF data analysis.

— *Vic Comello*

See: V. Petkov[1]* and S.D. Shastri[2], "Element-Specific Structure of Materials with Intrinsic Disorder by High-Energy Resonant X-ray Diffraction and Differential Atomic Pair-Distribution Functions: A Study of PtPd Nanosized Catalysts," Phys. Rev. B **81**, 165428 (2010).
DOI: 10.1103/PhysRevB.81.165428
Author affiliations: [1]Central Michigan University, [2]Argonne National Laboratory
Correspondence:
*petkov@phy.cmich.edu

Use of the Advanced Photon Source, an Office of Science User Facility operated for the U.S. Department of Energy (DOE) Office of Science by Argonne National Laboratory, was supported by the U.S. DOE under Contract No. DE-AC02-06CH11357.

1-ID • XSD • Materials science, physics, chemistry • High-energy x-ray diffraction • 50-90 keV, 50-130 keV • On-site • Accepting general users

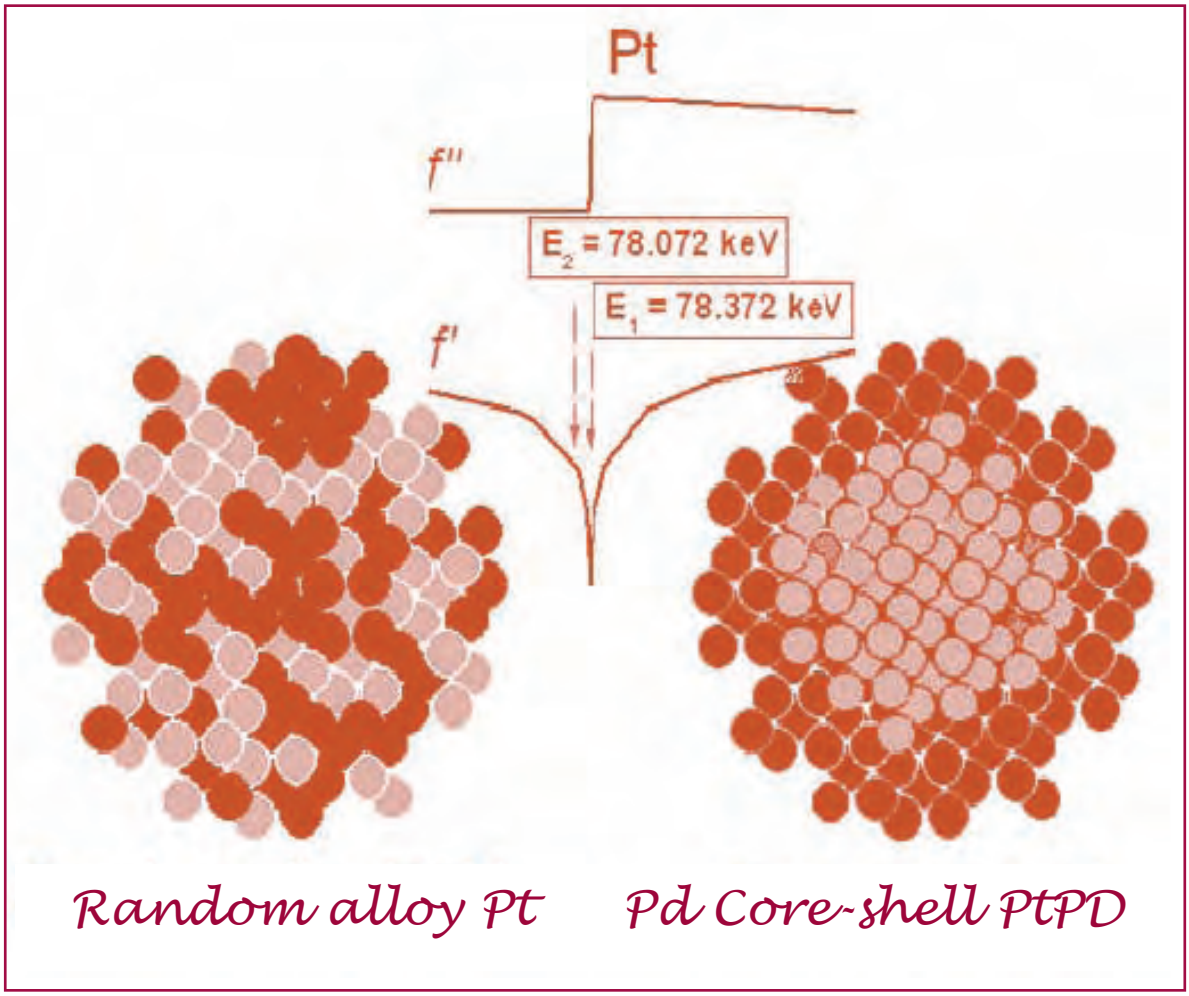

Fig. 1. Random alloy (left) and core-shell (right) PtPd nanoparticles. By probing the *K*-edge of Pt (central part), a "differential" atomic PDF is obtained that reflects correlations involving only Pt atoms, in this case Pt-Pt and Pt-Pd correlations. Thanks to its enhanced sensitivity, the Pt-differential PDF gives a very detailed snapshot of the atomic ordering in PtPd nanoparticles, and so provides a very precise structural basis for explaining their useful catalytic properties.

Negotiating a Disagreement between X-rays and Electrons

Bouncing electrons off atoms and molecules is a well-established technique for probing their internal electronic structure. Hitting the atoms or molecules with x-rays instead should in principle reveal the same information, but studies done at the XSD 20-ID beamline at the APS show a surprisingly large discrepancy between the two methods. The x-ray probe is a cleaner test of electronic structure, casting doubt on the accuracy of results that have traditionally been obtained using the electron technique.

Electron energy loss spectroscopy (EELS) is the measurement of energy lost by electrons when they scatter inelastically off an atom or molecule. In addition, the momentum exchanged between the electron and its target can be inferred from the probe electron's kinetic energy and the angle through which its path is deflected. The cross-section for this process is governed by a quantity known as the "dynamic structure factor," a function of the energy loss and momentum transfer.

Nonresonant inelastic x-ray scattering (NIXS) is the same process, except with an x-ray substituted for the electron. The basic theory of the two forms of scattering indicates that precisely the same dynamic structure factor should govern both. In its simplest realization, the central assumption in this proposition is that when either an x-ray or an electron scatters inelastically off an atom or molecule, it collides with a single electron in the target, bumping it from one quantum state to another. The full range of possible internal electronic transitions determines the form of the dynamic structure factor, which is why EELS and NIXS are such useful probes of the target's electronic configuration.

To test whether the dynamic structure factors inferred from EELS and NIXS are indeed the same, a team of researchers from the University of Washington, Los Alamos National Laboratory, McMaster University, the Australian National University, and the SLAC National Accelerator Laboratory made a precise comparison of the two methods using a classic target system, molecular nitrogen (N_2). The EELS measurements used standard practice in that community, while the NIXS study required development of a new gas-pressurized sample cell capable of working at a few atmospheres of pressure. Such pressures enhanced the NIXS signal while still ensuring single-molecule-like behavior. X-ray scattering measurements were done using the lower-energy resolution inelastic x-ray scattering spectrometer (LERIX) at 20-ID; EELS studies were done at McMaster University and the Australian National University.

For small-angle scattering, in which the momentum transfer is small, results from the two methods agreed well. But as the momentum transfer increased, the dynamic structure factors deduced from NIXS and EELS diverged strongly. The researchers found that the scattering rate for NIXS at high momentum transfer was generally low, especially as the energy loss increased. That is consistent with theoretical expectation, because only a limited momentum exchange is possible in connection with the lowest-energy single-electron transition within a nitrogen molecule. For EELS in the same energy loss range, on the other hand, the dynamic structure factor remained large for every possible electronic transition, implying some fundamental difference between inelastic scattering of x-rays and electrons in these experiments.

That also makes sense from a theoretical perspective. Electrons are far more sensitive than x-ray photons to the influence of all of the electrical charges in the system, both the electrons and the nucleus of any atom they encounter. The new results indicate that inelastic collisions with high momentum transfer come about when the incoming electron undergoes multiple collisions within the target, most likely involving a nearly-elastic scattering event from the nucleus together with an inelastic scattering event with an electron. When it scatters from the much more massive nucleus, the probe electron typically experiences little energy loss but high momentum transfer. While this nuclear scattering involves very little energy transfer, it can nevertheless have a major influence on the recorded energy-loss spectra because it results in a large

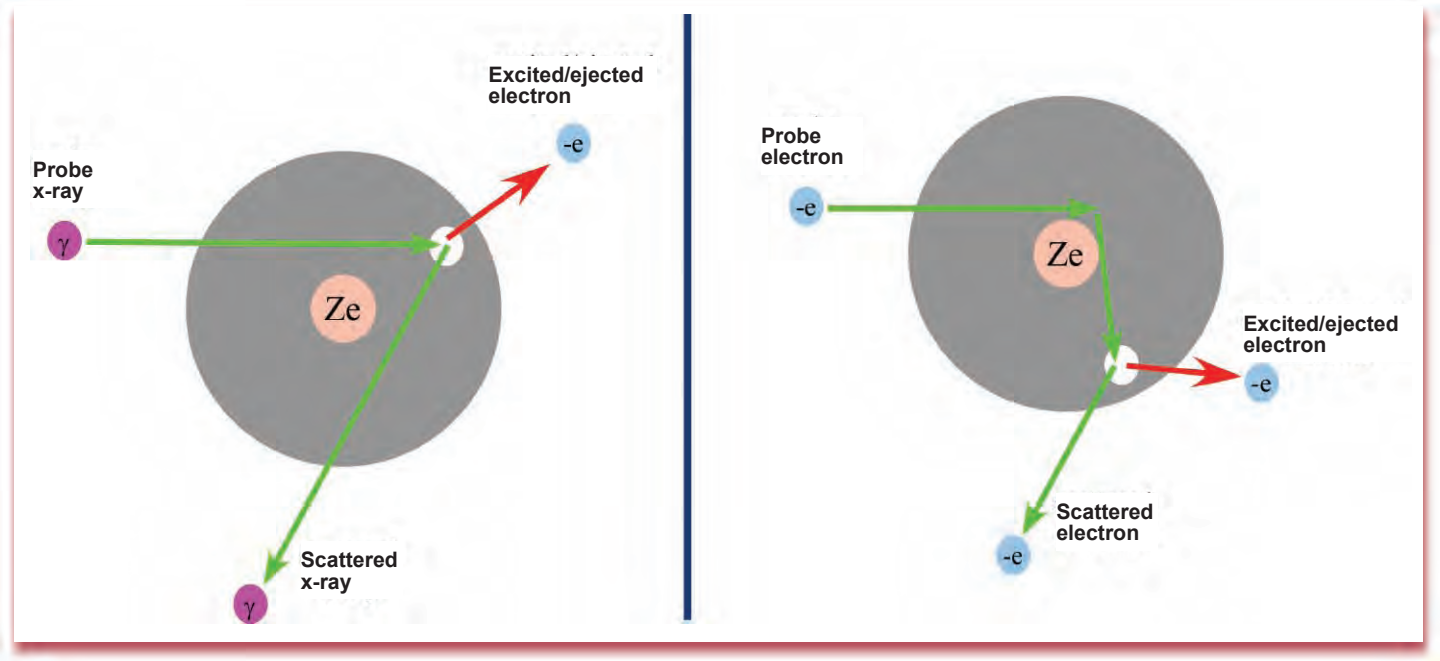

Fig. 1. (Left) A schematic representation of the inelastic scattering of a high-energy x-ray from a target atom. There is a simple interaction with one scattering event between the x-ray and a single electronic transition. The large scattering angle suggests a high momentum transfer. (Right) A schematic representation of a possible high-momentum transfer scattering event in which a high-energy electron is the probe particle. Most of the momentum transfer actually occurs at the nuclear scattering event, leaving the momentum transfer to the electronic transition highly uncertain.

uncertainty in the momentum exchanged in the electron-electron scattering event (Fig. 1). This uncertainty destroys any clean theoretical connection between the electron energy loss spectrum and the dynamic structure factor.

Although questions have been raised in the past about the validity of the usual theoretical treatment of EELS, this comparison with NIXS measurements represents an especially direct evidence of the need for a more sophisticated analysis. Although the EELS and NIXS results in the new work diverge markedly, EELS measurements at different incoming electron energies show considerable consistency. In the absence of other evidence, that consistency misleadingly suggested that the standard treatment of EELS was holding up reasonably well. The team is now exploring the implications of their findings for other systems, and possibly for more subtle phenomena involving the vibrational modes of molecules, another classic problem that has historically been an important field for EELS studies.

— David Lindley

See: J.A. Bradley[1,2], G.T. Seidler[1]*, G. Cooper[3], M. Vos[4], A.P. Hitchcock[3], A.P. Sorini[1,5], C. Schlimmer[1], and K.P. Nagle[1], "Comparative Study of the Valence Electronic Excitation of N2 by Inelastic X-Ray and Electron Scattering," Phys. Rev. Lett. **105**, 053202 (30 July 2010). DOI:10.1103/PhysRevLett.105.053202
Author affiliations: [1]University of Washington, [2]Los Alamos National Laboratory, [3]McMaster University, [4]Australian National University, [5]SLAC National Accelerator Laboratory
Correspondence: *seidler@uw.edu

This work was supported by the U.S. Department of Energy (DOE), the Natural Sciences and Engineering Research Council (NSERC) of Canada, and the Australian Research Council. Measurements at the APS were supported by the U.S. Depart-ment of Energy, NSERC of Canada, the University of Washington, Simon Fraser University. Use of the Advanced Photon Source, an Office of Science User Facility operated for the U.S. DOE Office of Science by Argonne National Laboratory, was supported by the U.S. DOE under Contract No. DE-AC02-06CH11357.

20-ID • XSD • Chemistry, environmental science, geoscience, materials science • Microfluorescence (hard x-ray), small x-ray absorbtion fine structure, surface diffraction, time-resolved x-ray absorption fine structure, x-ray absorption fine structure, x-ray emission spectroscopy, x-ray Raman scattering • 4.3-27 keV, 7-50 keV • On-site • Accepting general users

Probing Spin Liquids with a New Pulsed-Magnet System

Entirely new experimental vistas could be opened by a new pulsed-magnet system developed by an international team of scientists. This system can generate magnetic fields as high as 30 T for synchrotron x-ray scattering experiments. The researchers recently completed the first practical work using the system at the XSD 4-ID-D beamline at the APS to study magnetoelastic effects in the rare-earth pyrochlore terbium titanate ($Tb_2Ti_2O_7$). The study produced some unique insights into the $Tb_2Ti_2O_7$ system, and is the first step in developing this exciting new capability at the APS to address high-field science at the frontiers of contemporary condensed matter physics.

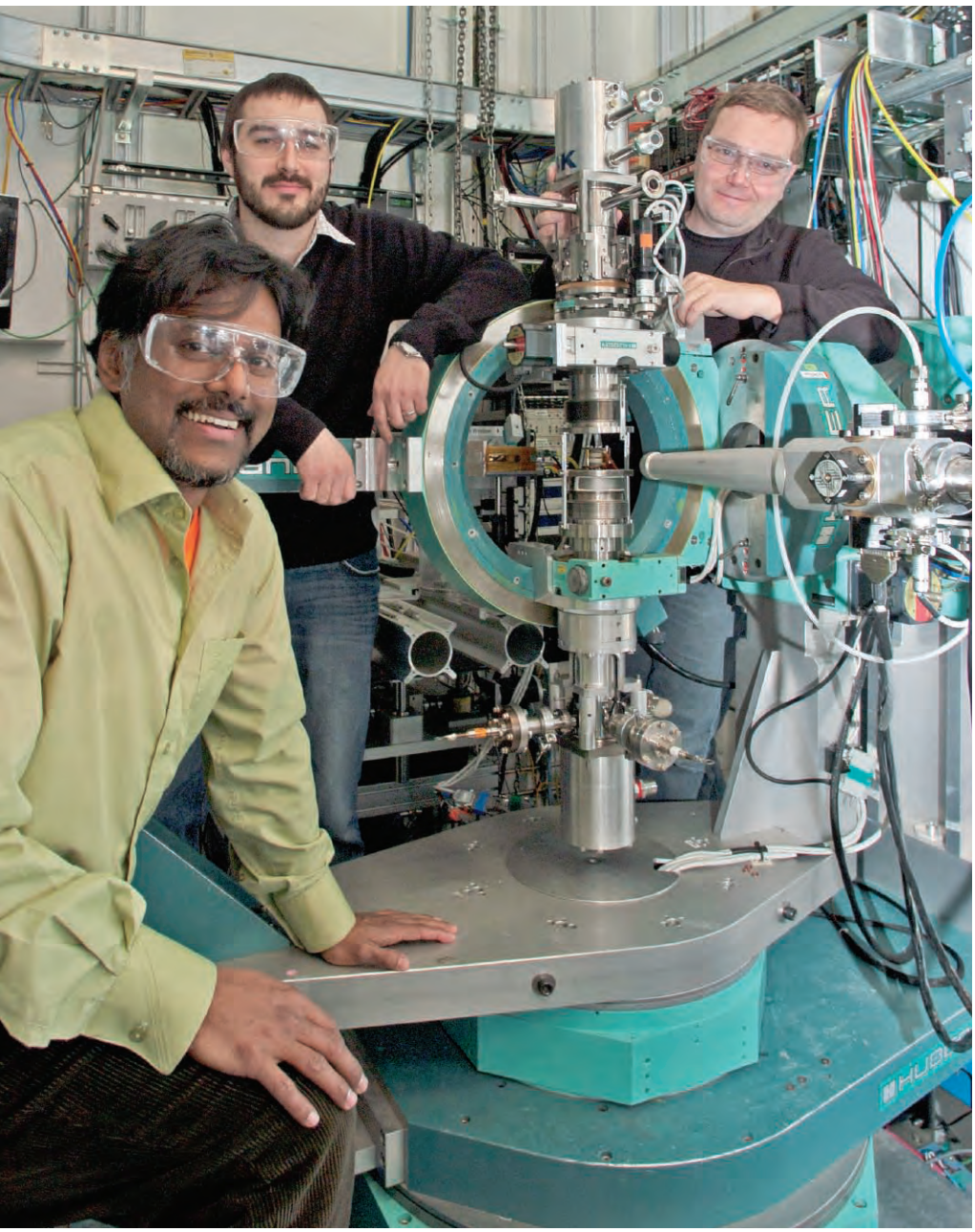

Co-authors and collaborators (l. to r.) Zahirul Islam , Jacob Ruff, and Jonathan Lang with the pulsed-magnet system in the XSD 4-ID-D research station.

Terbium titanate is a member of a class of materials called “frustrated magnets” because tetrahedral coordination of magnetic moments of Tb ions in the lattice structure prevents them from settling into a predictably ordered magnetic ground state. Such materials may exhibit magnetostrictive effects (a property that causes them to change their shape or dimensions when subjected to a magnetic field) and other exotic ferromagnetic and antiferromagnetic properties, which may be relevant to electronic transducers and switching applications.

Terbium titanate remains in a highly disordered spin-liquid ground state even at the lowest measurable temperature, while exhibiting magnetostriction exceeding that in commercial compounds such as Terfenol-D. Attempts to explain the material’s behavior theoretically have been inconclusive, awaiting experimental data on its lattice properties in the spin-liquid state. The problem in general for magnetoelastic effects, and in particular for systems that don’t order, hasn’t been well studied using structural probes such as x-rays.

The new pulsed-magnet system at the APS [1] has proven to be an ideal tool for direct structural observation of the $Tb_2Ti_2O_7$ compound at low temperatures using single-crystal x-ray diffraction and extreme magnetic fields on the 4-ID-D beamline. Prior to the work in question, there was much incidental evidence that the orientation of the

magnetic monments was strongly coupled to the actual positions of the atoms inside the crystal lattice. The new APS pulsed magnet allowed the experimenters to carefully constrain and measure that directly with x-rays. By applying high magnetic fields they could watch the lattice shift and bend and twist around.

Pulsed-magnet experiments provide some unique advantages for materials science work. Materials often display exotic phases under extreme conditions, which are fundamental to understanding their functionality, and the pulsed magnet is a way to generate this type of extreme condition in a contact-free way. Because the pulsed magnetic field is generated fast for a short duration, one may also combine it with the natural timing structure and high brilliance of synchrotron radiation for precision studies of structural relaxations and metastable phenomena on a micro-second level.

The researchers subjected $Tb_2Ti_2O_7$ crystals to pulsed magnetic fields of up to 30 T and temperatures as low as 4.4K, measuring the transverse magnetostriction in different conditions and observing the deformations of the crystal lattice via diffraction studies (Fig. 1). They found anisotropic magnetoelastic effects that have not been previously observed or predicted in the rare-earth titanates. At high temperatures, the $Tb_2Ti_2O_7$ system behaves much like a conventional paramagnet, but crosses over to display a collective response in the spin-liquid regime. Under moderate magnetic fields, some cubic pyrochlore symmetry is restored, but this gives way to a structural phase transition when the magnetic field is increased.

The results indicate a very large coupling between spin and lattice degrees of freedom in the spin-liquid state of $Tb_2Ti_2O_7$. Most likely, the reason it doesn't order at low temperature is that any ordered state would have internal magnetic fields and would have to distort or bend the lattice around.

The split-pair coil used in the APS dual-cryostat pulsed-magnet system was designed and fabricated by Hiroyuki Nojiri and Yasuhiro Matsuda at the Institute for Materials Research at Tohoku University. The experimental team is enthusiastic about the promise of the pulsed-magnet system and plans two complementary instruments that will allow different experimental orientations of the x-ray beam and magnetic fields, permitting researchers to design experiments utilizing various x-ray techniques.

While the pulsed magnets are certainly not the answer to every problem requiring magnetic fields, it is the only practical approach that is available in the foreseeable future for studying many materials at a synchrotron in high magnetic fields. The current work not only provides some unique insights into the $Tb_2Ti_2O_7$ system, but serves as the first major step in developing this exciting new capability at the APS to address high-field science at the frontiers of contemporary condensed matter physics. — *Mark Wolverton*

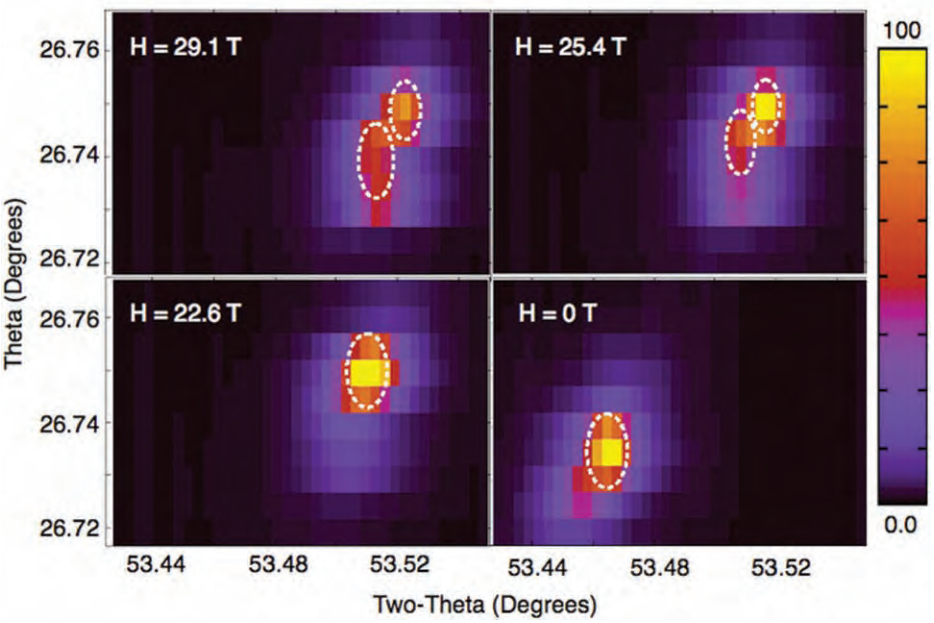

Fig. 1. The (008) intensity color map on a θ vs. 2θ mesh. With increasing magnetic field the peak splits at a critical field of H ~29 T, which is a hallmark of a structural phase transition with a reduction from cubic to tetragonal or orthorhombic symmetry. Above the critical field, the peak broadens and two subtly distinct lattice parameters are observed.

Reference

[1] Zahirul Islam, Jacob P.C. Ruff, Hiroyuki Nojiri, Yashuhiro H. Matsuda, Kathryn A. Ross, Bruce D. Gaulin, Zhe Qu, and Jonathan C. Lang, "A portable high-field pulsed-magnet system for single-crystal X-ray scattering studies," Rev. Sci. Instrum. **80**, 113902 (2009). DOI: 10.1063/1.3251273

See: J.P.C. Ruff[1,2*], Z. Islam[2**], J.P. Clancy[1], K.A. Ross[1], H. Nojiri[3], Y.H. Matsuda[4], H.A. Dabkowska[1], A.D. Dabkowski[1], and B.D. Gaulin[1,5], "Magnetoelastics of a Spin Liquid: X-Ray Diffraction Studies of $Tb_2Ti_2O_7$ in Pulsed Magnetic Fields," Phys. Rev. Lett. **105**, 077203 (2010). DOI:10.1103/PhysRevLett.105.077203
Author affiliations: [1]McMaster University, [2]Argonne National Laboratory, [3]Tohoku University, [4]University of Tokyo, [5]Canadian Institute for Advanced Research
Correspondence: *jpcruff@aps.anl.gov **zahir@aps.anl.gov

This work was supported by the International Collaboration Center at Tohoku University and by the Natural Sciences and Engineering Research Council of Canada. Use of the Advanced Photon Source, an Office of Science User Facility operated for the U.S. Department of Energy (DOE) Office of Science by Argonne National Laboratory, was supported by the U.S. DOE under Contract No. DE-AC02-06CH11357.

4-ID-D • XSD • Materials science, physics • Anomalous and resonant scattering (hard x-ray), magnetic circular dichroism (x-ray magnetic circular dichroism, hard x-ray), magnetic x-ray scattering • 2.5-50 keV • On-site • Accepting general users

Microanalysis for High Throughput at 8-BM

The APS recently added to its suite of beamlines a dedicated hard x-ray microanalysis facility for high-throughput approaches at XSD beamline 8-BM. The facility, currently accepting user proposals, was designed to address increasing user demand for x-ray fluorescence (XRF) microanalysis techniques. By supporting microscopy at low to medium resolution, and providing cutting-edge XRF techniques, the facility will complement existing and oversubscribed hard x-ray microprobes.

Planning for the facility began in 2007 as a project proposal through the APS, and a potential home for the project was found at 8-BM. The project was reviewed and endorsed by the APS Scientific Advisory Committee in early 2008. A final design report was prepared in the spring of 2009, and first light was brought into the redeveloped 8-BM station in the fall of 2009.

The beamline is remarkable in its re-purposing of existing equipment. Over a dozen major components of the beamline, including both the double-multilayer and double-crystal monochromators, were re-utilized from other APS sectors. These components now comprise a beamline with an energy range of 7 to 22 keV, focused by a toroidal mirror to deliver 4 x 10^{10} ph/s in a .5-mm beamspot at the entrance of the 8-BM research station.

The current facility plans call for support of three separate experimental stations within 8-BM. To complement imaging data on cellular metals, a pinhole imaging instrument has been commissioned to enable metallo-proteomic studies. This instrument provides microanalysis at the 0.15-0.5-mm length scale. The double-crystal monochromator adds the ability to probe chemical state, and possible coordination environment, using x-ray absorption near edge structure. The wet methods for this technique were developed by beamline staff [1] with the goal that a high level of support for this technique would be available to the users. This instrument is now completely commissioned and available through the APS General User Proposal System. This unique capability is enabling new research that connects science at multiple length scales, pushing questions from the organism level down to that of proteins.

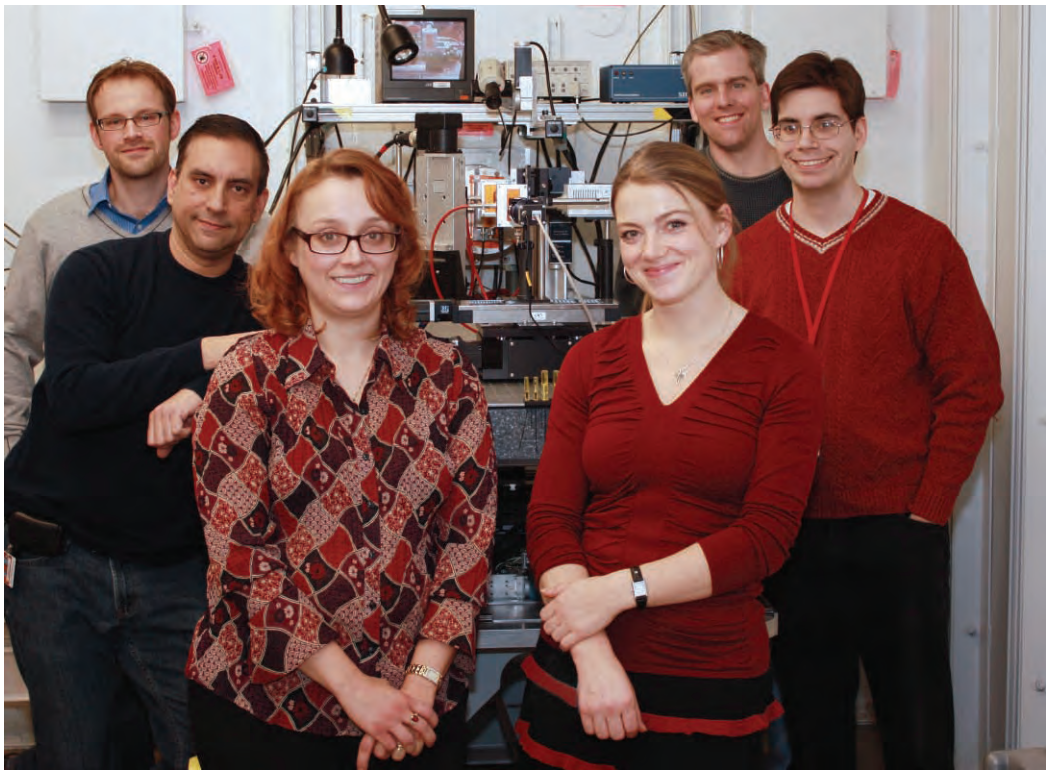

In the 8-BM-B research station, l. to r.: Stefan Vogt, Evan Maxey, Lydia Finney, Sophie-Charlotte Gleber, Christian Roehrig, and Jesse Ward. (Photo by Evan Maxey)

Additionally, work is currently under way to commission a medium-resolution microprobe (10-100 μm) using a Kirkpatrick-Baez mirror pair to provide focus. By ensuring that the system is entirely cross-compatible with existing high-resolution x-ray microprobes, this instrument will complement those capabilities and allow users to place their high-resolution images into a larger context. It is anticipated that this instrument will become available to APS general users in the fall of 2011.

Finally, a flow cytometer is also planned for 8-BM, and is expected to run simultaneously with other instrumentation; it holds great promise for improving throughput and sample statistics for XRF microanalysis.

The commissioning of 8-BM owes its successful completion to many people, including Mark Erdmann, Try Leng Kruy, Mohan Ramanthan, Joe Sullivan, and the Mechanical Operations and Maintenance Group, all in the APS Engineering Support Division; and Christian Roehrig, Rick Spence, and Ed Wrobel (all XSD), among others. The continued commissioning of instrumentation, and user support, is being carried out by Lydia Finney, Evan Maxey, Jesse Ward, Stefan Vogt, and Sophie-Charlotte Gleber (all XSD).

Contact: Lydia Finney, lfinney@anl.gov

References

[1] L. Finney et al., "Imaging Metals in Proteins by Combining Electrophoresis with Rapid X-ray Fluorescence Mapping," ACS Chem. Biol. **5**(6), 577 (2010), as well as a highlight by Nathan Zahler in the same issue.

The Catalyst Station at Beamline 9-BM

Catalysis is an essential technology for the development of energy production, solar energy utilization, clean and efficient combustion of twenty-first century fuels, and research needs for the hydrogen economy. In order to broaden catalysis research opportunities at the APS, significant upgrades have been carried out on the XSD beamline 9-BM-C end station for *in situ* catalyst studies using the x-ray absorption fine structure (XAFS) technique. XAFS is a "workhorse" technique that provides *in situ*, element-specific, atomic-level chemical and geometric information about a catalyst's structure.

9-BM is unique at the APS in that it is optimized for low energies (below 5 keV), and is the only XAFS beamline that can reach 2.1 keV. This makes the beamline excellent for XAFS at the phosphorus and sulfur *K*-edges, as well as for fifth-row transition metal *L*-edges. All of these materials are very important in catalysis.

The impetus for the 9-BM upgrade took root at a workshop on "Catalysis Research at the APS" that was held on September 12-13, 2005, in order to assess the requirements and opportunities for supporting catalysis research that makes use of the APS. Beamline 9-BM was selected as a focal point for these efforts, and a major upgrade was started in 2008. The main purpose of the beamline upgrade proposal was to instrument a beamline with the necessary infrastructure to support operando XAFS experiments, as well as provide infrastructure to support catalyst research at other APS beamlines.

XSD beamline scientist Trudy Bolin and Rodrigo Lobo (CSE/APS postdoc) inspect a grazing-incidence *in situ* sample cell in the 9-BM-C enclosure.

The 9-BM upgrade has been carried out in close collaboration with industrial, Argonne, and university researchers in order to insure that the needs of the catalyst research community were being addressed. Argonne has shown its commitment to catalysis research by hiring Rodrigo Lobo, a catalysis scientist in the Chemical Sciences and Engineering Division (CSE).

Beamline 9-BM has two end stations, 9-BM-B and 9-BM-C, and an energy range of 2.1 to 24 keV. The end stations have a moveable beam stop between them. The upgrade work was performed while the beamline was operational and supporting users. While equipment was being installed and tested, it was also possible to conduct *ex situ* and some *in situ* catalysis experiments at 9-BM-B. This allowed for exploring research opportunities and evaluating the beamline. Table 1 shows a list of the specific upgrades and new equipment, including a high-quality glove box and other equipment for sample preparation installed in the Sector 9 wet lab and already in use by several catalyst researchers from other sectors at the APS.

Future plans at 9-BM include performing concurrent XAFS and Fourier Transform Infrared (FT-IR) experiments to examine the vibrational modes of organic molecules while simultaneously looking at electronic transitions of other materials in a catalyst. There is a significant opportunity to explore many unanswered questions about how materials behave when subjected to "real" conditions. The first tests with a low-energy, *in situ*, high-temperature sample cell with the capability to flow varied mixtures of gases through it are planned for the 2011-1 run cycle.

Contact: Trudy Bolin, bolitru@aps.anl.gov

Table 1. Beamline 9-BM Catalyst Equipment Upgrades

EQUIPMENT	STATUS	COMMENTS
Innovative Technologies glove box	Operational; in use by many catalyst researchers at the APS	0.1 ppm O_2, ~1.5 ppm H_2O
House nitrogen system	Installation almost complete	Benefits four APS sectors
Second glove box	Installed	For "dirty " samples, ~1-10-ppm O_2
9-BM-C optical table, detectors, etc.	Operational and in use	Ion Chambers from Oxford
New 9-BM-C software	Operational and in use	
Flammable gas cabinets/ gas handling system/gas sensors	Operational and in use	
New exhaust fan	Operational and in use	Allows for future negative pressure in 9-BM-C (for H_2S, etc.)
Bruker Tensor 37 FT-IR spectrometer	Under commissioning	Sample cell by Harrick Scientific Products; allows for concurrent x-ray/IR sample characterization
Pfeiffer prisma plus mass spectrometer	Operational and in use	
13-element Ge detector	Due in March 2011	

Collaborative Advances in X-ray Instrumentation

In 2010, the APS continued a tradition of successful collaborations with sister light-source facilities.

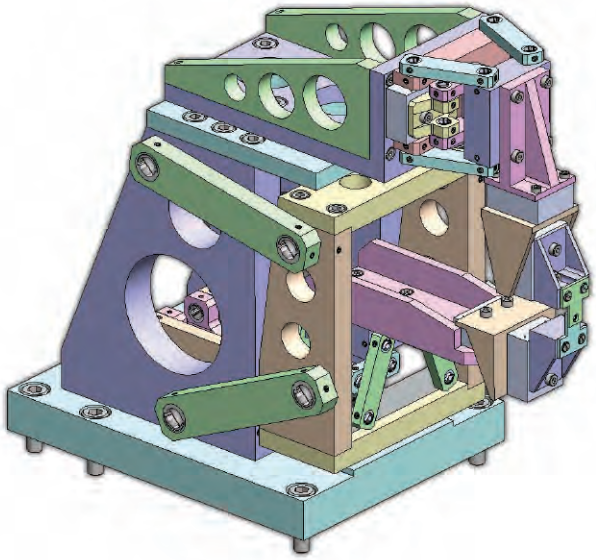

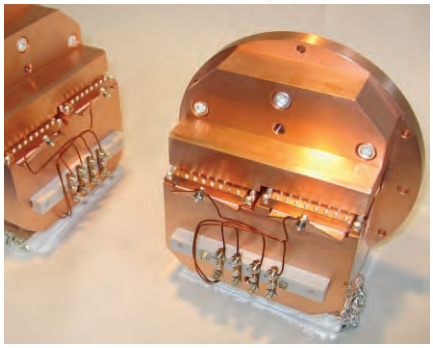

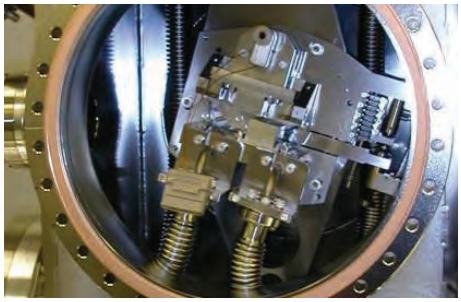

Fig. 1 (above): The APS 8-ID UHV-compatible artificial channel-cut crystal monochromator. Two similar monochromators were constructed and installed at the LCLS for XPCS and other applications. Fig. 2 (left): Rendering of the preliminary design for NSLS-II MLL optics alignment apparatus with seven degrees of the positioning freedom. Fig. 3 (below left): CVD-diamond-based x-ray beam position monitors for the 3-GeV Taiwan Photon Source Project.

Two APS-designed ultra-high-vacuum (UHV)-compatible, water-cooled, artificial channel-cut crystal monochromators for x-ray photon correlation spectroscopy (XPCS) and other applications were constructed and installed at the Linac Coherent Light Source (LCLS) at the SLAC National Accelerator Laboratory. The first such monochromator was commissioned and characterized on August 27, 2010.

The monochromator (Fig. 1) was originally developed by APS scientists and engineers to meet the challenging stability and optical requirements of the XPCS program at XSD) beamline 8-ID-I at the APS [1]. Using a laminar structure configured and manufactured by chemical etching and lithography techniques, a planar-shape, high-stiffness, high-precision weak-link module was designed and built [2]. The precision and stability of this mechanism allowed for alignment or adjustment of an assembly of crystals to achieve the same performance as does a single channel-cut crystal, so the device was called an "artificial channel-cut crystal." A similar monochromator has also been constructed for the HP-CAT beamline 16-BM at the APS for high-pressure research [3].

A zone-plate- and multilayer Laue lens (MLL)-compatible x-ray nanoprobe optics module was designed at the APS for the National Synchrotron Light Source-II project at Brookhaven National Laboratory. This work was carried out as a collaboration between Argonne and Brookhaven scientists and engineers. The preliminary design was based on the experience gained from the Argonne nanopositioning system designed for the Argonne Center for Nanoscale Materials/APS MLL-based hard x-ray nanoprobe project [4]. Figure 2 shows a conceptual three-dimensional model of the MLL optics alignment apparatus with seven degrees of the positioning freedom. The detailed design and analysis for the first prototype is in progress.

Finally, two chemical vapor deposition diamond-based x-ray beam position monitors (XBPMs) have been designed and constructed at the APS for the 3-GeV, 400-mA Taiwan Photon Source (TPS) project, as shown in Fig. 3. One of the BPMs is for the insertion device beamlines and one for the bending magnet beamlines. The XBPM prototypes were designed to meet stringent TPS requirements, including high monitor spatial resolution and mechanical structure stability, and the ability to withstand high power densities. This work is a collaboration between Argonne/APS and the Taiwan National Synchrotron Radiation Re-search Center (NSRRC) [5]. Scientists and engineers at the NSRRC provided design input and arranged and contributed to a pre-prototype test at beamline BL12XU of the SPring-8 light source in Japan.

Contact: Deming Shu, shu@aps.anl.gov

References

[1] S. Narayanan, A. Sandy, D. Shu, M. Sprung, C. Preissner, and J. Sullivan, J. Synchrotron Rad. **15**, 12 (2008).
[2] D. Shu, T. S. Toellner, and E. E. Alp, Nucl. Instrum. Methods A **467-468**, 771 (2001.
[3] W. Yang, D. Shu, E. Rod, G. Shen, and H-K. Mao, to be published in the proceedings of the Fifteenth Pan-American Synchrotron Radiation Instrumentation (SRI) Conference, Nucl. Instrum. and Methods A, (June 10-13, 2008, Saskatoon, Canada).
[4] D. Shu, H. Yan, and J. Maser, to be published in the proceedings of the Fifteenth Pan-American Synchrotron Radiation Instrumentation (SRI) Conference, Nucl. Instrum. and Methods A, (June 10-13, 2008, Saskatoon, Canada).
[5] C-K. Kuan, D. Shu et al., to be published in the proceedings of the Fifteenth Pan-American Synchrotron Radiation Instrumentation (SRI) Conference, Nucl. Instrum. and Methods A, (June 10-13, 2008, Saskatoon, Canada). ➲

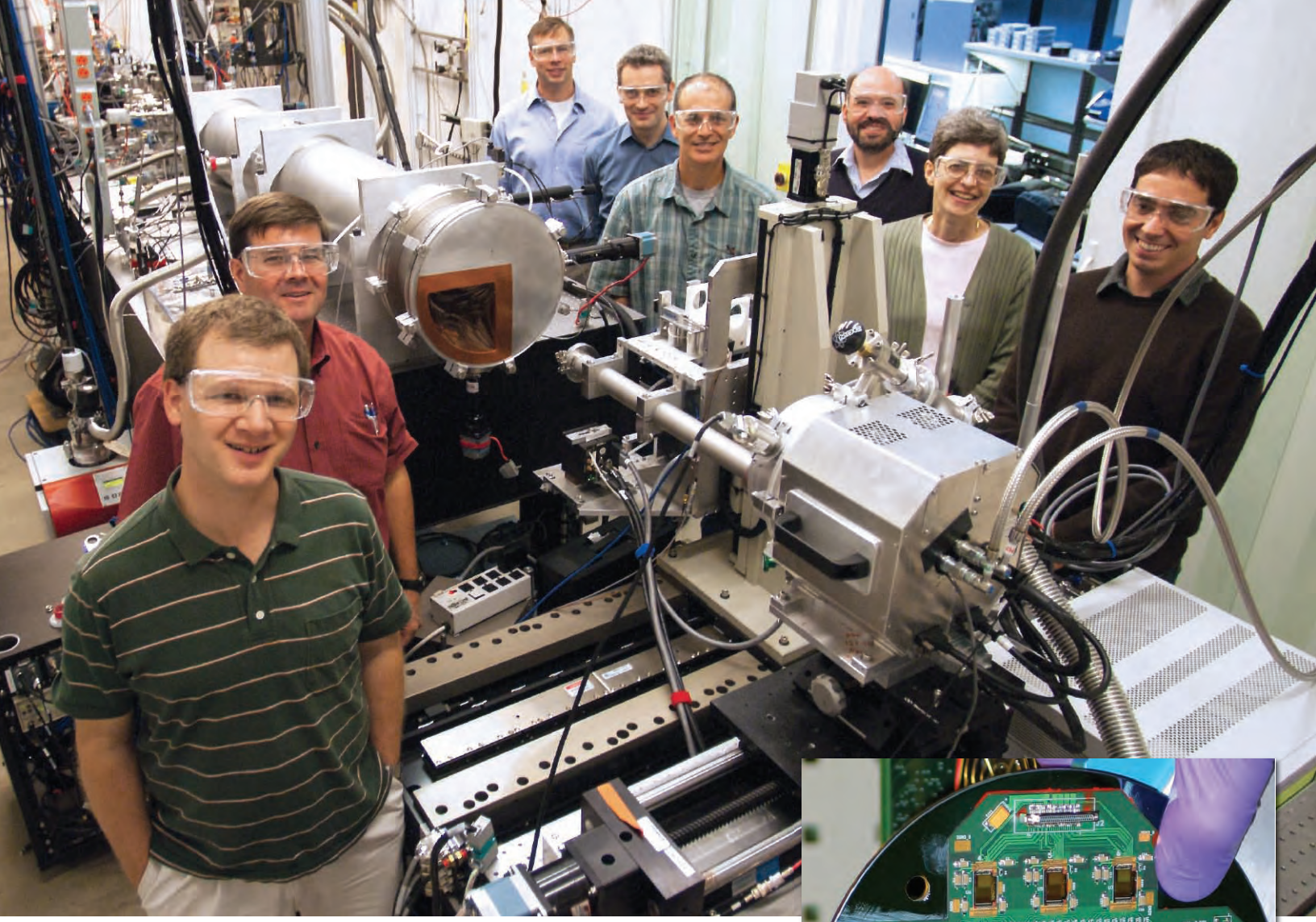

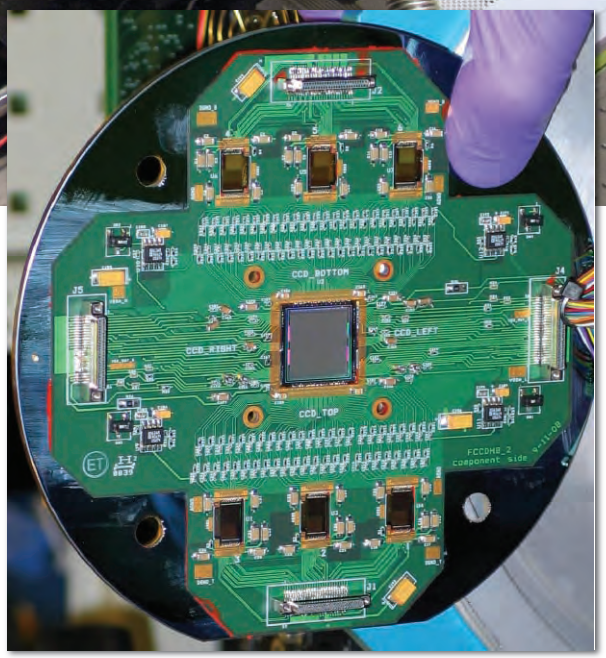

Above: The 480 × 480 Fast CCD x-ray detector (right foreground) and the project collaborators in the XSD beamline 8-ID research station. Left to right: Tim Madden (Argonne), John Weizeorick (Argonne), Alec Sandy (Argonne), Devis Contarato (LBNL), John Joseph (LBNL), Peter Denes (LBNL), Patricia Fernandez (Argonne), and Dionisio Doering (LBNL). Right: The detector's sensor exposed.

Since 2006, the staff of the Optics and Detectors Group in XSD has been collaborating with colleagues from Lawrence Berkeley National Laboratory (LBNL) to develop a unique, direct x-ray detector that provides small pixels, a fast frame rate, and high quantum efficiency. These features make this detector an ideal candidate for the XPCS experiments that are carried out at XSD beamline 8-ID at the APS. In 2010, the collaboration produced the first prototype of the 480 × 480 Fast CCD (charge-coupled device) x-ray detector.

One of the first sets of experiments to benefit from this new detector were conducted by Laurence Lurio and his students from Northern Illinois University. They used XPCS to study the dynamics of concentrated suspensions of alpha and gamma crystalline proteins extracted from bovine eye lenses. This fast, high-efficiency CCD camera used in parallel with other techniques has helped the researchers overcome the limitations of low flux and x-ray damage to their samples. With x-ray energies of 7.6 keV, the 480 × 480 Fast CCD x-ray detector gives Lurio's team a quantum efficiency near 100%, whereas older CCD cameras were only 50% efficient.

The success of the 480 × 480 Fast CCD detector has led to a new collaboration with LBNL to develop a larger, 1920 × 960 Fast CCD. This detector will retain the features of the smaller prototype, while adding the ability of operating in a 960 × 960 frame transfer mode. In a frame transfer mode users will be able to operate the camera at a high frame rate without a shutter. Shutterless operations have the advantage of being able to continuously collect photons without blocking x-rays while the CCD is being read-out.

Contact: John Weizeorick, weizeor@aps.anl.go

Greening the APS Booster

The electricity needed to power the technical components that produce APS x-ray beams is a significant segment of the APS operating budget, in terms of both energy and dollars. APS scientific and techical staff continually look for innovative schemes to reduce the facility energy footprint.

The APS electron booster ring uses two large power supplies in a push-and-pull configuration to power 68 dipole magnets connected in series. Each power supply has an output of up to 2000 V and 1000 A. The output of the power supplies ramps up from zero to the maximum as the beam energy increases from 325 MeV to 7 GeV. After the beam is extracted from the booster, the power supplies ramp down to zero and get ready for the next cycle. Figure 1 shows a set of typical dipole magnet voltage and current waveforms during one ramp cycle.

Because the booster ring operates at a rate of 2 Hz, the average power consumption of the dipole magnets and power supplies is about 500 kW, which amounts to 70% of the power consumed by all the booster magnets and power supplies. During top-up operation of the storage ring (when the electron current in the ring is maintained at a preset level by frequent injection of additional electrons) the beam in the booster is required only when there is a need to top up the ring. The dipole power supplies can be put in a standby mode (with a resulting minimum energy consumption) to keep the electronics alive, and awakened to ramp up when a top-up is needed. In order to achieve this energy-saving goal, the power supplies' regulation and stability had to be improved.

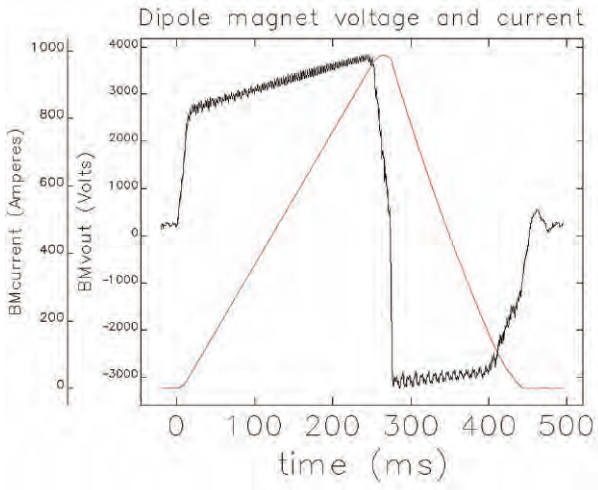

Fig. 1. Booster power supply output voltage (black line) and current (red line).

Hardware Improvements

The dipole magnet power supplies use a 12-pulse and AC-to-DC silicon-controlled rectifier. Its output contains harmonics of 12 multiples of the AC line frequency, dominated by the 720-Hz harmonics. Because of imperfections in the hardware, there is also a considerable amount of 360-Hz harmonics in the output voltage and current. After extensive studies and simulations, two mechanisms were found through which the harmonic currents got into the magnets: a differential mode and an unexpected common mode due to the capacitive coupling between the magnet coils and the system Earth ground through the magnet cores.

To reduce the differential mode harmonics, notch filters were installed at the output of the power supplies to trap the 360-Hz and 720-Hz harmonic voltages. To reduce the common harmonics, the impedance of the common mode circuit was increased. With these

"Greening" cont'd on page 140

Multi-Objective Evolutionary Optimization of APS-U Project Lattices

Among the many accelerator requirements for the APS Upgrade (APS-U) project is the need to change the electron storage ring optics or "lattice" to accommodate a number of long straight sections (LSSs). Two of these will be needed by the short-pulse x-ray (SPX) system in order to provide sufficient room for the cryostats that will contain the deflecting cavities. The other LSSs will accommodate the needs of certain beamlines for longer insertion devices. In addition, the APS will continue to accommodate the need for reduced horizontal beamsize (RHB) in one location.

The basic physical structure of the APS has a 40-fold periodicity, corresponding to the 40 storage ring sectors (35 of which can have beamlines). Within that structure, the option exists to tune individual magnets to either enforce or break the inherent translational symmetry of the machine. Most light source accelerators operate in highly symmetric lattices, because this is beneficial to improving the nonlinear dynamics of electrons. In developing lattices, accelerator physicists must tune the sextupole magnets in an attempt to ensure good injection efficiency and electron beam lifetime. Typically, this tuning is done using simulation codes that compute and minimize the strength of resonance driving terms. After this is completed, one would typically simulate ("track") the motion of individual electrons in the accelerator to determine the dynamic acceptance at the injection point (Fig. 1) and the momentum acceptance along the ring. (These determine, respectively, the injection aperture and the beam lifetime.) This process is problematic because minimizing the resonance driving terms does not ensure good dynamic acceptance and momentum acceptance. Hence, it is common to make use of a symmetric lattice, which reduces the difficulty of the problem.

"Lattices" cont'd on page 140

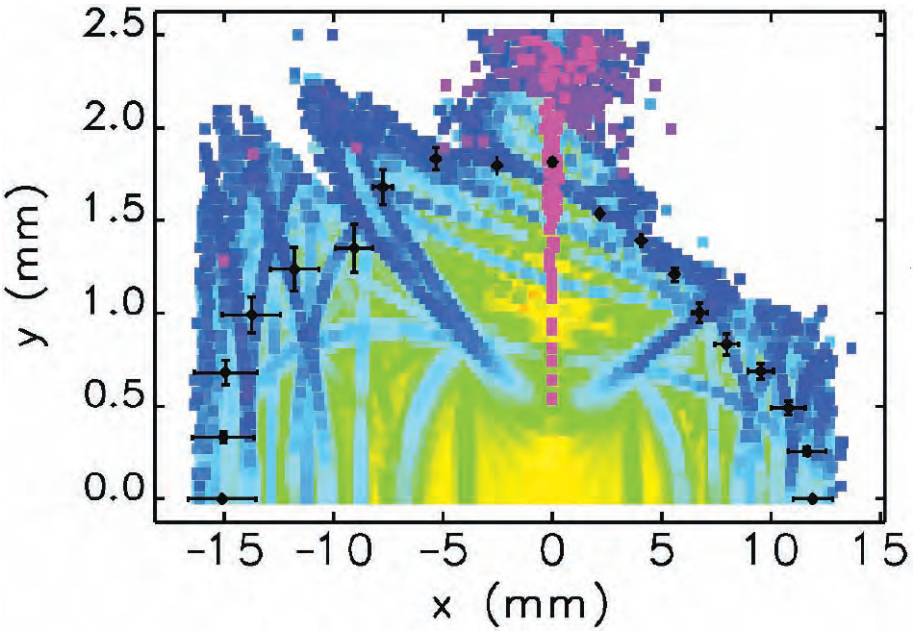

Fig. 1. Dynamic acceptance from 50 ensembles for the lattice with 8 LSS and chroamticity of 8 in both planes, superimposed on the frequency map for the machine with no errors. The frequency map is color-coded by the diffusion rate.

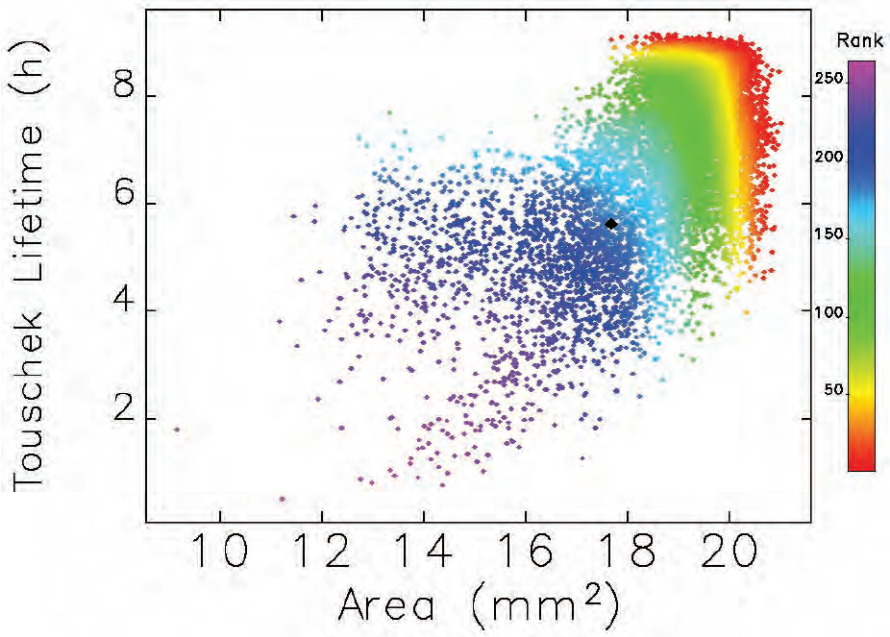

Fig. 2. Example of the evolution of the predicted Touschek lifetime and dynamic acceptance area during development of a configuration with eight non-symmetrically-placed LSSs The black diamond shows the starting point, which resulted from an optimization of a less difficult configuration.

THE SOFTGLUE SOLUTION

Many APS beamlines require custom digital electronics, and the APS has long served these needs with standard hardware such as the Generic Digital IO Board, a stand-alone, field-programmable gate array (FPGA)-based module, which is programmed offline by an electrical engineer armed with special software and an exact description of the requirement. This type of solution is well suited to the need for complex, high-performance hardware that does not require close cooperation with beamline software, that can be described completely and accurately in advance, and that can be tested before actual use.

Not all needs for digital electronics at the APS fit this pattern. Enter "softGlue," an Experimental Physics and Industrial Control System (EPICS) module that enables APS users to construct small, simple, digital electronic circuits, and to connect those circuits to field wiring, all by writing to EPICS variables. In this way, softGlue provides APS scientists and beamline-controls staff with the capability to analyze and solve simple digital electronics problems at run time, using tools they already have at hand, and already know how to use. softGlue solutions can be modified easily during an experiment, as the problems they address evolve or become better understood. softGlue solutions also can be set aside after an experiment is finished, and replaced by any custom electronics needed for the next experiment.

softGlue is not a new idea. Many APS users are familiar with the notion of a "userCalc": an EPICS record reserved for use by beamline staff and users, with which they can supplement deployed beamline software. The typical APS beamline has over 100 such records of various types, and beamline scientists have made extensive use of them. softGlue is the digital electronics equivalent of a collection of userCalcs. It can be "programmed" via the same user interfaces (motif editor and display manager, or MEDM, for example), and its "programming" can be saved and restored along with other beamline software, modified remotely, emailed to another user, and versioned as other beamline software is versioned.

Figure 1 shows the graphical user interface for two electronic components, which are implemented by softGlue in the FPGA of an Acromag IP-EP200 Industry Pack module. Signals are connected together by giving them the same name, so in this circuit, the output of the AND gate clocks the flip flop. A softGlue signal can also be driven directly by EPICS software, by writing a number instead of a name. The complexity of achievable circuitry is limited: only 15 signal names can be defined, and there is a fixed collection of components, including logic gates, flip flops, counters, multiplexers, and possibly additional application-specific components.

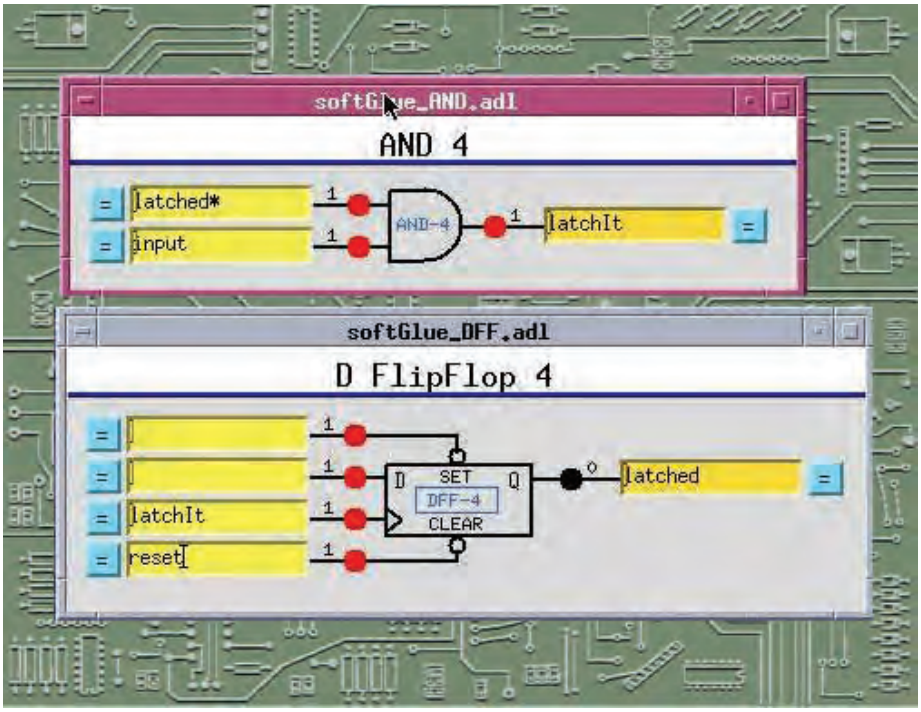

Fig. 1. Typical motif editor and display manager user interface.

The name "softGlue" is intended to suggest software-programmable "glue electronics." Glue electronics is typically simple circuitry that matches the output of one electronic device to the input requirements of another device. " "Glue" is a particularly appropriate notion when the electronic devices were not designed to communicate with each other, but experimental requirements call for their actions to be coordinated. For example, one might use pulses produced by a rotary encoder to direct the opening and closing of a shutter and to trigger data acquisition by a detector.

But softGlue is also useful in purely diagnostic applications. One might want to trigger an oscilloscope on the rising edge of signal A, but only if signal B is True, or only if signal C changed state within the past 20 μsec, etc.

Absent any programming (that is, when no signal names or values are defined) softGlue functions simply as an EPICS-supported 48-bit digital input/output (I/O) module, in which the I/O bits are designated as inputs or outputs at boot time. I/O signals can be enabled to generate interrupts, and softGlue defends the VME processor against interrupts occurring more frequently than they can be handled.

For more information, see: http://www.aps.anl.gov/bcda/synApps/softGlue/softGlueDoc.html.

Contact: Tim Mooney, mooney@aps.anl.gov

Useful Links on the APS Website @ www.aps.anl.gov

APS Upgrade Project: http://www.aps.anl.gov/Upgrade/

Become an APS User: http://www.aps.anl.gov/Users/New/

Beamline Directory: http://tinyurl.com/64dz5u6

APS Accelerator Systems Division: http://tinyurl.com/3gry2hw

APS Engineering Support Divsion: http://tinyurl.com/3v49smy

APS X-ray Science Division: http://tinyurl.com/3vxsqgq

APS Industrial Liaison Office: http://www.aps.anl.gov/industry/

APS Publications Database: http://tinyurl.com/3cgw6ch

APS Science and Research Highlights: http://tinyurl.com/5sfnczt

The APS and You: http://tinyurl.com/3qgkz5q

APS User News: http://tinyurl.com/3orwydu

APS News: http://www.aps.anl.gov/News/APS_News/

Conferences & Workshops: http://tinyurl.com/3e8wnjf

Lightsource Notes: http://tinyurl.com/43f3a7o

APS Technical Bulletins: http://tinyurl.com/3bbrlm3

APS Technical Updates: http://tinyurl.com/3m9fn7j

APS Brochure: http://www.aps.anl.gov/Science/Brochure/

APS Posters: http://www.aps.anl.gov/Science/Posters/

"Greening" cont'd from page 136
methods, the 360-Hz and 720-Hz harmonic currents in the dipole magnets have been reduced by 80% and 50%,

Software Improvements

The dipole magnet power supplies are equipped with voltage regulation circuits. To achieve the required full-range current tracking accuracy of 5×10^{-4}, two workstation-based programs are used. One program, called "bcontrol," regulates the ramp amplitude and delay; the other, called "autoRampCorrection," adjusts the voltage reference waveform to minimize the error between the magnet current and the expected current.

Two software upgrades have been implemented to autoRamp-Correction: a new normalization algorithm that eliminated an instability that caused continuous shift of ramp timing, and the addition of a smooth front-segment to the voltage reference that helped reduce the current transient at the injection point.

With these upgrades, the current tracking error has been greatly reduced. The error at the injection point has gone from 0.5% to 0.2% and the overall RMS error is 0.01%, down from 0.03%.

Energy-Saving Mode

Along with improvement of the power supplies, an energy-saving operation mode has been developed and tested. In this mode, the power supply ramp is disabled during the first minute in a typical 2-min top-up cycle. Ramp correction parameters are optimized to ensure the recovery of the current tracking accuracy after the power supplies "sleep" for one minute. Operating under this mode, an average power of 250 kW can be saved. Based on 5000 hours of user operations, 1.25 million kWh of energy can be saved annually.

Contact: Ju Wang, juw@anl.gov

"Lattices" cont'd from page 137

A direct (i.e., tracking-based) technique was recently developed for tuning sextupoles in order to maximize injection area and beam lifetime. This method uses either a single- or multi-objective parallel evolutionary optimizer running on a computing cluster. At any one time, the cluster is asked to perform particle tracking for many variants of a simulated accelerator, and to determine the dynamic acceptance and momentum acceptance of each. The optimizer then blends the properties of the best configurations, and in addition, adds some randomness to those properties in a deliberate imitation of the process of biological evolution. In this way, new trial configurations are created and submitted for evaluation, a process that continues until a sufficiently good solution has been obtained. Figure 2 shows an example of the progress of such an optimization.

The first application of this technique was to improving the lifetime of the APS electron beam in the standard 24-bunch mode; an improvement of about 25% was realized. In developing this lattice, it was serendipitously discovered that breaking the symmetry of the lattice could have a beneficial effect. At the same time, symmetric APS-U project lattices were being worked on that incorporated eight LSSs. This led to the exploration of non-symmetric LSS configurations for the APS-U project.

Early applications of this technique made use of a small computing cluster maintained by the Accelerator Systems Division. It soon became clear that additional resources were needed for the more challenging APS-U project lattices. Early access to the Argonne Laboratory Computing Resources Center's new "Fusion" cluster was instrumental in demonstrating the feasibility of configurations with eight non-symmetrically-placed LSSs. At the same time, software was ported to the BlueGene/P at the Argonne Leadership Computing Facility, which provides even more computing power.

Because of the unusual nature of the results and the importance of a good lattice for the APS-U project, experimental studies of "mock-up" LSS configurations were undertaken. These are developed in the same way as the APS-U project lattices, but the changes required in the Upgrade (removing and relocating magnets) are mocked-up by turning off and adjusting various magnets. In this way, it was feasible to experimentally test a close approximation of potential APS-U project lattices. So far, the lattices tested have mocked-up (1) eight non-symmetric long straights ("8RLSS") and (2) eight non-symmetric long straights with SPX and RHB included ("8RLSS+SPX+RHB").

Initial tests of the 8RLSS mock-up were disappointing, but the cause was soon discovered. Historically, significant steering of the electron beam has been accommodated to compensate for alignment issues between the storage ring and beamlines. This has resulted in significant vertical electron beam offsets in the sextupole magnets, which was found to drive a resonance. When the beam was moved to the "reference orbit," which is centered in the sextupoles, the performance of the mocked-up lattice was as good as the regular APS lattice. This provides a significant degree of confidence in the workability of an APS-U project configuration with non-symmetrically-placed LSSs. Even so, some discrepancies between simulations and experiments were found, which are being resolved. The 8RLSS+SPX+RHB mock-up is significantly more difficult, and work continues to improve the injection efficiency and lifetime.

Contact: M. Borland, borland@aps.anl.gov
V. Sajaev, sajaev@aps.anl.gov
L. Emery, emery@aps.anl.gov
A. Xiao, xiaoam@aps.anl.gov

Exploring the Synergy between Synchrotron Radiation and Advanced Nuclear Energy Systems

More than 100 people attended the January 27-28, 2010, "Workshop on the Role of Synchrotron Radiation in Solving Scientific Challenges in Advanced Nuclear Energy Systems," including registrants from universities, government laboratories, industries, and funding agencies. The registrants represented all aspects of nuclear energy production, from reactor materials, fuels, and simulation validation to separations for reprocessing, waste storage, and environmental remediation.

Convened at the request of the Argonne APS and Energy Sciences and Engineering directorates, the workshop was charged with assessing the potential contribution of synchrotron experiments to the scientific needs of the nuclear energy science and engineering community within the combined contexts of Argonne's Nuclear Energy Initiative and the APS Upgrade project. The workshop participants came to the unanimous conclusion that synchrotron studies hold enormous potential to make fundamental contributions in all aspects of nuclear energy research.

The workshop was divided into three breakout sessions for summary in the report [1], specifically: (1) Solutions, Amorphous Solids, and Environment; (2) Corrosion and Interfaces; and (3) Radiation Damage and Effects. It was clear from the workshop presentations that the community's efforts to date have focused largely on the first two areas. Numerous examples of x-ray scattering, spectroscopy, and imaging were presented with relevance to metal speciation for the purpose of linking structure, notably local and mesoscale, with chemical reactivity and bulk materials properties.

There was widespread interest in pursuing studies on radiation damage and effects but to date very few synchrotron experiments have been undertaken, in part because of the health and safety issues associated with bringing hazardous samples to a user facility. Highlighting specific interests with significant potential was the study on the aqueous corrosion of spent fuel

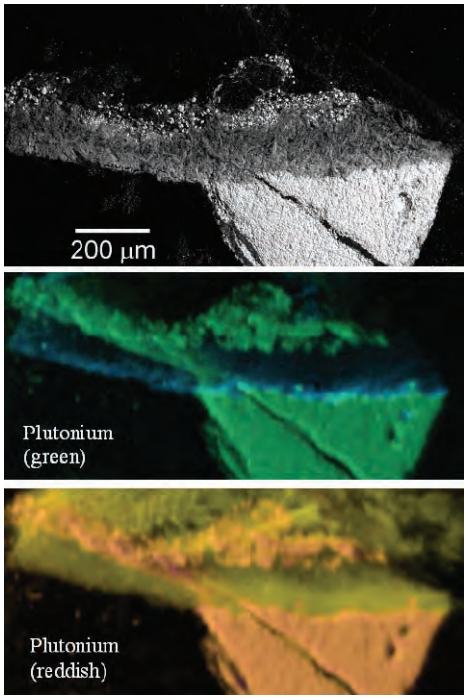

Fig. 1. Specimens of irradiated oxide nuclear fuel subjected to aqueous corrosion tests for 10 years, epoxy-embedded and cross sectioned in a hot cell for investigation. A small core was extracted and re-embedded in epoxy to form a specimen that was small enough to handle safely and was imaged with backscatter SEM (top), and x-ray fluorescence mapping and edge spectroscopy of key elemental components (center and bottom).

[2]. X-ray fluorescence mapping and edge spectroscopy were employed to investigate specimens of irradiated oxide nuclear fuel that had been subjected to aqueous corrosion tests for 10 years. Of specific interest was the local chemical environment of key elemental components. A backscatter scanning electron microscope (SEM) micrograph (top panel, Fig. 1) revealing intact fuel (light colored) with a 100-µm corrosion layer of uranyl silicate (gray), is compared with x-ray images of plutonium, strontium, and uranium (center and bottom panels) to show their relative distribution near the oxidation front.

The outcome of the workshop was a report summarizing the participants' recommendations. First amongst these was the request for continuation of the APS policy for access to state-of-the-art beamlines for experiments involving radioactive samples. APS assistance was requested with safety protocols,

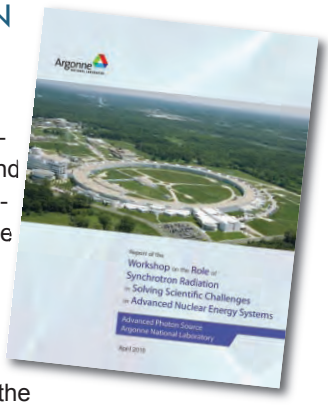

sample-containment design, and hardware development because many users encounter similar obstacles when trying to gain access to the APS experiment hall floor with hazardous samples. Along similar lines, recommendations were made to streamline safety approvals through more extensive communication. It was reasoned that assistance with these hurdles would greatly facilitate new users' efforts to conduct experiments on radioactive samples.

The most critical recommendations were associated with on-site radioactive sample handling. The community strongly recommended that the APS build a dedicated facility for handling radioactive materials. A stand-alone building located adjacent to the APS would permit open-sample manipulation and serve as a home base for the nuclear energy systems community, both of which were identified as needs by the user community.

Overall, the participants recognized the potential of synchrotron radiation studies, particularly those involving high-energy x-rays, as important but under-utilized probes of nuclear-energy related materials.

Contact: Lynda Soderholm, ls@anl.gov

References

[1] L. Soderholm, "Report of the Workshop on the Role of Synchrotron Radiation in Solving Scientific Challenges in Advanced Nuclear Energy Systems," www.aps.anl.gov/News/Conferences/2010/RAD/RAD-Workshop-Report.pdf

[2] A. Kropf, R. Finch, J. Fortner, S. Aase, C. Karanfil, C. Segre, J. Terry, G. Bunker, and L. Chapman, "Bent silicon crystal in Laue geometry to resolve x-ray fluorescence for x-ray absorption spectroscopy," Rev. Sci. Instrum. **74**, 4696 (2003).

CONFERENCES, MEETINGS, WORKSHOPS, ETC.

Workshop on the Role of Synchrotron Radiation in Solving Scientific Challenges in Advanced Nuclear Energy Systems • January 2-28, 2010 • The workshop brought together leading researchers in the field of advanced nuclear energy systems to discuss important scientific and technological issues in all areas of nuclear-energy systems, encourage communication between nuclear-energy researchers and synchrotron experts to optimize the use of synchrotron techniques for discovery in areas related to advanced nuclear energy systems, identify the user-community's future needs for synchrotron radiation facilities, and address scientific questions of importance in nuclear-energy technology and examine the adequacy of current capabilities and the need for new facilities. The workshop provided an important opportunity to assist the APS with identifying current and future synchrotron capabilities in the context of solving the pressing scientific and technological problems in advanced nuclear energy systems. Note; See the article on page xx. *Contact: ls@anl.gov, jstubbin@illinois.edu*

Small-Angle Scattering Short Course 2010: "Beyond RG" • March 27-31, 2010 • The objective of the course is to raise the capabilities of the small-angle scattering (SAS) community by providing an intermediate-level course for those in need of a better understanding of SAS theory and techniques utilized at the APS. The SAS short course offers an overview of SAS theory, capabilities, and data reduction and analysis tools to enable the community to submit highly effective beam time proposals and to facilitate better utilization of the resources at the APS. The course includes hands-on experiments at a selected APS small-angle x-ray scattering facility, and data reduction and evaluation. *Contact: ilavsky@aps.anl.gov*

Λ 2010 APS/EMC Users Meeting • May 3-5, 2010 • Rafael Jaramillo (Harvard University) received the 2010 Rosalind Franklin Young Investigator Award on May 4 at the 2010 APS/EMC Users Meeting (main photo). The APS Users Organization (APSUO) selects the winner of this biannual award, which recognizes an important technical or scientific accomplishment by a young investigator that depends on, or is beneficial to, the APS. Jaramillo was recognized for furthering understanding of itinerant magnetism and for contributions to the study of quantum matter at high pressure using synchrotron x-ray diffraction. Jaramillo is shown above receiving his award from Paul Fuoss (Argonne), chair of the APSUO Steering Committee, and Murray Gibson, Argonne Associate Laboratory Director for Photon Sciences. *Contact: strasser@aps.anl.gov*

Λ 12th National School on Neutron and X-ray Scattering • June 12-26, 2010 • The main purpose of the National School on Neutron and X-ray Scattering is to educate graduate students on the utilization of major neutron and x-ray facilities. Lectures, presented by researchers from academia, industry, and national laboratories, included basic tutorials on the principles of scattering theory and the characteristics of the sources, as well as seminars on the application of scattering methods to a variety of scientific subjects. Students conducted four short experiments at the APS and at the Oak Ridge National Laboratory Spallation Neutron Source and High Flux Isotope Reactor facilities to provide hands-on experience for using neutron and synchrotron sources. *Contact: nxschool@dep.anl.gov*

Λ 17th International Conference on Dynamical Processes in Excited States of Solids (DPC '10) • June 20-25, 2010 • This cross-disciplinary meeting is for scientists interested in theoretical and experimental aspects of the dynamics of excited states in condensed matter in physics, chemistry, life sciences and material sciences. Basic as well as applied science aspects are covered with emphasis on the dynamics of highly excited states of solids; excited states studies using synchrotron radiation and free electron lasers; excited states in clusters, spectroscopy of nanoscale and single nano objects; excited state dynamics of macromolecules and biomolecules; energy transfer and exciton dynamics; electron-phonon interaction and phonon dynamics; coherent, nonlinear, and high-resolution spectroscopy; ultrafast phenomena; and excited state dynamics under extreme conditions (such as pressure, magnetic fields, etc.). *Contact: dpc10@anl.gov*

Workshop on Computational Scattering Science 2010 • July 6-9, 2010 • The organizing principle for this workshop is how modern computations of the structure and dynamics of materials can predict the elastic and inelastic scattering observed by experiment. Ideas will also be sought to organize software development, and manage maintenance, upgrades, and user support. The Workshop Report will present possible paths forward, critically assessing their strengths, weaknesses, and cost-effectiveness. *Contact: btf@caltech.edu*

Λ APS/IIT Summer XAFS School • July 12-16, 2010 • The 2010 XAFS summer school was a continuation of the week-long summer school offered annually at the APS, with the classroom venue moved to the Illinois Institute of Technology in Chicago. Course material covers fundamental and practical aspects of x-ray absorption fine structure spectroscopy, including sample preparation, experiment, theory, and data analysis. Hands-on experiments are carried out at several APS beamlines, followed by a guided data analysis laboratory using Athena/iFEFFIT and other programs. The target audience is graduate students, postdocs, and other scientists who are new to XAFS and want to use it in their own research.
Contact: bunker@iit.edu

Λ Short Course on High Pressure Synchrotron Techniques • September 15-18, 2010 • Significant advances in high-pressure research have been made in recent years together with rapid progress in synchrotron radiation techniques. This short course provided an introduction for graduate students and postdoctoral researchers to high-pressure, synchrotron-based research. The chemical and physical fundamentals of matter at high densities were presented, as well as how high-pressure experiments, along with condensed matter theory, can provide a means to understand the changes that take place in matter under extreme conditions. Several high-pressure research frontiers were be introduced, and practical aspects of state-of-the-art x-ray synchrotron techniques were presented together with their current and potential applications. This short course formed a coherent introduction to the field of high-pressure research that is not generally taught in universities and provided a valuable background for students and young researchers to the field, regardless of the career paths they might pursue. *Contact: sgramsch@ciw.edu*

Λ The 16th Pan-American Synchrotron Radiation Instrumentation Conference • September 21-24, 2010 • Advances in synchrotron instrumentation, from sources through optics to detectors, have made possible the development of novel techniques to address pressing scientific questions that impact our daily life. SRI2010 is a forum to highlight these connections between synchrotron radiation instrumentation, science, and society. *Contact: sri2010@aps.anl.gov*

Λ Workshop on Evolution and Control of Complexity: Key Experiments Using Sources of Hard X-rays • October 11-13, 2010 • This workshop identified unexplored opportunities in the emerging field of non-equilibrium science where the focus will be on the use of hard x-ray spatiotemporal techniques. with no prior experience in inelastic x-ray scattering or synchrotron radiation. Experts in non-equilibrium science and engineering, laser science and technology, computational science, hard x-ray science, and source development explored the required hard x-ray characteristics and hard x-ray sources suitable to support a new community of users performing research in different focus areas of non-equilibrium science and engineering. The ultimate goal is to measure the time evolution of chaos or order using hard x-ray spatiotemporal tools.
Contact: ks@aps.anl.gov

X-RAY SOURCE & USER DATA

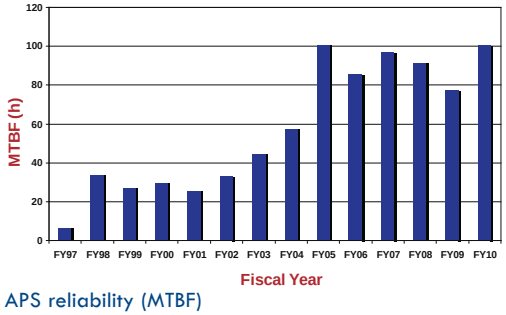

APS reliability (MTBF)

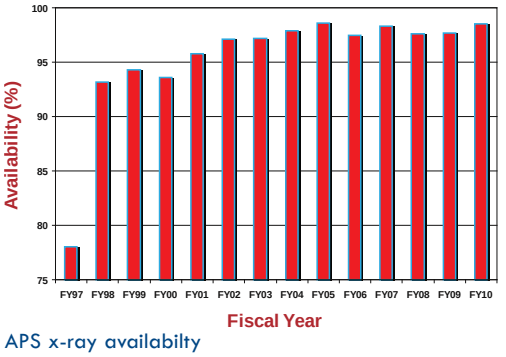

APS x-ray availabilty

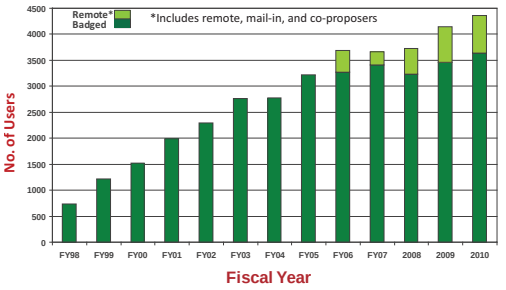

Number of APS users

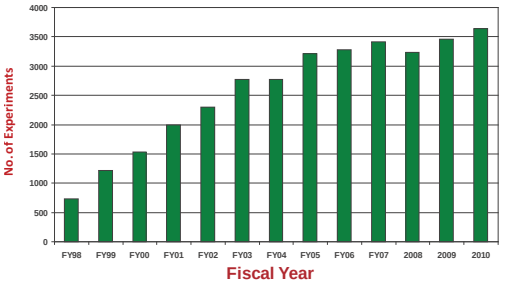

Number of experiments at the APS

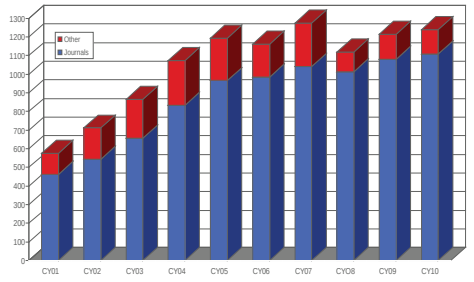

Number of APS publications

For complete lists of APS publications see the Publications Database at http://www.aps.anl.gov/Science/Publications/

In fiscal year 2010* the APS x-ray source continued to function as a highly reliable delivery system for synchrotron x-ray beams for research. Several factors support the overall growth in both the APS user community and the number of experiments carried out by that community. But there is a direct correlation between the number of x-ray hours available to users; the success of the APS experiment program; and the physicists, engineers, and technicians responsible for achieving and maintaining optimum x-ray source performance. Below are definitions of important measures for the delivery of x-ray beam to users (shown graphically at left).

Storage Ring Reliability: A measure of the mean time between beam losses (faults), or MTBF. MTBF is calculated by taking the delivered beam and dividing by the total number of faults. The APS targets, and routinely exceeds, 70 h MTBF. A fault is defined as complete unavailability of beam either via beam loss or removal of shutter permit not related to weather. A fault also occurs when beam has decayed to the point where stability and orbit can no longer be considered reliable. At the APS, this threshold is 50 mA.

X-ray Availability: The number of hours that the beam is available to the users divided by the number of hours of scheduled beam delivery prior to the beginning of a run. The specific definition of available beam is that the APS Main Control Room has granted permission to the users to open their shutters, *and* there is more than 50-mA stored beam in the storage ring.

* While the highlights in, and title of, this report cover calendar year 2010, data on accelerator performance and user statistics are measured on the basis of fiscal years.

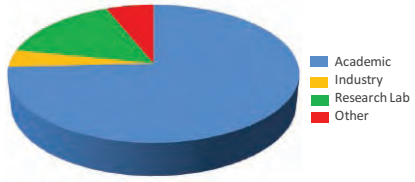

APS users by institution type

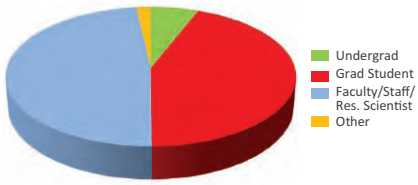

APS users by employment

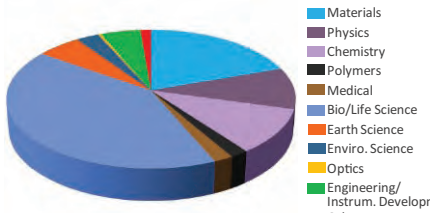

APS users by discipline

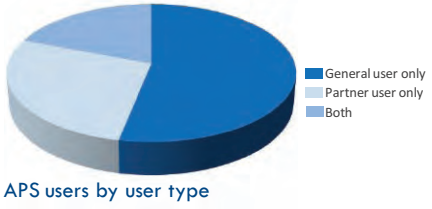

APS users by user type

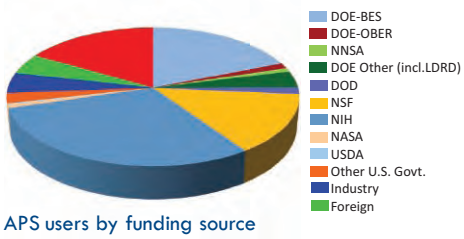

APS users by funding source

APS users by institutional geographic distribution

APS ORGANIZATION CHART

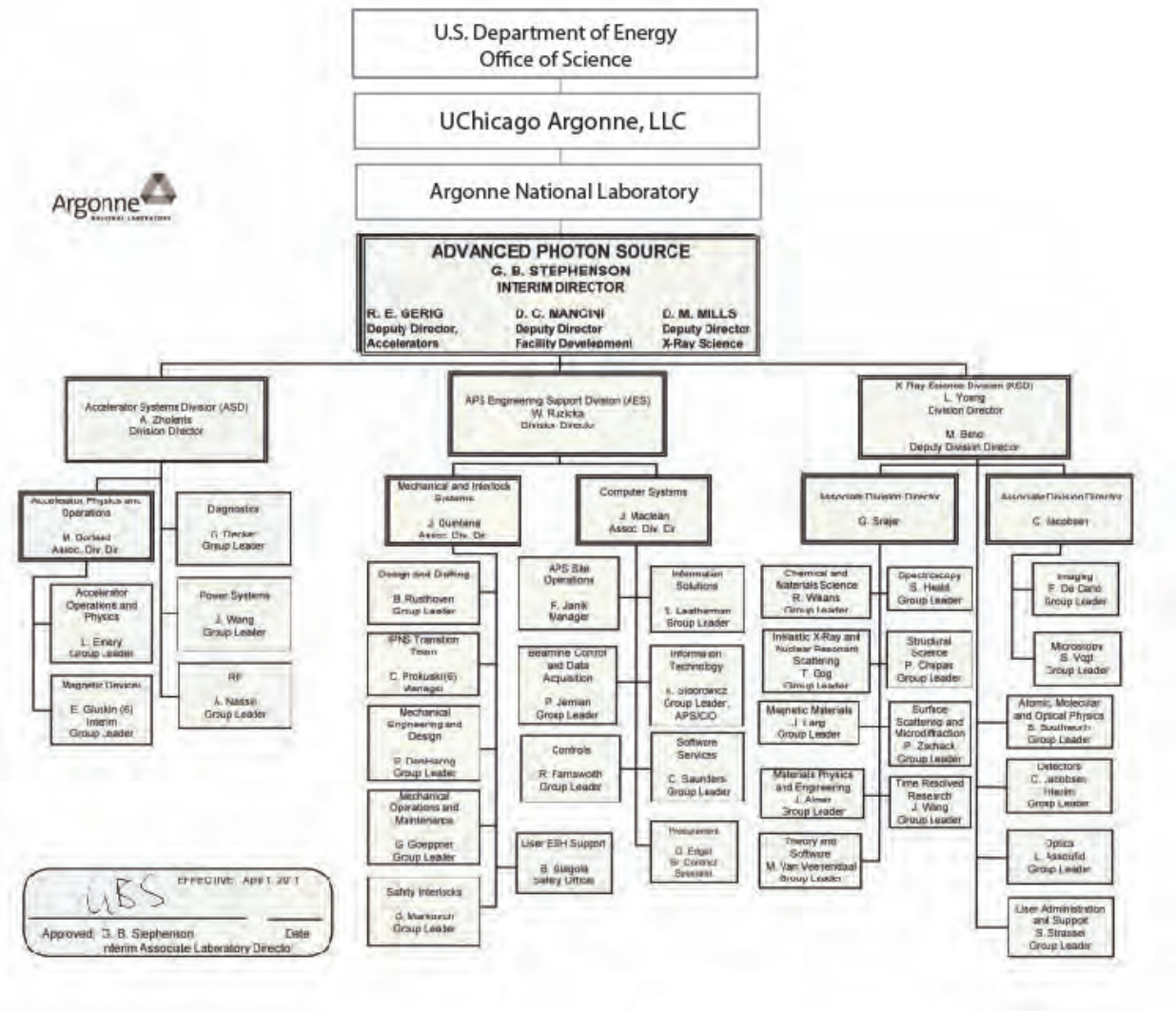

APS STAFFING AND FUNDING

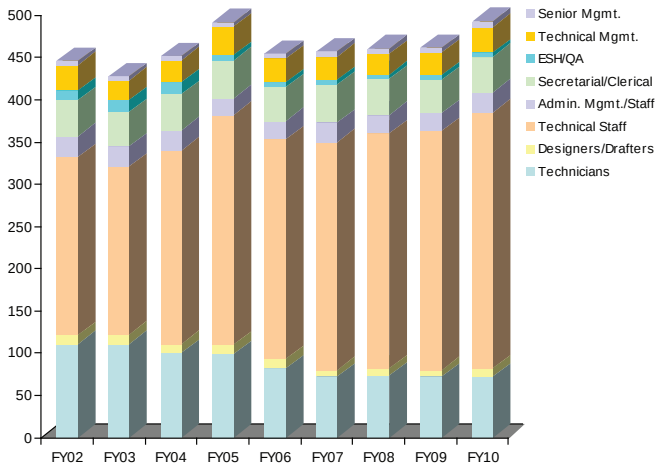

APS staffing levels, FY02-FY10

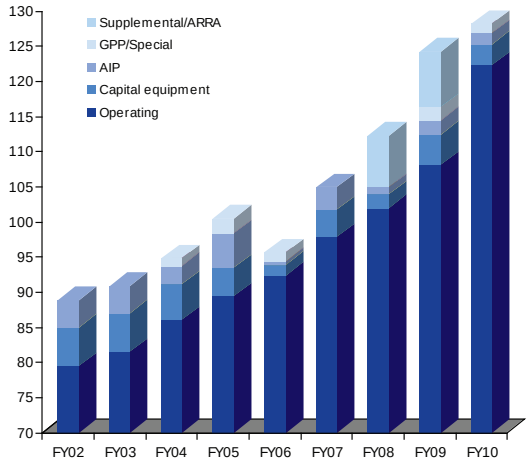

APS funding levels, FY02-FY10

TYPICAL APS MACHINE PARAMETERS

LINAC

Output energy	325 MeV
Maximum energy	450 MeV
Output beam charge	1–3 nC
Normalized emittance	10–20 mm-mrad
Frequency	2.856 GHz
Modulator pulse rep rate	30 Hz
Gun rep rate (1–6 pulses, 33.3 ms apart every 0.5 s)	2–12 Hz
Beam pulse length	8–15 ns
Bunch length	1–10 ps FWHM

PARTICLE ACCUMULATOR RING

Nominal energy	325 MeV
Maximum energy	450 MeV
Circumference	30.66 m
Cycle time	500 ms
Fundamental radio frequency (RF1)	9.77 MHz
12th harmonic rf frequency (RF12)	117.3 MHz
RMS bunch length (after compression)	0.34 ns

INJECTOR SYNCHROTRON (BOOSTER)

Nominal extraction energy	7.0 GeV
Injection energy	325 MeV
Circumference	368.0 m
Lattice structure	10 FODO cells/ quadrant
Ramping rep rate	2 Hz
Natural emittance	65 nm-rad-92 nm-rad
Radio frequency	351.930 MHz

STORAGE RING SYSTEM

Nominal energy	7.0 GeV
Circumference	1104 m
Number of sectors	40
Length available for insertion device	5.0 m
Nominal circulating current, multibunch	100 mA
Natural emittance	2.5 nm-rad
RMS momentum spread	0.096%
Effective emittance	3.1 nm-rad
Vertical emittance	0.040 nm-rad
Coupling	1.5%
Revolution frequency	271.554 kHz
Radio frequency	351.930 MHz
Number of bunches	24 to 1296
Time between bunches	153 to 2.8 ns
RMS bunch length	25 ps to 40 ps
RMS bunch length of 16 mA in hybrid mode	65 ps

APS SOURCE PARAMETERS

UNDULATOR A

Period: 3.30 cm
Length: 2.1 m in sectors 12, 21, 23, 24; 2.4 m in others
K_{max}: 2.75 (effective; at minimum gap)
Minimum gap: 10.5 mm
Tuning range: 3.0–13.0 keV (1st harmonic)
3.0–45.0 keV (1st-5th harmonic)
On-axis brilliance at 7 keV: 4.1 x 10^{19} ph/s/mrad^2/mm^2/0.1%bw (2.4 m)
3.3 x 10^{19} ph/s/mrad^2/mm^2/0.1%bw (2.1 m)
Source size and divergence at 8.0 keV:
Σ_x: 276 μm Σ_y: 11 μm
$\Sigma_{x'}$: 12.7 μrad (2.4 m), 12.9 μrad (2.1 m)
$\Sigma_{y'}$: 6.7 μrad (2.4 m), 7.1 μrad (2.1 m)

2.30-CM UNDULATOR (SECTORS 1, 11, 14)

Period: 2.30 cm
Length: 2.4 m
K_{max}: 1.20 (effective; at minimum gap)
Minimum gap: 10.5 mm
Tuning range: 11.8–20.0 keV (1st harmonic)
11.8–70.0 keV (1st-5th harmonic, non-contiguous)
On-axis brilliance at 12 keV: 6.9 x 10^{19} ph/s/mrad^2/mm^2/0.1%bw
Source size and divergence at 12.0 keV:
Σ_x: 276 μm Σ_y: 11 μm
$\Sigma_{x'}$: 12.3 μrad $\Sigma_{y'}$: 5.9 μrad

2.70-CM UNDULATOR (SECTORS 3 & 14)

Period: 2.70 cm
Length: 2.4 m
K_{max}: 1.76 (effective; at minimum gap)
Minimum gap: 10.5 mm
Tuning range: 6.7–16.0 keV (1st harmonic)
6.7–60.0 keV (1st-5th harmonic, non-contiguous)
On-axis brilliance at 12 keV: 5.7 x 10^{19} ph/s/mrad^2/mm^2/0.1%bw
Source size and divergence at 8.0 keV:
Σ_x: 276 μm Σ_y: 11 μm
$\Sigma_{x'}$: 12.7 μrad $\Sigma_{y'}$: 6.7 μrad

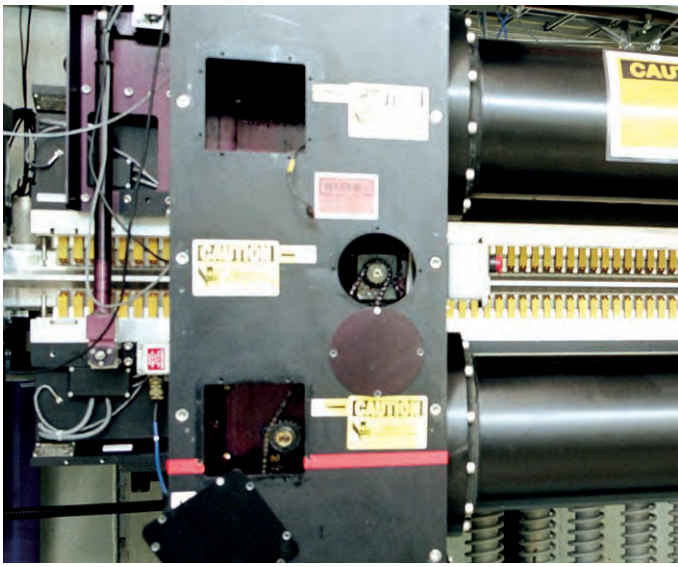

APS SOURCE PARAMETERS

3.00-cm UNDULATOR (SECTORS 12, 21, 23, 30)

Period: 3.00 cm
Length: 2.1 m in sectors 12, 21, and 23; 2.4 m in Sector 30
K_{max}: 2.20 (effective; at minimum gap)
Minimum gap: 10.5 mm
Tuning range: 4.6–14.5 keV (1st harmonic)
4.6–50.0 keV (1st-5th harmonic)
On-axis brilliance at 8 keV: 4.8×10^{19} ph/s/mrad^2/mm^2/0.1%bw (2.4 m)
3.9×10^{19} ph/s/mrad^2/mm^2/0.1%bw (2.1 m)
Source size and divergence at 8.0 keV:
Σ_x: 276 μm Σ_y: 11 μm
$\Sigma_{x'}$: 12.7 μrad (2.4 m), 12.9 μrad (2.1 m)
$\Sigma_{y'}$: 6.7 μrad (2.4 m), 7.1 μrad (2.1 m)

3.50-cm SmCo UNDULATOR (SECTOR 4)

Period: 3.50 cm
Length: 2.4 m
K_{max}: 3.08 (effective; at minimum gap)
Minimum gap: 9.5 mm
Tuning range: 2.3–12.5 keV (1st harmonic)
2.3–42.0 keV (1st-5th harmonic)
On-axis briliance at 7 keV: 3.7×10^{19} ph/s/mrad^2/mm^2/0.1%bw
Source size and divergence at 8.0 keV:
Σ_x: 276 μm Σ_y: 11 μm
$\Sigma_{x'}$: 12.7 μrad $\Sigma_{y'}$: 6.7 μrad

5.50-cm UNDULATOR (SECTOR 2)

Period: 5.50 cm
Length: 2.4 m
K_{max}: 4.97 (effective; at minimum gap)
Minimum gap: 14.0 mm
Tuning range: 0.6–7.0 keV (1st harmonic)
0.6–25.0 keV (1st-5th harmonic)
On-axis brilliance at 4 keV: 1.7×10^{19} ph/s/mrad^2/mm^2/0.1%bw
Source size and divergence at 4.0 keV:
Σ_x: 276 μm Σ_y: 11 μm
$\Sigma_{x'}$: 13.9 μrad $\Sigma_{y'}$: 8.8 μrad

APS SOURCE PARAMETERS

CIRCULARLY POLARIZING UNDULATOR (SECTOR 4)

Period: 12.8 cm
Length: 2.1 m
Circular mode:
K_{max}: 2.65 (effective; for both horizontal and vertical fields at maximum currents of 1.2 kA horizontal and 0.34 kA vertical)
B_{max}: 0.26 T (peak fields)
Tuning range: 0.5–3.0 keV (1st harmonic)
On-axis brilliance at 1.8 keV: 3.1×10^{18} ph/s/mrad^2/mm^2/0.1%bw
Linear mode:
K_{max}: 2.80 (effective; for both horizontal and vertical fields at maximum currents 1.4 kA horizontal and 0.40 kA vertical)
B_{max}: 0.29 T (peak fields)
Tuning range: 0.8–3.0 keV (1st harmonic)
0.8–10.0 keV (1st–5th harmonic)
On-axis brilliance at 2.1 keV: 2.3×10^{18} ph/s/mrad^2/mm^2/0.1%bw
Switching frequency: 0-5 Hz
Switching rise time: 20 ms
Source size and divergence at 1.5 keV:
Σ_x: 276 μm Σ_y: 12 μm
$\Sigma_{x'}$: 18.1 μrad $\Sigma_{y'}$: 14.5 μrad

APS BENDING MAGNET

Critical energy: 19.51 keV
Energy range: 1–100 keV
On-axis brilliance at 16 keV: 5.4×10^{15} ph/s/mrad^2/mm^2/0.1%bw
On-axis angular flux density:
9.6×10^{13} ph/s/mrad^2/0.1%bw at 16 keV
On-axis horizontal angular flux density:
1.6×10^{13} ph/s/mradh/0.1%bw at 6 keV
Source size and divergence at the critical energy:
Σ_x: 92 μm Σ_y: 31 μm
$\Sigma_{x'}$: 6 mrad $\Sigma_{y'}$: 47 μrad

Acknowledgments

***APS Science 2010* Editorial Board:**

Cele Abad-Zapatero (University of Illinois at Chicago), Mark A. Beno (ANL-XSD), Rodney E. Gerig (ANL-PSC), J. Murray Gibson (ANL-PSC), Thomas C. Irving (Illinois Institute of Technology), Derrick Mancini (ANL-PSC), Dennis M. Mills, (ANL-PSC), William G. Ruzicka (ANL-AES), George Srajer (ANL-XSD), G. Brian Stephenson (ANL-PSC, ANL-MSD), David M. Tiede (ANL-CSE), Linda Young (ANL-XSD), Alexander A. (Sasha) Zholents (ANL-ASD)

The research highlights in this report were written by:

William Arthur Atkins (waarc@grics.net)
David Bradley (david@sciencebase.com)
Yvonne Carts-Powell (yvonne.cartspowell@gmail.com)
Vic Comello (ANL-TSD, vcomello@anl.gov)
Sandy Field (sfield@fieldscientific.com)
Karen Fox (kfox@nasw.org)
Emma Hitt (emma@emmahitt.com)
Philip Koth (philkoth@comcast.net)
Elise LeQuire (cygnete@mindspring.com)
David Lindley (dlindley@nasw.org)
JR Minkel (jrminkel@gmail.com)
Mona A. Mort (monasbox@gmail.com)
Patricia E. Panatier (pep2@optonline.net)
Mark Wolverton (exetermw@earthlink.net)

Photography: Wes P. Agresta and George J. Joch (both ANL-TSD)
Aerial photograph of the APS: John Hill (Tigerhill Studio, http://www.tigerhillstudio.com)
Publications, contracts, rights and permissions, circulation: Jessie L. Skwarek (ANL-PSC)
Project coordination, art direction and design, photography: Richard B. Fenner (ANL-PSC)

Our thanks to the corresponding authors who assisted in the preparation of the research highlights, to the users and APS personnel who wrote articles for the report, and our apologies to anyone inadvertently left off this list. To all: your contributions are appreciated.

We note with deepest sadness the passing of our colleague JR Minkel. JR has been a contributor to *APS Science* since the inaugural issue in 2003. In fact, JR was the first of our science writers. He will always be remembered for his unfailing dedication and his ability to convey the wonder and excitement of science. On his former blog, “A Fistfull of Science,” JR described himself thus: “I’m a lab technician and freelance journalist based in Nashville, Tennessee. From 2006 to 2008 I worked as a web news reporter for *Scientific American*. Before that, I wrote for a number of popular science magazines. I’ve written one book, *Instant Egghead Guide: The Universe*. This is my blog. It reflects my current interest in the role of science in our collective construction of meaning.”

Advanced Photon Source
Argonne National Laboratory
9700 S. Cass Ave.
Argonne, IL 60439 USA

www.anl.gov
www.aps.anl.gov